INFORMATION TO USERS

This was produced from a copy of a document sent to us for microfilming. While the most advanced technological means to photograph and reproduce this document have been used, the quality is heavily dependent upon the quality of the material submitted.

The following explanation of techniques is provided to help you understand markings or notations which may appear on this reproduction.

1. The sign or "target" for pages apparently lacking from the document photographed is "Missing Page(s)". If it was possible to obtain the missing page(s) or section, they are spliced into the film along with adjacent pages. This may have necessitated cutting through an image and duplicating adjacent pages to assure you of complete continuity.

2. When an image on the film is obliterated with a round black mark it is an indication that the film inspector noticed either blurred copy because of movement during exposure, or duplicate copy. Unless we meant to delete copyrighted materials that should not have been filmed, you will find a good image of the page in the adjacent frame.

3. When a map, drawing or chart, etc., is part of the material being photographed the photographer has followed a definite method in "sectioning" the material. It is customary to begin filming at the upper left hand corner of a large sheet and to continue from left to right in equal sections with small overlaps. If necessary, sectioning is continued again—beginning below the first row and continuing on until complete.

4. For any illustrations that cannot be reproduced satisfactorily by xerography, photographic prints can be purchased at additional cost and tipped into your xerographic copy. Requests can be made to our Dissertations Customer Services Department.

5. Some pages in any document may have indistinct print. In all cases we have filmed the best available copy.

University Microfilms International

300 N. ZEEB ROAD, ANN ARBOR, MI 48106
18 BEDFORD ROW, LONDON WC1R 4EJ, ENGLAND

POPOWICZ, ANTHONY MICHAEL

CARBON-12/CARBON-13 AND HYDROGEN/DEUTERIUM VAPOR PRESSURE ISOTOPE EFFECTS OF FLUOROFORM: INTERMOLECULAR INTERACTIONS IN LIQUID FLUOROFORM

City University of New York PH.D. 1981

$^{12}C/^{13}C$ AND H/D VAPOR PRESSURE ISOTOPE EFFECTS OF FLUOROFORM: INTERMOLECULAR INTERACTIONS IN LIQUID FLUOROFORM

by

Anthony Michael Popowicz

A dissertation submitted to the
Graduate Faculty in Chemistry
in partial fulfillment of the
requirements for the degree of
Doctor of Philosophy,
The City University of New York

1981

This manuscript has been read and accepted by the Graduate Faculty in Chemistry in satisfaction of the dissertation requirements for the degree of Doctor of Philosophy.

March 14, 1981
date

Chairman of Examining Committee

Executive Officer

Supervisory Committee

The City University of New York

Abstract

$^{12}C/^{13}C$ AND H/D VAPOR PRESSURE:

ISOTOPE EFFECTS OF FLUOROFORM:

INTERMOLECULAR INTERACTIONS

IN LIQUID FLUOROFORM

BY

Anthony Michael Popowicz

Advisor: Professor Takanobu Ishida

A precision cryostat of the Bigeleisen-Brooks-Ribnikar-Ishida (BBIR) type with associated vacuum systems has been constructed and the appropriate temperature/pressure measurement and control systems designed and implemented. Various improvements in the cryostat design were incorporated in order to facilitate the assembly and repair processes. A major design change involved the incorporation of a digital stand alone computer to control cryostat operations. This apparatus was used to measure the $^{12}C/^{13}C$ and H/D Vapor Pressure Isotope Effects of Fluoroform.

Analysis of the measured VPIE results, in light of existing experimental data and theories, has demonstrated the need of a temperature dependent liquid force field, specifically a temperature-dependent interaction force constant between the C-H stretching motion and translational motion in the direction of the figure axis of CHF_3. This result is consistent with the observed spectroscopic data and vibrational and configurational models of fluoroform dimers. The intermolecular interaction is believed to be a weak hydrogen-bond in nature.

Come dance with the west wind
and touch on the mountain tops,
sail o'er the canyons and
up to the stars, and
reach for the heavens and
hope for the future and
all that we can be and
not what we are.

ACKNOWLEDGEMENTS

I would like to acknowledge with heartfelt appreciation, the contributions of all who have been involved in this project:

- Professor T. Ishida for his excellent guidance, limitless patience, and friendship,
- Professors V. Fried, J. Glickstein, A. Ronn and J. Schulman for their assistance and guidance,
- Mr. Armand Gazes for his invaluable assistance with the computer aspects of the project as well as his friendship,
- Mr. Sol Coltun and Mr. Martin Berman for their superb workmanship and professionalism in the construction of the cryostat,
- Professor J. Bigeleisen for his assistance, use of equipment and patience,
- Mr. Ottmar Safferling for his glassblowing efforts and friendship,
- Professor J. Howell for his assistance with Gaussian 70,
- Mr. Jan Shulman for his work on the purification of fluoroform samples and friendship,
- Mr. Peter Bratin and Mr. Michael Prencipe for their assistance in the electronics and friendship,
- Dr. Takao Oi for putting the cryostat back together again,
- Doctors Sene Bauman, Lucia Babcock, and Allan Rychtman for their friendship and support,
- Mr. Darrell Mayfield, Mr. Henry Wieck, and Mr. Lester Borodinsky for their supportive friendship,
- Lillian Richardson for her beautiful typing job,

- The Staff of the Brooklyn College Chemistry Department,
- The City University of New York Computer Center and Brooklyn College Data Acquisition Center for use of a great deal of computer time and facilities, and
- The Department of Energy who paid for it all.

TABLE OF CONTENTS

LIST OF TABLES

LIST OF FIGURES

I. INTRODUCTION

The understanding of the nature of intermolecular forces is of great scientific interest for both basic and applied reasons. Of particular concern is the liquid state. Due to the complexity of its structure, the interactions and motions of molecules are difficult to describe and characterize, and the applicability of spectroscopic techniques alone towards the elucidation of the nature of these forces is generally limited. Thus it is necessary to supplement spectroscopic data with information obtained from other experimental techniques. In particular, Vapor Pressure Isotope Effect (VPIE) measurements are ideally suited as a probe of intermolecular forces in condensed phases and coupled with spectroscopic and thermodynamic data of both the vapor and condensed states provides a powerful technique in examining intermolecular interactions and molecular motion in solid and liquid phases. It is therefore the objective of this research to apply the technique of VPIE towards elucidating intermolecular forces in liquid trifluoromethane (CHF_3).

Ia. VPIE Theory

In 1961 Jacob Bigeleisen[1] formulated the VPIE in terms of the reduced partition function ratios of the condensed and gas phase molecules:

$$\ln \frac{P'}{P} = \ln \frac{s}{s'} f_c - \ln \frac{s}{s'} f_g + k_1 + k_2 + k_3 , \qquad \text{I-(1)}$$

where

$$k_1 = (P'V' - PV)/RT , \qquad \text{I-(2)}$$

$$k_2 = (B_o P + \tfrac{1}{2} C_o P^2 + \ldots.) - (B_o P + \tfrac{1}{2} C_o P^2 + \ldots.)' , \qquad \text{I-(3)}$$

and

$$k_3 = \frac{1}{RT} \int_V^{V'} P' \, dV \qquad \text{I-(4)}$$

By convention primed quantities always refer to the lighter isotopic species under consideration. "c" and "g" refer to the condensed and gas phases, respectively, and the quantity "s" is the symmetry number for the molecule. P and V are the vapor pressure and molar volumes of the condensed state, and B_o, C_o, ... are the virial coefficients for the gas. The reduced partition function, s/s' f, is defined as

$$\frac{s}{s'} f = \frac{s}{s'} \frac{Q}{Q'} \prod_{i=1}^{N} \left(\frac{m_i'}{m_i} \right)^{3/2} = \frac{(Q/Q')qm}{(Q/Q')cl} , \qquad \text{I-(5)}$$

where Q_{qm} and Q_{cl} are the quantum mechanical and classical partition functions, respectively. m_i is the mass of the ith atom of an N-atom molecule. $\frac{s}{s'} f$ is thus the ratio of isotopic partition functions reduced in terms of the classical limit. Referring to equation 1, the term $\ln \frac{s}{s'} f_c - \ln \frac{s}{s'} f_g$ is the difference in the quantum mechanical

effects between the two phases. It is the vapor pressure difference that would be observed between two isotopic species with equivalent condensed phase molar volumes and gas phases whose behavior is ideal. The terms k_1, k_2 and k_3 are corrections to the VPIE. They account for changes in the vapor pressure when the condensed phase is subject to a pressure change from P to P', gas non-ideality, and condensed phase molar volume isotopic differences, respectively. Typically[2] one finds the magnitude of these corrections to the VPIE to be $k_1 \sim 1\%$, $k_2 \sim 0.1\%$ and $k_3 \sim 0.01\%$.

Due to the magnitude of most isotope effects ($\sim 1\%$) equation 1 can be given as

$$\ln \frac{f_c}{f_g} \approx \ln \frac{P'}{P} \left[1 + P \left(B_o - \frac{V}{RT} \right) \right] \qquad \text{I-(6)}$$

where the approximation $B_o' = B$, $V' = V$, and $\ln \frac{P'}{P} \approx \frac{P'-P}{P}$ used and the terms $\frac{1}{2}C_o P^2 - \frac{1}{2}C_o P'^2 + \ldots.$, and $\int_V^{V'} P' \, dV$ are neglected. These approximations are justified in that errors introduced are typically on the order of 0.01% or less, well within the limits of experimental error. Within the framework of the Harmonic Oscillator and Born Oppenheimer (HOBO) approximations and to the extent that internal and external motions of the molecules are separable

$$\frac{s}{s'} f = \prod_i \frac{u_i e^{-u_i/2} / (1-e^{-u_i})}{u_i' e^{-u_i'/2} / (1-e^{-u_i'})} , \qquad \text{I-(7)}$$

where $u_i = hc\nu_i/kT$. ν_i is the ith normal mode harmonic frequency in cm^{-1}.

In the gas phase, translational and rotational motions are treated independently from internal motions and, at ordinary temperature, the external motions are regarded to be classical. However, at low temperatures, correction for non-classical rotation may be required, depending on the particular molecular system under consideration. Neglecting any vibrational-rotational interaction, the reduced partition function ratio for the gas is thus given as

$$\frac{s}{s'} f_g = \left(\frac{Q_{vib}}{Q'_{vib}}\right)_{qm} \Big/ \left(\frac{Q_{vib}}{Q'_{vib}}\right)_{cl} = \prod_{i=1}^{3N-6} \frac{u_i e^{-u_i/2}/(1-e^{-u_i})}{u_i' e^{-u_i'/2}/(1-e^{-u_i'})}, \qquad \text{I-(8)}$$

where

$$(Q_{vib})_{qm} = \prod_{i=1}^{3N-6} e^{-u_i/2}/(1-e^{-u_i}) \qquad \text{I-(9)}$$

and

$$(Q_{vib})_{cc} = \prod_{i=1}^{3N-6} \frac{1}{u_i} \qquad \text{I-(10)}$$

It is noted that the energy zero is taken as the minimum of potential energy surface, to take advantage of the BO approximation. Upon condensation the molecule finds itself in a potential field which restricts the "free" motion experienced in the gas phase. The evaluation of f_c therefore depends upon the particular description of the potential surface the condensed phase molecule finds itself on. A model which has proved to be quite successful, due to the fact that configurational and other counting factors in the condensed phase partition function are invariant under isotopic substitution, is the

Simple Cell Model (SCM). SCM considers the condensed phase molecule to exist in and interact with a homogeneous and time-independent field. The 3N-6 vibrational modes thus are treated as in the gas phase and the six external modes are subject to a time-independent restoring force. Thus within the framework of HOBO approximations and SCM

$$\frac{s}{s'} f_c = \prod_{i=1}^{3N} \frac{u_i e^{-u_i/2}/(1-e^{-u_i})}{u_i' e^{-u_i'/2}/(1-e^{-u_i'})} , \qquad \text{I-(11)}$$

and thus

$$\frac{f_c}{f_g} = \prod_{i=1}^{3N-6} \left[\frac{(u_i/u_i')_c}{(u_i/u_i')_g} \cdot \frac{\exp((u_i'-u_i)_c/2)}{\exp((u_i'-u_i)_g/2)}\right] x$$

$$\left[\frac{(1-\exp(-u_i')_c / (1-\exp(-u_i)_c}{(1-\exp(-u_i')_g / (1-\exp(-u_i)_g}\right] x \qquad \text{I-(12)}$$

$$\prod_{i=1}^{6} \left[\frac{u_i \exp(-u_i/2) / (1-\exp(-u_i))}{u_i' \exp(-u_i'/2) / (1-\exp(-u_i'))}\right]_c$$

Taking the natural log of equation 12 shows that the magnitude and sign of $\ln f_c/f_g$ is determined by the net contribution of the external motions in the condensed phase and the perturbation of internal motions upon condensation by the intermolecular force field. Thus, given all the frequencies for the gas and condensed phases for the isotopic species under consideration, f_c/f_g is determined.

Ib. VPIE Methodology

Even though gas phase spectroscopic data is usually readily obtainable, information on the condensed phase is extremely limited, especially for liquids. However, the quantity f_c/f_g is given experimentally by equation I-(7). Thus from experimental P'/P and gas phase spectroscopic data, f_c can be obtained as a function of temperature. At this point the gas phase spectroscopic data can be used as a zeroth-order approximation to the internal force field of the condensed phase. Any available condensed phase spectroscopic and thermodynamic data, as well as models for intermolecular interaction are used to approximate the external force field and its interaction with the internal vibrations. A 3Nx3N vibrational secular equation is solved and f_c is calculated from 3N frequencies thus obtained. The calculated f_c can then be compared to the experimentally determined f_c and appropriate adjustments to the force constants can be made until the calculated and experimental results are in agreement. Such adjustments are limited in that the observed frequencies and any available thermodynamic data are reproduced to within the experimental error. Also the magnitude of these force constants and interaction force constants are constrained to certain "common sense" limits. The ability to reproduce the experimentally obtained f_c by the calculation, depends essentially on the adequacy of SCM, however, this model has proven to be quite successful in a variety of molecular systems. The application of VPIE based on SCM has led to a great deal of insight into condensed phase molecular forces. For example, the utilization of VPIE/SCM has led to the discovery of hindered rotation in methane,[3] nitrous oxide[4] and ethylene,[5] the hindered rotation about the C-C bond in ethane upon condensation,[6]

and molecular association in methyl acetylene[7] and nitric oxide.[8] SCM has also been modified and used to take into account cell occupancies by more than one molecule in the VPIE analysis of nitrous oxide[9] and carbon dioxide.[10,11]

Ic. Previous Investigations on CHF_3

Based on low temperature distillations by Borodinsky, et. al.,[12] it was found that CHF_3 exhibited an inverse VPIE ($P(^{13}CHF_3) > P(^{12}CHF_3)$) over the entire liquid region studied. The interesting result, however, was the slope of the $T \ln(f_c/f_g)$ vs $1/T$ plot. This is the first known occurrence of such a plot with a negative slope in the inverse region. Their analysis indicates a liquid force field with large external diagonal and external-internal interaction force constants. Their results and analysis were explained in terms of the large blue shift upon condensation of the C-H(ν_1) stretch.[13-15] Normally a red shift in vibrational frequency is found to occur upon condensation due to the "loosening" of the particular bond in question via delocalization of electron density from the bond to the external field. The anomaly here is that the shift in the C-H stretching frequency is positive and quite large ($\nu_1(g) = 3030 \rightarrow \nu_1(\ell) = 3062$). This fact has been postulated by Borodinsky and co-workers to be possibly due to some form of association between CHF_3 molecules.

Justification for such an interaction can be found in the literature. In 1961 Buckingham and Raab[16] postulated a loose antiparallel dimer configuration for gaseous CHF_3 based on dielectric constant measurements at 80°C and 160°C. More recent investigations[17,18] using far infrared and microwave spectroscopy on liquid CHF_3 indicate high

levels of alignment or local organization of CHF_3 molecules. A theoretical basis for such interactions has also been done[19] using CNDO/2 quantum mechanical calculations. Their results indicate a dimer in a linear C-H···F-C type interaction with a stabilization energy of 0.6 kcal/mole-dimer. An interaction of this magnitude tends to support the Buckingham and Raab analysis of association even in the gas phase. Further theoretical work by Kollman and co-workers[20] using ab-initio calculations indicate the ability of CHF_3 to form complexes with strong bases. Experimental verification of Kollman's work was done by cryo-spectroscopic studies[21] on CHF_3 - Me_3N solutions in liquid argon and krypton. Solutions 10^{-3} - 10^{-6} molar in CHF_3 and Me_3N were studied at temperature of 90°K - 160°K. Experimental stabilization energies of 3.5 kcal/mole-complex were reported.

As a preliminary study this author performed a detailed ab-initio calculation on a number of possible CHF_3 dimer configurations (Appendix A). It was found that two configurations provide stabilization energies on the order of 0.7 kcal/mole-dimer and that the interaction can be considered hydrogen-bonding in nature. Normal coordinate analysis of models of these hydrogen bonded system (Sec.VI.e) indicate a blue shift in the C-H stretching frequency upon formation of a hydrogen bond with fluorine. Infrared spectra of the ν_1 manifold of gaseous CHF, taken at 500°K, 300°K and 200°K and at pressure (25-50 torr), have shown that no frequency shift occurs in ν_1 as the temperature of the gas is changed from 500°K to 200°K within the resolution of the instrument, ± 1 cm^{-1}. Also no discernable peak, which might have indicated a significant concentration of the dimer, was found. This was expected due to the low concentrations of dimer. The low concentrations are predictable from

calculations based on the quantum mechanical and normal coordinate calculations at the pressures used to provide sufficient spectral resolution (Appendix B). To shed additional light on this subject the VPIE for CHF_3 has been studied.

Id. Outline of the Investigation

To obtain VPIE data on CHF_3 two techniques are available: (1) distillation and (2) differential manometry. The experimental requirements and precision of the two methods are markedly different. Requirements for distillation with respect to isotopic enrichment, chemical purity and temperature/pressure measurement and control are quite modest. On the other hand, differential manometry requires highly isotopically enriched (90% +) and chemically pure ($\sim$ 99.999%) samples. Temperature/pressure measurement and control require sophisticated equipment. The results obtained from differential manometry are, however, generally at least an order of magnitude more precise than that obtained from distillation studies. In order to obtain a quantitative understanding of this problem, it was decided that differential manometry would be the appropriate technique. Therefore, this investigation can be broken down to the following aspects:

1. construction of a low temperature thermostat and a differential manometry system with associated vacuum systems (Section II),

2. the design and implementation of an appropriate temperature/pressure measurement and control systems (Section III),

3. preparation of highly enriched ^{13}C and deuterium samples with total impurity levels of less than 50 ppm (Section IV),

4. measurement of VPIE for $^{13}CHF_3/^{12}CHF_3$ and $^{12}CDF_3/^{12}CHF_3$

systems (Section V), and

5. the analysis of experimental VPIE data in light of the existing experimental and theoretical information on CHF_3 (Section VI).

II. EXPERIMENTAL APPARATUS

The design of most low temperature thermostats is based upon the principles of the low temperature calorimeter of Eucken[22] and Nernst[23] developed in the early nineteen hundreds. The device consisted of a sample cell suspended in an evacuated chamber which was placed in a Dewar flask. This simple design provided sufficient thermal isolation to allow for reasonably accurate heat capacity measurements. The major drawback was that heat transfer by radiation had to be taken into account. The first major improvement of the Eucken/Nernst design was implemented by Gibson and Giauque[24] in which they made use of an adiabatic shield around the sample holder. By maintaining the temperature of this shield near that of the sample holder, heat radiation effects were minimized. Further improvements by Giauque and Egan[25] involved passage of heater, sensor wires and sample lines through large heat sinks, situated above the sample holder-lower shield assembly, to minimize heat leaks along these lines from the outside. Radiation effects were further minimized by Johnston and co-workers.[26] The heat sinks and the outermost container were supplied with heaters and thermal sensors and their temperatures maintained near that of the sample cell. The Johnston type cryostat has been applied successfully to isotopic vapor pressure measurements[27] and in 1968 Bigeleisen, Brooks, Ishida, and Ribnikar (BBIR) implemented major improvements on the Johnston design for precision isotopic vapor pressure measurements over a

temperature range of 2 - 300°K with long term thermal stabilities of the order of 10^{-3} degrees. The cryostat constructed to study vapor pressure isotope effects of fluoroform is of the BBIR design. Modifications have been implemented to improve thermal stability, facilitate assembly and repair processes as well as the ease of overall operation. The following aspects of the cryostat will be discussed:

1. cryostat design and function (Section IIa),
2. associated supporting vacuum systems (Section IIb),
3. temperature and pressure measurement and control design - description and specification (Section IIIa),
4. overall control design - analog and digital interface (Section IIIb), and
5. operation and control logic (Section IIIc).

IIa. Cryostat Design and Function

In this section the general design and function of the various sub-assemblies of the modified BBIR cryostat will be described. Detailed specifications concerning individual components and the assembly process can be found in the engineering drawings (Brookhaven National Laboratories - Job #561A: Vapor Pressure Cryostat, 11/65).

A simplified schematic of the assembled cryostat is shown in Figure 1. From this diagram the positioning and interconnections of the various cryostat components can be seen.

The heart of the cryostat is the sample holder (SH), which is shown in Figure 2. The SH is a cylinder of high purity copper (99.9999%) in which four symmetrically placed ports have been drilled out. It is in these ports ($\sim$ 0.6 cm^3 per port) that the isotopic samples reside. The high purity copper is required so as to assure the necessary degree of thermal uniformity between the four sample ports. To insure good thermal contact between the cell walls and the isotopic sample, the lower third of each port was packed with fine platinum mesh. This copper cylinder is concentrically positioned by means of four radial copper fins inside a copper cup and the space between the two cylinders is lead filled so as to increase the overall heat capacity. The copper cup is wound uniformly with Teflon coated constantan wire, which acts as a heater. The winding of the heating wire as in all other components is bifilar. The bifilar winding is necessary so as to not produce any induced magnetic fields which could affect the physical properties of the sample

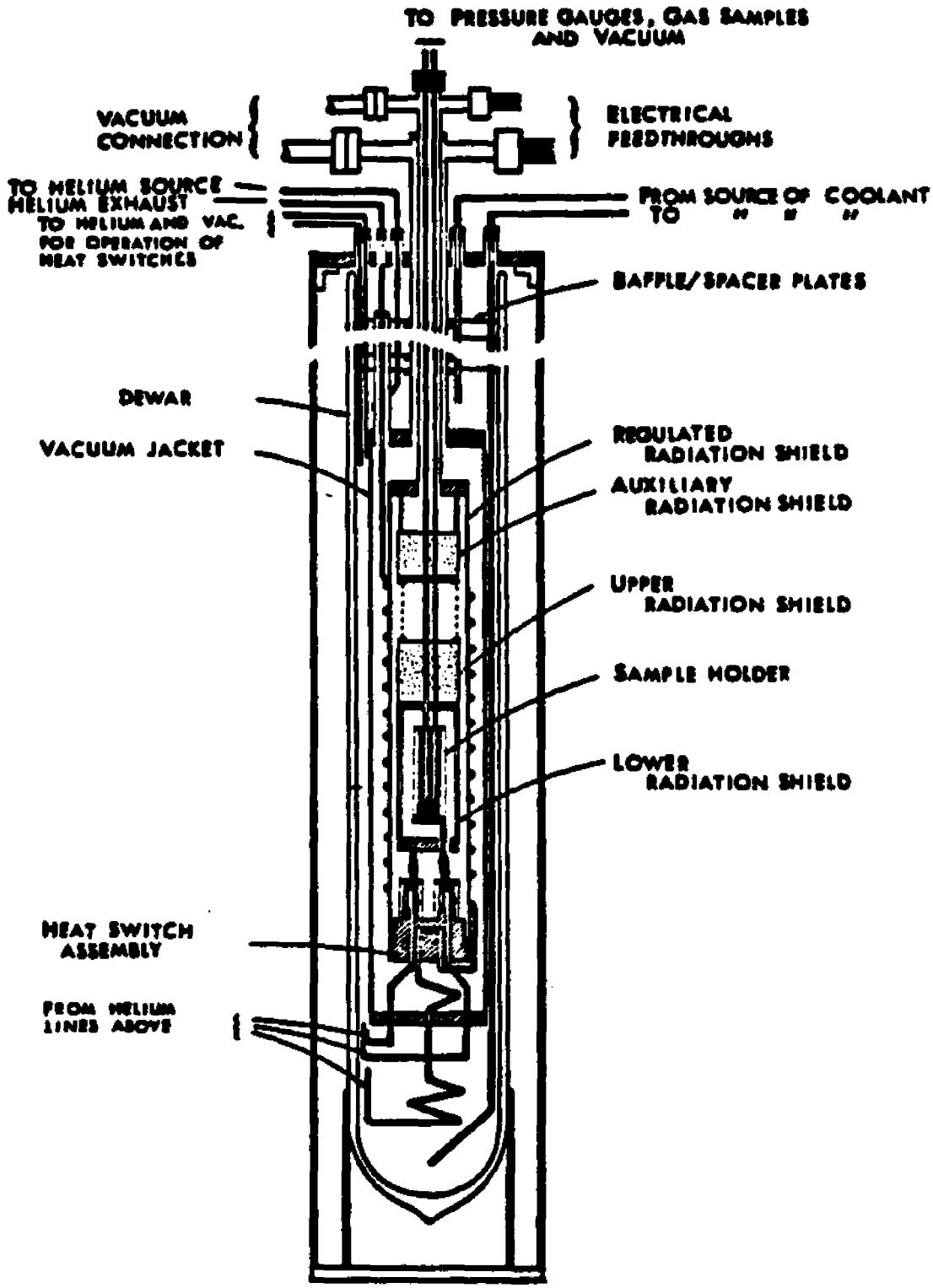

Figure 1. Assembly Drawing of the Cryostat

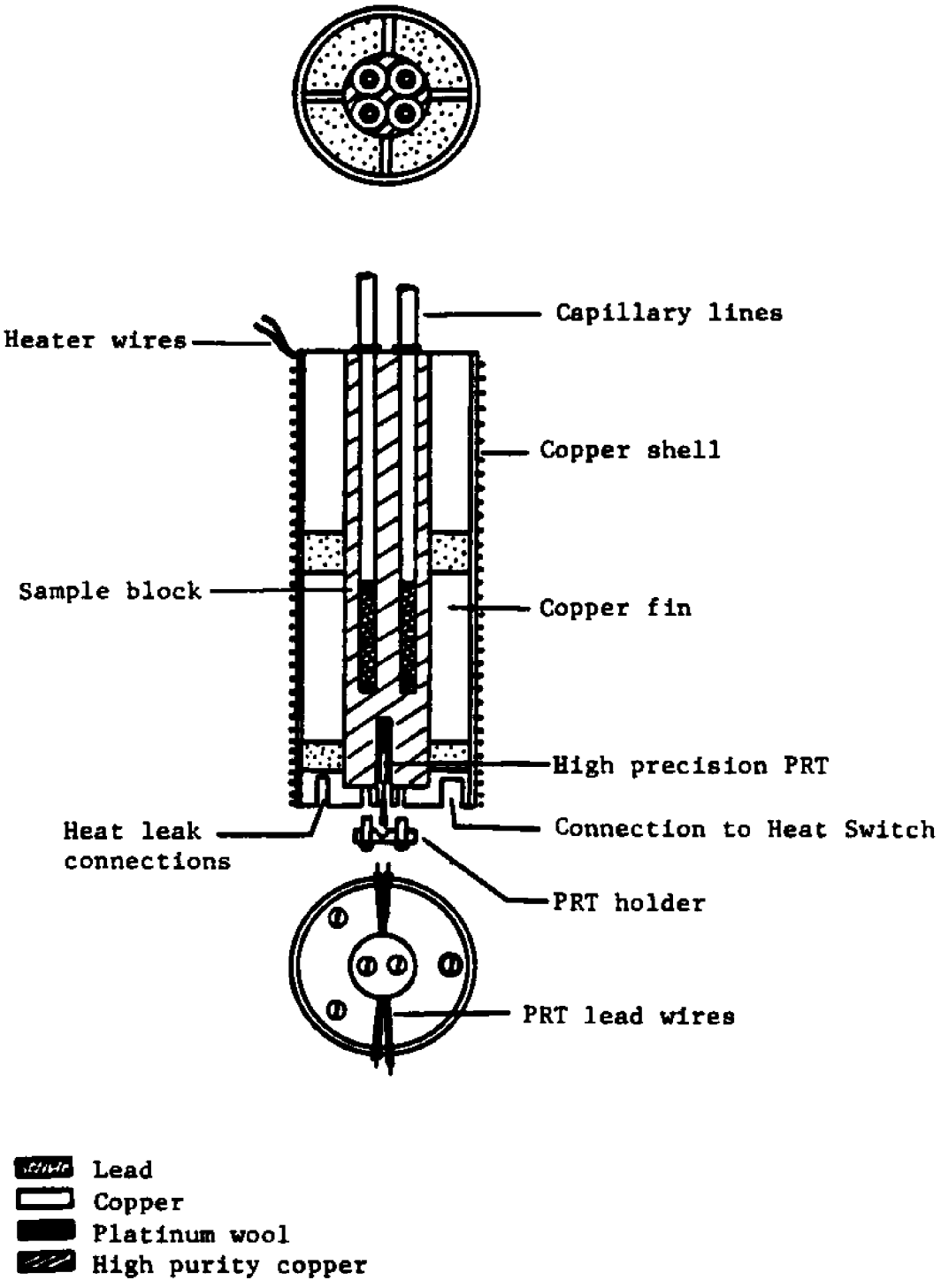

Figure 2. Sample Holder

(alignment-orientation effects). Drilled into the bottom of the SH are four additional holes. The one at the center penetrates into the bottom part of the high purity copper cylinder and is the receptacle for a resistance thermometer. The other three holes are shallow and tapped. Their function is to provide for thermal connections to another cryostat subassembly (Heat Switch). A thermocouple is positioned symmetrically with respect to the four ports on the top of the SH, and is physically in contact with the SH surface.

Silver-soldered to the SH are four thin walled stainless-steel tubes (Capillary Lines-CL) for the transfer of the samples to and from the sample holder. These lines run up the entire length of the cryostat to a vacuum feedthrough and connect into the sample handling system and pressure measurement devices.

In the original design the feedthrough is a set of four O-ring fittings mounted on a flange. The weight of the SH assembly is supported in the BBIR design by the press-fit of the four O-ring seals. This design has been modified (Figure 3) as follows: the four tubes were silver-soldered into a collar which was then passed through an o-ring connector mounted on a flange. This eliminates three possible sources of leak. This collar is threaded which allows the weight of the SH assembly to be supported by locking nuts and a stand-off collar. Thus the vacuum seal cannot be effected by the SH assembly weight or shift in position.

Due to the large temperature gradients which exist along the CL, condensation of the sample in the tubes rather than in the SH is a problem. In order to monitor and rectify such parasitic condensation, two thermocouples and constantan wire heaters were installed on the CL.

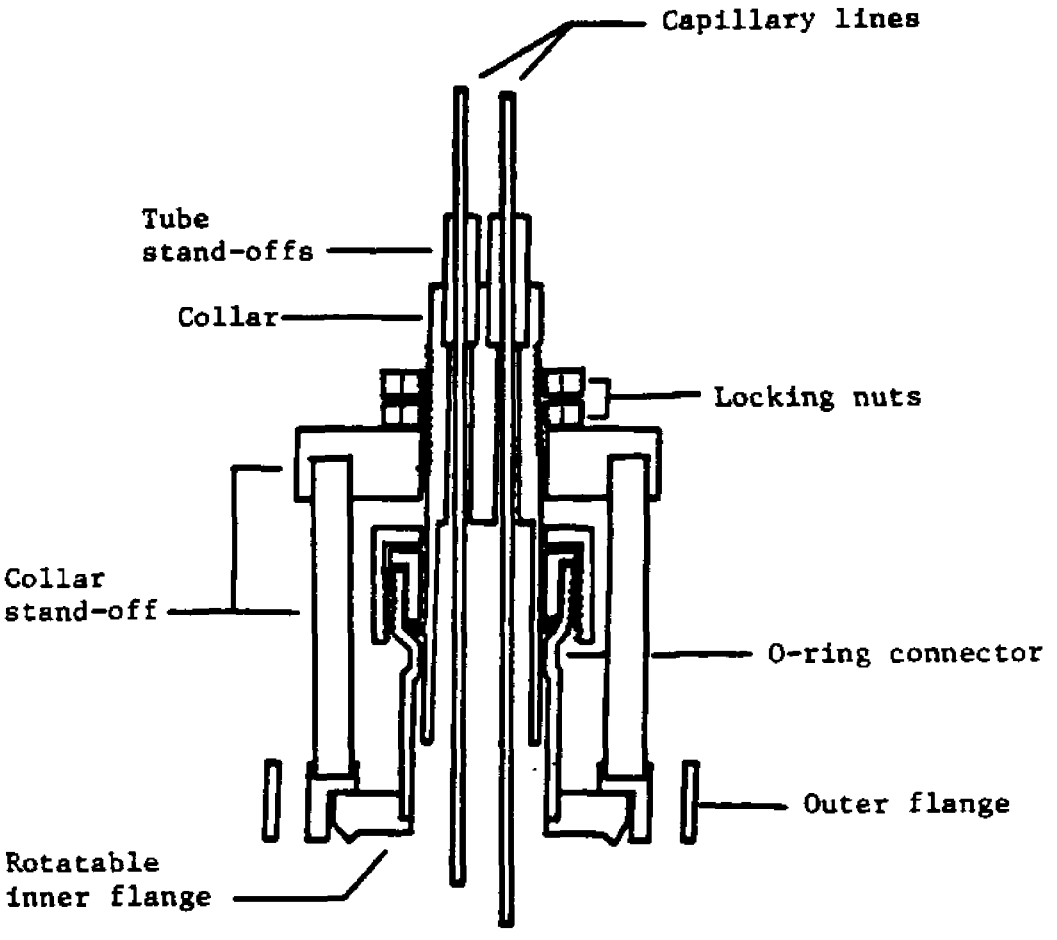

Figure 3. Capillary Line Feedthrough

The SH and CL assemblies are the only part of the cryostat to be in contact with the samples. The function of all other components is one of temperature control. Surrounding the SH is the Lower Radiation Shield (LRS), Figure 4. The LRS is a copper cup filled with lead wound with a constantan wire heater and supplied with a resistance thermometer and a thermocouple. The space between the SH and LRS is evacuated. The LRS is an adiabatic shield for minimizing thermal radiation effects. Directly above the SH and suspended from the LRS is the Upper Radiation Shield (URS), Figure 5. The URS is a lead-filled copper cup with holes drilled through to allow passage of the CL and electrical wiring. Its function is to minimize radiation effects from the upper regions of the cryostat as well as to buffer the SH from any heat transfer along the CL. Above the URS is the Auxiliary Radiation Shield. Its function is identical to that of the URS, though it is slightly smaller than the URS. The LRS and URS are hung from the ARS by No. 30 gauge stainless steel wires so as to provide thermal isolation from the ARS and the upper cryostat assemblies. The ARS itself is supported from the innermost flange (cf: Figure 6) by four threaded brass rods.

Located below the LRS is the Heat Switch (HS) Assembly, Figure 7. The HS is a major feature of the BBIR cryostat. This assembly consists of a set of bellows operated thermal switches, which allow for independent cooling of the LRS and SH. The HS is constantly cooled by the cryogenic liquid which circulates through its base. Pressurizing the bellows with helium gas expands the bellows making contact with a plate directly above, which connects to its respective component (LRS or SH). Evacuating the bellows breaks the thermal contact. Due to the small cross-sectional area of the bellows wall, heat transfer, from the bellows

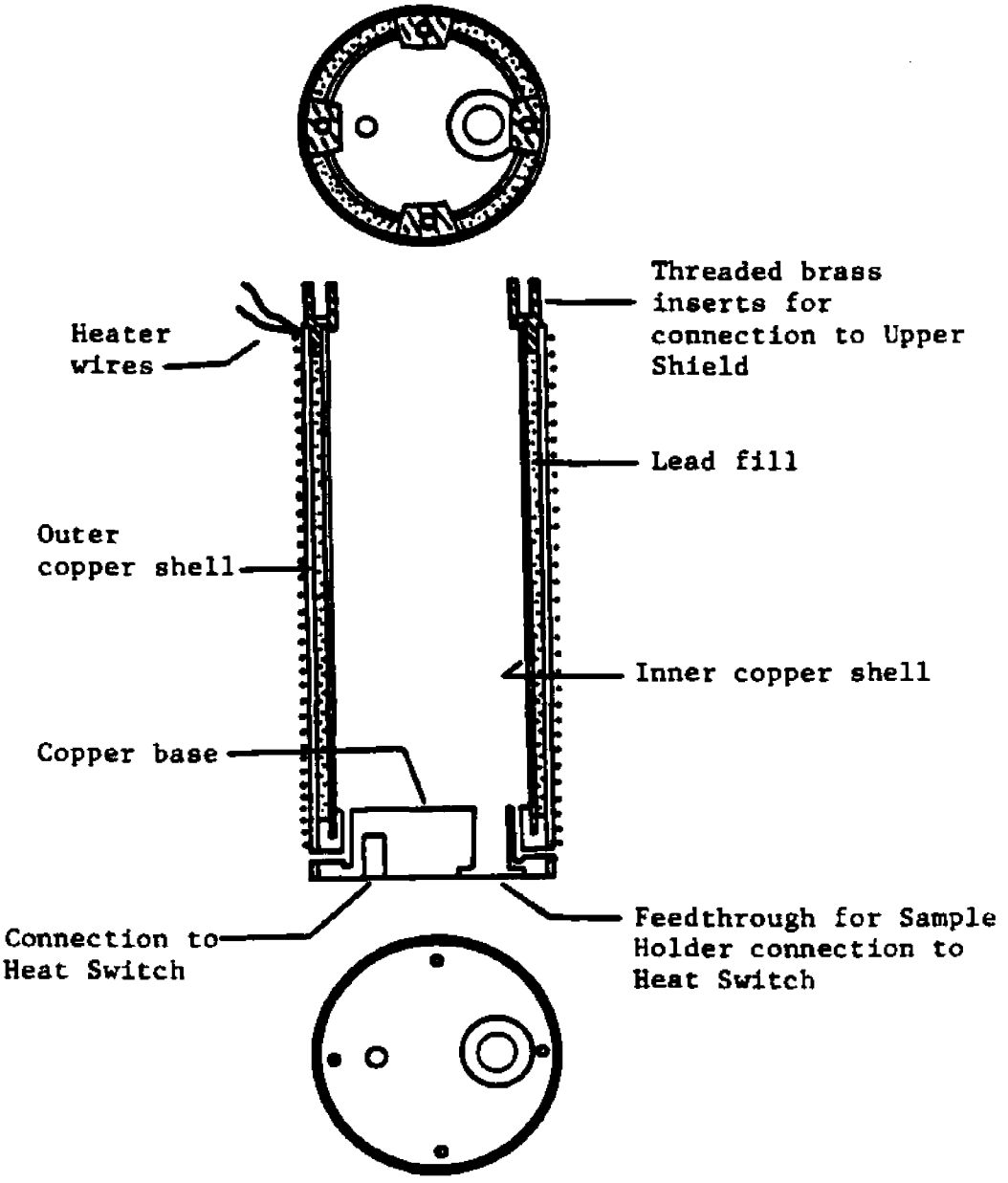

Figure 4. Lower Radiation Shield

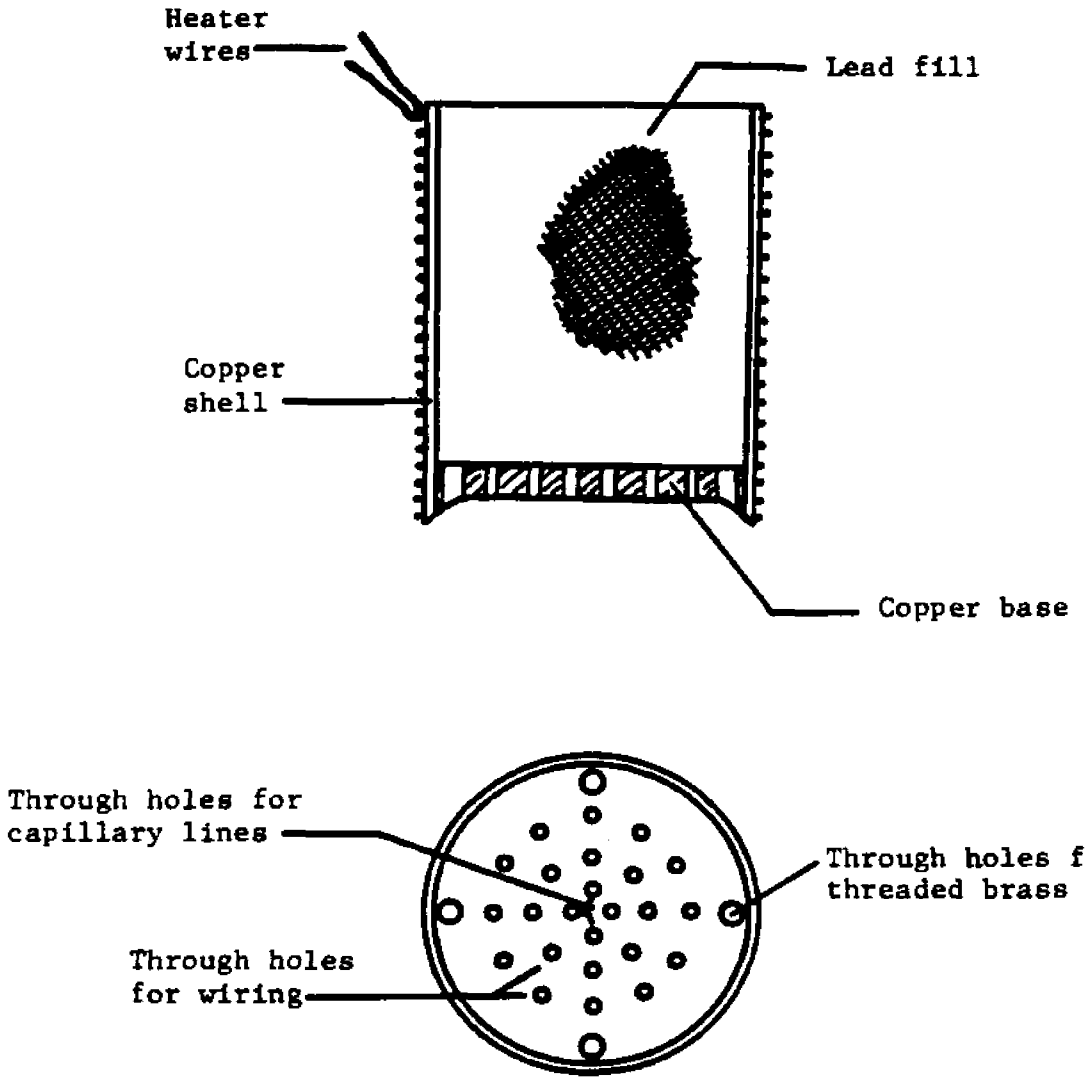

Figure 5. Upper Radiation Shield

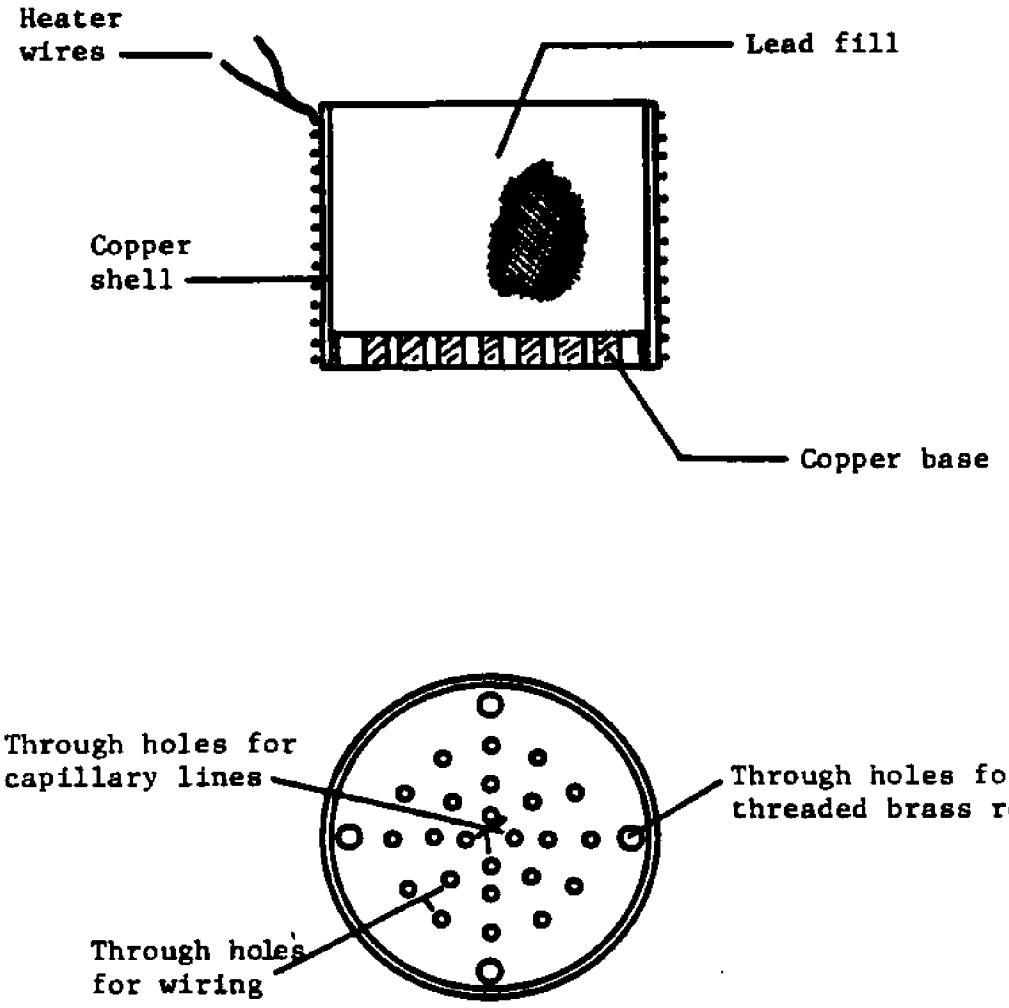

Figure 6. Auxiliary Radiation Shield

cap to the HS base, has had to be augmented by copper braids. The gold-plated contact plate on each heat switch is thermally isolated from the other. The connection between the sample holder contact plate and the sample holder base is fed through the bottom of the LRS, and the feed-through rod is thermally isolated from the LRS by means of a Teflon bushing.

Several modifications on the BBIR design of the heat switch have been incorporated: The pure nickel bellows, purchased from Servo-Meter, Inc., has been electron-beam welded to the copper upper and lower cups rather than being braised onto them. The bottom cups have been screwed down to the HS base and are then sealed with low-melting silver-solder, rather than being directly soldered to the HS base. The higher heat transfer rate between the upper and lower cups, while maintaining a reasonable flexibility of the braid connections, has been obtained by shortening the braids and letting them go through a bending motion rather than forcing them to do a stretching motion. For this purpose secondary caps have been braised onto each primary cap, and three copper braid support posts have been added to each switch.

Mating to the HS base and inner flange is the Regulated Radiation Shield (RRS), Figure 8. The SH, LRS, URS, ARS and HS assemblies are contained within the RRS. The outside of the RRS has a coil of copper tubing soft-soldered along its entire length. The lower end of the coil is connected to the coolant exit port on the HS base. The other end of the coil passes out through a vacuum feedthrough at the top of the cryostat assembly to a manifold for controlled pulling of coolant through the HS base and RRS coil. The RRS is also supplied with its own constantan wire heater, resistance thermometer and thermocouple.

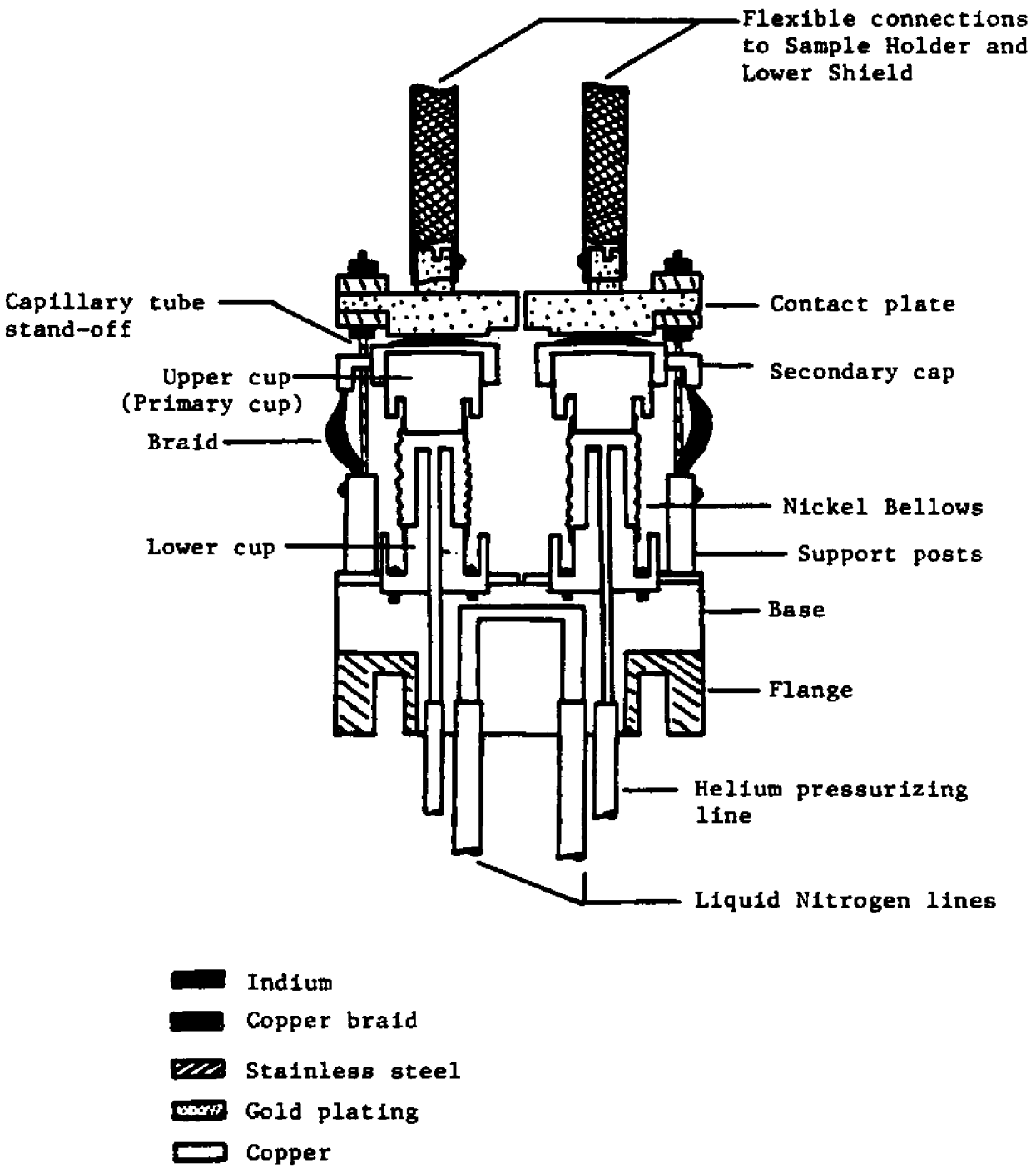

Figure 7. Heat Switch

The combination of cooling coil and heater allows for temperature control over a range determined at the low end by the cryogenic fluid temperature to ∿ 300°K at the high end. Thus the immediate environment (RRS) of the inner components (SH, LRS, URS, ARS) can be continually adjusted to the temperature of interest. This feature accounts, in part, for the excellent temperature controllability over a large temperature range.

Surrounding the RRS is another container (Outer Can, OC), Figure 9. The space between the OC and RRS, as is the space between the RRS and inner assemblies, is evacuated. The top of the OC is flanged to the outer flange. The bottom of the outer can has three vacuum feedthroughs; two for the helium gas supply lines for pressuring two HS bellows, and one for siphoning LN_2 from the pool of cryogenic fluid in the cryostat dewar through the HS-base and the RRS-cooling coil. The modification incorporated here is the jacketing of the vacuum feedthrough tubes on the OC base rather than direct soldering of the feedthrough tube to the OC-base. This allows for an easier disassembly and re-assembly process.

The assembly of all parts described so far hangs from the main flange by a 1 1/2 inch stainless steel tube through which passes the electrical wires for the RRS and the inner tube. A connection of the space between the OC and RRS to the vacuum system is made via this 1 1/2 inch tubing. The inner tube is welded to the 1 1/2 inch tube at the upper end. It contains the CL and the electrical wires for the assemblies within the RRS, and allows for the evacuation of the space inside the RRS. Coolant inlet, outlet and siphon tubes, heat switch helium gas lines and coolant level detector pass through the main flange via O-ring vacuum connectors. Wiring is fed out through high vacuum electrical ceramic feedthroughs, purchased from Perkin-Elmer/Ultek, Inc. Tube feedthroughs

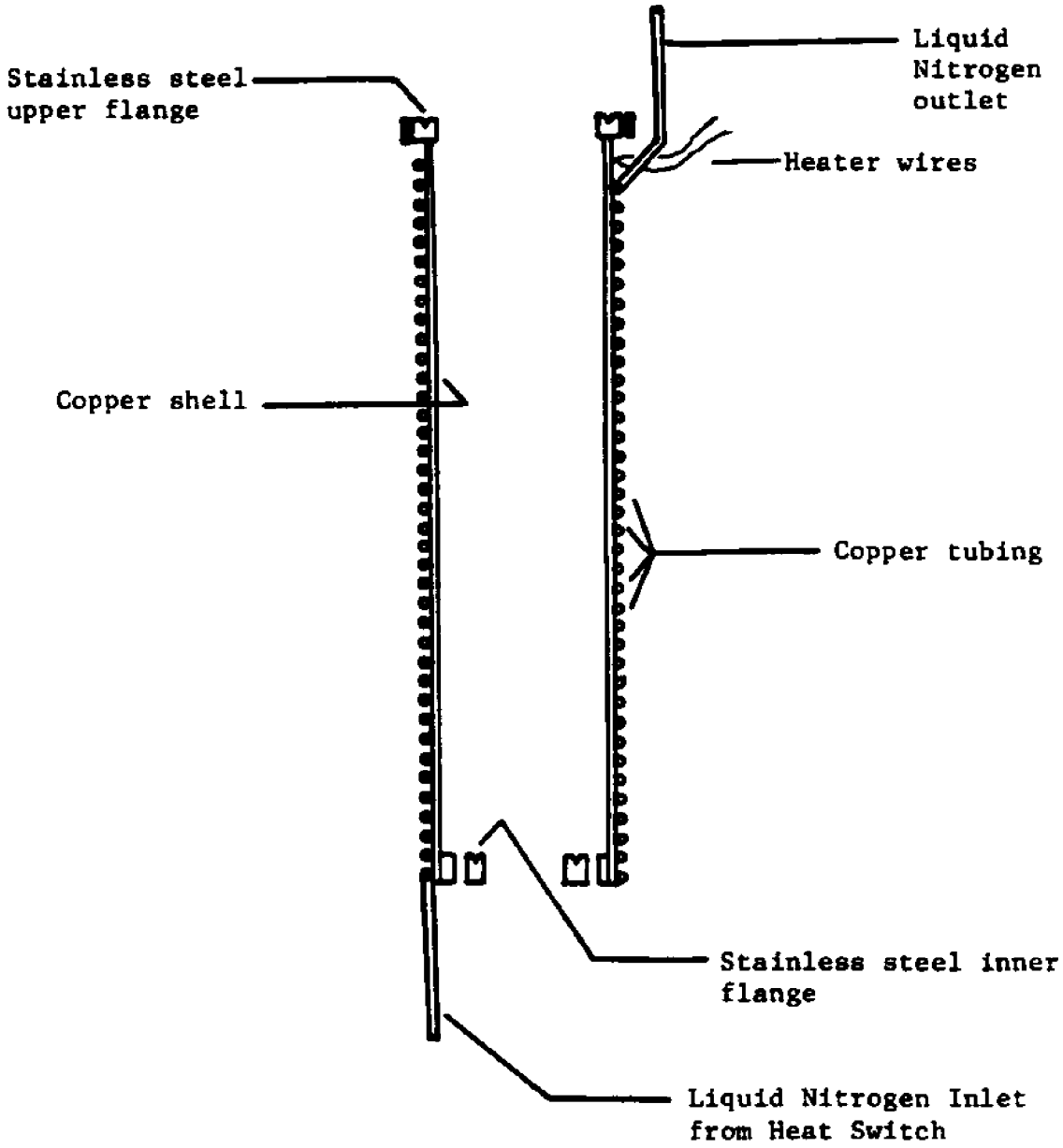

Figure 8. Regulated Radiation Shield

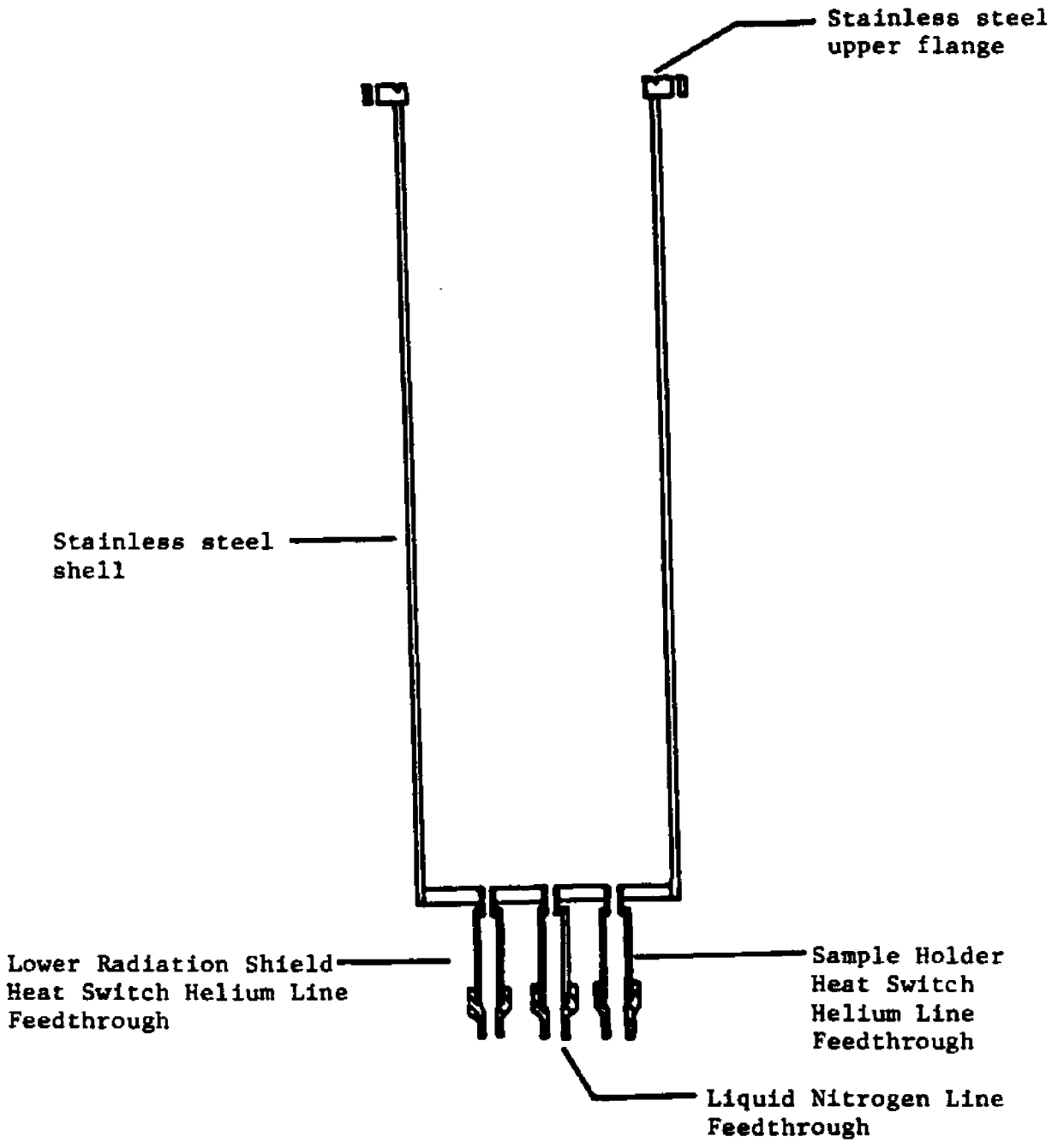

Figure 9. Outer Can

were used for thermocouple and resistance thermometer wires. Each wire is passed through its own capillary tube, which is electrically isolated from the other feedthrough tubes, and soft soldered in place, the wire insulation being removed only at the point of soldering. Solid pin feedthroughs were used for the heater wires. This entire assembly sits in a stainless steel dewar (Janis Model #RD-2185), which is suitable for cryogenic operation down to liquid helium temperature.

The flanges that may come in contact with the cryogenic temperature are sealed by means of hollow stainless steel O-rings coated with Teflon, purchased from Advance Products, Inc. These flanges are the seals between the HS and RRS, the RRS and the inner flange and the OC and outer flange.

IIb. Cryostat Vacuum Systems

Associated with the cryostat operation are three independent vacuum systems: The Sample Inlet System (SIS), Cryostat-Dewar System (CDS) and the Service Manifold (SM).

The SIS (Figure 10) is an all stainless-steel vacuum system with four independent manifolds servicing the four Sample Holder cells. These manifolds are themselves serviced by a common two inch, all stainless-steel, oil diffusion pumping station. The function of SIS is threefold:

1. introduction and storage of isotopic samples between runs,
2. transfer of isotopic samples to and from the sample holder, and
3. servicing the pressure measurement instrumentation.

Another two inch pumping station (CDS), Figure 11, is used to service the inner and outer vacuum regions of the cryostat as well as the vacuum jacket of the dewar. The operating pressures for both SIS and CDS is on the order of 10^{-7} torr. The third system (SM), Figure 12, has four functions:

1. pressurizing and evacuating the heat switch bellows,
2. controlled pulling of liquid nitrogen through the heat switch and regulated radiation shield,
3. siphoning out of liquid nitrogen from the dewar after the completion of a run, and
4. the introduction and removal of heat transfer gas to the inner and outer regions of the cryostat for initial cool down of cryostat

components.

The SM operating vacuum is on the order of 0.1 torr and is used in this purpose only for roughing out the large volumes of the cryostat and dewar vacuum jackets. SM connects into CDS for access to high vacuum.

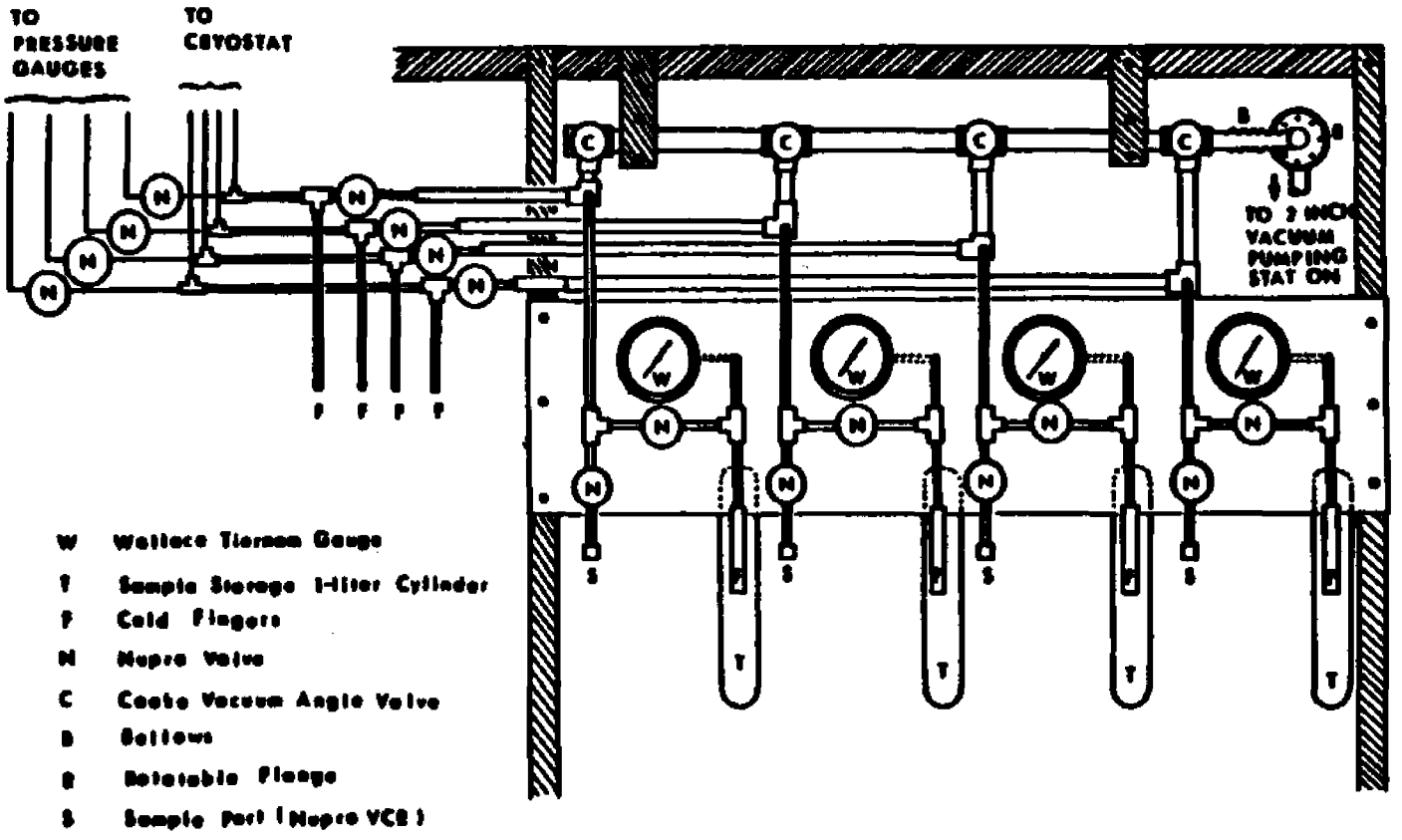

Figure 10. Sample Inlet System (SIS)

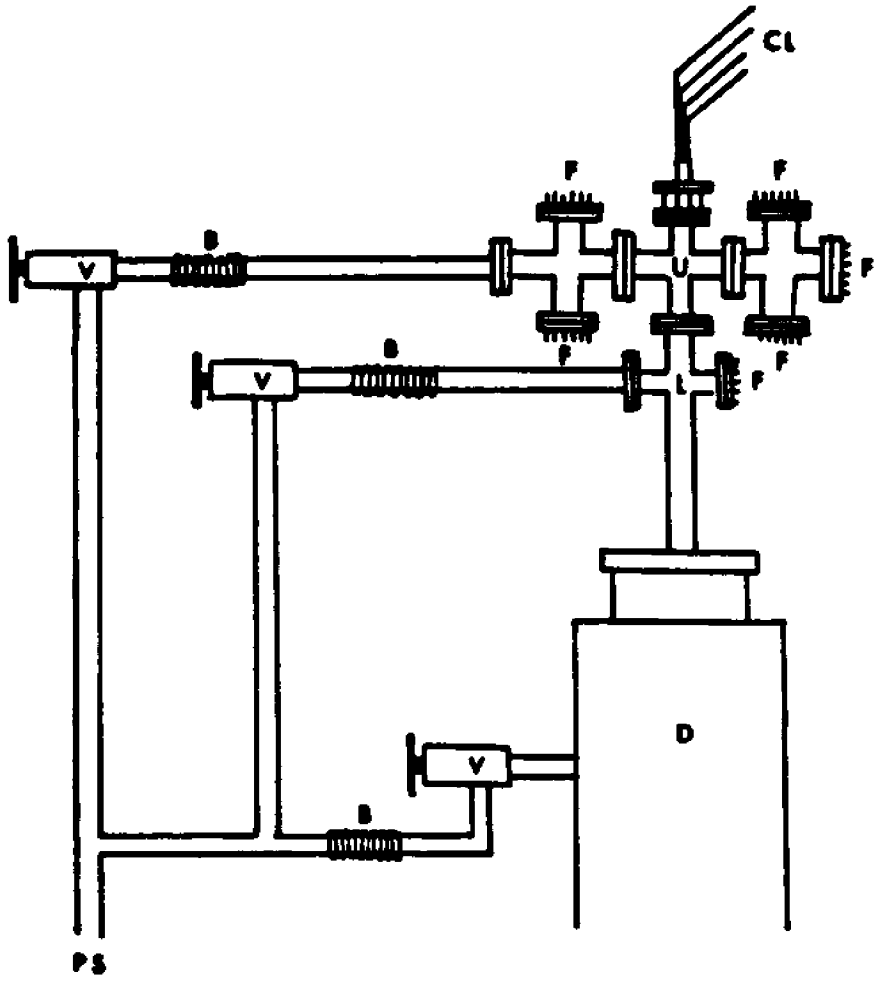

CL Capillary Lines
F High Vacuum Electrical Feedthroughs
V 3/4 inch Stainless Steel Bellows Valves
B 3/4 inch Bellows
U Upper Cross Assembly
L Lower Cross Assembly
D Cryostat Dewar
PS To a Stainless Steel Pumping Station

Figure 11. Cryostat-Dewar Vacuum System (CDS)

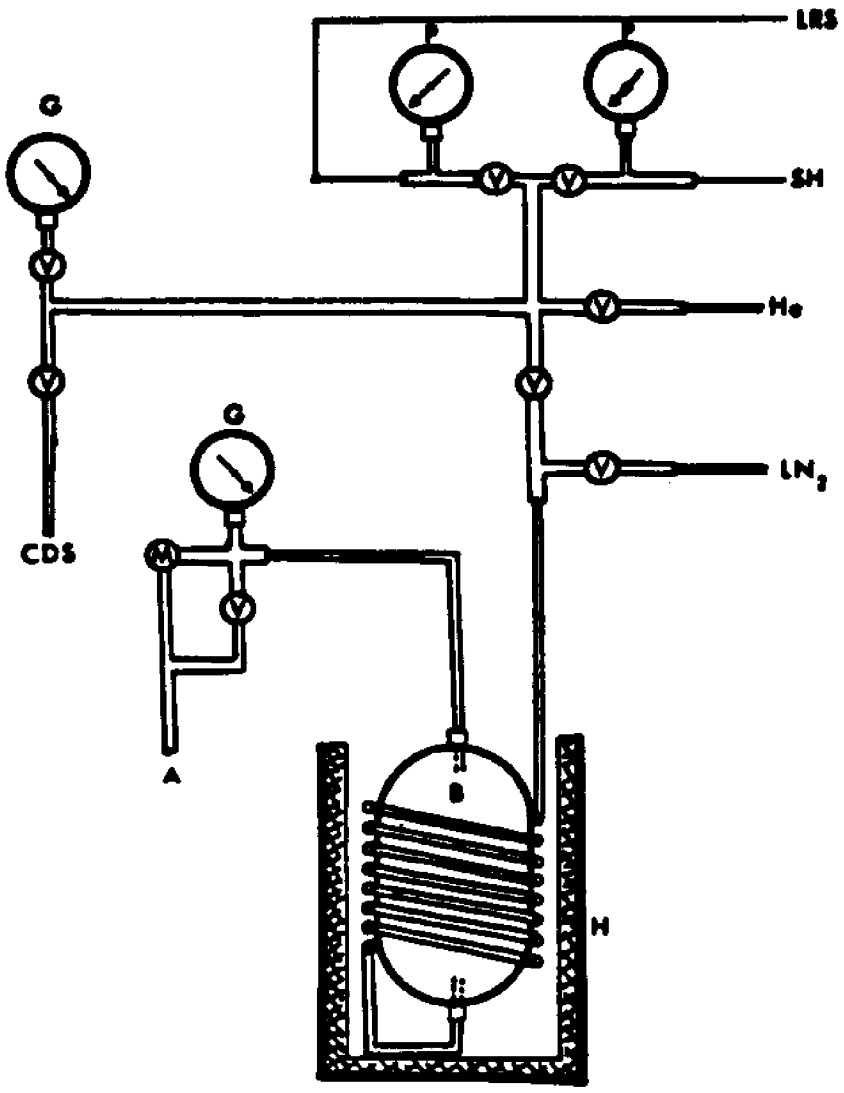

LRS Lower Radiation Shield-Heat Switch Helium Pressurizing Line
SH Sample Holder-Heat Switch Helium Pressurizing Line
P 0-30 inch vacuum/0-30 psi pressure gauge
G 0-30 inch vacuum gauge
He Helium gas inlet
LN_2 Connection to Cryostat Liquid Nitrogen Siphoning Line
V On/off valve
M Metering valve
B Ballast for warming up LN_2 Vapor
H Heating Mantle
A Connection to air pump

Figure 12. Service Manifold (SM)

III. TEMPERATURE/PRESSURE MEASUREMENT AND CONTROL SYSTEM

IIIa. Temperature/Pressure Measurement Sensors and Instrumentation

As previously indicated, each major cryostat assembly is supplied with two thermal sensors, i.e., a platinum resistance thermometer (PRT) and a copper-constantan thermocouple (TC). The PRTs used have resistance values of ∿ 100 ohms at 0°C and are all configured for four-wire resistance measurements to account for lead wire resistivity. Standard precision (± 0.05%) ceramic encased PRTs (Minco Model #S202) were placed on the RRS, ARS, URS and LRS, whereas a high precision (± 0.002%) gold encased-hermetically sealed PRT was inserted into the SH thermometer well (Minco Model #S1059). All PRT calibrations are traceable to the National Bureau of Standards. Each subassembly has one TC which acts essentially as a backup sensor. The capillary lines, CL, do not support any PRTs but are fitted with two TCs. These TCs are constructed of #30 gauge, Teflon coated, copper and constantan wire (Omega Engineering). These TCs were calibrated externally with respect to one of the Model S202 PRTs.

The calibration was done, in a thermostat specifically designed and constructed for this purpose (Figure 13), over a temperature range of -170°C to -50°C. The temperature control (± 0.05°C) for this calibration was achieved using a Scientific Systems Cryogenic Controller Model #3610A. The calibration results are summarized in Tables 1 and 2, which tabulate

the least-squares coefficients for the PRTs and TCs, respectively. The functional forms used for the least-squares fits are given in the footnotes of these tables. The four wire resistance measurements of the PRTs are readable to ± 0.001 ohm (Keithly Model 5900) which corresponds to ∿ ± 0.0025°C, whereas the TC voltages (Non Linear Systems MX-1) are read to ± 0.000001 V which in turn corresponds to ∿ ± 0.03°C.

The measurement of the absolute pressure and differential pressures are done using a spiral quartz gauge and three capacitance gauges, respectively.

The spiral quartz gauge (SQG) and its controller are manufactured by the Mensor Corp. The range of the SQG is 0 - 1500 torr with a resolution of ± 0.001% (± 0.015 torr). The SQG was calibrated in place using a Ruska Dead Weight Gauge Model #2460, courtesy of Dr. Jacob Bigeleisen. The dead weight gauge was calibrated by the National Bureau of Standards, Job #14662; 7/20/76. One hundred and fifty one calibration points were taken over the entire 1500 torr pressure range using atmospheric pressure as reference for both the SQG and Dead Weight Gauge. This data was then fit to several functional forms. The best fit was with a cubic polynomial. The calibration, however, is practically linear throughout a major part of the operating range of the gauge, each calibration point being within ± 0.01% of a linear relationship. Greater deviations occur at both extremes of the operating range, the deviations from the linear relationship increasing to 0.1%. The nonlinearity is accounted for by the cubic and quadratic terms in the best fit equation:

$$P = aQ^3 + bQ^2 + cQ \ , \qquad \text{II-(1)}$$

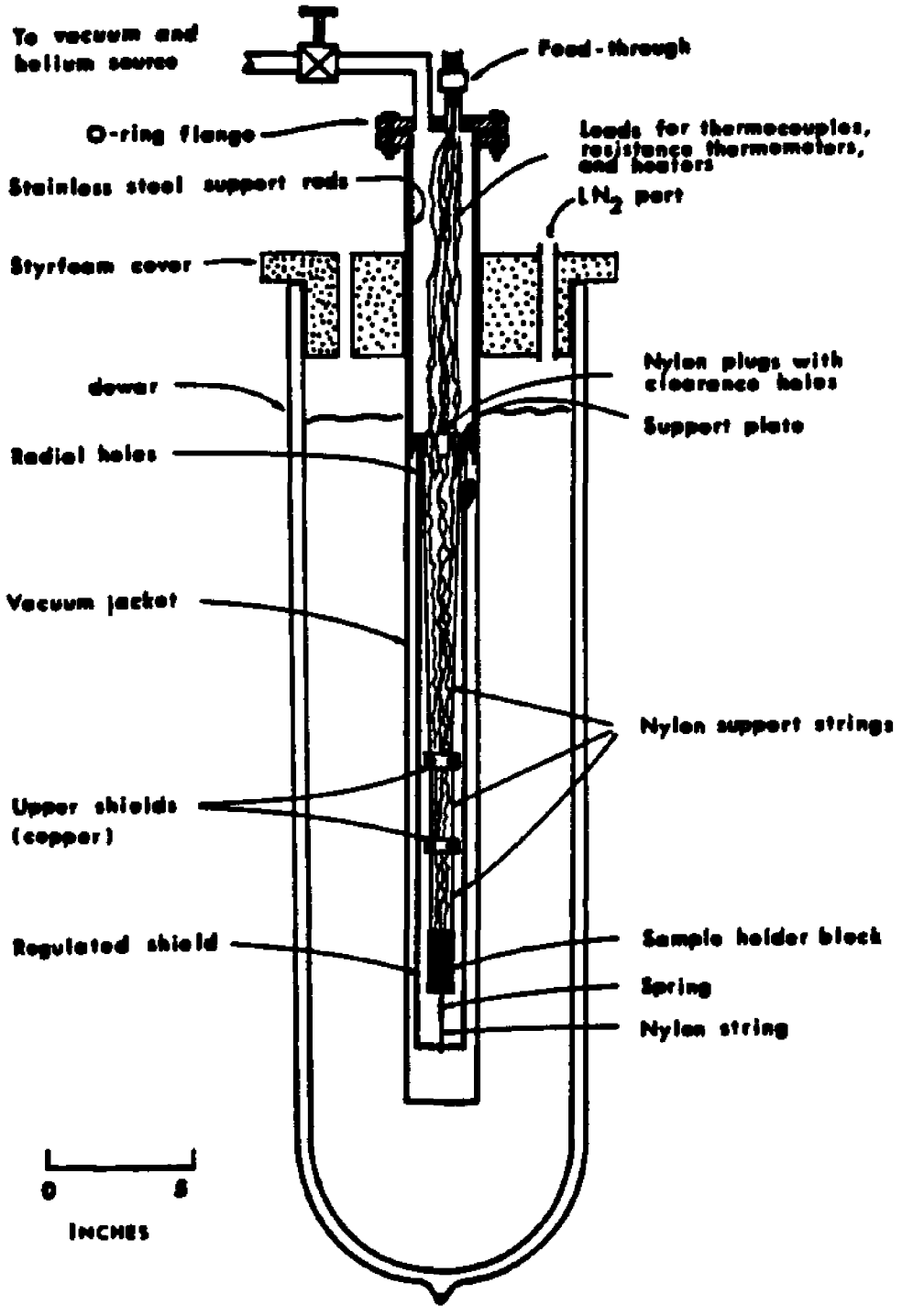

Figure 13. Thermocouple Calibration Thermostat

Table 1

Coefficients for the Temperature vs Resistance Fit for Cryostat PRTS[(a)]

PRT #	Location	a_1	a_2	a_3	a_4	a_5
Precision	Sample holder	3.3558	34.870	2.2008	0.0022642	-0.50296×10^{-5}
1	Lower Shield	2.8528	30.963	2.2742	0.0016939	-0.22344×10^{-5}
2	Upper Shield	3.6789	31.354	2.2489	0.0020573	-0.37857×10^{-5}
3	Regulated Shield	3.9408	30.803	2.2471	0.0021929	-0.41826×10^{-5}
5	Auxiliary Shield	3.8118	31.434	2.2452	0.0021355	-0.41016×10^{-5}

(a) Precision of the five-term fit is +/- 0.0002% for all PRTs. The functional form used is:

$$T = \frac{a_1}{R} + a_2 + a_3 R + a_4 R^2 + a_5 R^3 \quad ,$$

where T is in degrees Kelvin and R is in ohms.

Table 2

Coefficients for the Temperature vs Voltage Fit for Cryostat Thermocouples[(a)]

Thermocouple #	Location	$a_1 x10^3$	$a_2 x10^2$	$a_3 x10^1$	a_4
1	Not Used	0.27229	0.34415	0.15011	0.25361
2	Not Used	0.27930	0.37737	0.26516	0.40930
3	Auxiliary Shield	0.28776	0.42583	0.46939	0.69291
4	Upper Shield	0.28893	0.42701	0.48976	0.73749
5	Used as a sensor for control in the minicryostat				
6	Lower Capillaries	0.29537	0.47817	0.59273	0.78990
7	Regulated Shield	0.28950	0.44148	0.49115	0.68631
8	Sample Holder	0.28716	0.40510	0.42251	0.67485
9	Upper Capillaries	0.29436	0.47624	0.58376	0.77014
10	Lower Shield	0.28625	0.39781	0.40049	0.65301

(a) Precision of the four term fit is +/- 0.2%. The functional form used is:

$$T(°C) = A_1 - A_2|V| + A_3|V|^2 - A_4|V|^3 \ ,$$

where T is in degrees Kelvin and V is in millivolts relative to the ice point.

where

$$a = -1.9256 \times 10^{-14}$$

$$b = 1.6857 \times 10^{-9}$$

$$c = 1.5235 \times 10^{-2} \quad ,$$

in which P is the absolute pressure in torr and Q is the SQG decade counter reading (nominally, 100,000 counts per 1500 torr). The SQG pressure is normally read off a 6-decade counter for maximum precision, however two electronic outputs are also supplied:

a. a servo signal which indicates the degree from null balance of the opto-electronic circuit. This signal is used to measure pressure fluctuations and has the same sensitivity as the decade reading.

b. a 0-100 mv DC signal proportional to the decade reading but with an overall sensitivity of ± 0.1 torr.

The servo signal plays a very important role in the vapor pressure measurements in that it provides an indication of the thermal stability of the sample holder. The level of thermal stability required for measurement of isotopic differences in vapor pressures can be determined from the Clausius-Claperyon equation where the assumptions of gas ideality and the negligibility of liquid volume have been applied,

$$\frac{\Delta P}{P} \cdot \frac{RT^2}{\Delta H_{vap}} = \Delta T \qquad \text{II-(2)}$$

For a typical isotope effect of 1%, $\frac{\Delta P}{P} \sim 0.01$, and a 1% precision in the measurement, the absolute magnitude of the pressure fluctuation, δP, must be limited to $\frac{\delta P}{P} \sim 0.0001$. For the CHF_3 system ($\Delta H_{vap} \sim 4 \times 10^3 \frac{cal}{mole}$) the

thermal stability required for such vapor pressure measurements at various temperatures and the measurable temperature fluctuations as determined from thermal and pressure sensors are shown in Table 3. The SQG monitors only the pressure of the reference channel, in this case the absolute pressure of the $^{12}CHF_3$ sample.

The measurement of the differential pressures of the other three samples with respect to the reference sample is done using three Datametrics Capacitance Gauges (Model #572). The Gauges measure pressure differentials over seven full scale ranges from 100 torr down to 0.1 torr with a full scale precision of ± 0.01% of each full scale range. The capacitance gauges are calibrated by the manufacturer (NBS traceable) and provided with 0 - 10 volts DC full scale output at the rated precision of ± 0.01%. The specifications for the temperature and pressure sensors are summarized in Table 4.

Table 3

Thermal Stabilities Required for CHF_3 VP Measurement[a]

T(°K)	P(torr)[b]	δT required($x10^{-3}$deg)[c]	δT_{PRT} ($x10^{-3}$deg)[d]	δT_{SQG} ($x10^{-3}$deg)[e]
143	16.5	1.0	2.5	9.3
165	132	1.4	2.5	1.5
191	751	1.8	2.5	0.36

a. ΔH_{vap} (CHF_3) = $4x10^3$ cal/mole @ the Boiling Point

b. From experimental data (Sec. V)

c. Allowable thermal fluctuation for measurement of a 1% VPIE with 1% precision

d. Sensitivity of PRT reading

e. As determined from the Clausius Claperyon eqn with P and T as shown and ΔP = 0.015 torr (the SQG sensitivity).

Table 4

Cryostat Temperature and Pressure Sensor Specifications

Sensor	Sensitivity	Precision	Readability
PRT (SH)	.4Ω/deg	±.002%	2.5×10^{-3}°C
PRT (LRS,URS,ARS,RRS)	.4Ω/deg	±05%	2.5×10^{-3}°C
TC	30μV/deg	±.2%	0.03°C
SQG	$\frac{1500 \text{ torr}}{100{,}000 \text{ counts}}$	±0.001%	0.015 torr
CG	10.000V/Range	±0.01%/Range	@ X1: 10^{-2} torr
			@ X.1: 10^{-3} torr
			@ X.01: 10^{-4} torr
			@ X.001: 10^{-5} torr

IIIb. Overall Control/Measurement Design

Shown in Figure 14 is a flow-diagram of the cryostat electronics interface scheme. This system provides for cryostat operation, that is, temperature and pressure measurement and control, under manual, automatic (computer controlled) or computer assisted modes. The interface scheme can be broken down into five essential aspects:

1. thermocouple interface,
2. pressure instrumentation interface,
3. platinum resistance thermometer interface,
4. heater interface, and
5. computer system.

IIIb.1. Thermocouple Interface

The seven cryostat thermocouples are provided with reference junctions maintained at the ice-point. The sensor lines then feed to a terminal board from which the sensors are hardwired to a 12 channel thermocouple selector switch and to the first seven channels of a 12 channel 12-bit analog-digital converter. The output of the selection switch feeds into a Non-Linear Systems MX-1 6 digit Digital Volt-Ohm Meter (DVOM).* The readability of the thermocouples manually on the DVOM is ± 0.000001 V or ∿ ± 0.03°C whereas the precision of the thermocouple data acquired via the 12 bit A/D converter is ± 5μV or ∿ ± 0.15°C.

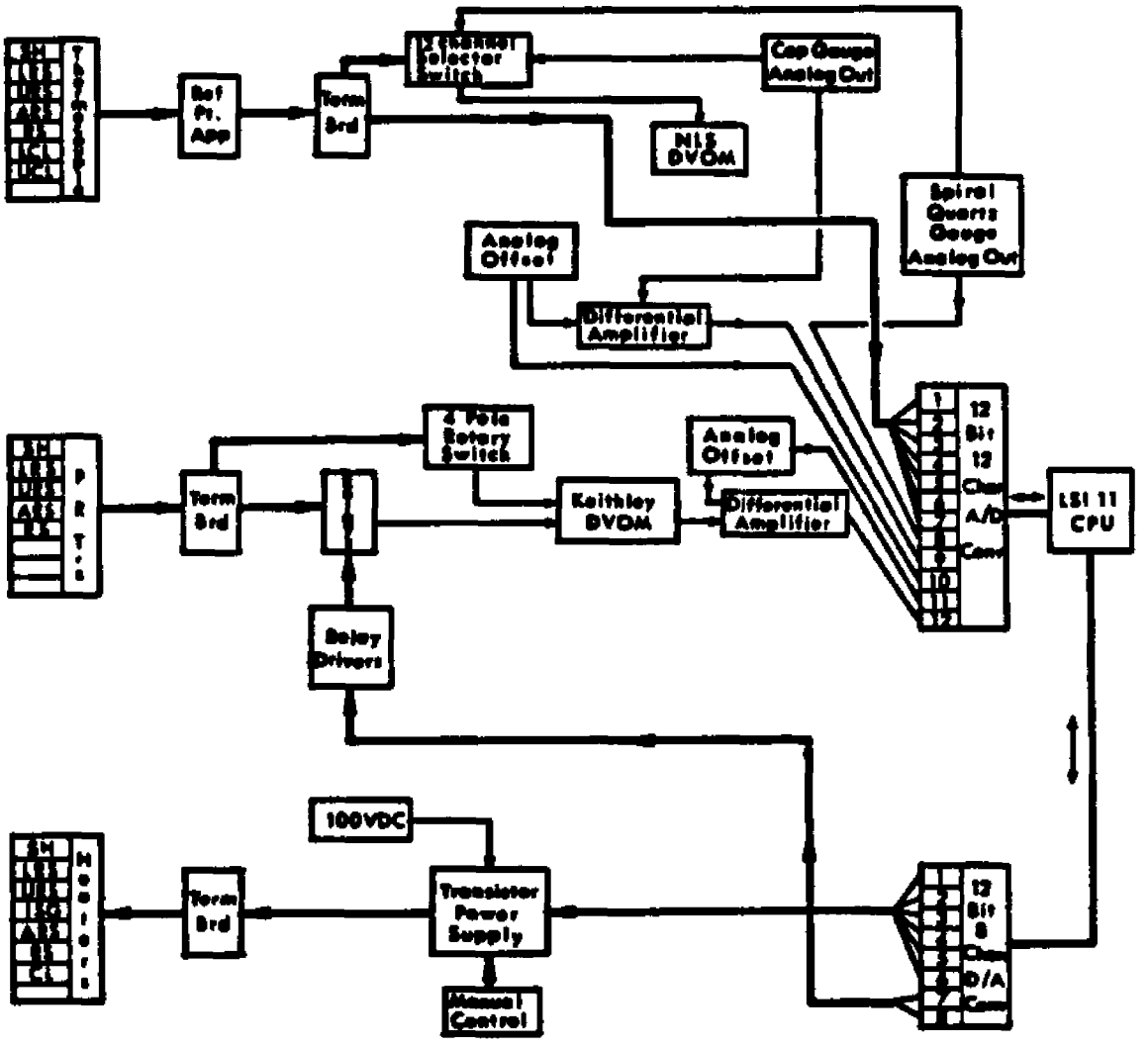

Figure 14. Cryostat Overall Electronics Interface Scheme

IIIb.2. Pressure Measurement Instrumentation Interface

Also connected to the 12 channel selector switch are the outputs of the spiral quartz gauge, capacitance gauge system and two Datel (Model #DVC8500) calibration voltage sources. Channels 8 and 9 of the A/D converter are connected to the SQG, and CG outputs, respectively. The capacitance gauge output is not the direct signal. The CG signal is fed through a differential amplifier which can be offset by a known voltage from the calibration source (Channel 10 of A/D converter).

By performing two 12 bit conversions, a conversion of 15 bit precision can be obtained as follows: For instance, to obtain a 15 bit A/D conversion of a value $X.ABCD_{10}$, an offset signal corresponding to the most significant digit X_{10} is applied to the unknown signal, the difference signal is amplified by a known gain of $\sim 10_{10}$, and a 12 bit conversion is taken. Separately, the offset signal X_{10} is converted, and this converted signal is added to the difference signal after the latter is scaled down by the value of the gain.

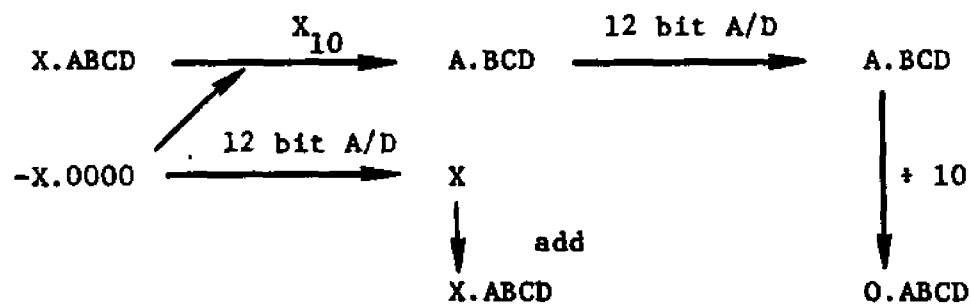

Thus in the manual mode the SQG signal is read directly off the decade counter for highest precision, i.e., ± 1 count or ± 0.015 torr. The readability of the SQG using the NLS DVOM is ± 10μV or ∿ ± 0.15 torr

IIIb.2. Pressure Measurement Instrumentation Interface

Also connected to the 12 channel selector switch are the outputs of the spiral quartz gauge, capacitance gauge system and two Datel (Model #DVC8500) calibration voltage sources. Channels 8 and 9 of the A/D converter are connected to the SQG, and CG outputs, respectively. The capacitance gauge output is not the direct signal. The CG signal is fed through a differential amplifier which can be offset by a known voltage from the calibration source (Channel 10 of A/D converter).

By performing two 12 bit conversions, a conversion of 15 bit precision can be obtained as follows: For instance, to obtain a 15 bit A/D conversion of a value $X.ABCD_{10}$, an offset signal corresponding to the most significant digit X_{10} is applied to the unknown signal, the difference signal is amplified by a known gain of $\sim 10_{10}$, and a 12 bit conversion is taken. Separately, the offset signal X_{10} is converted, and this converted signal is added to the difference signal after the latter is scaled down by the value of the gain.

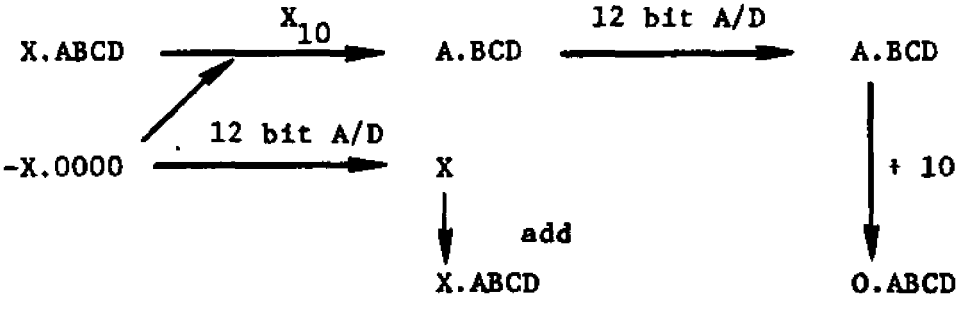

Thus in the manual mode the SQG signal is read directly off the decade counter for highest precision, i.e., ± 1 count or ± 0.015 torr. The readability of the SQG using the NLS DVOM is ± 10μV or ∿ ± 0.15 torr

and ± 25μV or ∿ ± .375 torr using the 12 bit A/D converter. The CG signal is readable on the DVOM to ± 0.1 mV or ± 0.01% of full scale and via the A/D converter to ± 0.25% and ± 0.03% of full scale for 12 bit and 15 bit precision, respectively.

IIIb.3. Platinum Resistance Thermometer Interface

Thermal measurements, with PRTs, are performed using four wires to account for lead wire effects. The PRT lines are fed to the cryostat terminal board and then to a switching circuit. The PRTs are hardwired to a 4 pole-6 throw Leeds and Northrup low resistance switch for manual selection and to a series of Magnetic Mercury-Wetted 2 pole-1 throw Reed Relays (2/PRT) for automatic selection of the PRTs. The four-wire connections are then fed into a Keithley Model 5900 6-digit DVOM for resistance measurements to ± 0.001 ohm (∿ ± 0.0025°C). Automatic selection requires the manual switch to be in the open setting. Automatic Selection of the PRTs is done by using the six available digital outputs of two-digital-analog converter channels (3 bits/channel) to selectively drive a transistor (GE-28 NPN Silicon) which in turn drives the appropriate set of relays. The Keithley DVOM provides a high precision analog output which along with the output from a calibration source is fed into a differential amplifier (Analog Devices J-52). The amplifier output is connected to channel 11 of the A/D convertor and the calibration source to channel 12. Automatic PRT readings correspond to ± 0.025 ohms (± 0.0625°C) and ± 0.0031 ohms (± 0.0075°C) for 12 bit and

15 bit conversions, respectively.

IIIb.4. Heater Interface

Each of the seven cryostat heaters are supplied with an independently controllable power supply. These power supplies are adjustable under manual as well as computer control. A schematic for a heater power supply is shown in Figure 15. It is built around a GE-251 NPN Silicon power transistor. Eight such transistors (seven active heaters and one spare) are connected in parallel to a single 100 VDC at 3.5 amps power supply. By controlling the voltage on the transistor base the voltage drop across the heater is also controlled. The seven base voltages for manual control of the seven heaters are supplied by seven ten turn pots with a common 5.7 VDC at 10 ma power supply. Automatic control is accomplished by using the output from the eight (six 12 bit precision and two 8 bit precision) independently controllable digital-analog converter channels. With appropriate heat sinking of the power transistors the circuit has been found to be reliable and stable even at maximum power settings.

IIIb.5. Computer Specifications

The computer used is a DEC-LSI-11 16 bit microprocessor with 28 K bytes of RAM. The system also supports a programable real time

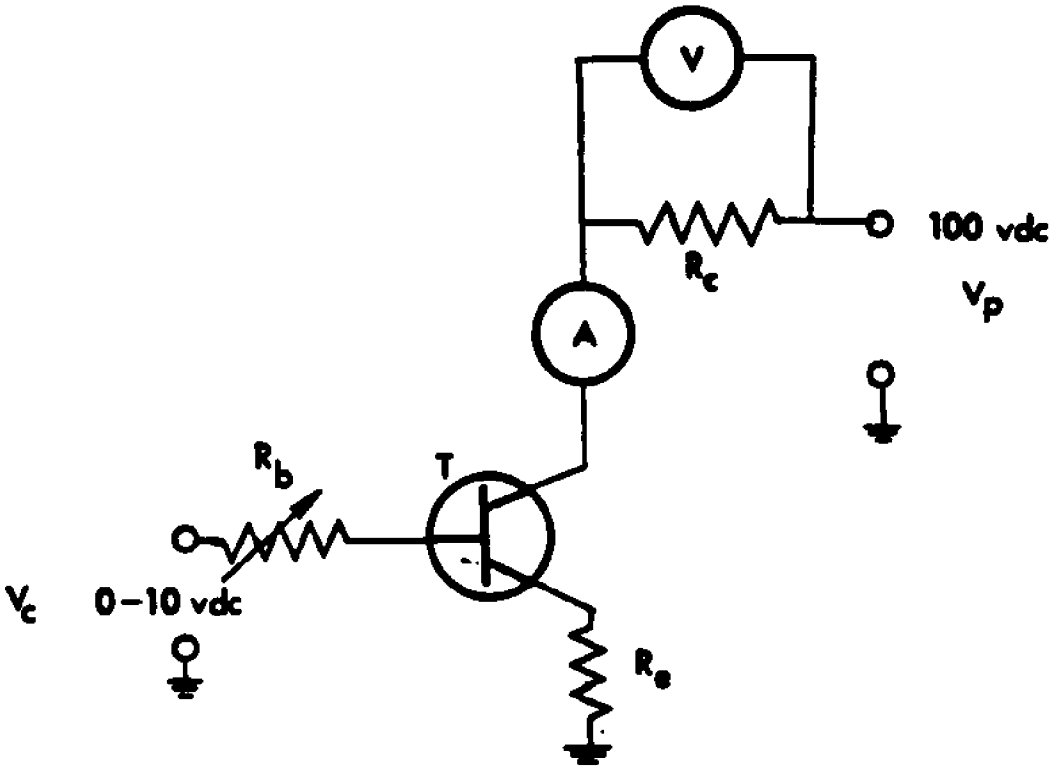

V	Voltmeter
A	Ammeter
R_c	Cryostat Heater
R_b	Base Resistor
R_e	Emiter Resistor
T	GE-251 NPN Transistor
V_p	100 VDC-3.5 Amp Regulated Power Supply
V_c	Control Voltage

Figure 15. Cryostat Heater Circuit

clock, a Data Translation 12 channel 12 bit analog-digital converter (with programable gain), Data Translation 8 channel 12 bit digital-analog converter and dual single density Shugart Floppy Disk drives (500 K bytes available soft storage). Software control of the computer and its associated hardware is accomplished under DEC's RT-11 operating system and RT-11 Fortran programing language. This software allows for interactive operation with the benefits (programing, calculation) of a high level language such as Fortran. RT-11 Fortran is a fully structured Fortran language exhibiting true usage of subroutines, overlays and libraries, as well as the individual memory access and manipulation of assembler languages.

IIIc. Cryostat Temperature Control and Operation

IIIc.1. Thermal Control Logic

The control and operation of the cryostat is a rather involved process, in that the absolute temperature of six independent assemblies, as well as various temperature differentials, must be controlled and maintained over extended periods of time. The operation of the cryostat can be broken down into three basic parts, i.e., sample introduction, initial point set-up and normal point to point operation. In order to introduce the samples, the inner assemblies of the cryostat are chilled down to below the normal freezing points of the samples. This is accomplished by siphoning LN_2 through the RRS coil and by the addition of helium gas to the inner vacuum jackets. Once a sufficiently low temperature has been reached, the transfer gas, helium, is removed and the jackets brought to high vacuum. Typically this procedure, starting from ambient temperature, requires approximately three hours. Heater current is then applied to all the cryostat heaters, except to that of the SH. The heat switch to the SH has been actuated and the temperatures of all components are raised to slightly above the normal freezing point. The gas samples are now condensed into the sample holder, the coldest inner assembly component. From this point on, the SH must always be colder than the other inner assemblies, so as not to cause parasitic condensation in the capillary lines. After the samples have been introduced into the SH, the entire system is brought to the

desired temperature range for the first reading. Shown in Table 5 are the various thermal differentials that must be maintained constantly throughout a reading.

All inner assemblies are kept at temperatures greater than that of the SH to avoid parasitic condensation. However, the RRS is kept colder than the SH so as to keep the heat switch near the LN_2 temperature and to provide for a heat leak environment which is necessary for the temperature control process. Except for the minor cooling capabilities of the heat switch for the SH and LRS, none of the other inner assemblies can be cooled individually. For this reason the trend is always towards higher temperature. Due to the inability to cool and the thermal sluggishness of the system, continuous rather than on-off control has been used. The thermal control logic can be best understood by referring to Figure 16. For simplicity, consider only one assembly. An initial current (typically 150 - 350 ma-DC) sufficient to supply enough power to bring the component to within $\sim$ -0.2°C of the desired temperature within a few minutes is applied to the heater. The current is cut back to a lower level ($\sim$ 5 - 10 ma) allowing the component temperature to level-off. In this fashion the system asymptotically approaches the set-point as the heat input balances the heat loss. The initial current values are necessary to raise the component temperature, whereas the low level currents are to offset the heat loss to the environment. The system is allowed to reach equilibrium at whatever temperature the heat input balances the heat loss. Although the temperature settability is not very good ($\sim \pm$ 0.5°K), the temperature controllability is very good ($\sim \pm$ 0.001°K) for this mode of operation. This procedure is applied to all components such that the SH is always the coldest inner assembly

Table 5

Cryostat Component Temperature Differentials

Assembly	Thermal Differential (with respect to SH temperature)
LRS	+0.2°K
URS	+0.2°K
ARS	+0.5°K
RRS	-2.0°K

Note: CL are physically converted to the component through which they pass, and thus reflect that component thermal differential.

component and that at equilibrium the thermal differentials in Table 5 are maintained. In actuality, this process is applied to the LRS, URS and ARS simultaneously. Once the desired temperature has been reached, the SH temperature is subsequently adjusted. The RRS, due to its large heat capacity and proximity to LN_2, requires the greatest amount of time to reach the desired temperature. Because of this it is heated almost continuously (Figure 17). Once equilibrium has been reached, as indicated by temperature fluctuations of the SH as determined from PRT or vapor pressure readings, the vapor pressure data and temperature data is recorded. The procedure is repeated for each data point (Figure 18).

Typically each point requires $\sim$ one hour if no complications, such as parasitic condensation, occur. Overnight the SH power is turned off, its heat switch turned on and the other component heaters maintained at low level current settings. In this way the SH is kept coldest so as to avoid parasitic condensation and the system may be restarted around the last desired set-point. In general, this procedure works well. However, once parasitic condensation occurs, the sample from the channel with parasitic condensation is removed. The CL are warmed up, the SH chilled down, and the sample re-introduced into the SH slowly. Parasitic condensation is generally corrected easily at sample pressures greater than 10 torr, because such pressures provide sufficiently high mass transfer rates. Once a run has been completed, heat is applied to all components. The samples are driven out of the SH into their respective manifolds and returned to the storage containers.

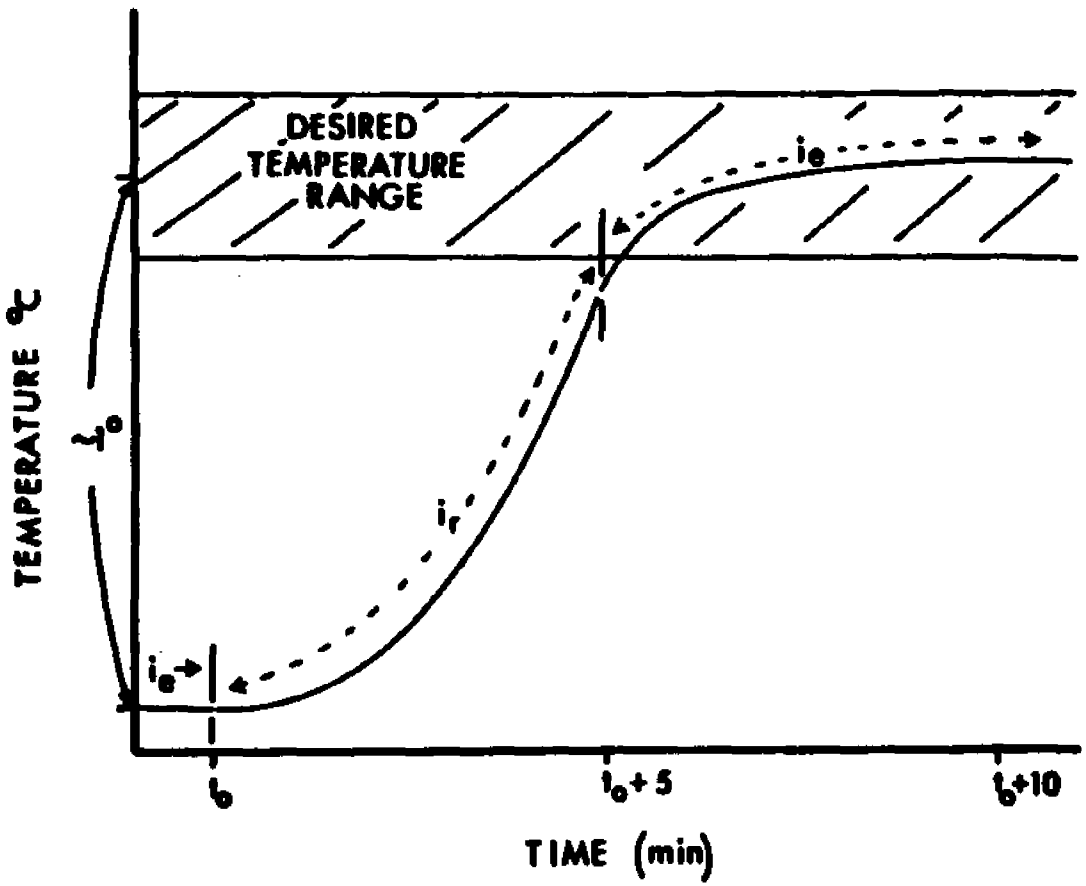

Figure 16. Thermal Control Logic for One Component

(i_r and i_e refer to current settings for raising and maintaining at equilibrium the component temperature, respectively)

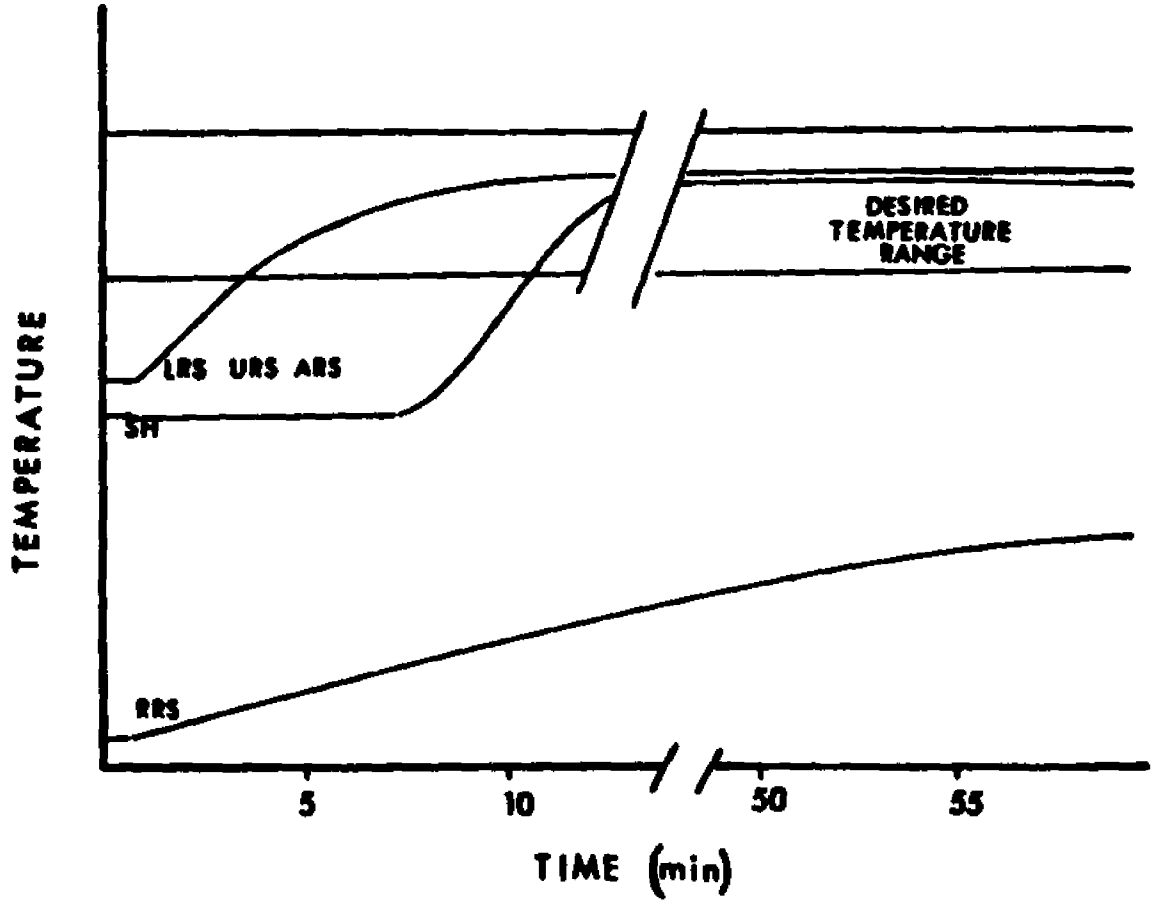

Figure 17. Thermal Control Logic for All Cryostat Components

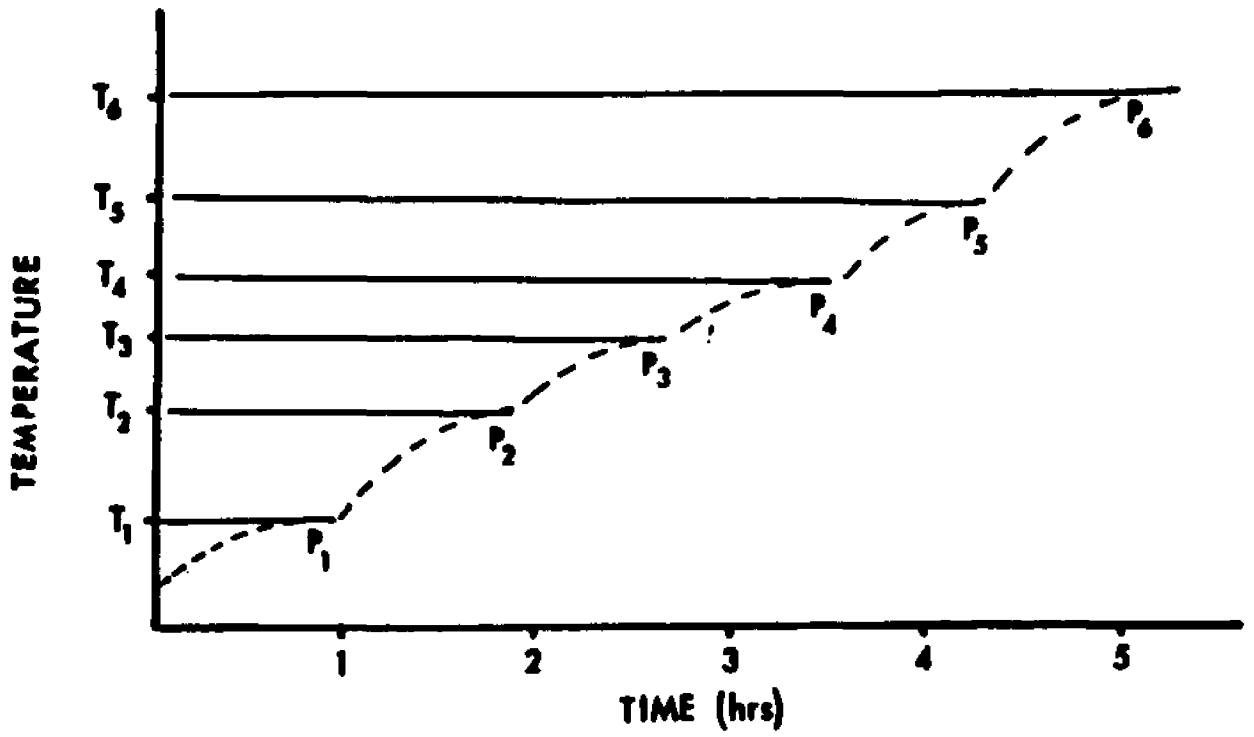

Figure 18. Approach to Equilibrium for a Number of Data Points (P_i refers to Vapor Pressure Readings)

IIIc.2. Operation/Control Software

The operation and control of the cryostat has been designed to function from a completely manual to a fully automatic mode depending on the extent of computer interaction. The software developed mirrors the thermal control logic previously described and allows for as flexible a control system as possible.

The Cryostat Pressure/Temperature Interactive Control program, or CRYPTIC, is structured in the following manner: Various routines or subprograms which perform a specific task (temperature readings using thermocouple or platinum resistance thermometer, heater feedback, pressure measurements, etc.), are accessed via interaction of the console operator with the program main. The operator calls the desired subroutine and, once its operation is complete, control is transferred back to the main program and the console operator. Some routines can cycle continuously, and control can be transferred back to the main program using operator generated interrupts from the console terminal. This scheme allows for maximum flexibility and allows routines to be added or deleted as required. Presently the program CRYPTIC consists of the main program and eleven subroutines. Their functions are outlined in the following.

1. KBQ (KeyBoard Query) is the main program and it allows for the operator access to the various subroutines.

2. TCAR (ThermoCouple Automatic Read) is subroutine #1, and it measures the temperatures of the cryostat components twice over a specified period of time. The routine calculates the rate of change of temperatures. This data is printed out on the console terminal as

well as made available to other routines.

3. RTAR (Resistance Thermometer Automatic Read) is subroutine #2, and is identical in function as TCAR, but the temperature measurements are performed with PRTs.

4. HAMAN (Heater Adjust MANual) is subroutine #3, and it allows the operator to access the D/A converter channels from the console terminal to adjust the cryostat heaters.

5. HAUTO (Heater Adjust AUTOmatic) is subroutine #4, and it automatically adjusts the cryostat heaters. The feedback data is determined by HAUTO which calls TCAR or RTAR. The feedback logic is essentially a proportional control type with a built-in damping/amplification and power factors. The input parameters used are the temperature-differences between various cryostat components, e.g., sample holder, lower radiation shield, etc., and set points (Cf: NUTEM) and also the differences among the cryostat components. Rates of approach to the temperature set point are also used. This routine cycles constantly and the return to KBQ can occur by console interrupt only.

6. PTIN (Pressure/Temperature INput) is subroutine #5, and accepts as input from the console terminal the precision pressure and temperature data read from the spiral quartz gauge, capacitance gauges and sample holder PRT. This data is printed out and stored for later access.

7. NUTEM (New TEMperature) is subroutine #6. This routine allows the operator to set the next desired set point temperature, which would be an approximate value of the temperature at which the next VPIE data will be taken.

8. INPUT (INPUT of control program data) is subroutine #7. This subroutine accepts from the console terminal the necessary operating

parameters and constants. For example: The run's starting temperature, temperature increment, wait time between sensor readings for TCs and PRTs, query wait time for automatic operation, and the various power gain and damping factors for heater control operations. This information is made available to all other subroutines.

9. DDUMP (Data DUMP) is subroutine #8, and its function is to dump all the pressure and temperature data obtained from PTIN onto a disk. A full printout on the console terminal is also provided.

10. PRESS (PRESSure measurement) is subroutine #9. This routine performs a 12-bit measurement of the absolute pressure of the reference gas on one of the capacitance gauge channels; the particular channel is manually set by the operator.

11. INSTR (INSTRuctions) is subroutine #10, and is simply a printout of CRYPTIC's operating instructions for the operator.

12. CONV (CONVersion) is subroutine #11, and it provides conversions of sensor signals (voltage, resistance, etc.) to physical parameters (temperature, pressure, etc.)

A listing of CRYPTIC can be found in Appendix C.

However, such factors as the time lags between the initiation of a new heater power level and the corresponding response at one of the temperature sensors, power damping factors, cycle time, etc., are peculiar to each component and system temperature. Such information can only be obtained empirically. Thus, the present study was performed under a computer assisted mode, that is, the computer has been used to convert analog data from keyboard input to temperature/pressure data for use at the terminal by the operator. Records of the operation and operating conditions from this and subsequent studies will be used to fix the necessary parameters for fully automatic-computer control.

IV. PURIFICATION AND ISOTOPIC ANALYSIS OF $^{12}CHF_3$, $^{12}CDF_3$ and $^{13}CHF_3$

IVa. Chemical Purification

$^{12}CHF_3$ was obtained from Linde-Union Carbide and one liter @ NTP each of $^{13}CHF_3$ and $^{12}CDF_3$ were purchased from Stohler Isotopes Corporation. The $^{13}CHF_3$ sample was supposed to have about 90% ^{13}C-enrichment, and the $^{12}CDF_3$ sample was expected to contain about 98% D.

Initial chemical analysis by gas chromatographic techniques indicated purity levels on the order of 98.8%, 99.99% and 95.5% for $^{12}CHF_3$, $^{12}CDF_3$ and $^{13}CHF_3$, respectively. The major impurities were CO_2, H_2O and an unknown in $^{12}CHF_3$ and $^{12}CDF_3$. $^{13}CHF_3$ was found to contain CO_2, CO, H_2O and seven additional impurities whose identities have not been determined.

The following procedures were used to purify these compounds to acceptable levels:

$^{12}CHF_3$ and $^{12}CDF_3$: The samples were passed, under vacuum, through an ascarite column (1.5 cm in diameter x 60 cm in length) three times to remove CO_2. Subsequent bulb-to-bulb distillation removed H_2O.

$^{13}CHF_3$: The sample was initially cleaned by bulb-to-bulb distillation. It was subsequently purified by passage through an ascarite column five times and a Chromosorb 102 60/80 mesh column at -50°C eight times. The sample was repassed three times through ascarite and a final bulb-to-bulb distillation was performed.

This procedure removed CO_2, CO and H_2O and five of the seven unknown impurities. The total impurity at this point was ∿ 1.0%. Further purification on the $^{13}CHF_3$ sample was done using preparative gas chromatography. The $^{13}CHF_3$ sample was passed through two columns in tandem: A Silica Gel (60/80 mesh) column (3/8" O.D. x 1/4" I.D. x 6 feet) and an Alumina (80/200 mesh) column (3/8").D. x 1/4" I.D. x 6 feet) at 25°C with Helium as the carrier gas. Numerous fractions were collected over a period of several hours and analyzed. The two impurities, which were not removed by bulb-to-bulb and adsorption techniques, eluted before the $^{13}CHF_3$. Therefore only middle and end fractions which showed minimal amounts of these impurities were recombined. The final sample size after this procedure was ∿ 135 cc at NTP.

The final chemical analysis was performed on a Perkin-Elmer 9000 Gas Chromatograph using Alumina 80/200 mesh and Spherocarb 80/100 mesh columns (3/32" I.D. x 6 feet) with Helium as the carrier gas. A thermal conductivity detector (225 ma) was used with a column flow rate of 19 cc/min at temperatures ranging from 60°C - 225°C. The level of impurity as determined by this assay after the procedures described above are ∿ 18 ppm, 16 ppm and 300 ppm for $^{12}CHF_3$, $^{12}CDF_3$ and $^{13}CHF_3$ respectively (Table 6). The $^{13}CHF_3$ sample could not be further purified, because to do so would not leave us with enough material to cover a sufficient temperature range in the VPIE analysis.

Table 6

Fluoroform Final Chemical Analysis and Analytical Gas Chromatographic Conditions

Sample	Impurity	#PPM	Coloumn	Temperature (°C)	Flow Rate ($\frac{cc}{minutes}$)	Retention Time (min)*
$^{12}CHF_3$	CO_2	3	Spherocarb	117	19	5.4
	H_2O	5	Spherocarb	117	19	6.5
	Unknown A	10	Spherocarb	173	19	>30
$^{12}CDF_3$	CO_2	10		117	19	5.4
	H_2O	1		117	19	6.5
	Unknown A	5		173	19	>30
$^{13}CHF_3$	Unknown B	200	Alumina	60	19	0.50
	Unknown C	50	Alumina	60	19	1.20

*Retention time is with respect to air.

IVb. Isotopic Analysis

After purification, the samples were analyzed for their isotopic content. The analysis was performed on a Kratos MS30 Dual Beam Mass Spectrometer - DS50 Data Base System (courtesy of Dr. Iden, Mass Spectrometry Laboratory, Departments of Chemistry and Pharmacology, State University of New York at Stony Brook). The data after being corrected for relative intensities[29] yielded the results tabulated in Table 7. Note that the chemical purities are also summarized in Table 7.

Table 7

Chemical and Isotopic Analysis of Purified Isotopic Fluoroform Samples

Sample	$^{12}CHF_3$	$^{12}CDF_3$	$^{13}CHF_3$
% Chem Purity	99.998	99.998	99.97
	Isotopic Content		
% $^{12}CHF_3$	99.3	3.0	17.6
% $^{13}CHF_3$	0.7	-	82.4
% $^{12}CDF_3$	-	96.1	-
% $^{13}CDF_3$	-	0.9	-

V. EXPERIMENTAL RESULTS

Va. Experimental Vapor Pressure Data

The experimental vapor pressure obtained, over several weeks, is summarized in Tables 8 and 9 for the (12/13) and (H/D) effects, respectively. In these tables P' is the pressure of $^{12}CHF_3$, P the pressure of $^{13}CHF_3$ and $^{12}CDF_3$ in Tables 7 and 8, respectively, and $\Delta P = P'-P$. This data is plotted in Figures 19 and 20 for the (12/13) and (H/D) effects, respectively. The temperature range covered was from $\sim$ 126°K (-147°C) to $\sim$ 212°K (-61°C) which corresponds to a vapor pressure range of approximately 1.6 torr to 2204 torr. The (12/13) VPIE is an inverse effect ($P(^{13}CHF_3) > P(^{12}CHF_3)$) whereas the (H/D) effect was found to be normal ($P(^{12}CHF_3) > P(^{12}CDF_3)$). The vapor pressure data of the reference sample ($^{12}CHF_3$) was compared to that of Giauque, Brodale and Valentine,[30] and our temperature scale was consistent with their temperature scale to within 0.05°K. No attempt to correct our temperature scale was made due to the limited amount of Giauque's data (13 points) especially at the low vapor pressure end.

Table 8: Carbon Vapor Pressure Isotope Effects in Fluoroform

No.	T (°K)	$10^3/T$ ($°K^{-1}$)	P (Torr)	T $\ln(P'_{12}/P_{13})$	Date
1	133.71	7.479	4.8871	-0.6646	10/28
2	134.69	7.424	5.5502	-0.6732	10/23
3	135.17	7.398	5.9221	-0.6742	10/28
4	135.72	7.368	6.3596	-0.6664	10/29
5	136.17	7.344	6.7179	-0.6576	10/23
6	136.64	7.319	7.1478	-0.6642	10/28
7	137.04	7.297	7.5106	-0.6417	10/29
8	137.66	7.265	8.1112	-0.6544	10/23
9	138.06	7.243	8.5472	-0.6459	10/29
10	139.06	7.191	9.6494	-0.6444	10/29
11	139.18	7.185	9.7927	-0.6461	10/23
12	139.75	7.156	10.496	-0.6510	10/29
13	140.43	7.121	11.386	-0.6500	10/29
14	141.27	7.079	12.570	-0.6449	10/29
15	142.05	7.040	13.761	-0.6313	10/29
16	143.02	6.992	15.327	-0.6174	10/24
17	143.24	6.981	15.723	-0.6324	10/29
18	144.64	6.914	18.343	-0.6404	10/24
19	144.95	6.899	19.023	-0.6227	10/30
20	145.76	6.861	20.773	-0.6312	10/30
21	146.14	6.843	21.662	-0.6366	10/24
22	146.64	6.819	22.883	-0.6302	10/30
23	147.65	6.773	25.484	-0.6246	10/24
24	148.56	6.731	28.032	-0.6102	10/30
25	149.16	6.704	29.796	-0.6246	10/24
26	149.94	6.670	32.274	-0.6134	10/30

[continued]

[Table 8; continued]

No.	T (°K)	$10^3/T$ ($°K^{-1}$)	P (Torr)	T $\ln(P'_{12}/P_{13})$	Date
27	150.65	6.638	34.661	-0.6160	10/24
28	151.13	6.617	36.375	-0.6061	10/25
29	151.94	6.581	39.452	-0.6126	10/25
30	152.18	6.571	40.372	-0.6089	10/24
31	152.66	6.550	42.310	-0.6028	10/30
32	153.16	6.529	44.441	-0.6026	10/25
33	153.67	6.508	46.622	-0.6070	10/24
34	154.17	6.486	48.907	-0.6000	10/25
35	155.15	6.445	53.711	-0.5947	10/25
36	156.16	6.404	59.009	-0.5901	10/25
37	157.16	6.363	64.668	-0.5859	10/25
38	157.43	6.352	66.279	-0.5944	10/30
39	158.17	6.322	70.916	-0.5828	10/25
40	159.23	6.280	77.870	-0.5906	10/30
41	160.26	6.240	85.247	-0.5926	10/30
42	160.61	6.226	87.963	-0.5752	10/21
43	161.55	6.190	95.287	-0.5852	10/30
44	162.13	6.168	100.18	-0.5716	10/26
45	162.64	6.149	104.63	-0.5764	10/21
46	163.17	6.129	109.12	-0.5716	10/26
47	163.95	6.100	116.49	-0.5752	10/30
48	164.75	6.070	124.41	-0.5649	10/26
49	165.16	6.055	128.59	-0.5687	10/21
50	165.86	6.029	136.14	-0.5737	10/30
51	166.75	5.997	146.03	-0.5593	10/26
52	167.14	5.983	150.76	-0.5592	10/21

[continued]

[Table 8; continued]

No.	T (°K)	$10^3/T$ ($°K^{-1}$)	P (Torr)	T $\ln(P'_{12}/P_{13})$	Date
53	168.15	5.947	163.02	-0.5580	10/26
54	169.14	5.912	176.10	-0.5578	10/21
55	170.44	5.867	194.24	-0.5511	10/26
56	171.16	5.842	205.27	-0.5522	10/21
57	171.65	5.826	212.58	-0.5492	10/26
58	172.18	5.808	221.24	-0.5608	10/22
59	172.85	5.785	232.40	-0.5476	10/26
60	174.16	5.742	255.53	-0.5551	10/22
61	174.64	5.726	264.29	-0.5428	10/26
62	175.64	5.694	283.80	-0.5419	10/26
63	176.17	5.676	294.49	-0.5485	10/22
64	177.53	5.633	323.66	-0.5370	10/27
65	178.23	5.611	339.15	-0.5470	10/22
66	179.56	5.569	370.96	-0.5329	10/27
67	180.14	5.551	385.91	-0.5417	10/22
68	180.94	5.527	406.58	-0.5310	10/27
69	181.64	5.505	425.71	-0.5223	10/22
70	182.30	5.486	444.18	-0.5283	10/27
71	183.64	5.445	484.05	-0.5203	10/23
72	184.58	5.418	512.83	-0.5244	10/31
73	185.21	5.399	534.05	-0.5197	10/27
74	185.62	5.387	547.73	-0.5206	10/23
75	186.06	5.375	562.51	-0.5218	10/27
76	187.63	5.330	618.52	-0.5161	10/23
77	188.62	5.302	656.53	-0.5140	10/27
78	189.22	5.285	680.81	-0.5140	10/27

[continued]

[Table 8; continued]

No.	T (°K)	$10^3/T$ ($°K^{-1}$)	P (Torr)	T $\ln(P'_{12}/P_{13})$	Date
79	189.66	5.273	698.02	-0.5155	10/23
80	190.54	5.248	735.06	-0.5104	10/31
81	191.24	5.229	766.14	-0.5050	10/27
82	192.05	5.207	802.20	-0.5064	10/27
83	193.02	5.181	847.59	-0.5057	10/31
84	194.24	5.148	906.83	-0.4955	10/27
85	195.12	5.125	952.43	-0.4961	10/27
86	196.02	5.101	1000.9	-0.5054	10/31
87	197.05	5.075	1056.9	-0.4977	10/27
88	198.10	5.048	1118.5	-0.4914	10/31
89	198.64	5.034	1150.5	-0.4916	10/27
90	199.66	5.008	1215.0	-0.4824	10/31

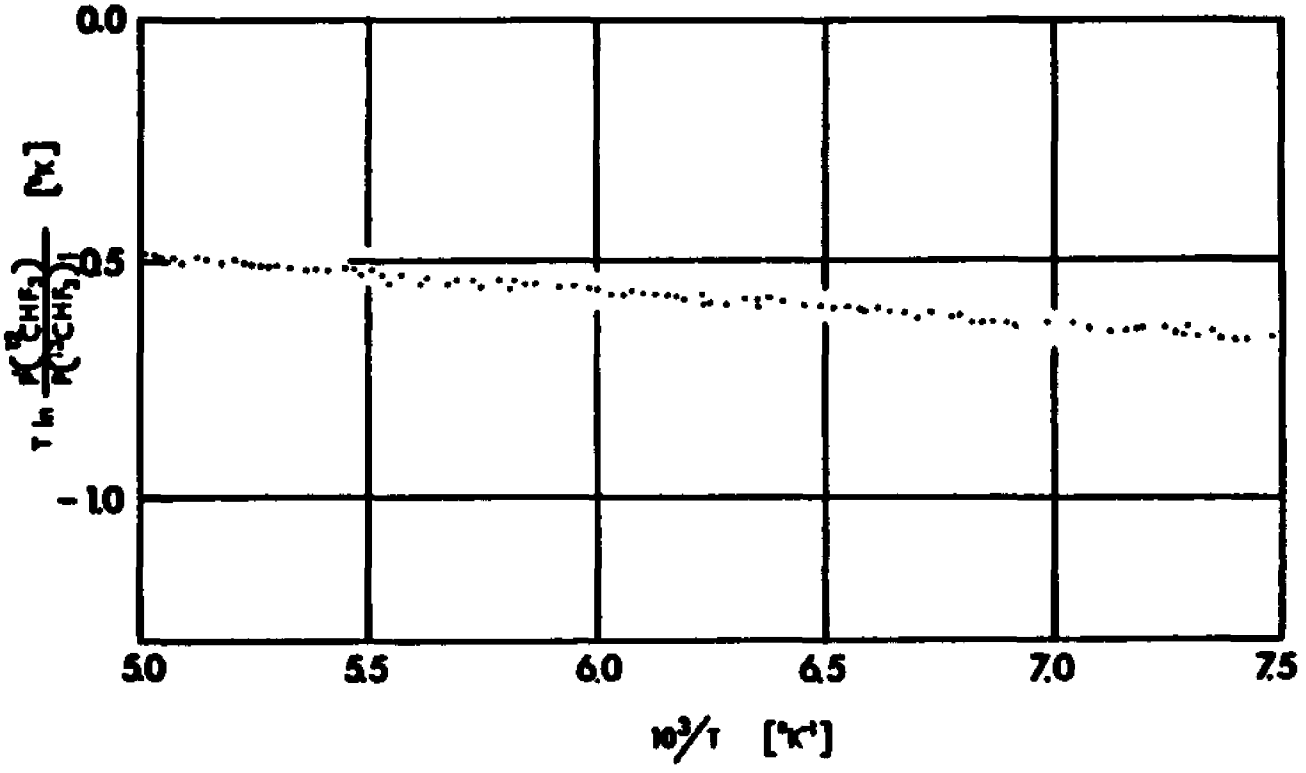

Figure 19. 12/13 Vapor Pressure Isotope Effect in Fluoroform

Table 9: Hydrogen Vapor Pressure Isotope Effects in Fluoroform

No.	T (°K)	$10^3/T$ ($°K^{-1}$)	P (Torr)	$T \ln(P'_H/P_D)$	Date
1	126.00	7.936	1.6478	+4.406	09/08
2	126.95	7.877	1.8993	+4.369	09/08
3	127.84	7.822	2.1600	+4.418	09/08
4	128.72	7.769	2.4587	+4.347	09/08
5	129.16	7.742	2.6142	+4.679	10/28
6	129.64	7.714	2.8124	+4.308	09/08
7	129.97	7.694	2.9252	+4.578	10/28
8	130.51	7.662	3.1630	+4.277	09/08
9	131.55	7.602	3.6554	+4.264	09/08
10	132.54	7.545	4.1889	+4.233	09/08
11	133.01	7.518	4.4587	+4.611	10/23
12	133.53	7.489	4.7712	+4.391	08/13
13	133.71	7.479	4.8871	+4.440	10/28
14	133.75	7.477	4.9099	+4.263	09/08
15	134.15	7.454	5.1828	+4.367	08/13
16	134.15	7.454	5.1828	+4.273	09/02
17	134.69	7.424	5.5502	+4.463	10/23
18	135.14	7.400	5.8993	+4.350	08/13
19	135.17	7.398	5.9221	+4.405	10/28
20	135.17	7.398	5.9237	+4.218	09/02
21	135.72	7.368	6.3596	+4.516	10/29
22	136.16	7.344	6.7148	+4.341	08/13
23	136.17	7.344	6.7179	+4.513	10/23
24	136.64	7.319	7.1478	+4.394	10/28
25	136.66	7.317	7.1615	+4.257	09/02
26	137.04	7.297	7.5106	+4.457	10/29

[continued]

[Table 9; continued]

No.	T (°K)	$10^3/T$ ($°K^{-1}$)	P (Torr)	T $\ln(P'_H/P_D)$	Date
27	137.14	7.292	7.5914	+4.317	08/13
28	137.66	7.265	8.1112	+4.470	10/23
29	137.78	7.258	8.2454	+4.267	09/02
30	138.06	7.243	8.5472	+4.406	10/29
31	138.16	7.238	8.6433	+4.307	08/13
32	138.32	7.230	8.8475	+4.247	09/08
33	138.44	7.223	9.0091	+4.202	08/19
34	138.96	7.196	9.5564	+4.243	09/02
35	139.06	7.191	9.6494	+4.361	10/29
36	139.16	7.186	9.8171	+4.183	08/19
37	139.18	7.185	9.7927	+4.426	10/23
38	139.65	7.161	10.422	+4.207	09/08
39	139.75	7.156	10.496	+4.342	10/29
40	140.13	7.137	11.014	+4.233	09/02
41	140.15	7.135	11.052	+4.146	08/19
42	140.43	7.121	11.386	+4.324	10/29
43	140.79	7.103	11.927	+4.314	09/15
44	140.84	7.100	11.979	+4.215	09/08
45	141.15	7.085	12.416	+4.189	08/19
46	141.27	7.079	12.570	+4.311	10/29
47	141.41	7.072	12.778	+4.222	09/02
48	142.05	7.040	13.761	+4.301	10/29
49	142.17	7.034	13.967	+4.238	09/15
50	142.17	7.034	13.985	+4.131	08/19
51	142.53	7.016	14.563	+4.201	09/02
52	142.64	7.010	14.757	+4.198	08/20

[continued]

[Table 9; continued]

No.	T (°K)	$10^3/T$ ($°K^{-1}$)	P (Torr)	T $\ln(P'_H/P_D)$	Date
53	143.02	6.992	15.327	+4.321	10/24
54	143.14	6.986	15.595	+4.192	08/19
55	143.24	6.981	15.723	+4.262	10/29
56	143.64	6.962	16.501	+4.223	09/15
57	143.74	6.957	16.697	+4.213	09/02
58	144.14	6.938	17.438	+4.185	08/19
59	144.64	6.914	18.343	+4.291	10/24
60	144.95	6.899	19.023	+4.238	10/30
61	144.98	6.898	19.102	+4.204	09/02
62	145.14	6.890	19.474	+4.201	09/15
63	145.14	6.890	19.489	+4.165	08/20
64	145.76	6.861	20.773	+4.223	10/30
65	146.13	6.843	21.668	+4.241	09/08
66	146.14	6.843	21.662	+4.248	10/24
67	146.14	6.843	21.712	+4.142	08/20
68	146.55	6.824	22.683	+4.189	09/03
69	146.64	6.819	22.883	+4.203	10/30
70	146.69	6.817	23.019	+4.192	09/15
71	147.15	6.796	24.199	+4.120	08/20
72	147.17	6.795	24.232	+4.118	09/15
73	147.43	6.783	24.923	+4.191	09/08
74	147.55	6.777	25.260	+4.163	09/03
75	147.60	6.775	25.405	+4.148	09/15
76	147.65	6.773	25.484	+4.199	10/24
77	148.15	6.750	26.915	+4.107	08/20
78	148.43	6.737	27.724	+4.145	09/16

[continued]

[Table 9; continued]

No.	T (°K)	$10^3/T$ ($°K^{-1}$)	P (Torr)	T $\ln(P'_H/P_D)$	Date
79	148.56	6.731	28.032	+4.170	10/30
80	148.76	6.722	28.659	+4.143	09/03
81	149.15	6.705	29.816	+4.097	08/20
82	149.16	6.704	29.796	+4.167	10/24
83	149.16	6.704	29.879	+4.170	09/08
84	149.44	6.692	30.689	+4.134	09/16
85	149.94	6.670	32.274	+4.143	10/30
86	149.96	6.668	32.410	+4.125	09/03
87	150.15	6.660	33.048	+4.089	08/20
88	150.44	6.647	33.988	+4.125	09/16
89	150.64	6.638	34.705	+4.147	09/08
90	150.65	6.638	34.661	+4.138	10/24
91	151.13	6.617	36.375	+4.120	10/25
92	151.13	6.617	36.438	+4.103	09/03
93	151.16	6.616	36.546	+4.076	08/20
94	151.44	6.603	37.561	+4.112	09/16
95	151.94	6.581	39.452	+4.087	10/25
96	152.16	6.572	40.374	+4.066	08/20
97	152.18	6.571	40.372	+4.105	10/24
98	152.35	6.564	41.138	+4.081	09/03
99	152.47	6.559	41.613	+4.093	09/16
100	152.66	6.550	42.318	+4.100	10/30
101	152.66	6.550	42.486	+4.078	08/21
102	153.12	6.531	44.415	+4.077	09/11
103	153.14	6.530	44.446	+4.052	08/20
104	153.16	6.529	44.441	+4.068	10/25

[continued]

[Table 9; continued]

No.	T (°K)	$10^3/T$ ($°K^{-1}$)	P (Torr)	T $\ln(P'_H/P_D)$	Date
105	153.55	6.513	46.244	+4.062	09/03
106	153.67	6.508	46.622	+4.086	10/24
107	154.17	6.486	48.907	+4.058	10/25
108	154.36	6.478	49.939	+4.056	08/21
109	154.65	6.466	51.272	+4.077	09/11
110	154.77	6.461	51.919	+4.043	09/03
111	155.15	6.445	53.711	+4.047	10/25
112	155.15	6.445	53.830	+4.042	08/21
113	155.65	6.425	56.470	+4.070	09/08
114	155.94	6.413	57.947	+4.024	09/03
115	155.95	6.412	58.040	+4.062	09/16
116	156.16	6.404	59.009	+4.032	10/25
117	156.16	6.404	59.128	+4.024	08/21
118	157.12	6.365	64.579	+4.042	09/08
119	157.14	6.364	64.607	+4.009	09/03
120	157.16	6.363	64.668	+4.023	10/25
121	157.16	6.363	64.804	+4.009	08/21
122	157.24	6.360	65.183	+4.041	09/11
123	157.43	6.352	66.270	+4.022	10/30
124	157.62	6.344	67.661	+4.036	08/27
125	158.15	6.323	70.803	+3.994	08/21
126	158.17	6.322	70.916	+4.008	10/25
127	158.34	6.316	72.083	+3.987	09/03
128	158.67	6.302	74.251	+4.035	09/12
129	158.95	6.291	76.132	+4.018	09/08
130	159.15	6.283	77.481	+3.978	08/21

[continued]

[Table 9; continued]

No.	T (°K)	$10^3/T$ ($°K^{-1}$)	P (Torr)	T $\ln(P'_H/P_D)$	Date
131	159.23	6.280	77.870	+3.994	10/30
132	159.31	6.277	78.599	+3.997	08/27
133	159.54	6.268	80.177	+3.973	09/03
134	160.16	6.244	84.670	+4.003	09/12
135	160.19	6.243	84.785	+3.998	09/08
136	160.26	6.240	85.247	+3.975	10/30
137	160.74	6.221	89.042	+3.953	09/03
138	160.74	6.221	89.127	+3.977	08/27
139	161.55	6.190	95.287	+3.956	10/30
140	161.68	6.185	96.487	+3.972	09/12
141	161.70	6.184	96.633	+3.940	09/03
142	161.94	6.175	98.582	+3.937	09/03
143	162.07	6.170	99.763	+3.956	08/27
144	162.13	6.168	100.18	+3.944	10/26
145	162.64	6.149	104.63	+3.911	10/21
146	162.94	6.137	107.31	+3.920	09/03
147	163.12	6.131	108.98	+3.946	09/12
148	163.17	6.129	109.12	+3.921	10/26
149	163.26	6.125	110.15	+3.938	08/27
150	163.66	6.110	113.82	+3.898	10/20
151	163.95	6.100	116.49	+3.921	10/30
152	164.15	6.092	118.64	+3.902	09/04
153	164.36	6.084	120.67	+3.917	08/27
154	164.75	6.070	124.41	+3.900	10/26
155	164.75	6.070	124.58	+3.919	09/12
156	165.14	6.056	128.62	+3.920	09/09

[continued]

[Table 9; continued]

No.	T (°K)	$10^3/T$ ($°K^{-1}$)	P (Torr)	T $\ln(P'_H/P_D)$	Date
157	165.16	6.055	128.59	+3.887	10/21
158	165.36	6.048	130.78	+3.885	09/04
159	165.57	6.040	133.12	+3.900	08/27
160	165.86	6.029	136.14	+3.884	10/30
161	166.12	6.020	139.30	+3.907	09/16
162	166.15	6.019	139.39	+3.881	10/22
163	166.27	6.014	140.86	+3.894	09/12
164	166.56	6.004	144.01	+3.868	09/04
165	166.65	6.000	145.31	+3.888	09/09
166	166.75	5.997	146.03	+3.870	10/26
167	166.79	5.996	146.74	+3.881	08/27
168	167.14	5.983	150.76	+3.860	10/21
169	167.50	5.970	155.31	+3.858	09/04
170	167.76	5.961	158.53	+3.851	09/04
171	167.86	5.957	159.48	+3.870	09/12
172	167.97	5.954	161.06	+3.870	08/28
173	168.15	5.947	163.02	+3.849	10/26
174	168.73	5.927	170.70	+3.836	09/04
175	169.09	5.914	175.47	+3.849	09/09
176	169.14	5.912	176.10	+3.832	10/21
177	169.19	5.911	176.96	+3.843	08/28
178	169.45	5.901	180.40	+3.844	09/12
179	169.96	5.884	187.54	+3.816	09/04
180	170.36	5.870	193.42	+3.820	08/28
181	170.44	5.867	194.24	+3.815	10/26
182	171.04	5.847	203.57	+3.819	09/12

[continued]

[Table 9; continued]

No.	T (°K)	$10^3/T$ ($°K^{-1}$)	P (Torr)	T $\ln(P'_H/P_D)$	Date
183	171.14	5.843	205.16	+3.800	09/04
184	171.16	5.842	205.27	+3.808	10/21
185	171.55	5.829	211.46	+3.800	08/28
186	171.65	5.826	212.58	+3.798	10/26
187	172.18	5.808	221.24	+3.797	10/22
188	172.37	5.801	224.62	+3.779	09/04
189	172.76	5.788	231.08	+3.791	09/12
190	172.76	5.788	231.25	+3.782	08/28
191	172.85	5.785	232.60	+3.780	10/26
192	173.56	5.762	244.84	+3.762	09/04
193	173.94	5.749	252.02	+3.764	08/28
194	174.04	5.746	253.60	+3.770	09/09
195	174.16	5.742	255.53	+3.765	10/22
196	174.45	5.732	261.18	+3.763	09/12
197	174.64	5.726	264.29	+3.755	10/26
198	174.74	5.723	266.78	+3.745	09/04
199	175.15	5.709	274.60	+3.746	08/28
200	175.64	5.694	283.80	+3.741	10/26
201	175.66	5.693	284.40	+3.742	09/09
202	175.95	5.684	290.61	+3.728	09/04
203	176.14	5.677	294.46	+3.736	09/12
204	176.17	5.676	294.49	+3.740	10/22
205	176.36	5.670	298.74	+3.728	08/28
206	177.16	5.645	315.69	+3.710	09/04
207	177.53	5.633	323.66	+3.715	10/27
208	177.55	5.632	324.20	+3.713	08/28

[continued]

[Table 9; continued]

No.	T (°K)	$10^3/T$ ($°K^{-1}$)	P (Torr)	T $\ln(P'_H/P_D)$	Date
209	177.84	5.623	330.95	+3.710	09/12
210	178.13	5.614	337.45	+3.709	09/09
211	178.23	5.611	339.15	+3.707	10/22
212	178.44	5.604	344.60	+3.696	09/04
213	178.76	5.594	352.13	+3.695	08/28
214	179.54	5.570	371.16	+3.686	09/13
215	179.56	5.569	370.96	+3.686	10/27
216	179.61	5.568	372.98	+3.682	09/09
217	179.75	5.563	376.52	+3.674	09/04
218	179.95	5.557	381.21	+3.678	08/28
219	180.14	5.551	385.91	+3.681	10/22
220	180.94	5.527	406.58	+3.666	10/27
221	181.05	5.523	410.09	+3.655	09/04
222	181.13	5.521	412.32	+3.666	09/16
223	181.16	5.520	412.87	+3.661	08/28
224	181.25	5.517	415.32	+3.661	09/13
225	181.64	5.505	425.71	+3.668	10/22
226	181.67	5.505	427.08	+3.653	09/09
227	182.30	5.486	444.18	+3.647	10/27
228	182.35	5.484	445.91	+3.637	09/05
229	182.35	5.484	445.98	+3.643	08/28
230	182.95	5.466	463.59	+3.636	09/13
231	183.56	5.448	481.78	+3.627	08/28
232	183.63	5.446	484.25	+3.621	09/05
233	183.64	5.445	484.05	+3.641	10/23
234	184.13	5.431	499.66	+3.620	09/09

[continued]

[Table 9; continued]

No.	T (°K)	$10^3/T$ ($°K^{-1}$)	P (Torr)	T $\ln(P'_H/P_D)$	Date
235	184.58	5.418	512.83	+3.595	10/31
236	184.64	5.416	515.66	+3.611	09/13
237	184.75	5.413	519.55	+3.612	08/28
238	184.97	5.406	526.37	+3.608	09/05
239	185.21	5.399	534.05	+3.615	10/27
240	185.62	5.387	547.73	+3.611	10/23
241	185.94	5.378	558.75	+3.597	08/28
242	186.06	5.375	562.51	+3.601	10/27
243	186.26	5.369	569.64	+3.587	09/05
244	186.35	5.366	572.95	+3.589	09/13
245	187.13	5.344	601.00	+3.579	09/16
246	187.14	5.344	601.28	+3.574	09/09
247	187.14	5.344	601.34	+3.579	08/29
248	187.54	5.332	616.16	+3.570	09/05
249	187.63	5.330	618.52	+3.581	10/23
250	188.13	5.316	638.23	+3.564	09/13
251	188.35	5.309	646.25	+3.560	08/29
252	188.62	5.302	656.53	+3.565	10/27
253	188.86	5.295	666.32	+3.549	09/05
254	189.22	5.285	680.81	+3.555	10/27
255	189.65	5.273	698.61	+3.537	09/10
256	189.66	5.273	698.02	+3.550	10/23
257	189.93	5.265	709.63	+3.536	09/13
258	190.15	5.259	719.08	+3.529	09/05
259	190.54	5.248	735.06	+3.526	10/31
260	191.15	5.232	762.86	+3.516	09/16

[continued]

[Table 9; continued]

No.	T (°K)	$10^3/T$ ($°K^{-1}$)	P (Torr)	T $\ln(P'_H/P_D)$	Date
261	191.24	5.229	766.14	+3.529	10/27
262	191.44	5.224	775.41	+3.509	09/05
263	191.63	5.218	783.28	+3.509	10/23
264	191.67	5.217	785.74	+3.511	09/13
265	192.05	5.207	802.20	+3.514	10/27
266	192.15	5.204	807.74	+3.501	09/10
267	193.02	5.181	847.59	+3.489	10/31
268	193.12	5.178	853.16	+3.489	09/05
269	193.14	5.178	853.41	+3.491	09/16
270	193.63	5.164	875.88	+3.475	10/23
271	194.24	5.148	906.83	+3.492	10/27
272	194.63	5.138	927.92	+3.470	09/10
273	195.12	5.125	952.43	+3.474	10/27
274	195.12	5.125	953.20	+3.464	09/05
275	195.14	5.124	953.96	+3.464	09/16
276	195.65	5.111	980.03	+3.432	10/23
277	196.02	5.101	1000.9	+3.433	10/31
278	197.05	5.075	1056.9	+3.432	10/27
279	197.12	5.073	1063.4	+3.441	09/10
280	197.15	5.072	1063.8	+3.437	09/16
281	197.15	5.072	1064.1	+3.440	09/05
282	197.66	5.059	1091.8	+3.412	10/23
283	198.10	5.048	1118.5	+3.408	10/31
284	198.64	5.034	1150.5	+3.418	10/27
285	199.15	5.021	1183.8	+3.416	09/05
286	199.61	5.010	1210.9	+3.378	$10/2_3$

[continued]

[Table 9; continued]

No.	T (°K)	$10^3/T$ ($°K^{-1}$)	P (Torr)	T $\ln(P'_H/P_D)$	Date
287	199.66	5.008	1215.0	+3.386	10/31
288	200.15	4.996	1247.2	+3.407	09/10
289	201.15	4.971	1313.6	+3.392	09/05
290	203.14	4.923	1452.6	+3.385	09/16
291	203.17	4.922	1455.6	+3.357	09/05
292	205.14	4.875	1607.6	+3.324	09/16
293	207.13	4.828	1770.6	+3.271	09/16
294	212.16	4.713	2237.2	+3.179	09/16

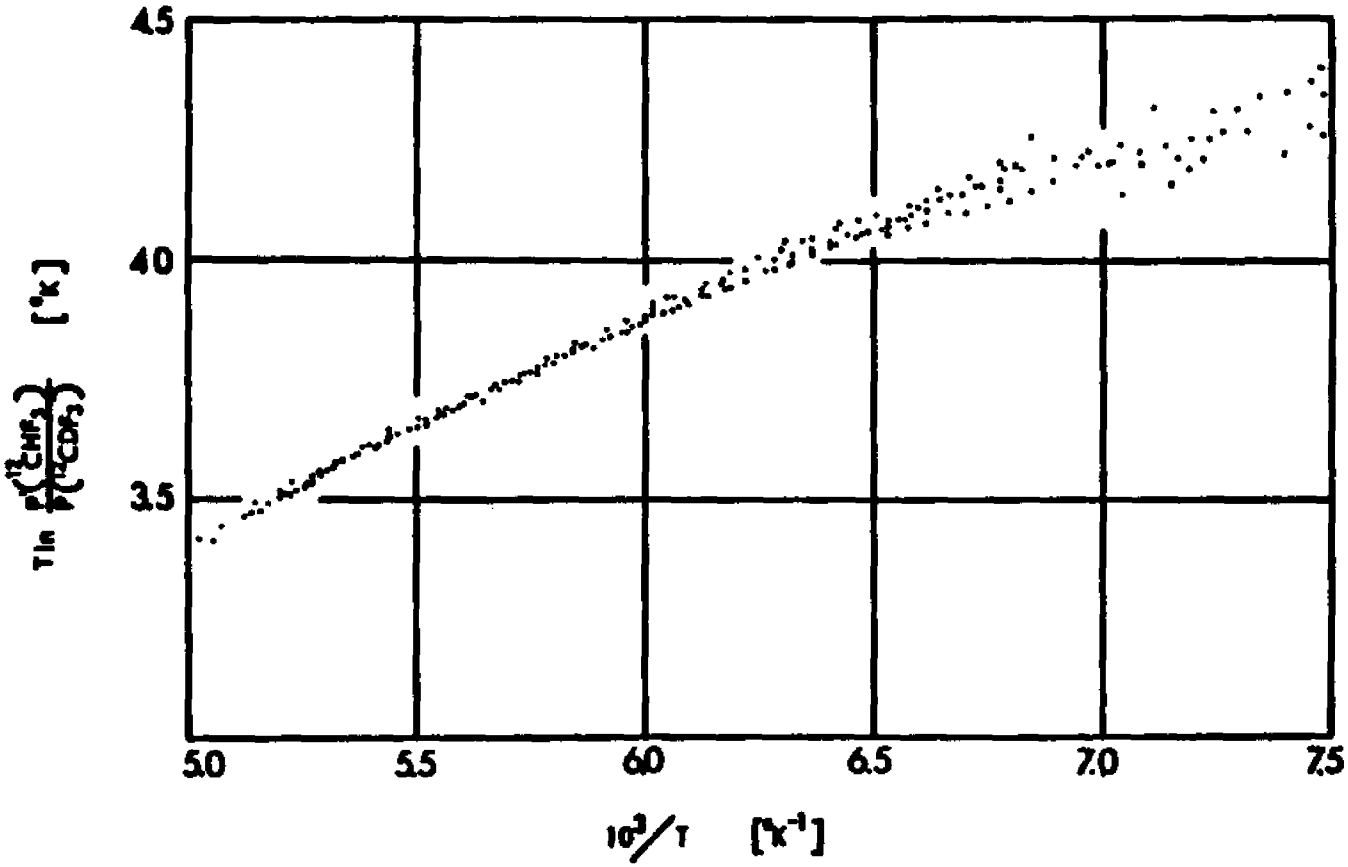

Figure 20. H/D Vapor Pressure Isotope Effect in Fluoroform

Vb. Data Reduction

1. Correction for Isotopic Content

The experimentally observed data of $P_{reference}$ and ΔP ($\equiv P_{reference} - P_{sample}$) for each effect had to be corrected for isotopic content so that the quantity P'/P could be obtained. The isotopic mixtures are treated ideally. Application of isotopic analysis (Section IV) yields the following:

$$\frac{12}{13} : \frac{P'}{P} = \left[\frac{1}{1 - 1.216\left(\frac{\Delta P}{P_{ref}}\right)}\right] , \qquad \text{V-(1)}$$

and

$$\frac{H}{D} : \frac{P'}{P} = \left[\frac{1}{1 - 1.031\left(\frac{\Delta P}{P_{ref}}\right)}\right] , \qquad \text{V-(2)}$$

where the following approximations have been made: $P_{ref} = P'$ and, for the calculation of the H/D effect, $P(^{13}CHF_3) \approx P(^{12}CHF_3)$. These approximations are valid based on the isotopic content data and the level of the observed isotope effect. The errors introduced by these approximations are on the order of 0.010% and 0.014% for the 12/13 and H/D effects, respectively.

2. Non-Ideality Corrections

In order to obtain f_c/f_g data, the P'/P data must be corrected for gas non-ideality[30] and condensed phase molar volume isotopic

differences.[31] These terms are given in Eq. I-(6).

$$\ln \frac{f_c}{f_g} = \ln \frac{P'}{P} \left[1 + P_{ref}\left(B_o - \frac{V}{RT}\right)\right] , \qquad \text{I-(6)}$$

where $$B_o(\text{torr}^{-1}) = \frac{-397.2}{T^3}$$

and

$$\frac{V}{RT}\ (\text{torr}^{-1}) = \frac{1.12\text{x}10^{-3}}{2.10T - 3.37\text{x}10^{-3}T^2}$$

The VPIE for CHF_3 as a function of temperature can be summarized as follows:

12/13 VPIE:

$$\ln\left(\frac{f_c}{f_g}\right)_T = \left[\ln \frac{1}{1-1.216\left(\frac{\Delta P}{P_{ref}}\right)_T}\right]\left[1+\left(P_{ref}\right)_T\left(\frac{-397.2}{T^3} - \frac{1.12\text{x}10^{-3}}{2.10T-3.37\text{x}10^{-3}T^2}\right)\right] \qquad \text{V-(3)}$$

and

H/D VPIE:

$$\ln\left(\frac{f_c}{f_g}\right)_T = \left[\ln \frac{1}{1-1.031\left(\frac{\Delta P}{P_{ref}}\right)_T}\right]\left[1+\left(P_{ref}\right)_T\left(\frac{-397.2}{T^3} - \frac{1.12\text{x}10^{-3}}{2.10T-3.37\text{x}10^{-3}T^2}\right)\right] \qquad \text{V-(4)}$$

f_c/f_g data is tabulated in Tables 10 and 11 for the 12/13 and H/D effects, respectively, and plotted in Figures 21 and 22 for the respective effects.

Table 10: Corrected Carbon Vapor Pressure Isotope Effect in Fluoroform

No.	T (°K)	$10^3/T$ ($°K^{-1}$)	$\ln f_c/f_g$	$T \ln f_c/f_g$ (°K)
1	133.71	7.4789	-0.6036D-02	-0.8070
2	134.69	7.4245	-0.6069D-02	-0.8174
3	135.17	7.3981	-0.6056D-02	-0.8186
4	135.72	7.3681	-0.5961D-02	-0.8091
5	136.17	7.3438	-0.5863D-02	-0.7984
6	136.64	7.3185	-0.5901D-02	-0.8063
7	137.04	7.2971	-0.5684D-02	-0.7790
8	137.44	7.2643	-0.5770D-02	-0.7943
9	138.06	7.2432	-0.5678D-02	-0.7840
10	139.06	7.1911	-0.5624D-02	-0.7820
11	139.18	7.1849	-0.5634D-02	-0.7841
12	139.75	7.1556	-0.5653D-02	-0.7900
13	140.43	7.1210	-0.5616D-02	-0.7887
14	141.27	7.0786	-0.5538D-02	-0.7824
15	142.05	7.0398	-0.5391D-02	-0.7658
16	143.02	6.9920	-0.5236D-02	-0.7488
17	143.24	6.9813	-0.5354D-02	-0.7669
18	144.64	6.9137	-0.5368D-02	-0.7764
19	144.95	6.8989	-0.5208D-02	-0.7549
20	145.76	6.8606	-0.5249D-02	-0.7651
21	146.14	6.8428	-0.5279D-02	-0.7715
22	146.64	6.8194	-0.5208D-02	-0.7637
23	147.65	6.7728	-0.5125D-02	-0.7567
24	148.56	6.7313	-0.4975D-02	-0.7391
25	149.16	6.7042	-0.5071D-02	-0.7564
26	149.94	6.6693	-0.4953D-02	-0.7426

[continued]

[Table 10; continued]

No.	T (°K)	$10^3/T$ ($°K^{-1}$)	$\ln f_c/f_g$	T $\ln f_c/f_g$ (°K)
27	150.65	6.6379	-0.4949D-02	-0.7456
28	151.13	6.6168	-0.4853D-02	-0.7335
29	151.94	6.5815	-0.4878D-02	-0.7411
30	152.18	6.5712	-0.4840D-02	-0.7366
31	152.66	6.5505	-0.4776D-02	-0.7291
32	153.16	6.5291	-0.4758D-02	-0.7287
33	153.67	6.5075	-0.4776D-02	-0.7339
34	154.17	6.4863	-0.4704D-02	-0.7253
35	155.15	6.4454	-0.4631D-02	-0.7185
36	156.16	6.4037	-0.4564D-02	-0.7127
37	157.16	6.3629	-0.4500D-02	-0.7072
38	157.43	6.3520	-0.4557D-02	-0.7174
39	158.17	6.3223	-0.4445D-02	-0.7031
40	159.23	6.2802	-0.4472D-02	-0.7121
41	160.26	6.2399	-0.4456D-02	-0.7141
42	160.61	6.2263	-0.4315D-02	-0.6930
43	161.55	6.1900	-0.4362D-02	-0.7046
44	162.13	6.1679	-0.4244D-02	-0.6880
45	162.64	6.1485	-0.4264D-02	-0.6935
46	163.17	6.1286	-0.4214D-02	-0.6875
47	163.95	6.0994	-0.4218D-02	-0.6915
48	164.75	6.0698	-0.4120D-02	-0.6787
49	165.16	6.0547	-0.4136D-02	-0.6831
50	165.86	6.0292	-0.4152D-02	-0.6887
51	166.75	5.9970	-0.4024D-02	-0.6709
52	167.14	5.9830	-0.4012D-02	-0.6706

[continued]

[Table 10; continued]

No.	T (°K)	$10^3/T$ ($°K^{-1}$)	$\ln f_c/f_g$	T $\ln f_c/f_g$ (°K)
53	168.15	5.9471	-0.3976D-02	-0.6686
54	169.14	5.9123	-0.3948D-02	-0.6677
55	170.44	5.8672	-0.3866D-02	-0.6589
56	171.16	5.8425	-0.3854D-02	-0.6597
57	171.65	5.8258	-0.3821D-02	-0.6558
58	172.18	5.8079	-0.3887D-02	-0.6693
59	172.85	5.7854	-0.3778D-02	-0.6531
60	174.16	5.7418	-0.3796D-02	-0.6611
61	174.64	5.7261	-0.3699D-02	-0.6461
62	175.64	5.6935	-0.3668D-02	-0.6442
63	176.17	5.6763	-0.3699D-02	-0.6517
64	177.53	5.6329	-0.3587D-02	-0.6369
65	178.23	5.6107	-0.3637D-02	-0.6482
66	179.56	5.5692	-0.3510D-02	-0.6303
67	180.14	5.5512	-0.3554D-02	-0.6402
68	180.94	5.5267	-0.3464D-02	-0.6268
69	181.64	5.5054	-0.3391D-02	-0.6159
70	182.30	5.4855	-0.3414D-02	-0.6223
71	183.64	5.4454	-0.3330D-02	-0.6116
72	184.58	5.4177	-0.3334D-02	-0.6155
73	185.21	5.3993	-0.3290D-02	-0.6093
74	185.62	5.3874	-0.3286D-02	-0.6099
75	186.06	5.3746	-0.3283D-02	-0.6108
76	187.63	5.3296	-0.3211D-02	-0.6025
77	188.62	5.3017	-0.3175D-02	-0.5989
78	189.22	5.2849	-0.3161D-02	-0.5982

[continued]

[Table 10; continued]

No.	T (°K)	$10^3/T$ ($°K^{-1}$)	$\ln f_c/f_g$	$T \ln f_c/f_g$ (°K)
79	189.66	5.2726	-0.3161D-02	-0.5994
80	190.54	5.2482	-0.3109D-02	-0.5924
81	191.24	5.2290	-0.3061D-02	-0.5853
82	192.05	5.2070	-0.3051D-02	-0.5859
83	193.02	5.1808	-0.3025D-02	-0.5839
84	194.24	5.1483	-0.2937D-02	-0.5706
85	195.12	5.1251	-0.2922D-02	-0.5701
86	196.02	5.1015	-0.2956D-02	-0.5795
87	197.05	5.0749	-0.2887D-02	-0.5693
88	198.10	5.0480	-0.2830D-02	-0.5606
89	198.64	5.0342	-0.2819D-02	-0.5601
90	199.66	5.0085	-0.2745D-02	-0.5481

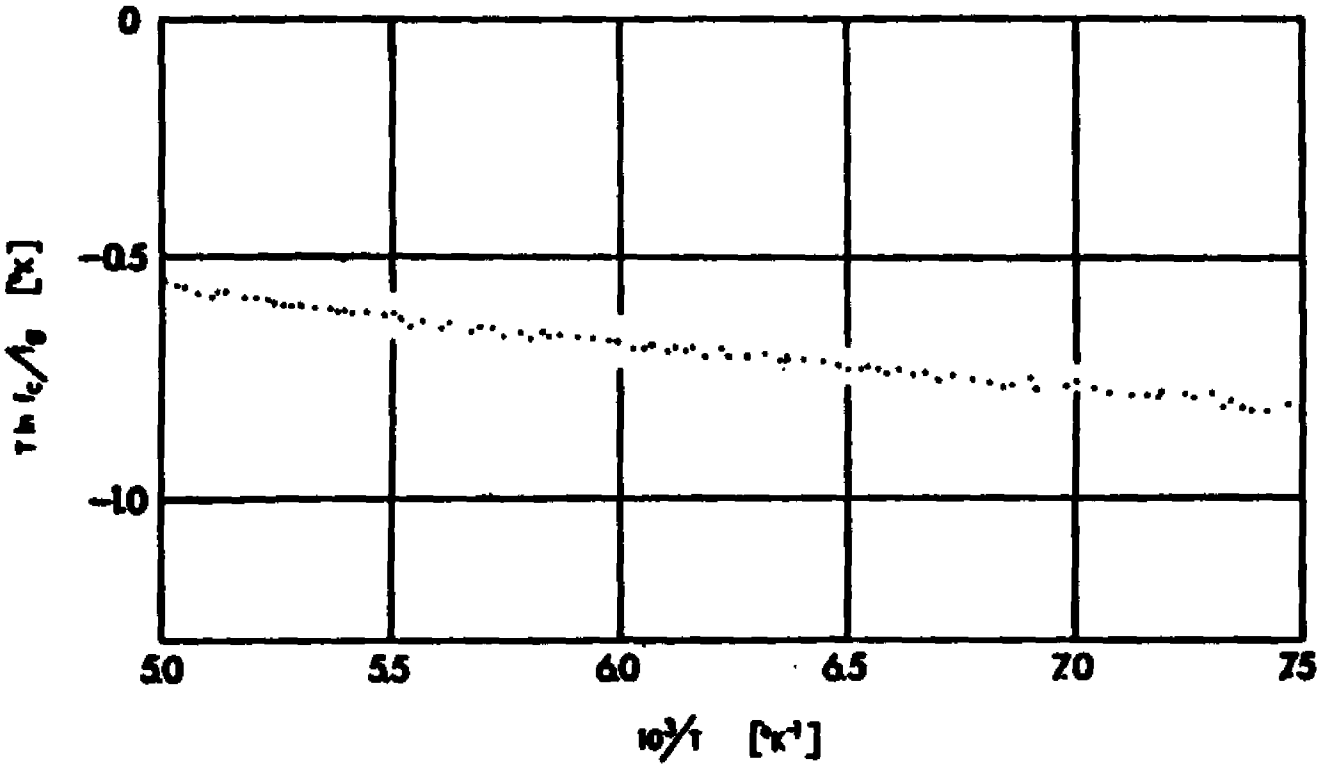

Figure 21. Corrected 12/13 Vapor Pressure Isotope Effect in Fluoroform

Table 11: Corrected Hydrogen Vapor Pressure Isotope Effect in Fluoroform

No.	T (°K)	$10^3/T$ ($°K^{-1}$)	$\ln f_c/f_g$	T $\ln f_c/f_g$ (°K)
1	126.00	7.9365	0.3606D-01	4.544
2	126.95	7.8771	0.3549D-01	4.505
3	127.84	7.8223	0.3563D-01	4.556
4	128.72	7.7688	0.3482D-01	4.482
5	129.16	7.7423	0.3735D-01	4.824
6	129.64	7.7137	0.3426D-01	4.442
7	129.97	7.6941	0.3632D-01	4.720
8	130.51	7.6622	0.3379D-01	4.409
9	131.55	7.6017	0.3341D-01	4.396
10	132.54	7.5449	0.3292D-01	4.363
11	133.01	7.5182	0.3573D-01	4.753
12	133.53	7.4890	0.3389D-01	4.526
13	133.71	7.4789	0.3422D-01	4.576
14	133.75	7.4766	0.3285D-01	4.394
15	134.15	7.4543	0.3355D-01	4.501
16	134.15	7.4543	0.3283D-01	4.404
17	134.69	7.4245	0.3369D-01	4.538
18	135.14	7.3997	0.3317D-01	4.483
19	135.17	7.3981	0.3350D-01	4.539
20	135.17	7.3981	0.3216D-01	4.347
21	135.72	7.3681	0.3429D-01	4.654
22	136.16	7.3443	0.3285D-01	4.473
23	136.17	7.3438	0.3415D-01	4.650
24	136.64	7.3185	0.3313D-01	4.527
25	136.66	7.3174	0.3209D-01	4.386
26	137.04	7.2971	0.3351D-01	4.592

[continued]

[Table 11; continued]

No.	T (°K)	$10^3/T$ ($°K^{-1}$)	$\ln f_c/f_g$	T $\ln f_c/f_g$ (°K)
27	137.14	7.2918	0.3243D-01	4.448
28	137.66	7.2643	0.3345D-01	4.605
29	137.78	7.2579	0.3190D-01	4.396
30	138.06	7.2432	0.3288D-01	4.539
31	138.16	7.2380	0.3211D-01	4.437
32	138.32	7.2296	0.3163D-01	4.375
33	138.44	7.2233	0.3126D-01	4.328
34	138.96	7.1963	0.3145D-01	4.370
35	139.06	7.1911	0.3230D-01	4.492
36	139.16	7.1860	0.3096D-01	4.308
37	139.18	7.1849	0.3275D-01	4.559
38	139.65	7.1608	0.3103D-01	4.333
39	139.75	7.1556	0.3200D-01	4.472
40	140.13	7.1362	0.3111D-01	4.359
41	140.15	7.1352	0.3046D-01	4.269
42	140.43	7.1210	0.3171D-01	4.453
43	140.79	7.1028	0.3155D-01	4.442
44	140.84	7.1003	0.3082D-01	4.340
45	141.15	7.0847	0.3056D-01	4.313
46	141.27	7.0786	0.3142D-01	4.439
47	141.41	7.0716	0.3074D-01	4.347
48	142.05	7.0398	0.3117D-01	4.428
49	142.17	7.0338	0.3069D-01	4.363
50	142.17	7.0338	0.2991D-01	4.252
51	142.53	7.0161	0.3034D-01	4.324
52	142.64	7.0107	0.3029D-01	4.321

[continued]

[Table 11; continued]

No.	T (°K)	$10^3/T$ ($°K^{-1}$)	$\ln f_c/f_g$	T $\ln f_c/f_g$ (°K)
53	143.02	6.9920	0.3110D-01	4.447
54	143.14	6.9862	0.3014D-01	4.314
55	143.24	6.9813	0.3062D-01	4.384
56	143.64	6.9618	0.3026D-01	4.346
57	143.74	6.9570	0.3016D-01	4.336
58	144.14	6.9377	0.2988D-01	4.306
59	144.64	6.9137	0.3052D-01	4.415
60	144.95	6.8989	0.3008D-01	4.360
61	144.98	6.8975	0.2983D-01	4.325
62	145.14	6.8899	0.2978D-01	4.322
63	145.14	6.8899	0.2952D-01	4.285
64	145.76	6.8606	0.2980D-01	4.344
65	146.13	6.8432	0.2985D-01	4.362
66	146.14	6.8428	0.2990D-01	4.369
67	146.14	6.8428	0.2915D-01	4.260
68	146.55	6.8236	0.2940D-01	4.308
69	146.64	6.8194	0.2948D-01	4.322
70	146.69	6.8171	0.2939D-01	4.311
71	147.15	6.7958	0.2879D-01	4.236
72	147.17	6.7949	0.2877D-01	4.234
73	147.43	6.7829	0.2923D-01	4.309
74	147.55	6.7774	0.2901D-01	4.280
75	147.60	6.7751	0.2889D-01	4.265
76	147.65	6.7728	0.2924D-01	4.317
77	148.15	6.7499	0.2850D-01	4.222
78	148.43	6.7372	0.2870D-01	4.260

[continued]

[Table 11; continued]

No.	T (°K)	$10^3/T$ ($°K^{-1}$)	$\ln f_c/f_g$	T $\ln f_c/f_g$ (°K)
79	148.56	6.7313	0.2885D-01	4.286
80	148.76	6.7222	0.2862D-01	4.258
81	149.15	6.7047	0.2823D-01	4.210
82	149.16	6.7042	0.2871D-01	4.282
83	149.16	6.7042	0.2873D-01	4.285
84	149.44	6.6916	0.2842D-01	4.248
85	149.94	6.6693	0.2839D-01	4.256
86	149.96	6.6684	0.2826D-01	4.238
87	150.15	6.6600	0.2798D-01	4.201
88	150.44	6.6472	0.2817D-01	4.237
89	150.64	6.6383	0.2828D-01	4.259
90	150.65	6.6379	0.2821D-01	4.250
91	151.13	6.6168	0.2800D-01	4.231
92	151.13	6.6168	0.2788D-01	4.214
93	151.16	6.6155	0.2769D-01	4.186
94	151.44	6.6033	0.2788D-01	4.222
95	151.94	6.5815	0.2762D-01	4.196
96	152.16	6.5720	0.2743D-01	4.174
97	152.18	6.5712	0.2769D-01	4.214
98	152.35	6.5638	0.2750D-01	4.189
99	152.47	6.5587	0.2755D-01	4.201
100	152.66	6.5505	0.2756D-01	4.208
101	152.66	6.5505	0.2742D-01	4.185
102	153.12	6.5308	0.2732D-01	4.184
103	153.14	6.5300	0.2715D-01	4.158
104	153.16	6.5291	0.2725D-01	4.174

[continued]

[Table 11; continued]

No.	T (°K)	$10^3/T$ ($°K^{-1}$)	$\ln f_c/f_g$	$T \ln f_c/f_g$ (°K)
105	153.55	6.5125	0.2714D-01	4.168
106	153.67	6.5075	0.2728D-01	4.192
107	154.17	6.4863	0.2700D-01	4.162
108	154.36	6.4784	0.2695D-01	4.160
109	154.65	6.4662	0.2704D-01	4.181
110	154.77	6.4612	0.2679D-01	4.146
111	155.15	6.4454	0.2674D-01	4.149
112	155.15	6.4454	0.2671D-01	4.144
113	155.65	6.4247	0.2680D-01	4.172
114	155.94	6.4127	0.2645D-01	4.124
115	155.95	6.4123	0.2669D-01	4.163
116	156.16	6.4037	0.2646D-01	4.132
117	156.16	6.4037	0.2641D-01	4.124
118	157.12	6.3646	0.2635D-01	4.140
119	157.14	6.3638	0.2613D-01	4.106
120	157.16	6.3629	0.2622D-01	4.121
121	157.16	6.3629	0.2613D-01	4.106
122	157.24	6.3597	0.2632D-01	4.139
123	157.43	6.3520	0.2616D-01	4.119
124	157.62	6.3444	0.2622D-01	4.133
125	158.15	6.3231	0.2585D-01	4.089
126	158.17	6.3223	0.2594D-01	4.103
127	158.34	6.3155	0.2577D-01	4.081
128	158.67	6.3024	0.2603D-01	4.130
129	158.95	6.2913	0.2587D-01	4.112
130	159.15	6.2834	0.2557D-01	4.070

[continued]

[Table 11; continued]

No.	T (°K)	$10^3/T$ ($°K^{-1}$)	$\ln f_c/f_g$	T $\ln f_c/f_g$ (°K)
131	159.23	6.2802	0.2566D-01	4.086
132	159.31	6.2771	0.2567D-01	4.089
133	159.54	6.2680	0.2547D-01	4.064
134	160.16	6.2438	0.2556D-01	4.093
135	160.19	6.2426	0.2552D-01	4.088
136	160.26	6.2399	0.2536D-01	4.065
137	160.74	6.2212	0.2514D-01	4.041
138	160.74	6.2212	0.2529D-01	4.065
139	161.55	6.1900	0.2502D-01	4.042
140	161.68	6.1851	0.2510D-01	4.058
141	161.79	6.1843	0.2489D-01	4.025
142	161.94	6.1751	0.2483D-01	4.021
143	162.07	6.1702	0.2493D-01	4.040
144	162.13	6.1679	0.2484D-01	4.028
145	162.64	6.1485	0.2455D-01	3.993
146	162.94	6.1372	0.2456D-01	4.001
147	163.12	6.1305	0.2469D-01	4.027
148	163.17	6.1286	0.2453D-01	4.002
149	163.26	6.1252	0.2462D-01	4.019
150	163.66	6.1102	0.2430D-01	3.977
151	163.95	6.0994	0.2439D-01	4.000
152	164.15	6.0920	0.2424D-01	3.979
153	164.36	6.0842	0.2430D-01	3.994
154	164.75	6.0698	0.2413D-01	3.976
155	164.75	6.0698	0.2425D-01	3.995
156	165.14	6.0555	0.2419D-01	3.995

[continued]

[Table 11; continued]

No.	T (°K)	$10^3/T$ ($°K^{-1}$)	$\ln f_c/f_g$	T $\ln f_c/f_g$ (°K)
157	165.16	6.0547	0.2398D-01	3.961
158	165.36	6.0474	0.2394D-01	3.959
159	165.57	6.0397	0.2400D-01	3.973
160	165.86	6.0292	0.2385D-01	3.956
161	166.12	6.0197	0.2395D-01	3.978
162	166.15	6.0187	0.2379D-01	3.952
163	166.27	6.0143	0.2385D-01	3.965
164	166.56	6.0038	0.2364D-01	3.937
165	166.65	6.0006	0.2375D-01	3.957
166	166.75	5.9970	0.2362D-01	3.939
167	166.79	5.9956	0.2368D-01	3.950
168	167.14	5.9830	0.2350D-01	3.927
169	167.50	5.9701	0.2343D-01	3.924
170	167.76	5.9609	0.2334D-01	3.916
171	167.86	5.9573	0.2344D-01	3.935
172	167.97	5.9534	0.2343D-01	3.935
173	168.15	5.9471	0.2327D-01	3.913
174	168.73	5.9266	0.2310D-01	3.898
175	169.09	5.9140	0.2312D-01	3.909
176	169.14	5.9123	0.2301D-01	3.892
177	169.19	5.9105	0.2307D-01	3.903
178	169.45	5.9014	0.2303D-01	3.903
179	169.96	5.8837	0.2279D-01	3.873
180	170.36	5.8699	0.2275D-01	3.875
181	170.44	5.8672	0.2271D-01	3.870
182	171.04	5.8466	0.2264D-01	3.872

[continued]

[Table 11; continued]

No.	T (°K)	$10^3/T$ ($°K^{-1}$)	$\ln f_c/f_g$	T $\ln f_c/f_g$ (°K)
183	171.14	5.8432	0.2251D-01	3.852
184	171.16	5.8425	0.2255D-01	3.860
185	171.55	5.8292	0.2244D-01	3.850
186	171.65	5.8258	0.2242D-01	3.848
187	172.10	5.8079	0.2233D-01	3.845
188	172.37	5.8015	0.2220D-01	3.826
189	172.76	5.7884	0.2221D-01	3.836
190	172.76	5.7884	0.2215D-01	3.827
191	172.85	5.7854	0.2213D-01	3.825
192	173.56	5.7617	0.2192D-01	3.804
193	173.94	5.7491	0.2187D-01	3.804
194	174.04	5.7458	0.2189D-01	3.810
195	174.16	5.7418	0.2184D-01	3.804
196	174.45	5.7323	0.2179D-01	3.801
197	174.64	5.7261	0.2171D-01	3.792
198	174.74	5.7228	0.2164D-01	3.781
199	175.15	5.7094	0.2158D-01	3.780
200	175.64	5.6935	0.2148D-01	3.773
201	175.66	5.6928	0.2149D-01	3.774
202	175.95	5.6834	0.2136D-01	3.759
203	176.14	5.6773	0.2138D-01	3.766
204	176.17	5.6763	0.2140D-01	3.770
205	176.36	5.6702	0.2130D-01	3.757
206	177.16	5.6446	0.2108D-01	3.735
207	177.53	5.6329	0.2106D-01	3.738
208	177.55	5.6322	0.2104D-01	3.736

[continued]

[Table 11; continued]

No.	T (°K)	$10^3/T$ ($°K^{-1}$)	$\ln f_c/f_g$	T $\ln f_c/f_g$ (°K)
209	177.84	5.6230	0.2098D-01	3.731
210	178.13	5.6139	0.2093D-01	3.729
211	178.23	5.6107	0.2091D-01	3.727
212	178.44	5.6041	0.2082D-01	3.714
213	178.76	5.5941	0.2076D-01	3.712
214	179.54	5.5698	0.2060D-01	3.699
215	179.56	5.5692	0.2060D-01	3.699
216	179.61	5.5676	0.2057D-01	3.694
217	179.75	5.5633	0.2050D-01	3.686
218	179.95	5.5571	0.2050D-01	3.689
219	180.14	5.5512	0.2049D-01	3.691
220	180.94	5.5267	0.2029D-01	3.671
221	181.05	5.5233	0.2021D-01	3.660
222	181.13	5.5209	0.2026D-01	3.670
223	181.16	5.5200	0.2023D-01	3.665
224	181.25	5.5172	0.2022D-01	3.665
225	181.64	5.5054	0.2020D-01	3.669
226	181.67	5.5045	0.2011D-01	3.654
227	182.30	5.4855	0.1999D-01	3.645
228	182.35	5.4840	0.1993D-01	3.634
229	182.35	5.4840	0.1996D-01	3.640
230	182.95	5.4660	0.1984D-01	3.630
231	183.56	5.4478	0.1971D-01	3.617
232	183.63	5.4457	0.1966D-01	3.611
233	183.64	5.4454	0.1977D-01	3.631
234	184.13	5.4309	0.1959D-01	3.607

[continued]

[Table 11; continued]

No.	T (°K)	$10^3/T$ ($°K^{-1}$)	$\ln f_c/f_g$	T $\ln f_c/f_g$ (°K)
235	184.50	5.4177	0.1939D-01	3.580
236	184.64	5.4159	0.1947D-01	3.595
237	184.75	5.4127	0.1946D-01	3.595
238	184.97	5.4063	0.1941D-01	3.590
239	185.21	5.3993	0.1941D-01	3.596
240	185.62	5.3874	0.1934D-01	3.589
241	185.94	5.3781	0.1922D-01	3.573
242	186.06	5.3746	0.1922D-01	3.576
243	186.26	5.3688	0.1912D-01	3.561
244	186.35	5.3662	0.1912D-01	3.563
245	187.13	5.3439	0.1896D-01	3.548
246	187.14	5.3436	0.1894D-01	3.544
247	187.14	5.3436	0.1896D-01	3.547
248	187.54	5.3322	0.1885D-01	3.536
249	187.63	5.3296	0.1890D-01	3.546
250	188.13	5.3155	0.1874D-01	3.526
251	188.35	5.3093	0.1869D-01	3.521
252	188.62	5.3017	0.1868D-01	3.524
253	188.86	5.2949	0.1857D-01	3.506
254	189.22	5.2849	0.1855D-01	3.510
255	189.65	5.2729	0.1840D-01	3.489
256	189.66	5.2726	0.1846D-01	3.502
257	189.93	5.2651	0.1835D-01	3.484
258	190.15	5.2590	0.1829D-01	3.478
259	190.54	5.2482	0.1822D-01	3.472
260	191.15	5.2315	0.1809D-01	3.458

[continued]

[Table 11; continued]

No.	T (°K)	$10^3/T$ ($°K^{-1}$)	$\ln f_c/f_g$	$T \ln f_c/f_g$ (°K)
261	191.24	5.2290	0.1814D-01	3.470
262	191.44	5.2236	0.1801D-01	3.449
263	191.63	5.2184	0.1799D-01	3.447
264	191.67	5.2173	0.1799D-01	3.449
265	192.05	5.2070	0.1796D-01	3.449
266	192.15	5.2043	0.1788D-01	3.436
267	193.02	5.1808	0.1771D-01	3.417
268	193.12	5.1781	0.1769D-01	3.417
269	193.14	5.1776	0.1770D-01	3.419
270	193.63	5.1645	0.1756D-01	3.399
271	194.24	5.1483	0.1756D-01	3.411
272	194.63	5.1380	0.1740D-01	3.386
273	195.12	5.1251	0.1736D-01	3.387
274	195.12	5.1251	0.1731D-01	3.377
275	195.14	5.1245	0.1730D-01	3.377
276	195.65	5.1112	0.1708D-01	3.342
277	196.02	5.1015	0.1704D-01	3.339
278	197.05	5.0749	0.1690D-01	3.330
279	197.12	5.0731	0.1693D-01	3.338
280	197.15	5.0723	0.1691D-01	3.334
281	197.15	5.0723	0.1693D-01	3.337
282	197.66	5.0592	0.1673D-01	3.306
283	198.10	5.0480	0.1665D-01	3.298
284	198.64	5.0342	0.1663D-01	3.303
285	199.15	5.0213	0.1655D-01	3.297
286	199.61	5.0098	0.1631D-01	3.256

[continued]

[Table 11; continued]

No.	T (°K)	$10^3/T$ (°K-1)	$\ln f_c/f_g$	T $\ln f_c/f_g$ (°K)
287	199.66	5.0085	0.1634D-01	3.263
288	200.15	4.9963	0.1638D-01	3.279
289	201.15	4.9714	0.1619D-01	3.256
290	203.14	4.9227	0.1590D-01	3.231
291	203.17	4.9220	0.1577D-01	3.204
292	205.14	4.8747	0.1537D-01	3.153
293	207.13	4.8279	0.1489D-01	3.083
294	212.16	4.7134	0.1388D-01	2.945

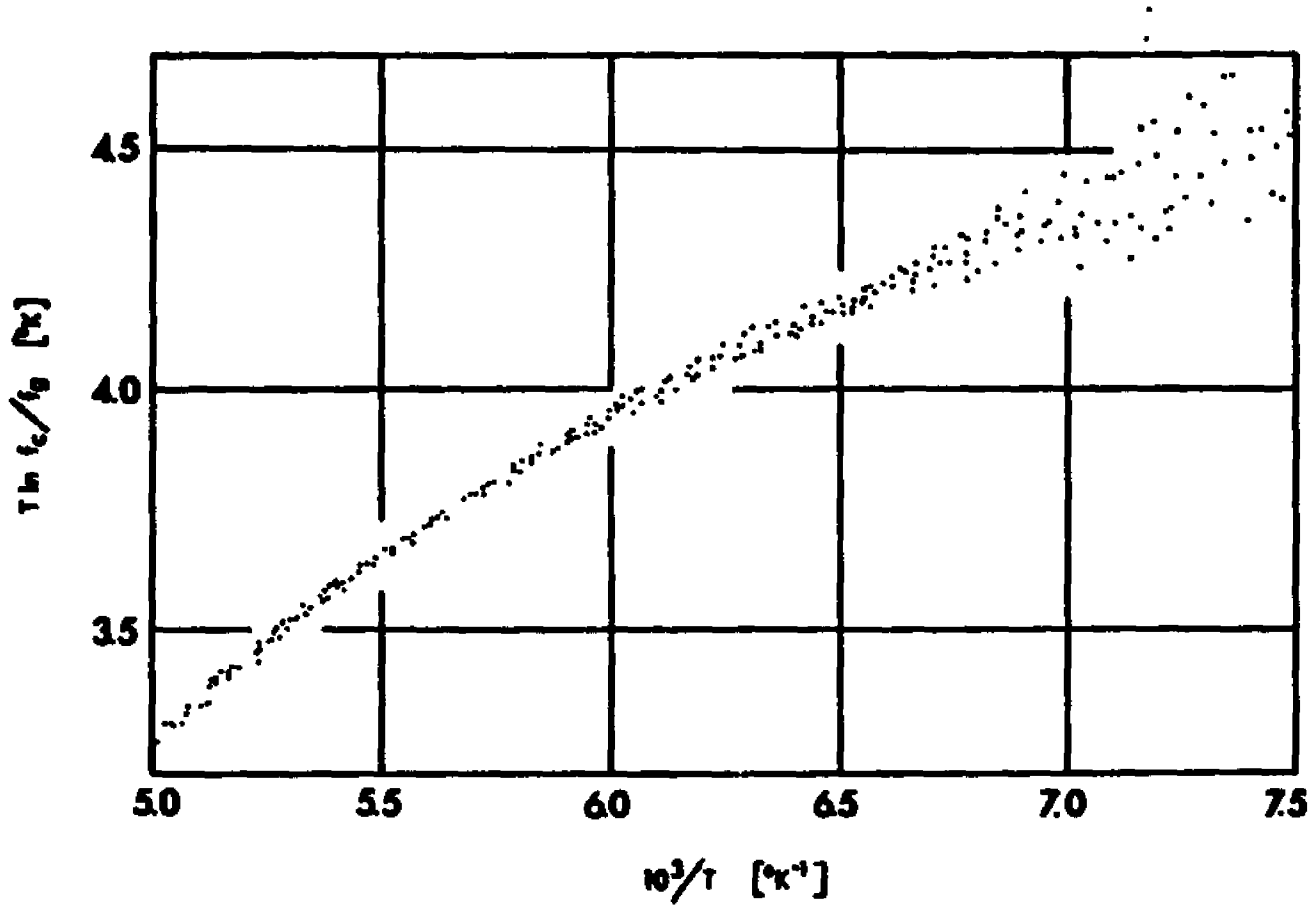

Figure 22. Corrected H/D Vapor Pressure Isotope Effect in Fluoroform

VI. DISCUSSION

Referring to Figures 22 and 21 for the D/H and 12/13 VPIE in fluoroform, respectively, the following observations can be made:

1. The H/D effect is normal in that its magnitude and slope ($\Delta(T \ln f_c/f_g)/\Delta(1/T)$) are positive, and

2. The 12/13 effect is inverse with a slope ($\Delta(T \ln f_c/f_g)/\Delta(1/T)$) that is negative.

The 12/13 VPIE measured compares reasonably well with the distillation results, on natural abundance ^{13}C-fluoroform, of Borodinsky, et. al.[12] (cf. Figure 23). Any discrepancy in results can be attributed to problems associated with the distillation technique. Also for qualitative comparison, the H/D VPIE(---) and 12/13 VPIE(——) for methane,[3] methyl fluoride[32] and fluoroform are shown in a simplified plot in Figure 24. Unfortunately there is no available experimental VPIE data for difluoromethane and carbon tetrafluoride to complete the $CH_X F_{4-X}$ series. But considering these three species, the following points are of interest:

1. The D/H effect in methane is inverse whereas it is normal in fluoroform and methyl fluoride,

2. The 12/13 effect in methane is normal as opposed to the inverse effects observed in fluoroform and methyl fluoride, and

3. The 12/13 VPIE in fluoroform exhibits a negative slope ($\Delta(T \ln f_c/f_g)/\Delta(1/T)$) whereas methane and methyl fluoride have positive slopes for both the D/H VPIE and the 12/13 VPIE.

The observed VPIE in fluoroform will be discussed in light of the experimentally observed blue-shifting C-H stretching frequency and proposed intermolecular association in the liquid phase.

VIa. Vibrational Analysis

As was discussed earlier (Section I), the VPIE data can be used to provide insight on the condensed phase, and specifically the liquid phase of fluoroform. From experimental spectroscopic data on the gas and liquid phase, the VPIE for fluoroform can be calculated and compared to the observed experimental VPIE results. The liquid force field can be modified until an appropriate fit is made. This vibrational problem consists of solving a 3N-6 x 3N-6 vibrational secular equation for the gas phase and a 3N x 3N secular equation for the liquid phase. Within the framework of the Simple Cell Model, Harmonic Oscillator and Born-Oppenheimer approximations, this problem can be treated by standard methods of normal coordinate analysis. The Wilson F-G matrix procedure[33] provides a mathematical tool for the vibrational analysis and computer programs for performing such calculations on high speed machines have been developed by Schachtschneider and Snyder.[34] There are two programs, the first calculates the $\underset{\sim}{G}$ matrix for each isotopic molecule which is given once the molecular geometry, orientation and masses are fixed, and the second program uses these $\underset{\sim}{G}$ matrices with the isotope independent force constant matrix, $\underset{\sim}{F}$, to solve the secular equation

$$|\underset{\sim}{FG} - \lambda \underset{\sim}{I}| = 0 \,, \qquad \text{VI-(1)}$$

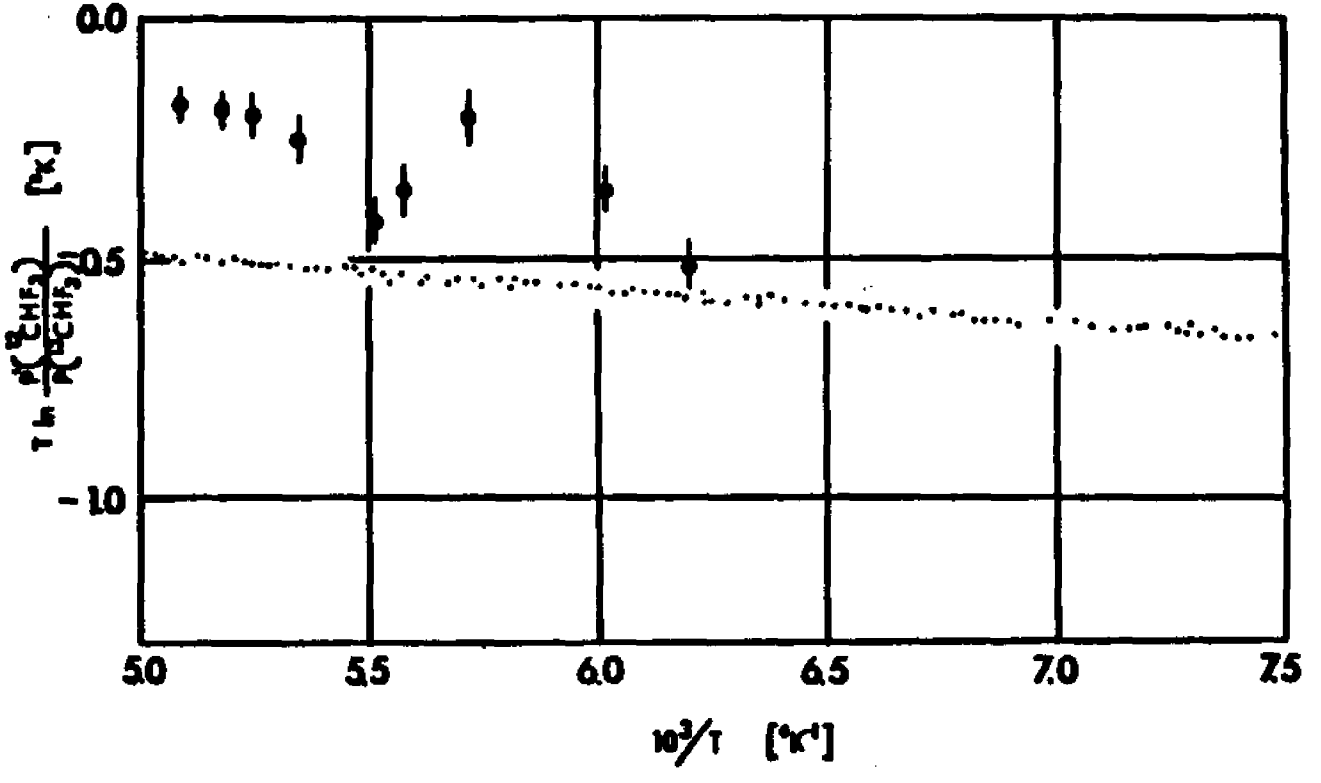

Figure 23. $^{12}C/^{13}C$ Vapor Pressure Isotope Effects from Differential Manometric and Distillation $^{12}(\phi)$ Measurements

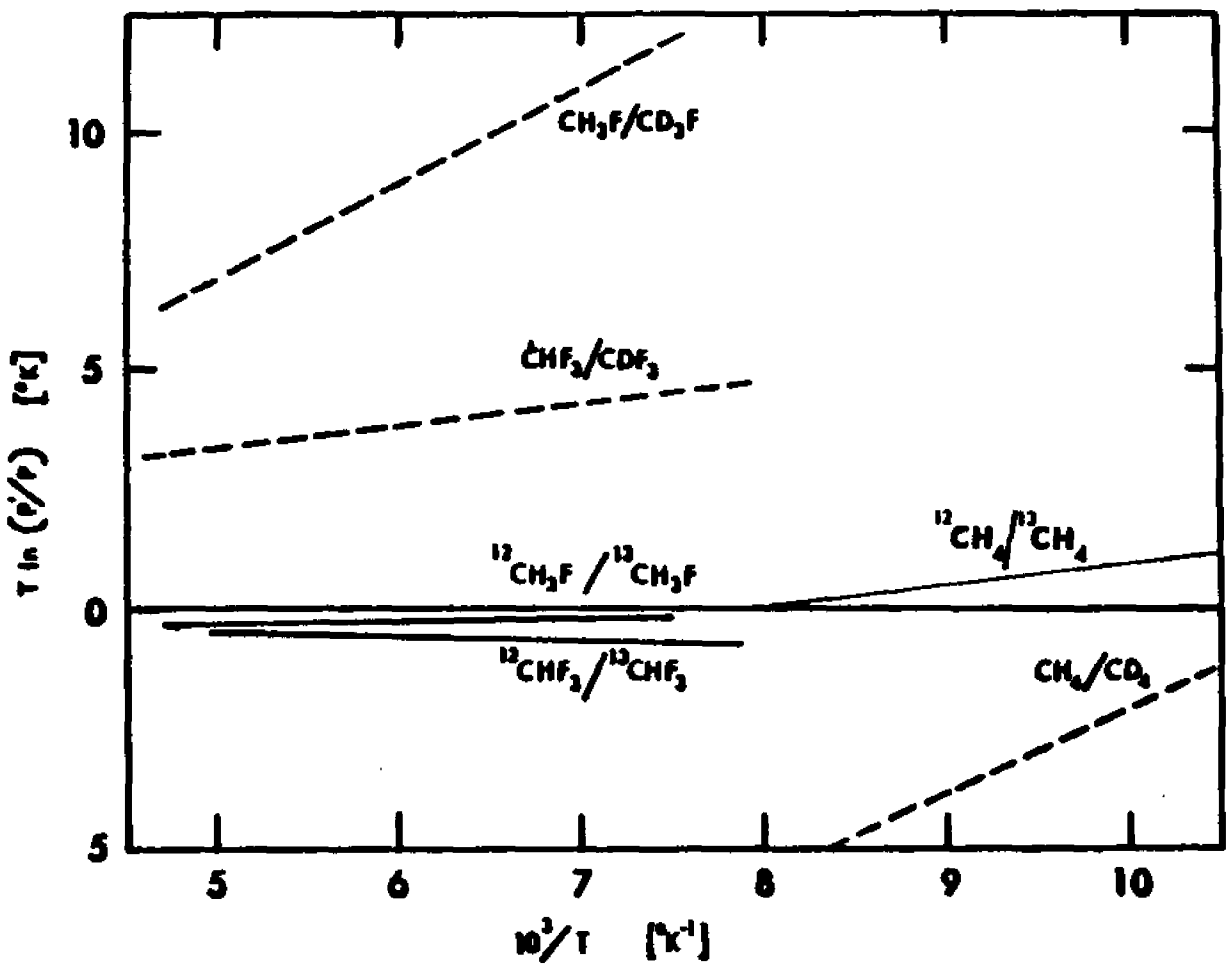

Figure 24. Comparison of Vapor Pressure Isotope Effects in Methane, Methyl Fluoride and Fluoroform

where $\underset{\sim}{I}$ is the identity matrix and λ is the eigenvalue. The vibration frequency is obtained directly from

$$\lambda_i = 4\pi^2 \nu_i^2 \qquad \text{VI-(2)}$$

The second program, which solves the secular equation, was modified by Bigeleisen and Ishida to calculate the reduced partition function ratio, as defined in equation I-(12), as a function of temperature. The program was further modified, for this particular application, to allow for series of changes in the liquid $\underset{\sim}{F}$ matrix so that differential effects to the vibrational frequencies and VPIE could be calculated directly and appropriately tabulated. The program (P9042DQ) is listed in Appendix C.

VIb. Internal Coordinate Definition of Fluoroform

The internal coordinates and cartesian coordinates are listed in Tables 12 and 13, respectively and shown in Figure 25. The mass scale used is that based on carbon-12 (^{12}C = 12.000000 amu, ^{13}C = 13.003334 amu, H = 1.007825 amu, D = 2.0144000 amu, ^{19}F = 18.998400 amu).

Table 12

Definition of Internal Coordinates[a] for Fluoroform

Coordinate number	Definition
1	C-H stretch
2	C-F stretch
3	C-F stretch
4	C-F stretch
5	H-C-F bend[b]
6	H-C-F bend[b]
7	H-C-F bend[b]
8	F-C-F bend[b]
9	F-C-F bend[b]
10	F-C-F bend[b]

(a) Refer to Figure 25 for the schematic diagram of internal coordinates.

(b) Weighted by the C-F bond length, 1.322 Å.

Table 13

Cartesian Coordinate Definition for Fluoroform

Atom	X Coordinate	Y Coordinate	Z Coordinate
C	0.000000	0.000000	0.000000
H	0.000000	0.000000	1.098000
F_2	1.083050	0.625299	-0.458505
F_3	-1.083050	0.625299	-0.458505
F_4	0.000000	-1.250599	-0.458505

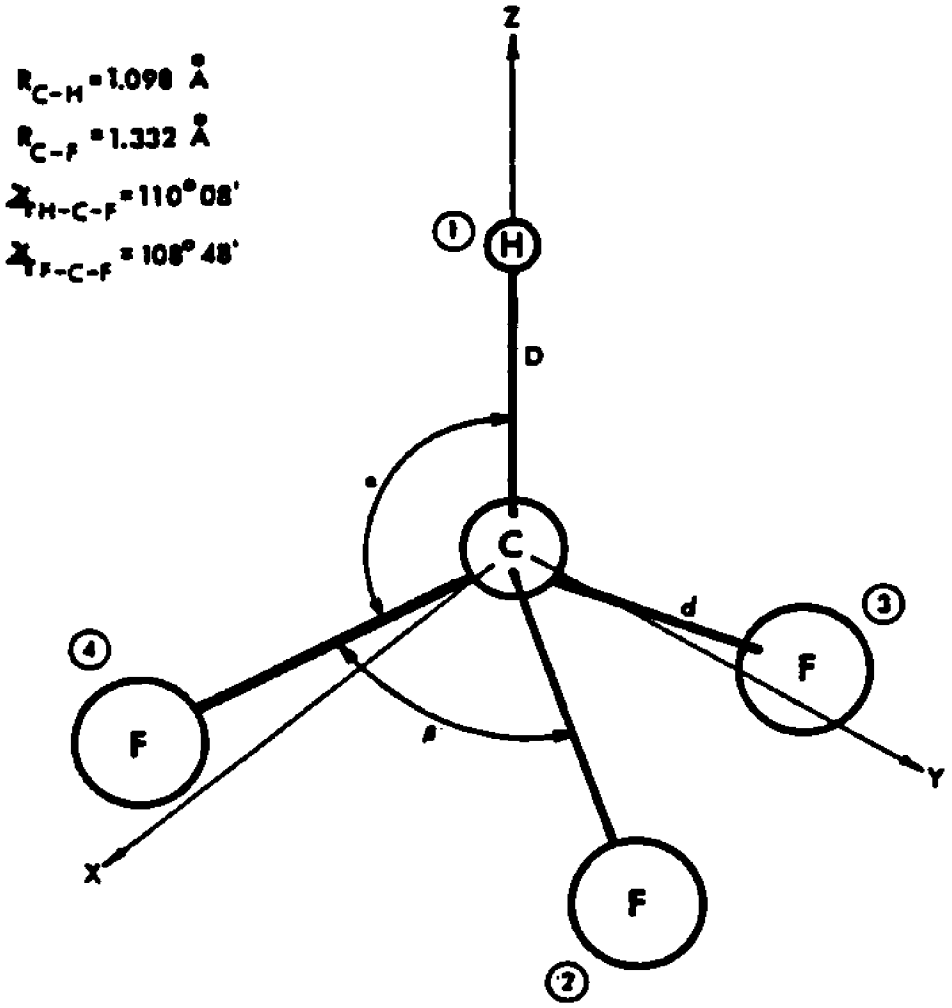

Figure 25. Internal Coordinate Definition for Fluoroform

VIc. Gas Phase $\underset{\sim}{F}$ Matrix of Fluoroform

The gas phase $\underset{\sim}{F}$ matrix used for this study is that of Borodinsky, Wick, Mayfield and Ishida.[12] The description of this force constant matrix is given in Table 14. The gas phase frequencies produced with this $\underset{\sim}{F}$ matrix are compared to that found in the literature in Table 15. As can be seen, this $\underset{\sim}{F}$ matrix agrees well with the experimentally observed frequencies and was used for this study to describe the gas phase force field of fluoroform.

Table 14

F_c Matrix of Gaseous Fluoroform[a]

Diagonals			Off-diagonals	
Description	Notation	Value (mdyne/Å)	Notation	Value (mdyne/Å)
C-H stretch	f_D	5.0000	f_{Dd}	1.1720
C-F stretch	f_d	6.0179	f_{dd}	0.7499
HCF bend	f_α	0.4913	$f_{D\alpha}$	-0.1674
FCF bend	f_β	0.7646	$f_{D\beta}$	0.1674
			$f_{d\alpha}$	0.1943
			$f_{d\alpha'}$	-0.2657
			$f_{d\beta}$	0.2560
			$f_{d\beta'}$	-0.1808
			$f_{\alpha\alpha}$	0.0393
			$f_{\beta\beta}$	-0.0973
			$f_{\alpha\beta}$	-0.1517
			$f_{\alpha\beta'}$	-0.2667

[a]The internal coordinate system consists of one CH bond stretch D, three CF bond stretches d, three HCF angle bends α, and three FCF angle bends β. All bending coordinates are weighted by the equilibrium C-F bond length of 1.332 Å. An F-matrix element with one subscript is a diagonal element, and one with two subscripts is an off-diagonal element. When two off-diagonal elements are listed for a similar interaction, e.g., $f_{d\alpha}$ and $f_{d\alpha'}$, the one without a prime refers to the interaction between two coordinates which share a common C-F bond, while the line with a prime refers to the interaction between two coordinates which do not share a common C-F bond. The molecular geometry used[35]: D_0(C-H) = 1.098 Å, d_0(C-F) = 1.332 Å, α_0(H-C-F) = 110° 08', and β_0(F-C-F) = 108° 48'.

Table 15

Frequencies of Gaseous Fluoroform

Molecule	Mode	Experimental (cm^{-1}) Long[36]	Galasso[37]	D'Cunha[38]	Wilt[45]	Calculated (cm^{-1})
$^{12}CHF_3$	$\nu_1(A_1)$	3035	3031	3031	3035	3036.224
	$\nu_2(A_1)$	1137	1140	1140	1141	1138.888
	$\nu_3(A_1)$	700	700	700	693	701.408
	$\nu_4(E)$	1376	1372	1372	1377	1380.999
	$\nu_5(E)$	1152	1152	1152	1158	1151.835
	$\nu_6(E)$	508	507	507	508	507.690
$^{12}CDF_3$	$\nu_1(A_1)$	2257	2273	2257	2261	2256.455
	$\nu_2(A_1)$	1110	1109	1109	1111	1109.181
	$\nu_3(A_1)$	693	693	693	694	690.428
	$\nu_4(E)$	1210	1207	1207	1211	1205.379
	$\nu_5(E)$	977	974	974	975	973.713
	$\nu_6(E)$	502	504	504	502	500.657
$^{13}CHF_3$	$\nu_1(A_1)$				3025	3026.179
	$\nu_2(A_1)$				1116	1108.880
	$\nu_3(A_1)$				695	699.294
	$\nu_4(E)$				1368	1371.870
	$\nu_5(E)$				1132	1125.381
	$\nu_6(E)$				507	506.739

VId. Liquid Phase $\underset{\sim}{F}$ Matrix of Fluoroform

In the liquid phase there are six additional motions to consider, that is three translational and three rotational modes as well as the possible interaction of these external modes with the internal motions. The Schachtschneider-Snyder $\underset{\sim}{G}$ matrix program takes these external motions into account appropriately. The process of fitting the liquid force constant matrix is complicated by the general lack of liquid spectroscopic data, especially for low boiling compounds such as fluoroform. The experimentally observed vibrational frequencies, reported in the literature, are listed in Table 16. Note that only internal modes were measured and no data on the external motions in either the liquid or solid are available. Using these observed internal frequencies the internal part of the liquid $\underset{\sim}{F}$ matrix was adjusted until the calculated and experimental results matched. The gas phase $\underset{\sim}{F}$ matrix with translational force constants ($T_X = T_Y = T_Z = 0.01$ mdynes/Å) and rotational force constants ($R_X = R_Y = R_Z = 0.01$ mdynes-Å) added was the starting point for the fitting process. This procedure consisted of first observing the individual effect of small changes to the force constants to the vibrational modes. From this information one employs an iterative process until the calculated and observed results converge such that the modifications employed are within the accepted "common sense" limits. This was accomplished by adjusting only f_D, f_d, f_α, f_{Dd} and f_{dd}, corresponding to the C-H stretching, C-F stretching, HCF bending, CH-CF interaction and CF-CF interaction force constants, respectively. All other force constants are as per the gas. These

Table 16

Observed Frequencies of ^{12}C Liquid Fluoroform

Mode	Glockler[39] (cm^{-1})	Rank[40] (cm^{-1})
$\nu_1(A)$	3062	3062
$\nu_2(A)$	1117	1117
$\nu_3(A)$	697	697
$\nu_4(E)$	1376	1376
$\nu_5(E)$	...	1160
$\nu_6(E)$	508	508

force constants and the corresponding ones in the gas phase $\mathcal{F}$ matrix as well as the calculated and observed frequencies are given in Table 17. The increase in f_D and decrease in f_d are consistent with the observed blue and red shift of the CH and CF stretching frequencies upon condensation, respectively. The decrease in the other force constants are also reasonable in that one normally expects a general "loosening-up" of internal forces upon condensation. Thus the internal part depicts fairly well the internal motions in liquid fluoroform. Up to this point the fitting process has relied only on the observed internal frequencies as the criterion of the "goodness" of the fit. Examination of the calculated VPIE using the above internal force constants and diagonal translation (mdynes/Å) and rotational (mdynes-Å) force constants of 0.01 shows that it fails to represent the liquid force field, as a whole, adequately. A comparison of the calculated and observed VPIE is given in Table 18. As can be seen the calculated 12/13 VPIE has the wrong sign for both magnitude and slope, and the magnitude of the effect and slope for both the 12/13 VPIE and H/D VPIE are too small. This discrepancy is attributable to the inadequacy of the external field description. It is now necessary to look at the external motions as well as the internal-external interactions. Increasing the external force constants increased the magnitude of the H/D VPIE significantly and its slope to some extent, but it also made the 12/13 VPIE more positive, which is in the wrong direction. It was found necessary to use internal-external interaction force constants. The interaction force constants DT_Z, dT_Z, αT_Z and βT_Z, which describe the interaction of the indicated internal mode with translation along the Z axis, were found to have the only significant effect. This result is corroborated by the analysis of Borodinsky et. al.[12] Their results indicate the need of large internal-external force

Table 17

Comparison of Internal Force Constants for the Gas and Liquid $\underset{\sim}{F}$ Matrices of Fluoroform

	Force Constants (mdynes/Å)		Liquid Frequencies (cm^{-1})	
	Gas	Liquid[a]	Calculated	Observed
f_D	5.0000	5.0726	3062.03	3062
f_d	6.0179	5.9097	1375.65	1376
f_α	0.4913	0.4872	1159.70	1160
f_{Dd}	1.1720	1.0400	1117.46	1117
f_{dd}	0.7499	0.5650	696.84	697
all others: as per gas c.f. Table 14			507.86	508

[a] $T_X = T_Y = T_Z = 0.01$ mdynes/Å and $R_X = R_Y = R_Z = 0.01$ mdynes-Å

Table 18

Comparison of Calculated and Observed 12/13 VPIE and H/D VPIE[a] for Fluoroform

	12/13 VPIE[b] (°K)		H/D VPIE[b] (°K)	
T(°K)	Calculated	Observed	Calculated	Observed
140	0.3634	-0.79	1.7200	4.41
165	0.3522	-0.67	1.6884	4.04
190	0.3439	-0.59	1.6678	3.52

[a] F_{ζ} (liquid) defined in Table 17

[b] $T \ln f_c/f_g$

constants along the translational Z axis to force the 12/13 VPIE into the inverse region with negative slope. This is indicated even though their internal force constant description of the liquid is considerably different. Utilization of their liquid $\underset{\sim}{F}$ matrix produces a 12/13 VPIE which reproduces the observed liquid frequencies and generally reproduces the observed 12/13 VPIE but fails to reproduce the observed H/D effect. The calculated H/D VPIE using their $\underset{\sim}{F}$ (liquid) produces a H/D effect of the wrong sign in both magnitude and slope. This is understandable in light of the limited amount of experimental data that was used for fitting the $\underset{\sim}{F}$ matrix. Only the 12/13 VPIE and $^{12}CHF_3$ liquid internal frequencies were available to them. The "best" single liquid $\underset{\sim}{F}$ matrix determined in the present study, which best reproduces the observed liquid frequencies and 12/13 VPIE and H/D VPIE, is given in Table 19. Due to the lack of external frequency data the external force constants were set so as to produce external frequencies of reasonable magnitude (50-100 cm^{-1}). The 12/13 VPIE and H/D VPIE generated by using this liquid $\underset{\sim}{F}$ matrix, which will be defined as $\underset{\sim}{F}_\ell{}^1$, is shown in Figures 26 and 27, respectively. The solid line is the calculated result. As can be seen, it fails to reproduce the observed slopes for both effects. Eight different liquid $\underset{\sim}{F}$ matrices were tested to see if the slopes for the 12/13 and H/D effects could be increased. These trial liquid $\underset{\sim}{F}$ matrices ($\underset{\sim}{F}_\ell{}^1 \rightarrow \underset{\sim}{F}_\ell{}^8$) are described in Tables 20 and 21. Also tabulated in Table 21 are the calculated 12/13 VPIE and H/D VPIE. For comparison the experimental effects are also listed. The calculated internal and external frequencies for $\underset{\sim}{F}_\ell{}^1 \rightarrow \underset{\sim}{F}_\ell{}^8$ and the experimentally observed internal frequencies are listed in Table 22.

Table 19

$\underset{\sim}{F}$ Matrix of Liquid Fluoroform[a] (F_{ℓ}^{-1})

	Diagonals (mdyne/Å)[b]		Off-diagonals (mdyne/Å)[b]	
C-H stretch	f_D	5.0726	f_{dd}	0.5650
C-F stretch	f_d	5.9097	f_{Dd}	1.0400
HCF bend	f_α	0.4872	$f_{D\alpha}$	-0.1674
FCF bend	f_β	0.7650	$f_{D\beta}$	0.1674
			$f_{d\alpha}$	0.1943
			$f_{d\alpha'}$	-0.2657
			$f_{d\beta}$	0.0256
			$f_{d\beta'}$	-0.1808
			$f_{\alpha\alpha}$	0.0393
			$f_{\beta\beta}$	-0.0973
			$f_{\alpha\beta}$	-0.1517
	f_{T_x}	0.20	$f_{\alpha\beta'}$	0.2667
	f_{T_y}	0.20		
	f_{T_z}	0.40	f_{DT_z}	-0.73
	f_{R_x}	0.20	f_{dT_z}	0.13
	f_{R_y}	0.20	$f_{\alpha T_z}$	0.13
	f_{R_z}	0.05	$f_{\beta T_z}$	-0.13

[a]For definitions of the internal coordinates and F-matrix element notations see the footnote of Table IV.

[b]All F-matrix elements are in the units of mdyne/Å except f_R, which are in the units of mdyne Å.

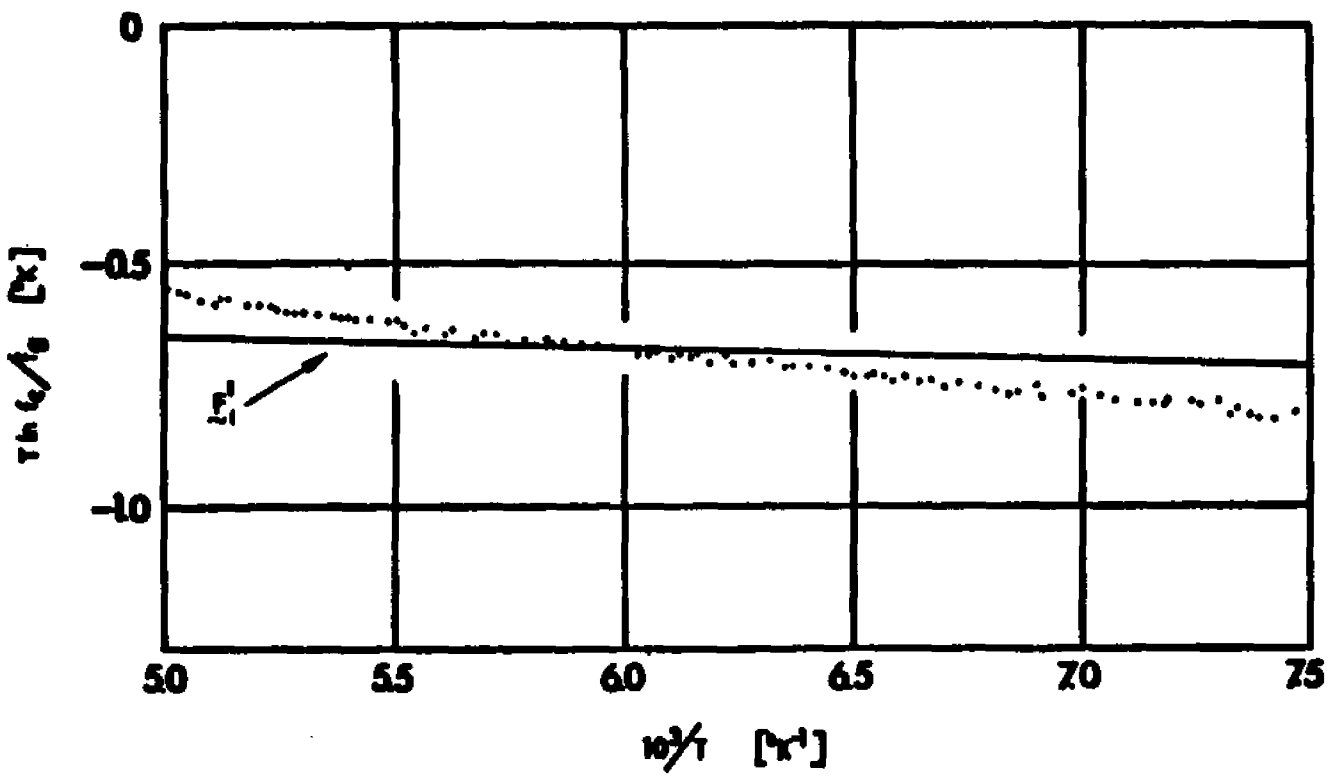

Figure 26. Comparison of Experimental and Calculated $^{12}C/^{13}C$ (——) Vapor Pressure Isotope Effects Using $F_{i\ell}^{1}$

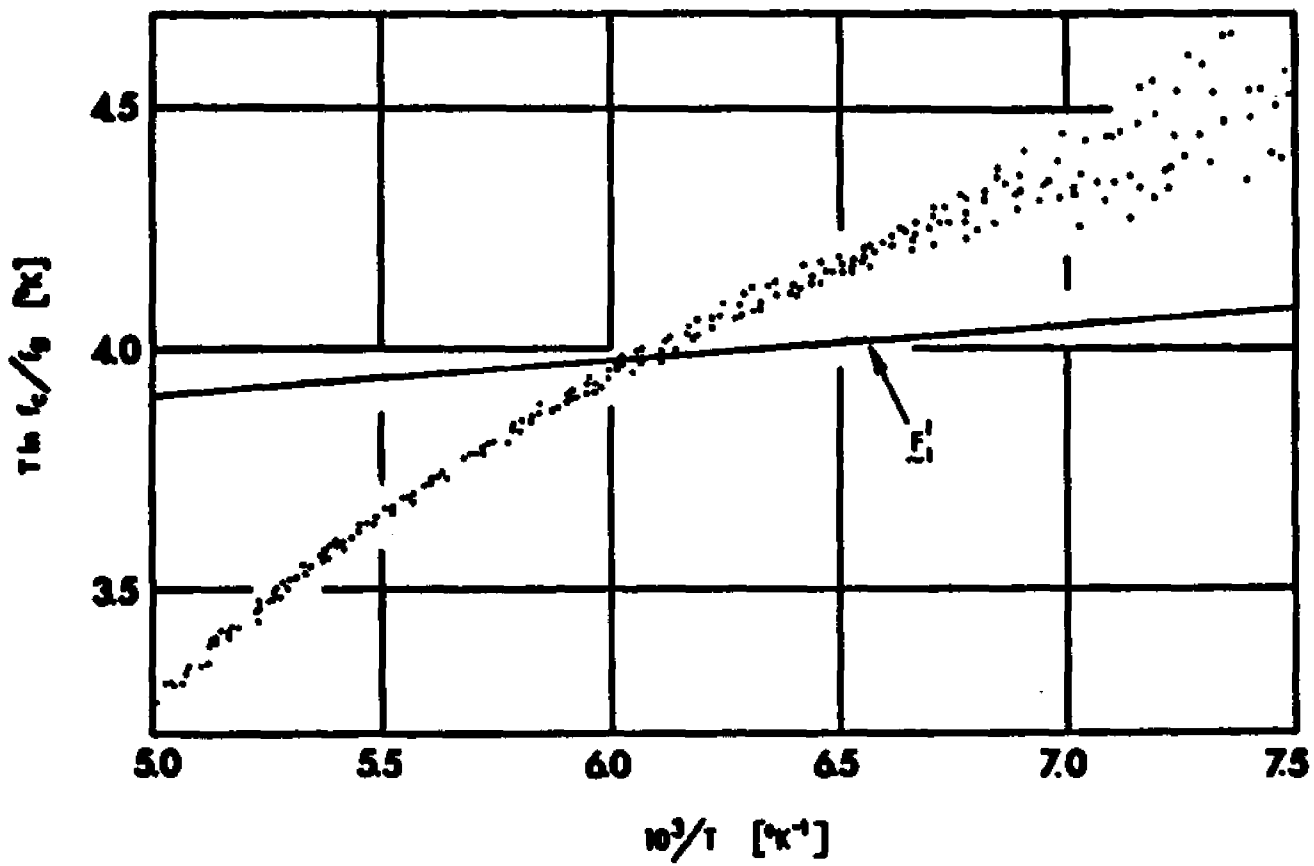

Figure 27. Comparison of Experimental and Calculated H/D (——) Vapor Pressure Isotope Effects Using F_{ℓ}^{1}

Table 20

Three Basis Sets of $\underset{\sim}{F}$ Matrix Elements for Liquid Fluoroform

f_{ij}	A	B	C
D	5.0726	5.0000	4.8147
d	5.9097	6.0179	6.2063
dd	0.5650	0.7499	0.8594
Dd	1.0400	1.1720	0.4744
Dβ	0.1674	0.1674	0.3104
Dα	-0.1674	-0.1674	-0.3104
dβ	0.0256	0.2560	0.2560
dβ'	-0.1808	-0.1808	-0.1808
dα	0.1943	0.1943	0.1943
dα'	-0.2657	-0.2657	-0.2657
β	0.7650	0.7646	0.7654
ββ	-0.0973	-0.0973	-0.0973
α	0.4872	0.4913	0.4895
αα	0.0393	0.0393	0.0413
αβ	-0.1517	0.1517	-0.1252
αβ'	-0.2667	-0.2667	-0.2402
T_x	0.20	0.01	0.30
T_y	0.20	0.01	0.30
T_z	0.40	0.01	0.30
R_x	0.20	0.01	0.10
R_y	0.20	0.01	0.10
R_z	0.05	0.01	0.10
DT_z	-0.73	0	-0.84
dT_z	0.13	0	0.84
αT_z	0.13	0	0.30
βT_z	-0.13	0	-0.30

A is $\underset{\sim}{F}_\ell{}^1$; the best single $\underset{\sim}{F}$ matrix for the liquid

B is $\underset{\sim}{F}_\ell{}^2$; internal part is as per the gas

C is $\underset{\sim}{F}_\ell{}^4$; as per reference 12

Table 21

Trial $\underset{\sim}{F}$ (Liquid) for Fluoroform

#	internal	external[a]	internal/ external	T ln f_c/f_g 12/13	T ln f_c/f_g H/D	VPIE @ 140°K - VPIE @ 190°K °K	12/13	H/D
1	A	A	A	-0.689	4.058	140		
				-0.676	3.975	165	-0.04	+0.15
				-0.658	3.912	190		
2	B	T=.01	0	0.0177	0.0225	140		
		R=.01		0.0166	0.0191	165	+0.002	+0.006
				0.0157	0.0166	190		
3	C	T=.01	0	1.903	-22.844	140		
		R=.01		1.908	-22.827	165	-0.02	-0.06
				1.917	-22.788	190		
4	C	C	C	-0.403	-20.952	140		
				-0.350	-20.944	165	-0.12	-0.05
				-0.282	-20.903	190		
5	A	C	C	-2.093	3.873	140		
				-2.052	3.820	165	-0.10	+0.09
				-1.996	3.787	190		
6	A (except C-H C-F as per ref. 12)	C	C	-0.830	-11.281	140		
				-0.788	-11.336	165	-0.10	+0.09
				-0.734	-11.370	190		
EXPERIMENTAL DATA:				-0.79	4.44	140		
				-0.67	3.97	165	-0.20	+0.95
				-0.59	3.49	190		

[continued]

[Table 21; continued]

#	internal	external[a]	internal/ external	T ln f_c/f_g 12/13	T ln f_c/f_g H/D	VPIE @ 140°K - VPIE @ 190°K °K	12/13	H/D
7	A	T_z=1.00	A	-0.357	5.248	140		
		$T_{x,y}$=0.50		-0.394	4.967	165	+0.05	+0.49
		$R_{x,y}$=1.00 R_z=0.25		-0.412	4.755	190		
8	A	T=.50	$DT_z=\beta T_z=-1.0$	-3.426	5.166	140		
		R=.50	$dT_z=\alpha T_z=1.0$	-3.457	4.984	165	+0.01	+0.30
				-3.437	4.870	190		
EXPERIMENTAL DATA:				-0.79	4.44	140		
				-0.67	3.97	165	-0.20	+0.95
				-0.59	3.49	190		

[a] T in units of mdynes/Å and R in units of mdynes-Å

Table 22

$^{12}CHF_3$ Frequencies Produced from Trial F (liquid)

	F (liq)								
	#1	#2	#3	#4	#5	#6	#7	#8	EXP.
ν_1	3063	3036	3061	3062	3063	2986	3063	3064	3062
ν_4	1376	1381	1376	1376	1376	1380	1376	1376	1376
ν_5	1160	1152	1160	1160	1160	1188	1160	1160	1160
ν_2	1118	1139	1109	1117	1127	1140	1118	1170	1117
ν_3	697	702	677	697	697	702	697	704	697
ν_6	508	508	508	508	508	509	508	508	508
X_1	83	19	19	126	142	141	187	361	-
X_2	83	19	19	85	85	85	187	132	-
X_3	70	16	16	85	85	85	138	132	-
X_4	70	16	16	59	59	59	110	110	-
X_5	67	16	16	59	59	59	110	110	-
X_6	31	14	14	44	44	44	69	98	-

Note: ν_i are the internal frequencies in cm^{-1}

X_i are the external frequencies listed in descending order (cm^{-1})

Examination of these results shows that no single liquid $\underset{\sim}{F}$ matrix can reproduce all the experimental data with a large enough slope. $\underset{\sim}{F}_{\ell}^{7}$ and $\underset{\sim}{F}_{\ell}^{8}$ generate an H/D VPIE with slopes that are within a factor of 2 and 3, respectively, of the observed effect. But the 12/13 VPIE is wrong and very large external frequencies are produced. $\underset{\sim}{F}_{\ell}^{4}$, $\underset{\sim}{F}_{\ell}^{5}$ and $\underset{\sim}{F}_{\ell}^{6}$ produce a 12/13 effect with slopes within a factor of 2 of the observed with "reasonable" external frequencies but generate H/D VPIE that are wrong. All these trial $\underset{\sim}{F}$ matrices fail to show the marked temperature dependency that is observed experimentally. It is felt that these trial $\underset{\sim}{F}$ matrices incorporate significant changes as can be seen by the swings in VPIE magnitudes, slope direction, internal and external frequencies. The failure of any one liquid $\underset{\sim}{F}$ matrix to produce the marked temperature dependency of the observed 12/13 VPIE and H/D VPIE necessitates the examination of temperature dependent force constants.

The nature of this temperature dependency is believed to be due to intermolecular association, specifically a dimer, which based on quantum mechanical calculations (Appendix A) has been termed as weak hydrogen bonding, and as such is strongly orientation dependent. That is, the hydrogen bond is linear in nature and deviation from linearity would effect the interaction energy significantly. An increase in the available thermal energy would allow for more freedom in the external modes which would affect the VPIE. With this idea in mind the T_Z and DT_Z force constants were adjusted to simulate a change in temperature and the 12/13 VPIE and H/D VPIE were subsequently calculated. The Z direction was chosen because this would be the direction of interaction of the proton with the external field. Changing T_Z (0.40 mdynes/Å) by ± 0.05 mdynes/Å in an effort to simulate the effects of a temperature

change of 165°K ± 25°K produced no significant change in the T ln f_c/f_g vs 1/T plots for either the 12/13 or H/D effects. However, changing DT_Z (-0.73 mdynes/Å) by ± .12 units produced an interesting result. It generated a result which reproduces the observed result for both effects. The results for changing T_Z and DT_Z are given in Table 23 and 24, and the DT_Z results are plotted in Figures 28 and 29 for the 12/13 VPIE and H/D VPIE, respectively. The description for the final liquid F matrix for fluoroform, $F_\ell(T)$, is given in Table 25. This temperature dependency in DT_Z also reproduces the observed internal frequencies and generates "reasonable" external frequencies. These results are given in Table 26, and the calculated frequencies for all isotopic species using $F_\ell(T)$ are in Table 27.

The fact that changing T_Z didn't produce a significant effect whereas DT_Z did is reasonable if one considers that T_Z is an indication of the interaction of the molecule as a whole, without regard to a particular orientation, with the external field in the Z direction. Whereas DT_Z is more orientation dependent in that it is the level of interaction of specifically the C-H motion with the external field along the Z-axis, the axis of the proposed hydrogen bonding (c.f. Dimer Type A, Appendix A). The observed temperature dependency is inherently coupled to this particular interaction.

Table 23

Effect of Changing f_{T_z} on 12/13 VPIE and H/D VPIE[a] for Fluoroform

T(°K)	T_z(mdynes/Å)	12/13 VPIE[a] (°K)		H/D VPIE[a] (°K)	
		Calculated	Observed	Calculated	Observed
140	0.45	-0.67	-0.79	4.07	4.44
165	0.40	-0.67	-0.67	3.97	3.97
190	0.35	-0.67	-0.59	3.91	3.49

[a] $T \ln f_c/f_g$

[b] Note F_{ℓ}^{1} used

Table 24

Effect of Changing f_{DT_z} on 12/13 VPIE[a] and H/D VPIE[a] for Fluoroform

T(°K)	DT_z(mdynes/Å)	12/13 VPIE[a] (°K)		H/D VPIE[a] (°K)	
		Calculated	Observed	Calculated	Observed
140	-0.85	-0.74	-0.79	4.47	4.44
165	-0.73	-0.67	-0.67	3.97	3.97
190	-0.60	-0.61	-0.59	3.47	3.49

[a] T ln f_c/f_g

[b] Note F_{ℓ}^{1} used

Table 25

Final $\underset{\sim}{F}$ Matrix, $\underset{\sim}{F}_{\ell}(T)$, of Liquid Fluoroform

	Diagonals (mdyne/Å)[b]		Off-diagonals (mdyne/Å)[b]	
C-H stretch	f_D	5.0726	f_{dd}	0.5650
C-F stretch	f_d	5.9097	f_{Dd}	1.0400
HCF bend	f_α	0.4872	$f_{D\alpha}$	-0.1674
FCF bend	f_β	0.7650	$f_{D\beta}$	0.1674
			$f_{d\alpha}$	0.1943
			$f_{d\alpha'}$	-0.2657
			$f_{d\beta}$	0.0256
			$f_{d\beta'}$	-0.1808
			$f_{\alpha\alpha}$	0.0393
			$f_{\beta\beta}$	-0.0973
			$f_{\alpha\beta}$	-0.1517
	f_{T_x}	0.20	$f_{\alpha\beta'}$	0.2667
	f_{T_y}	0.20		
	f_{T_z}	0.40	f_{DT_z}	$-0.73 + 5.0\times10^{-3}(T-165°K)$
	f_{R_x}	0.20	f_{dT_z}	0.13
	f_{R_y}	0.20	$f_{\alpha T_z}$	0.13
	f_{R_z}	0.05	$f_{\beta T_z}$	-0.13

[a] For definitions of the internal coordinates and F-matrix element notations see the footnote of Table IV.

[b] All F-matrix elements are in the units of mdyne/Å except f_R, which are in the units of mdyne Å.

Table 26

Calculated Internal and External Frequencies Using $F_{\ell\ell}(T)$

		Calculated Frequencies (cm^{-1}) $^{12}CHF_3$ f_{DT_z} (mdynes/Å)		
Experimental (cm^{-1}) frequencies		-0.85	-0.73	-0.60
ν_1	3062	3062.68	3062.52	3062.38
ν_4	1376	1375.65	1375.65	1375.65
ν_5	1160	1159.70	1159.70	1159.70
ν_2	1117	1118.45	1118.45	1118.45
ν_3	697	696.85	696.84	696.85
ν_6	580	507.86	507.86	507.86
T_x	-	83.4	83.4	83.4
T_y	-	83.4	83.4	83.4
T_z	-	59.0	66.8	73.1
R_x	-	69.7	69.7	69.7
R_y	-	69.7	69.7	69.7
R_z	-	30.9	30.9	30.9

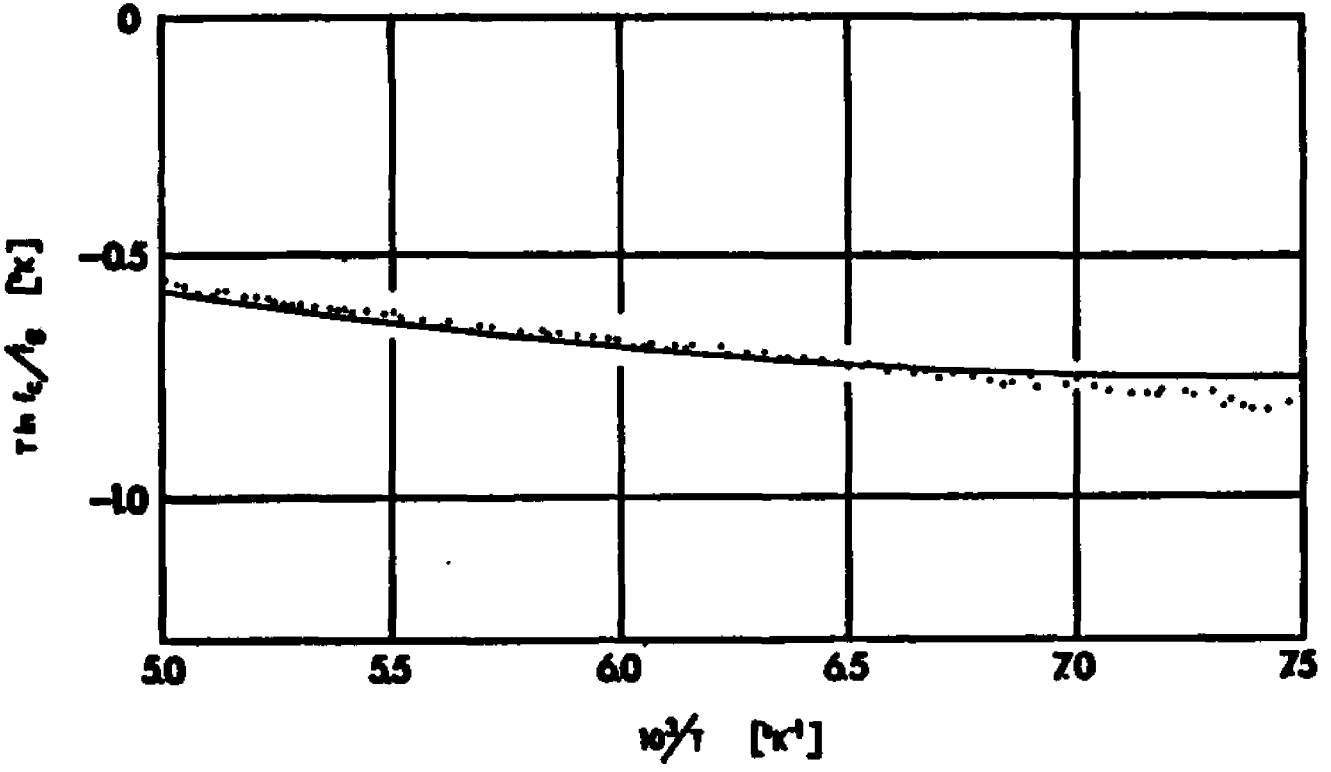

Figure 28. Comparison of Experimental and Calculated 12/13 (——) Vapor Pressure Isotope Effect Using $F_{\ell}(T)$

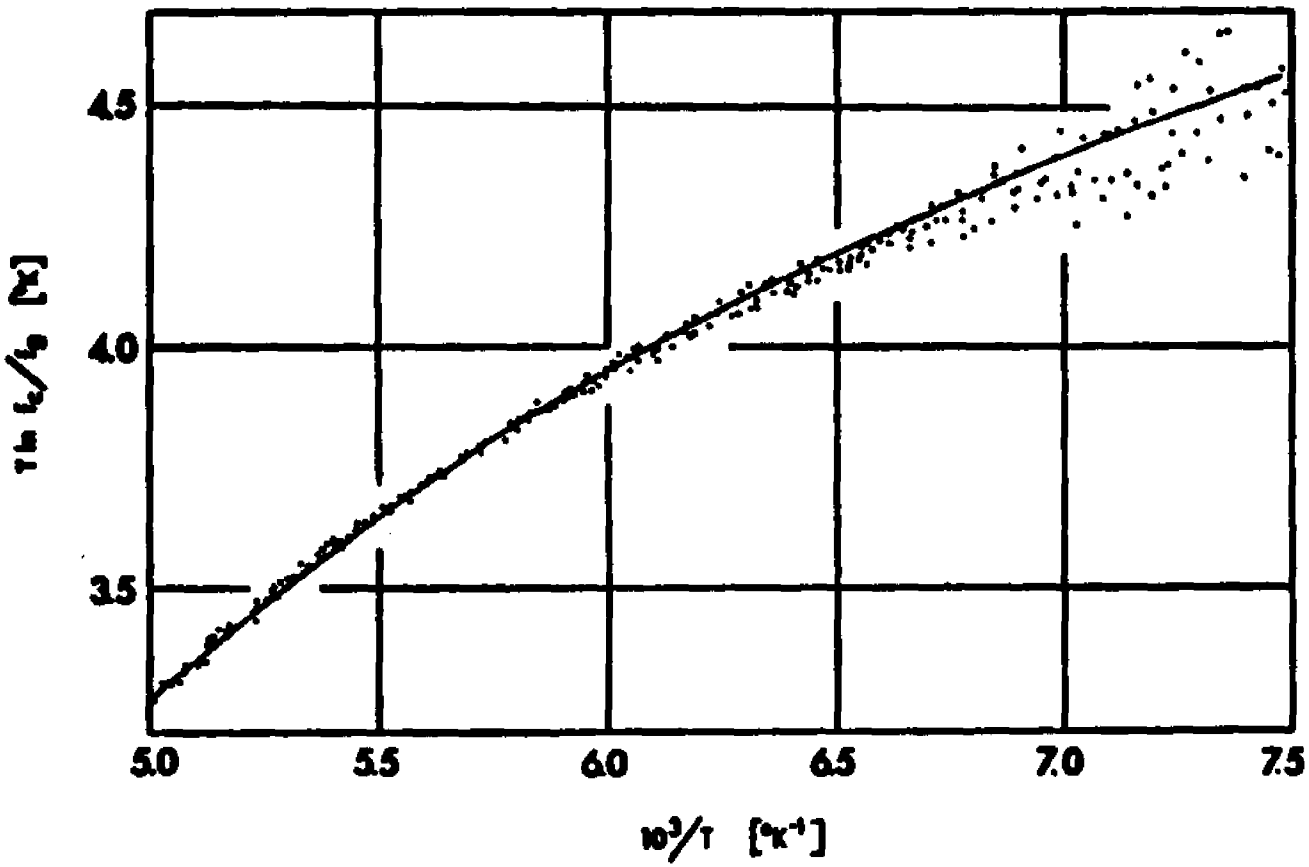

Figure 29. Comparison of Experimental and Calculated H/D (——) Vapor Pressure Isotope Effect Using $F_{\ell\ell}(T)$

Table 27

Calculated Internal and External Frequencies for Liquid Fluoroform Using $F_{\ell}(T)$ at T=165°K

	$^{12}CHF_3$ (cm^{-1})	$^{13}CHF_3$ (cm^{-1})	$^{12}CDF_3$ (cm^{-1})
ν_1	3062.52	3052.38	2274.71
ν_4	1375.65	1366.12	1211.48
ν_5	1159.70	1133.46	1086.61
ν_2	1118.45	1090.09	972.00
ν_3	696.84	695.03	687.46
ν_6	507.86	506.90	500.70
T_x	83.4	83.3	81.7
T_y	83.4	83.3	81.7
T_z	66.8	66.7	66.3
R_x	69.7	69.2	69.1
R_y	69.7	69.2	69.1
R_z	30.9	30.9	30.9

VIe. Correlation of the VPIE in Fluoroform with the Blue Shifting C-H Stretching Frequency upon Condensation and Intermolecular Hydrogen Bonding

The normal VPIE with the positive slope for the H/D effect and the inverse VPIE with the negative slope for the 12/13 effect can be simultaneously explained by a blue-shift of the C-H stretching frequency of fluoroform upon condensation. The large external-internal interaction force constants used to reproduce both the observed H/D VPIE and 12/13 VPIE are in agreement with specific, short-range intermolecular interactions such as the hydrogen bonding between the molecules of fluoroform. Figure 22 shows for the H/D VPIE a normal isotope effect at all temperatures investigated and a positive slope of the plot of Tln vs 1/T. On the other hand, Figure 21 shows for the $^{13}C/^{12}C$ substitution an inverse VPIE at all temperatures and a negative slope in the plot. How is this marked difference between two substitutions possible? In both substitutions the molecular symmetry does not change (C_{3v}). The molecular mass increases by the similar amount (by 1 amu) in both cases, so that the translational contributions to the overall T $\ln(f_c/f_g)$ is similar for both cases. The change in the principal moments of inertia in the D/H-substitution is somewhat greater for the D/H substitution than for the $^{13}C/^{12}C$ substitution, because the latter substitution is made near the center of mass of the molecule. However, the magnitude of the change even in the former is not large, because the fluoroform has three heavy (F) atoms at the peripheral positions. Thus, the rotational contribution to T $\ln(f_c/f_g)$ would not be so different between the two isotopic substitutions.

Internal vibrational contributions to T $\ln(f_c/f_g)$ may be expressed as a sum of 3N-6 independent contributions. When the temperature is not sufficiently high ($h\nu_i >> kT$), the vibrational excited states are not accessible and they do not contribute appreciably to the partition functions. These ground state contributions to T $\ln(f_c/f_g)$ are depicted in Figure 29. It is noted that the internal vibrations usually red-shift upon condensation and only in rare occasions does a vibrational frequency blue-shift upon condensation. When it does, an internal vibration contributes positively to $\ln(f_c/f_g)$. As the Boltzmann excitation sets in with an increasing temperature, the magnitude of vibrational contribution starts to decrease toward zero.

With these trends shown in Figure 30 in mind, the marked difference observed between the H/D VPIE and the 12/13 VPIE is explainable as follows. The isotope shift of the C-H stretching frequency in fluoroform is very large in the D-for-H substitution, while it is small for the ^{13}C-for-^{12}C substitution. If the C-H stretching frequency were red shifting upon condensation, its contribution to T $\ln(f_c/f_g)$ would have been that of the R2-line of Figure 30 for D/H and that of the R1-line of Figure 30 for $^{13}C/^{12}C$. Since all the other vibrational frequencies red-shift upon condensation, the sum of the "External" line and all the red-shift lines would have yielded a plot for the D/H-substitution which would lie below (more inverse than) the corresponding plot for the $^{13}C/^{12}C$-substitution. Figures 21 and 22 show otherwise. The normal VPIE with a positive slope for the D/H-effect is possible only if the contribution of the C-H stretching motion looks like the B1 or B2 line of Figure 30. Thus, for the D/H-substitution, the C-H stretching contribution is like that of the B2-line, while for the $^{13}C/^{12}C$-effect, the contribution is

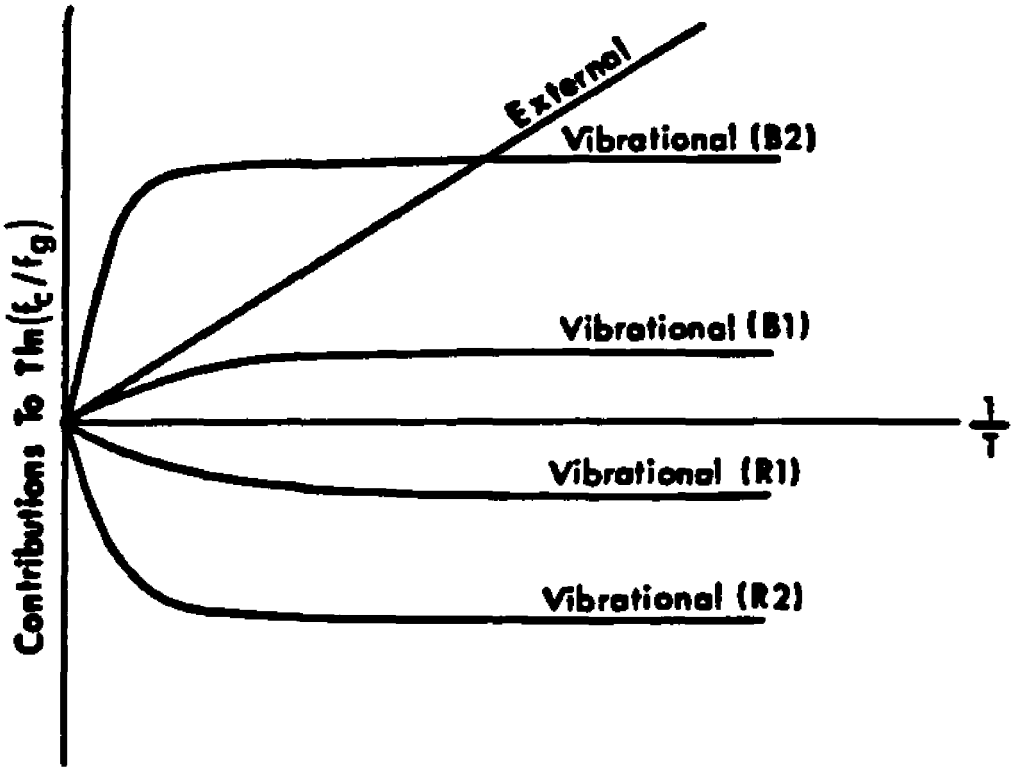

Vibrational R1: **Frequencies that red-shift upon condensation, Low frequency and/or small isotope shift**

Vibrational R2: **Frequencies that red-shift upon condensation, High frequency and/or large isotope shift**

Vibrational B1: **Frequencies that blue-shift upon condensation, Low frequency and/or small isotope shift**

Vibrational B2: **Frequencies that blue-shift upon condensation, High frequencies and/or large isotope shift**

Figure 30. Schematic Plots of Various Contributions to T ln f_c/f_g

that of the B1-line. The sum of the "External" line and B2-line thus yields a straight line with the positive slope in the positive VPIE-region when the temperatures are not sufficiently high for the Boltzmann excitation to set in for the C-H stretching mode. On the other hand, since the isotope shift upon ^{13}C-for-^{12}C substitution is so small (10 cm^{-1} for $^{13}C/^{12}C$, as compared to 780 cm^{-1} for D/H), the magnitude of its contribution to T $\ln(f_c/f_g)$ is very small (B1-line), resulting in the negative VPIE largely due to the effects of other red-shifting frequencies. The VPIE data supports the blue-shifting of the C-H stretching frequency upon condensation. But what is responsible for the blue shift upon condensation?

The possibility of hydrogen-bonding has been explored by carrying out an Ab-initio molecular orbital study using the Gaussian-70 program with an STO-3G basis set of functions (c.f. Appendix A). Several dimer configurations of fluoroform exhibited a small stabilization energy. One such stable configuration (called DT-A in Appendix A) and the energy plot of the DT-A configuration as a function of H_1-F_{21} distance are reproduced in Figures 31 and 32, respectively. Based on the linearity of the interaction and the observed charge redistribution upon bond formation, the interaction is being termed "Hydrogen Bonding".

The DT-A dimer configuration shows a stabilization energy of -0.72 kcal/mole dimer (or -0.36 kcal/mole monomer) with the equilibrium H···F distance of 2.34 Å, corresponding to the carbon-to-carbon intermolecular separation of 4.83 Å. These are in fair agreement with a published[41] Lennard-Jones' 12-6 potential constants ϵ = 0.391 kcal/mole and σ = 4.26 Å, the latter being obtained from the second virial coefficient of gaseous CHF_3. These equilibrium intermolecular separations are also in surprisingly good agreement with the molecular volume data: At -95°C (178°K), the molar volume of liquid fluoroform[42] is 25.33 ml/mole, the

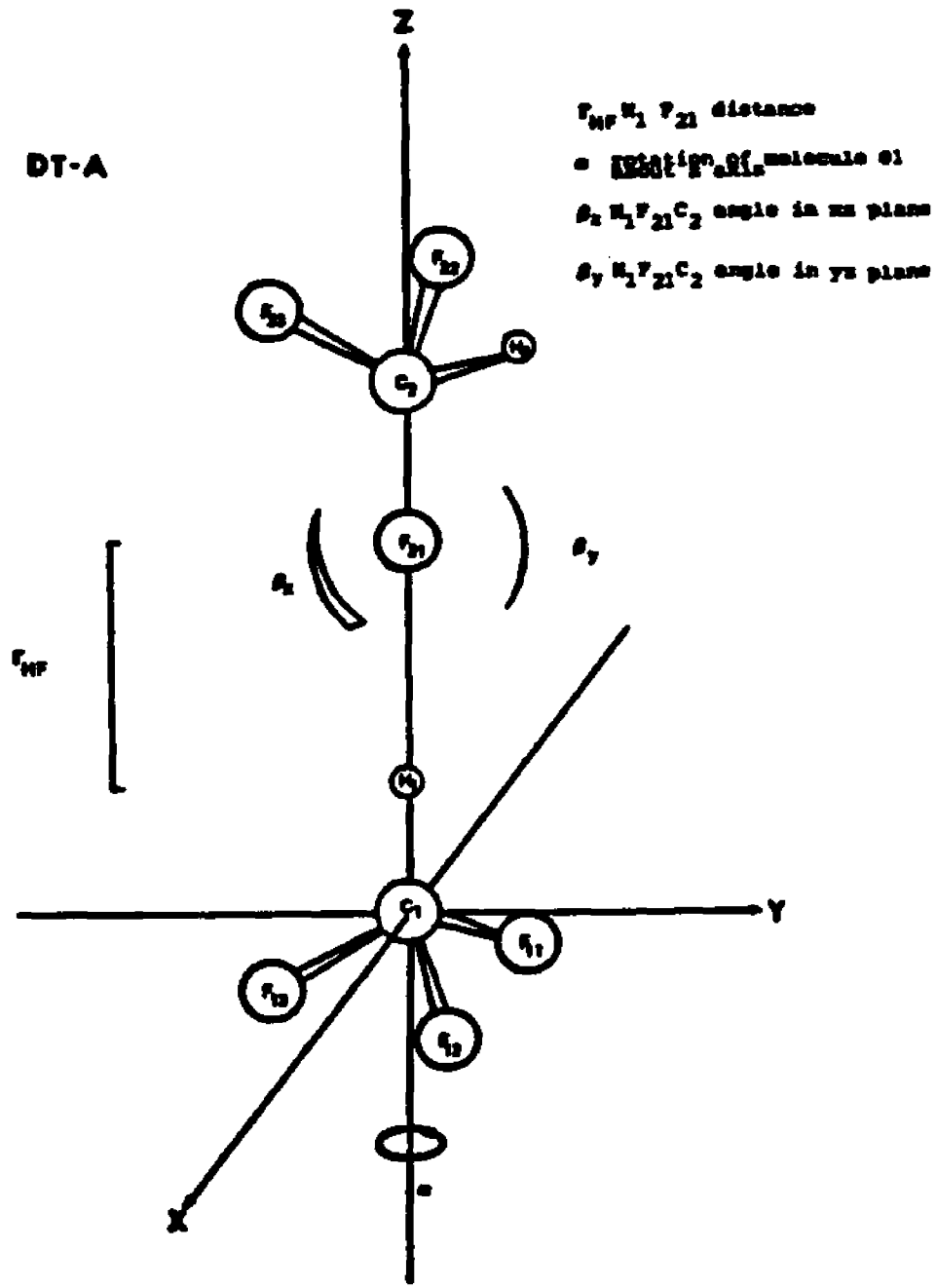

Figure 31. Dimer Type A (DT-A) Configuration of Fluoroform

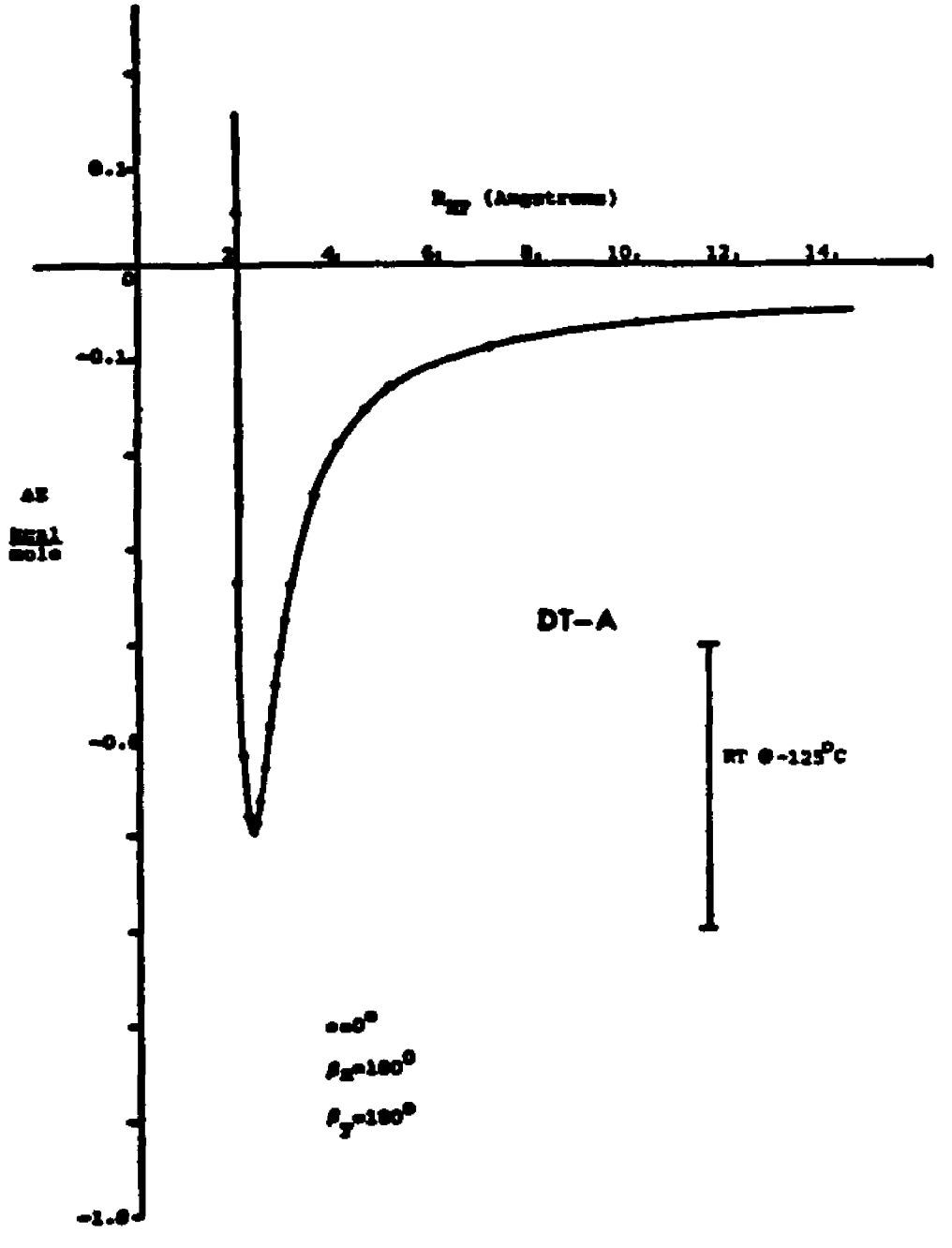

Figure 32. Stabilization Energy vs R_{HF} for DT-A Configuration of Fluoroform

corresponding diameter of a molecular sphere being 4.314 Å.

A hydrogen bond with an energy of the order of 0.4 kcal/mole is a very weak one compared to bona-fide hydrogen bonds having the bond energies of the order of 5 ∿ 20 kcal/mole. The fact that the liquid molecular volume data gives the average intermolecular separation (4.31 Å) which is similar to the equilibrium distance (4.83 Å) obtained by the M.O. calculation indicates that on the average the intermolecular forces of the magnitudes similar to that of our "hydrogen bond" are acting between every pair of molecules in the liquid. This is so in spite of the fact that any CHF_3 molecule can contribute only one hydrogen to the hydrogen bonding. Such an extra interaction could be that of London dispersion forces.

As far as can be determined, the literature on hydrogen bonding contains not a single instance of blue-shift of X-H stretching frequency upon formation of a X-H····Y bond: The X-H stretching frequency always red-shifts upon a hydrogen bond formation. The explanation is that the formation of a hydrogen bond necessarily modifies the electronic charge distribution around the X-H bond, making it less stiff. But then, the literature on hydrogen bonding concerns itself with bona fide hydrogen bonds and sometimes even regard a bond energy of 5 kcal/mole marginal in order to qualify to be a hydrogen bond. If a "hydrogen bond" is as weak (∿ 0.4 kcal/mole monomer) as in CHF_3, could it be that the shift in electronic distribution around the X-H bond upon formation of the C-H····F bond is so small that other effects, such as an effect of the new H····F bond on the C-H stretching frequency, more than just compensate for the weakening of the C-H bond?

Chloroform, an accepted and well studied proton donor, undergoes

no shift of its C-H stretching frequency[43] when dissolved in such electron donor solvents as ketones and nitriles. In CCl_4 solutions of strong proton acceptors such as pyridine-d_5 and dimethyl sulfoxide-d_6, the spectral shifts were found[44] to be in the order $CHBr_3$ > CHI_3 > $CHCl_3$, with fluoroform exhibiting inconclusive results.

In the simplest model of hydrogen bonding one would assume that the carbon and fluorine atoms are infinitely heavy and can be simulated by two solid walls. In this model the potential energy and the kinetic

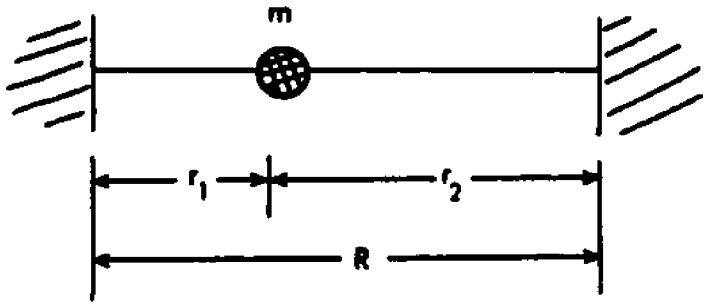

energy are given by

$$2V = f_1 (r_1-r_{10})^2 + f_2 (r_2-r_{20})^2$$

$$= f_1 (\Delta r_1)^2 + f_2 (\Delta R-\Delta r_1)^2$$

$$= (f_1+f_2) (\Delta r_1)^2 - 2f_2 \Delta R\Delta r_1 + f_2(\Delta R)^2 , \qquad \text{VI-(3)}$$

and

$$2T = m(\dot{\Delta r_1})^2 + M(\dot{\Delta R})^2 , \qquad \text{VI-(4)}$$

where f_1 and f_2 are the harmonic force constants, r_{10} and r_{20} are the equilibrium distances, $\Delta r_1=r_1-r_{10}$, $\Delta R_2=R_2-R_{20}$, and $\Delta R=R-R_e$, R_e being equal to $r_{10}+r_{20}$, and M is a certain reduced mass of the two-wall system. The eigenvalues of this two-dimensional problem are:

$$\lambda_{\pm} = \frac{1}{2mM}\left([M(f_1+f_2)+mf_2] \pm \sqrt{[M(f_1+f_2)+mf_2]^2-4mMf_1f_2} \right) \qquad \text{VI-(5)}$$

λ_+ of Eq. VI-(5) corresponds to the C-H stretching frequency, and it can be approximated by

$$\frac{\lambda_+}{\lambda_o} = \frac{[1+(1+\frac{m}{M})\frac{f_2}{f_1}]^2 - \frac{m}{M}\frac{f_2}{f_1}}{1+(1+\frac{m}{M})\frac{f_2}{f_1}} \quad , \qquad \text{VI-(6)}$$

where $\lambda_o = f_1/m$, the eigenvalue of a free C-H stretching motion. When f_2 tends to zero, Eq. VI-(6) reduces to

$$\frac{\lambda_+}{\lambda_o} = 1 \quad , \qquad \text{VI-(7)}$$

as it should. When M tends to infinity, Eq. VI-(6) reduces to

$$\frac{\lambda_+}{\lambda_o} = \frac{f_1+f_2}{f_1} \quad , \qquad \text{VI-(8)}$$

which implies a blue-shift of the C-H stretching frequency, unless the value of f_1 in the numerator becomes smaller than the f_1 value in the denominator. Apparently for bona fide hydrogen bonds, f_1 in the H-bonded configuration which we might call f_1' is so small compared to the f_1-value of a free C-H configuration that the relation,

$$f_1' + f_2 < f_1 \quad , \qquad \text{VI-(9)}$$

is satisfied, thus leading to the red-shift. A further analysis of the quantity λ_+/λ_o given by Eq. VI-(6) as a function of two ratios, m/M and f_2/f_1, has proved that λ_+ is always greater than λ_o as long as f_2 is positive. Therefore, the condition, $f_1' < f_1$, is the necessary condition for the red-shift under all circumstances. The minimum value of the decrease in f_1 that one should have for the red-shifting depends on the ratios m/M and f_2/f_1 and if this minimum decrease in f_1 is not met, the frequency will blue-shift.

Another model is a linear triatomic model with the center of mass kept stationary. In this model the effect of an off-diagonal F-matrix element is considered:

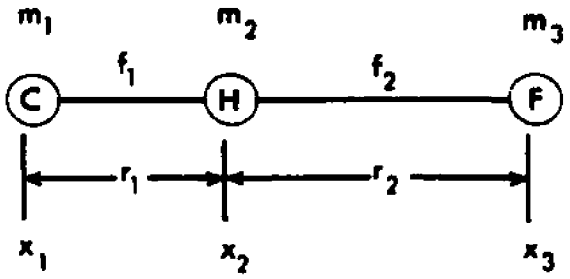

$$2V = f_1(x_2-x_1-r_{10})^2 + f_2(x_3-x_2-r_{20})^2 + 2f_{12}(x_2-x_1-r_{10})(x_3-x_2-r_{20}) \qquad \text{VI-(10)}$$

and

$$2T = m_1\dot{x}_1^2 + m_2\dot{x}_2^2 + m_3\dot{x}_3^2 \qquad \text{VI-(11)}$$

The standard transformation to the internal coordinate system yielded

$$2V = f_1(\Delta r_1)^2 + f_2(\Delta r_2)^2 + 2f_{12}(\Delta r_1)(\Delta r_2) \quad , \qquad \text{VI-(12)}$$

$$2T = \mu_{1-23}(\Delta\dot{r}_1)^2 + \mu_{3-12}(\Delta\dot{r}_2)^2 + 2\frac{m_1m_3}{M}(\Delta\dot{r}_1)(\Delta\dot{r}_2) \quad , \qquad \text{VI-(13)}$$

where

$$\frac{1}{\mu_{1-23}} = \frac{1}{m_1} + \frac{1}{m_2+m_3} \quad , \qquad \text{VI-(14)}$$

and

$$\frac{1}{\mu_{3-12}} = \frac{1}{m_3} + \frac{1}{m_1+m_2} \quad . \qquad \text{VI-(15)}$$

One of the roots of this secular problem λ_+ can be approximated by

$$\frac{\lambda_+}{\lambda_o} = \left(1 + \frac{f_2-2f_{12}}{f_1}\right)\left(1 - \frac{m_2}{m_1}\right)(1 - x) \quad , \qquad \text{VI-(16)}$$

where

$$\lambda_o = \frac{f_1}{\mu_{12}} = \frac{f_1(m_1+m_2)}{m_1m_2} \quad , \text{ and} \qquad \text{VI-(17)}$$

$$x = \frac{2m_2(m_1+m_3)}{m_1m_3}\,\frac{(f_1f_2-f_{12}^2)}{(f_1+f_2-2f_{12})^2} \quad . \qquad \text{VI-(18)}$$

Eq. VI-(16) reduces to Eq. VI-(8) when $f_{12} = 0$, $m_2 \ll m_1$ and $m_2 \ll m_3$. In the limit of heavy m_1 and m_3,

$$\frac{\lambda_+}{\lambda_o} = \frac{f_1+f_2-2f_{12}}{f_1} \quad , \qquad \text{VI-(19)}$$

which clearly shows the role of off-diagonal force constant between the "internal" motion, which is the C-H stretching motion, and the "external"

motion represented by the distance between m_2(H) atom and m_3(F) atom. A positive f_{12} tends to give a red shift, while a negative f_{12} tends to lead to a blue shift. Numerical restriction on the absolute magnitude of f_{12} in a stable configuration is given by $f_{12} < (f_1 f_2)^{1/2}$. Since $f_1 >> f_2$, $|f_{12}|$ may be bigger than f_2 and thus become more important than f_2 in its role in the blue-shift/red-shift argument. The role of f_{12} or rather f_{DT_Z} has already been explored and the result is consistent with and is supported by the above vibrational analysis of hydrogen bonded models of liquid fluoroform.

VIf. Concluding Remarks

To summarize, the following has been shown:

1. The need of a temperature dependent force field, specifically the f_{DT_Z} element, in order to reproduce the observed VPIE in fluoroform,
2. Observed temperature dependency is associated with intermolecular association, specifically weak "hydrogen bonding,"
3. The liquid $\underset{\sim}{F}$ matrix is consistent with the experimentally observed vibrational frequencies,
4. The observed H/D VPIE and 12/13 VPIE are explainable in terms of the experimentally observed blue shifting of the C-H stretching vibration, and
5. Models of the weakly hydrogen-bonded system support the liquid $\underset{\sim}{F}$ matrix formulated and observed C-H blue shift upon condensation.

To gain further insight into this problem, the VPIE for CH_2F_2 and CF_4 should be investigated as well as detailed liquid and solid phase spectra obtained in order to solidify the analysis of the liquid state in the CH_XF_{4-X} series.

VII. REFERENCES

1. J. Bigeleisen, J. Chem. Phys. 34, 1485 (1961).
2. G. Jansco and W. A. Van Hook, Chem. Rev. 74(b), 689 (1974).
3. J. Bigeleisen, C. B. Crazg, and M. Jeevanandam, J. Chem. Phys. 47, 4335 (1967).
4. J. Bigeleisen and S. V. Ribnikar, J. Chem. Phys. 35, 1297 (1961).
5. J. Bigeleisen, S. V. Ribnikar, and W. A. Van Hook, J. Chem. Phys. 38, 489 (1963).
6. W. A. Van Hook, J. Chem. Phys. 44, 234 (1966).
7. W. A. Van Hook, J. Chem. Phys. 46, 1907 (1967).
8. D. M. Eshelman, F. J. Torre, and J. Bigeleisen, J. Chem. Phys. 60, 490 (1974).
9. Y. Yato, M. Lee, and J. Bigeleisen, J. Chem. Phys. 63, 1555 (1975).
10. Z. Bilkadi, M. Lee, and J. Bigeleisen, J. Chem. Phys. 62, 2087 (1975).
11. M. Lee, J. Chem. Phys. 62, 2094 (1975).
12. L. Borodinsky, H. Wieck, D. Mayfield, and T. Ishida, J. Chem. Phys. 68, 3279 (1978).
13. D. Long, R. Gravenor, and T. Jones, Trans. Faraday Soc. 60, 1509 (1964).
14. G. Glocker and W. Edgell, J. Chem. Phys. 9, 224 (1941).
15. D. Rank, E. Shull, and E. Pace, J. Chem. Phys. 18, 885 (1950).
16. A. Buckingham and R. Raab, J. Chem. Soc. 5511 (1961).
17. M. Evans, J. Che. Soc., Faraday Trans. 2, 71 (4), 843 (1975).
18. A. Gerschel, et. al., Molecular Physics 32, 679 (1976).
19. A. Goel and N. R. Rao, Trans. Faraday Soc. 67 (10), 2828 (1971).

20. P. Kollman, et. al., J. Am. Chem. Soc. 97, 955 (1975).

21. V. Bertseo, N. Goluber, and D. Shchepkin, Opt. Spektrosk. 40, 951 (1976).

22. A. Eucken, Phys. Z. 10, 586 (1909).

23. W. Nernst, Ann. Phys. 36, 395 (1911).

24. G. Gibson, and M. Giauque, J. Am. Chem. Soc. 45, 93 (1923).

25. W. Giauque and C. Egan, J. Chem. Phys. 5, 45 (1937).

26. H. Johnston, J. Clarke, E. Rifkin, and E. Kerr, J. Am. Chem. Soc. 72, 3933 (1950).

27. J. Bigeleisen and E. Roth, J. Chem. Phys. 35, 68 (1961).

28. J. Bigeleisen, F. Brooks, T. Ishida, and S. Ribnikar, Rev. Sci. Inst. 39, 353 (1968).

29. American Petroleum Institute, Mass Spectral Data Serial #468, 1950.

30. W. Giauque, G. Brodale, and R. Valentine, J. Chem. Phys. 66, 392 (1962).

31. O. Ruff, Ber. 69, 299 (1936).

32. T. Oi and J. Shulman, State University of New York at Stony Brook (private communication).

33. E. Wilson, J. Decius, and P. Cross, Molecular Vibrations (New York: McGraw-Hill Book Co.), 1955.

34. J. Schachtschneider and R. Snyder, Spectrochim. Acta 19, 117 (1963).

35. A. Rogers, J. Chao, R. Wilhoit, and B. Zwolinski, J. Phys. Chem. Ref. Data 3, 117 (1974).

36. D. Long, R. Gravenor, and D. Jones, Trans. Faraday Soc. 60, 1509 (1964).

37. V. Galasso, D. DeAlti, and G. Costa, Spectrochim. Acta 21, 669 (1965).

38. R. D'Cunha, J. Mol. Spec. 43, 282 (1972).

39. G. Glocker and W. Edgell, J. Chem. Phys. 9, 224 (1941).

40. D. Rank, E. Shull and E. Pace, J. Chem. Phys. 18, 885 (1950).

41. R. Hajjar and G. MacWood, J. Chem. Phys. 49, 4567 (1968).

42. Handbook of Fundamentals, American Society of Heating, Refrigerating and Air Conditioning Engineers, Inc., (New York), 1974.

43. R. Green, Hydrogen Bonding by C-H Groups (New York: John Wiley & Sons), 1974.

44. A. Allerhand and P. Schluyer, J. Am. Chem. Soc. 85, 1765 (1963).

45. P. Wilt, et. al., Journal of Molecular Spectroscopy 58, 76-110 (1975).

APPENDIX A

Ab-Initio Calculations on Model CHF_3 Dimer Systems

Calculation Description

Hydrogen bonding interactions could be expected to occur in CHF_3. This is reasonable judging from the polarity and substituents. In order to get some idea of the extent of this interaction as well as the structure of the interacting system, quantum mechanical calculations have been carried out on CHF_3 monomer and four basic dimer configurations. Various investigators[1,2,3,4] have applied ab-initio molecular orbital studies to interacting systems, especially to hydrogen bonding. This approach has met with a good deal of success both qualitatively and quantitatively.

Gaussian 70,[5] a Fortran IV ab-initio SCF molecular orbital routine was used in studying intermolecular interactions in CHF_3. Gaussian 70 utilizes gaussian functions to describe the basis set. The basis functions are chosen to be fixed linear combinations of gaussian functions, for example

$$G_s(\alpha,r) = (2\alpha/\pi)^{3/4} \exp(-\alpha r^2) \qquad \text{A-(1)}$$

and

$$G_{p_x}(\alpha,r) = (128\alpha^5)/\pi^3)^{1/4} x \cdot \exp(-\alpha r^2) \ . \qquad \text{A-(2)}$$

The use of these gaussian functions allows the explicit integration of the Hamiltonian operator.

Two types of basis sets are made available as part of the program, the minimal STO-NG[6,7] and extended N-31G[8,9] sets, however, provision is

made for input of any basis sets such that a maximum of 70 basis functions is not exceeded. The STO-3G basis set was used in examining the interactions between two CHF_3 molecules. In Table A1 are found the basis set descriptions used for CHF_3 calculations. Presently only calculations of CHF_3 dimers have been considered, however, polymers of up to six CHF_3 monomers can be performed using Gaussian 70.

Dimer Configurations

The number of viable geometric forms of two interacting molecules is limited if a hydrogen bonding interaction is expected. The four basic dimer configurations and the dimer internal coordinates considered for each are shown in Figures A1, A2, A3, and A4.

In order to achieve internal consistency of results, the geometry of the CHF_3 monomer was first optimized starting with experimentally determined parameters. Comparison of the experimental and calculated results are tabulated in Table A2.

Also internal force constants have been calculated from the cartesian force constants determined by the best fit of calculated energies to a harmonic potential for the x, y, and z coordinates for each atom. From the best fit coefficients the force constants can be calculated. A list of the cartesian force constants, obtained by varying each coordinate (x,y,z) by ± 0.005 angstroms for each atom are found in Table A3. Note that the average deviation listed for each force constant, in parts per

Table A1

CHF_3 Basis Set Description (STO-3G)

ATOM	NO.	ATOMIC ORBITAL TYPE	SCALE FACTOR	GAUSSIAN FUNCTIONS EXPONENT	S COEF	P COEF
C	1	1S	5.67000			
				7.16168D 01	1.54329D-01	0.0
				1.30451D 01	5.35328D-01	0.0
				3.53051D 00	4.44635D-01	0.0
	2 - 5	2SP	1.72000			
				2.94125D 00	-9.99672D-02	1.55916D-01
				6.83483D-01	3.99513D-01	6.07684D-01
				2.22290D-01	7.00115D-01	3.91957D-01
H	6	1S	1.24000			
				3.42525D 00	1.54329D-01	0.0
				6.23913D-01	5.35328D-01	0.0
				1.68855D-01	4.44635D-01	0.0
F_1	7	1S	8.65000			
				1.66679D 02	1.54329D-01	0.0
				3.03608D 01	5.35328D-01	0.0
				8.21682D 00	4.44635D-01	0.0
	8 - 11	2SP	2.55000			
				6.46480D 00	-9.99672D-02	1.55916D-01
				1.50228D 00	3.99513D-01	6.07684D-01
				4.88589D-01	7.00115D-01	3.91957D-01

[continued]

[Table A1; continued]

ATOMIC ORBITAL			GAUSSIAN FUNCTIONS		
ATOM NO.	TYPE	SCALE FACTOR	EXPONENT	S COEF	P COEF
F_2 12	1S	8.65000			
			1.66679D 02	1.54329D-01	0.0
			3.03608D 01	5.35328D-01	0.0
			8.21682D 00	4.44635D-01	0.0
3 - 16	2SP	2.55000			
			6.46480D 00	-9.99672D-02	1.55916D-01
			1.50228D 00	3.99513D-01	6.07684D-01
			4.88589D-01	7.00115D-01	3.91957D-01
F_3 17	1S	8.65000			
			1.66679D 02	1.54329D-01	0.0
			3.03608D 01	5.35328D-01	0.0
			8.21682D 00	4.44635D-01	0.0
8 - 21	2SP	2.55000			
			6.46480D 00	-9.99672D-02	1.55916D-01
			1.50228D 00	3.99513D-01	6.07684D-01
			4.88589D-01	7.00115D-01	3.91957D-01

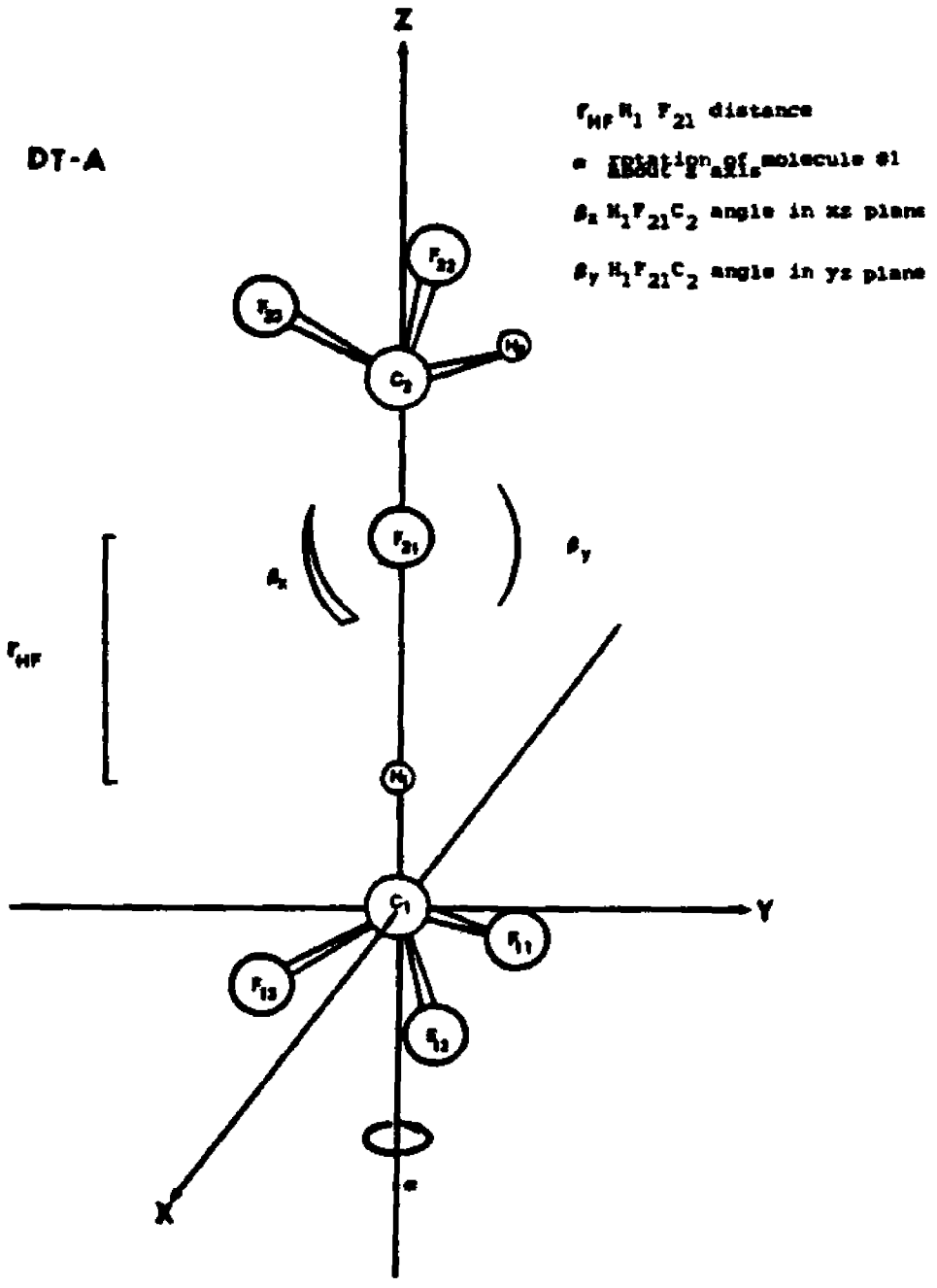

Figure A1. Dimer Type A Configuration

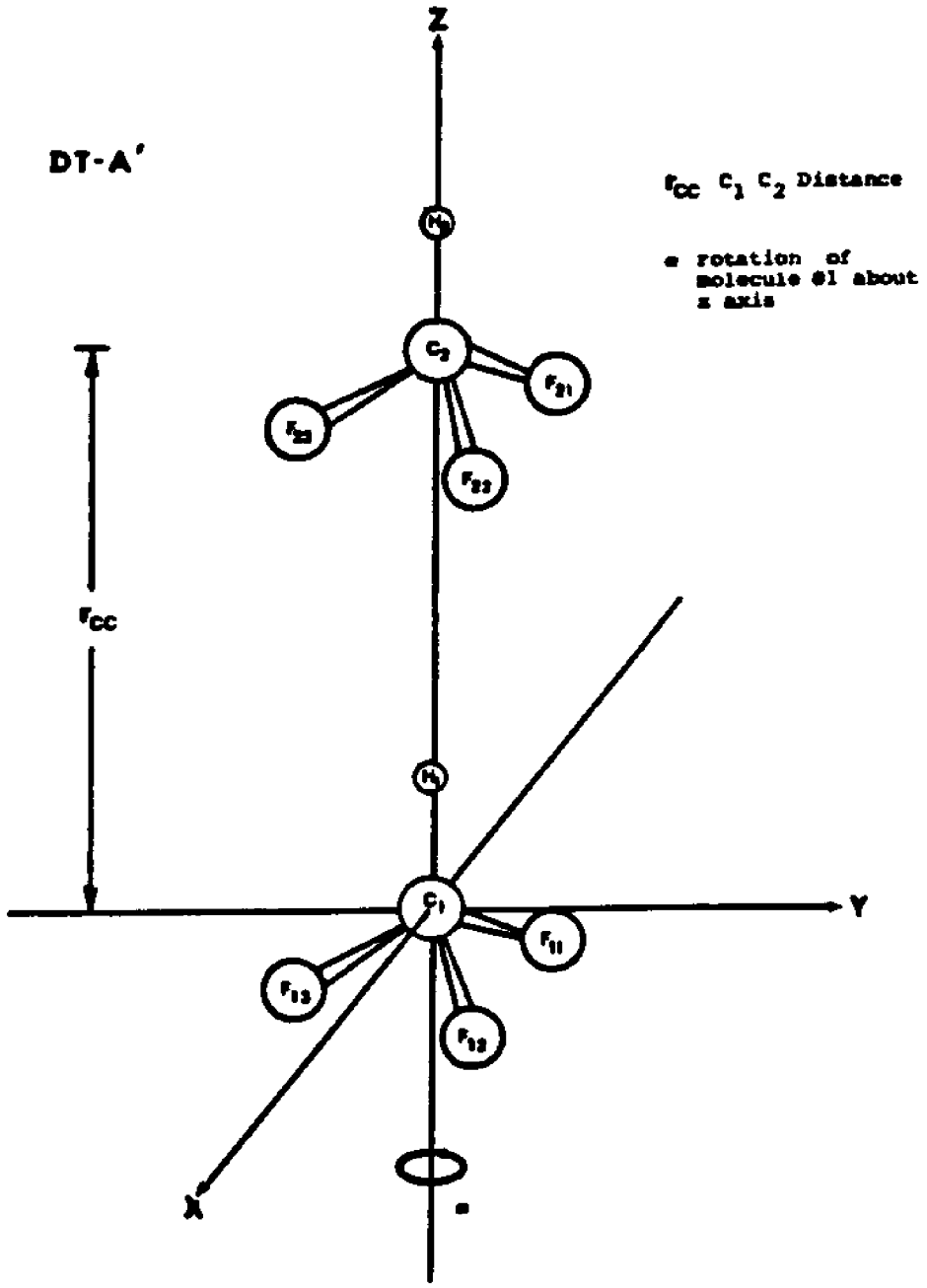

Figure A2. Dimer Type A' Configuration

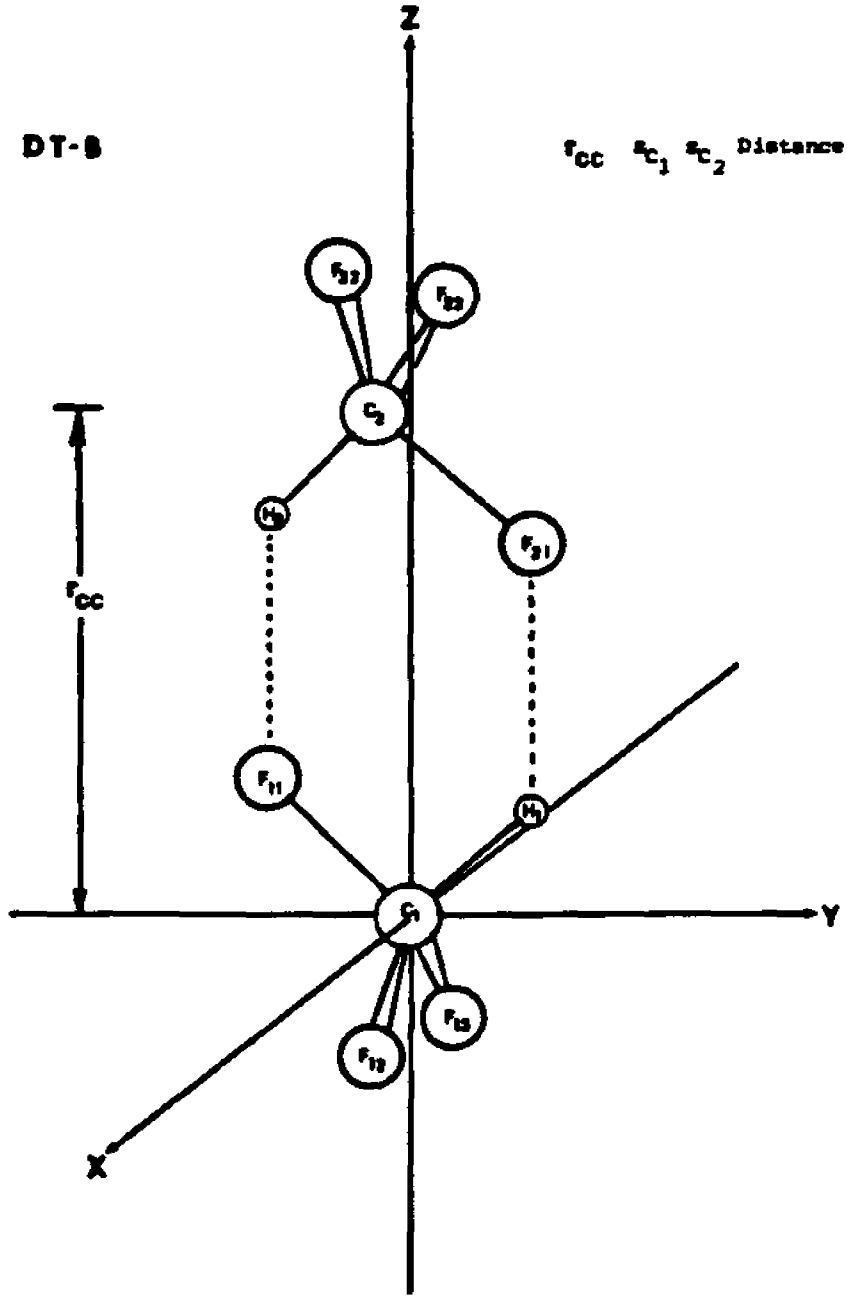

Figure A3. Dimer Type B Configuration

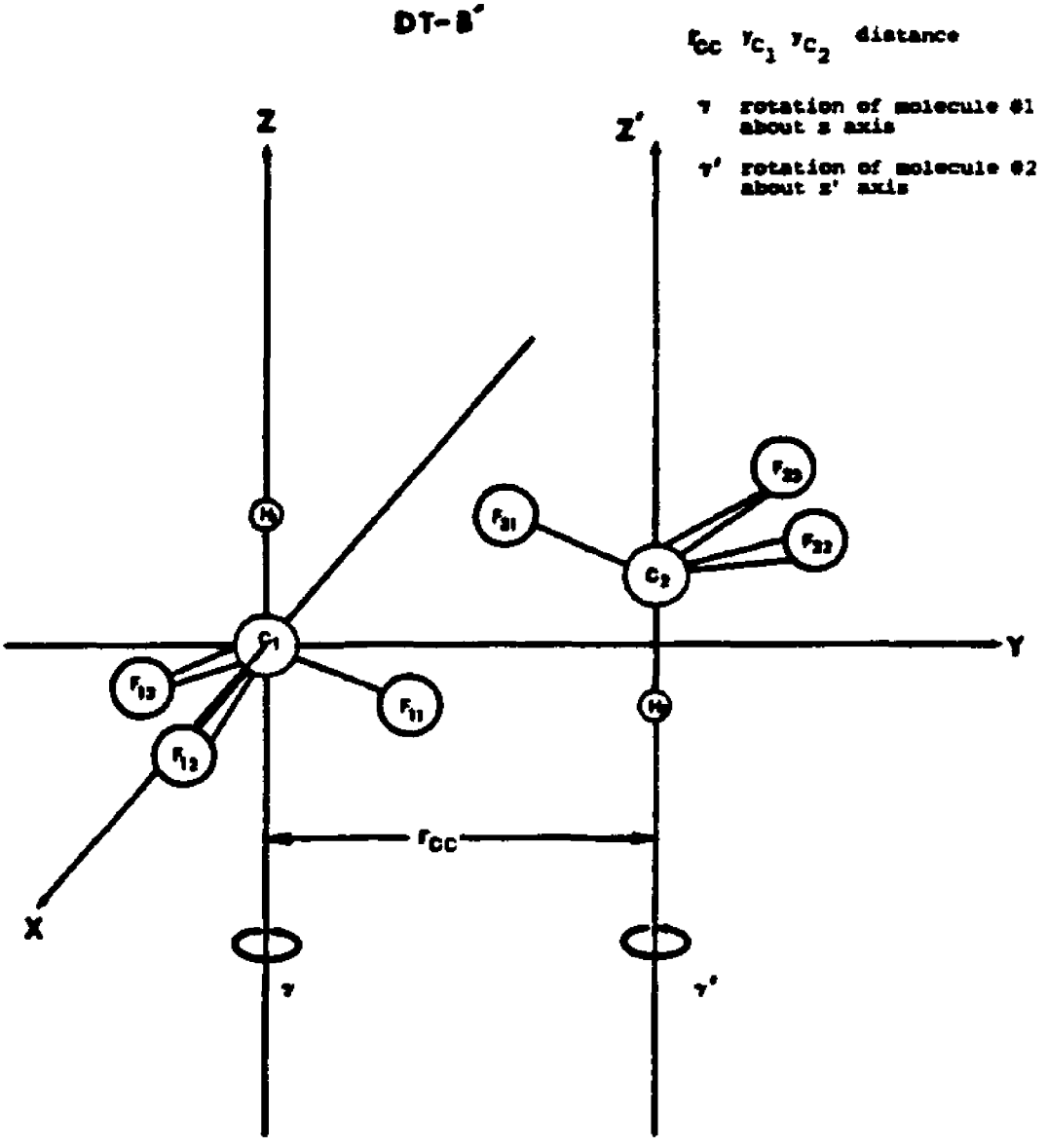

Figure A4. Dimer Type B' Configuration

Table A2

Comparison of Experimental and Calculated Results for CHF_3

	EXPERIMENTAL	CALCULATED
r_{CH} (angstroms)	1.098	1.11817
r_{CF} (angstroms)	1.332	1.36981
FCF angle (deg)	108.8	108.801
HCF angle (deg)	110.1	110.133
μ (debyes)	1.65	1.110
f_{CH} (mdynes/angstrom)	5.0000	7.0155*
f_{CF} (mdynes/angstrom)	6.0179	8.7258*

*Deviation from harmonicity is less than 0.1 ppt.

Table A3

CHF_3 Cartesian Force Constants*

ATOM		FORCE CONSTANT (mdynes/angstroms)	a.d.(ppt)**
C	xx	12.4609	3.3
	yy	12.4487	3.8
	zz	12.5185	3.5
H	xx	4.8469	0.7
	yy	1.2680	0.5
	zz	3.2036	0.6
F_1	xx	7.4273	2.4
	yy	1.0727	1.6
	zz	3.4261	2.0
F_2	xx	1.3185	5.3
	yy	6.1437	4.0
	zz	3.7603	1.8
F_3	xx	1.3185	5.3
	yy	6.1437	4.0
	zz	3.7603	1.8

*Calculations for monomer in Type B geometry (see Fig. A3 molecule #1)
**Deviation from harmonicity

thousand, is a level of harmonicity of the potential as determined from the least squares reduction.

Results

The extent of interaction experienced will be measured by the amount of stabilization energy, ΔE, achieved.

$$\Delta E = E_T \text{ (dimer)} - 2E_T \text{ (monomer)} \quad , \qquad \text{A-(3)}$$

where E_T is defined as

$$E_T = E_{\text{Electronic}} + E_{\text{nuclear}} \qquad \text{A-(4)}$$

where $E_{\text{Electronic}}$ and E_{Nuclear} refer to the total electronic and nuclear repulsion energy, respectively.

Following are summarizations of results obtained for each dimer configuration:

1. Dimer Type A (DT-A): ΔE was found to be -0.72 kcal/mole, corresponding to r_{HF} = 2.3 angstroms, α = 60 deg, $\beta_x = \beta_y$ = 235 deg (cf. Figure A8). The stabilization energy was found to be relatively insensitive to changes in α. The bending motions β_x and β_y show a minimum in the potential at +/- 45 deg for β_y and +45 deg for β_x. These results indicate that there would be free rotation about the z axis and bending motion unhindered to angles of +/- 90 deg for temperatures as low as 150°K. Plots of the stabilization energy vs r, α, β_y, β_x can be seen in Figures A5, A6, A7, and A8, respectively.

2. Dimer Type A'(DT-A'): A slight stabilization of -0.15 kcal/mole

was found for this configuration. Calculations for α = 0 and 60 degrees show little change in the potential with variations of r_{CC} until the nature of the interaction becomes repulsive. The minimum in both cases was found to occur at r_{CC} = 5.0 angstroms. Plots of ΔE vs r_{CC} for α = 0 deg and 60 deg is shown in Figure A9.

3. Dimer Type B (DT-B): An energy minimum of -0.68 kcal/mole was found to occur at r_{CC} = 4.1 angstroms (refer to Figure A10).

4. Dimer Type B' (DT-B'): Two thermally distinct energy minima were found for this configuration. A ΔE of -0.50 kcal/mole at r_{CC} = 4.2 angstroms and γ,γ' = 0,0 degrees, and a ΔE = -0.22 kcal/mole at r_{CC} = 5.2 angstroms for γ,γ' = 60,0 degrees (cf. Figure A4). This result is shown in Figure A11.

Discussion

All four dimer configurations considered were found to exhibit some stabilization energy as compared to that of the free dimer. Roughly there is a difference of 0.6 kcal/mole in stabilization energy between dimer forms A and A'. The energies of forms A', B', B,A fall in a thermal energy range corresponding to 75°-375°K. This can be considered a form of temperature dependent association. Focusing attention on the most stable forms, a stabilization energy of approximately 0.7 kcal/mole is found for types A and B. The magnitude of this stabilization is that found for "strong" Van der Waals interactions or "weak" hydrogen bonds. The essential difference between these two configurations is the linearity of the C---H·····F interaction. In type A a single linear interaction is found as opposed to two bent interactions in the B case. Tabulation of the overlap population of interacting atoms, atom electron

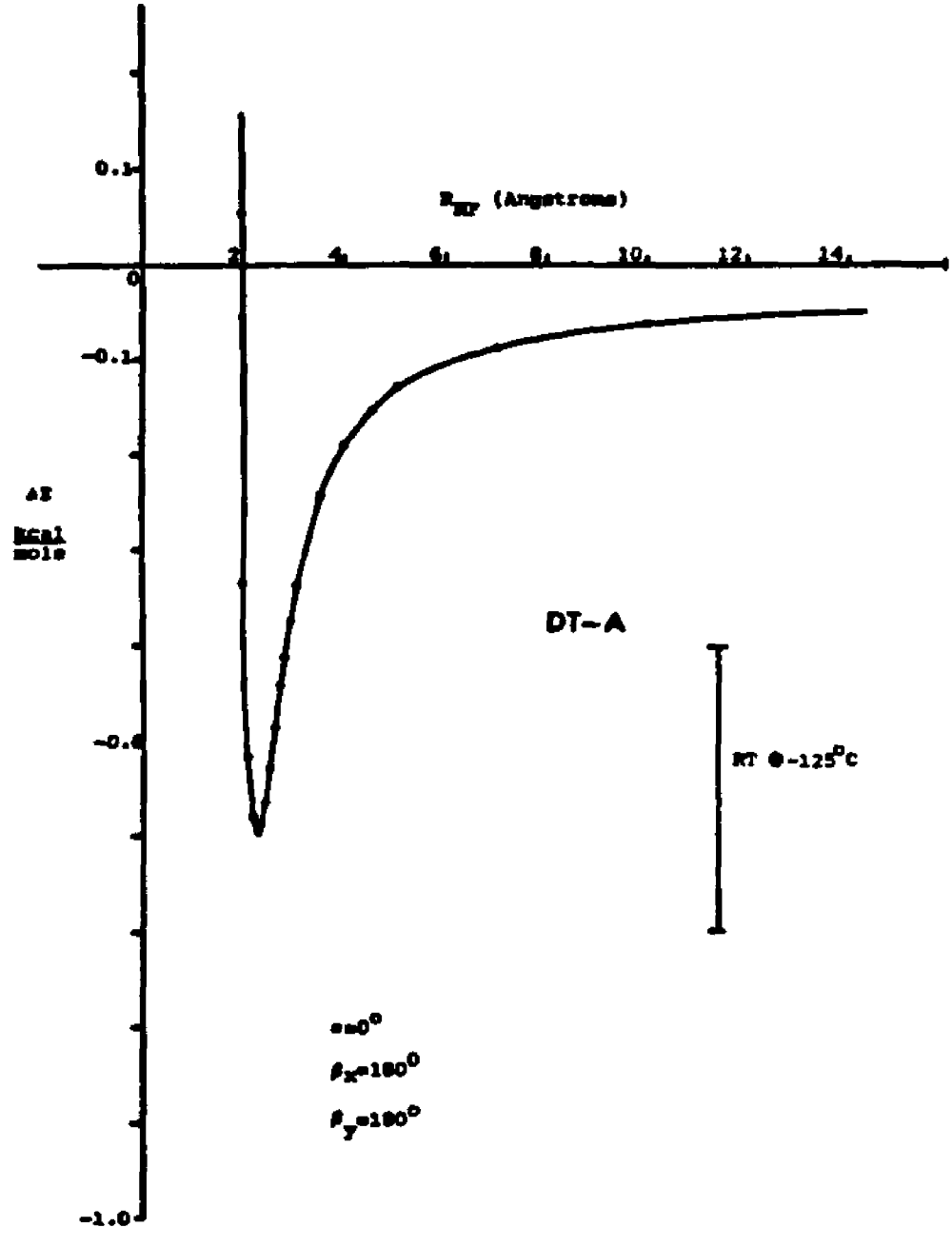

Figure A5. Stabilization Energy vs R_{HF} for Dimer Type A

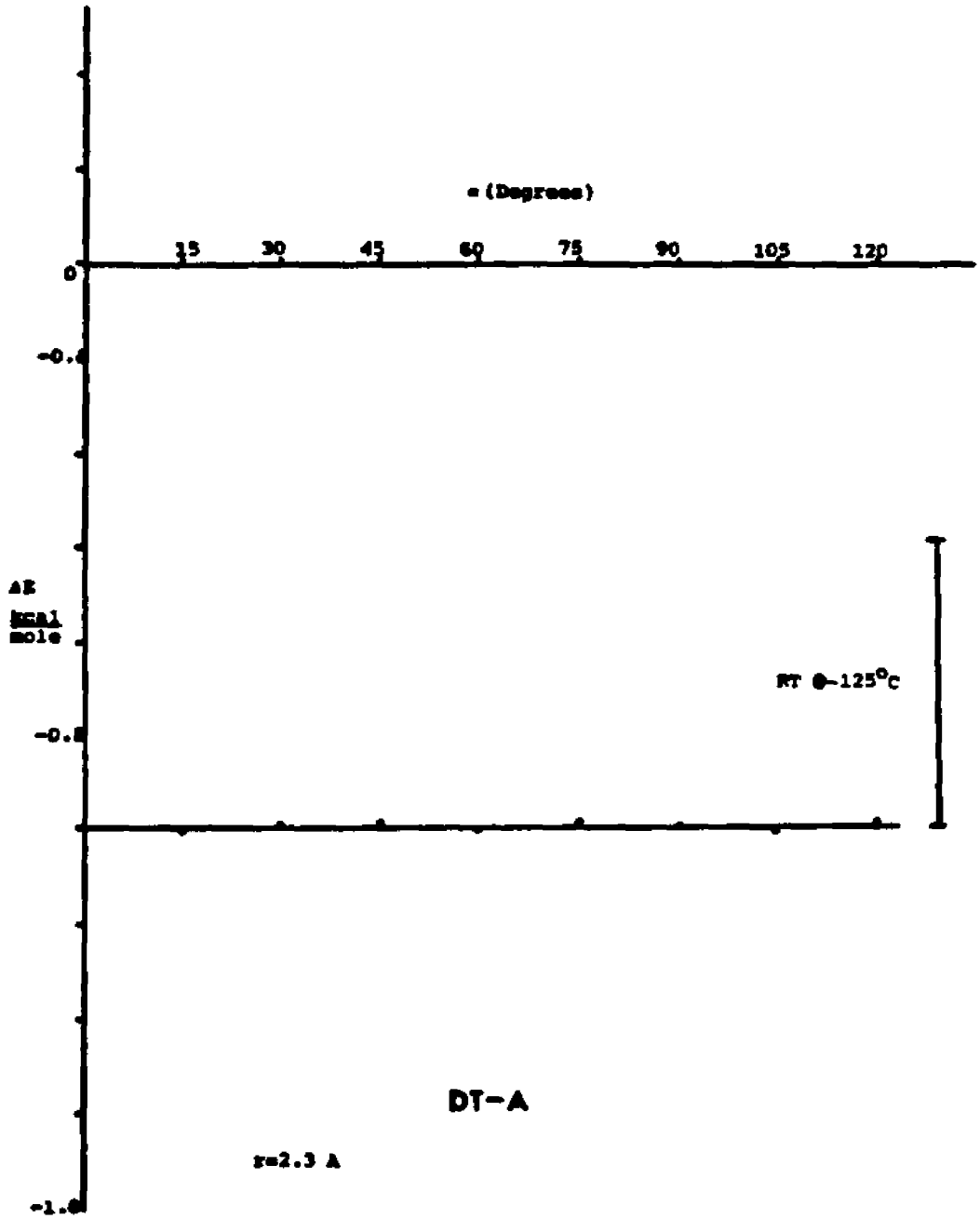

Figure A6. Stabilization Energy vs α for Dimer Type A

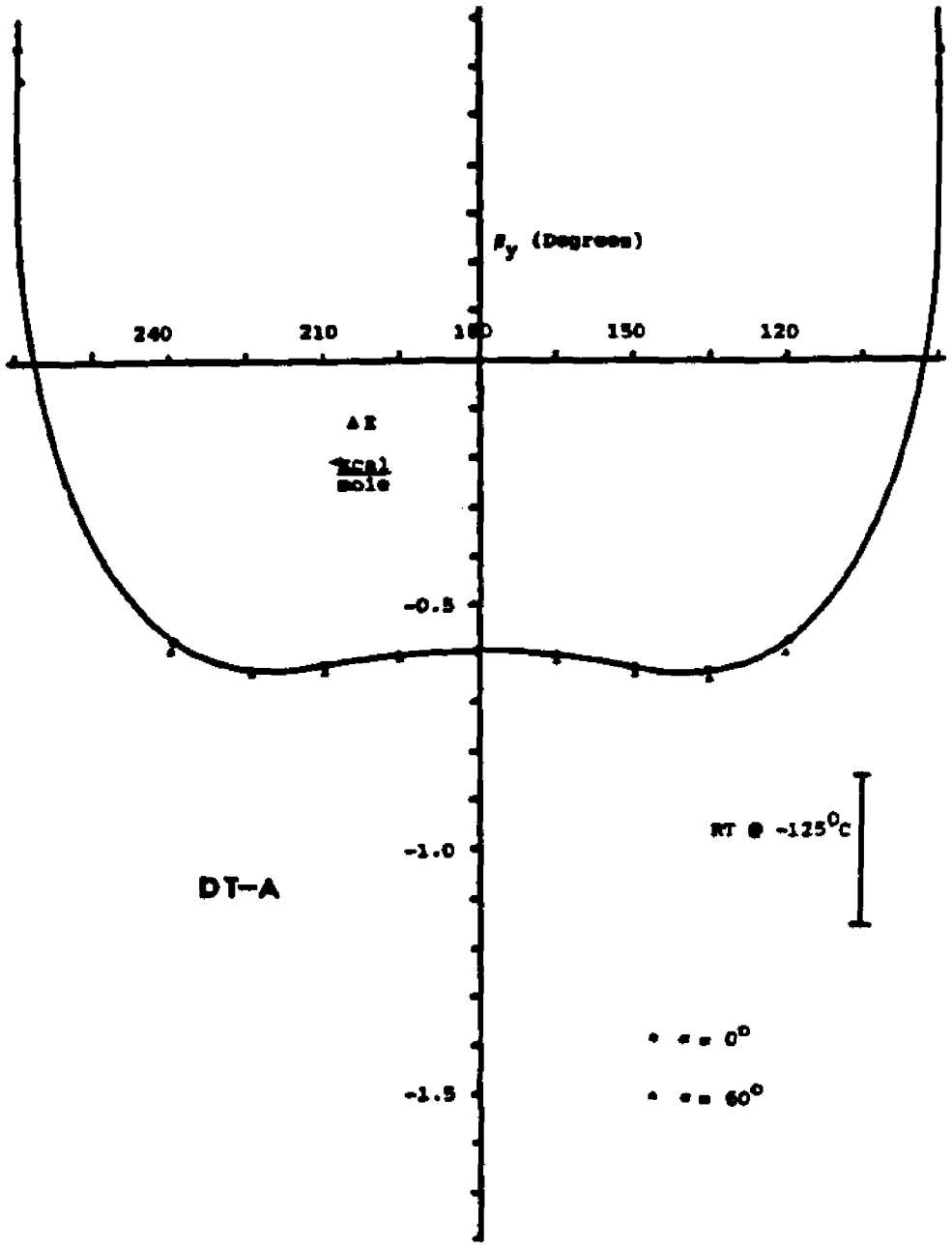

Figure A7. Stabilization Energy vs β_y for Dimer Type A

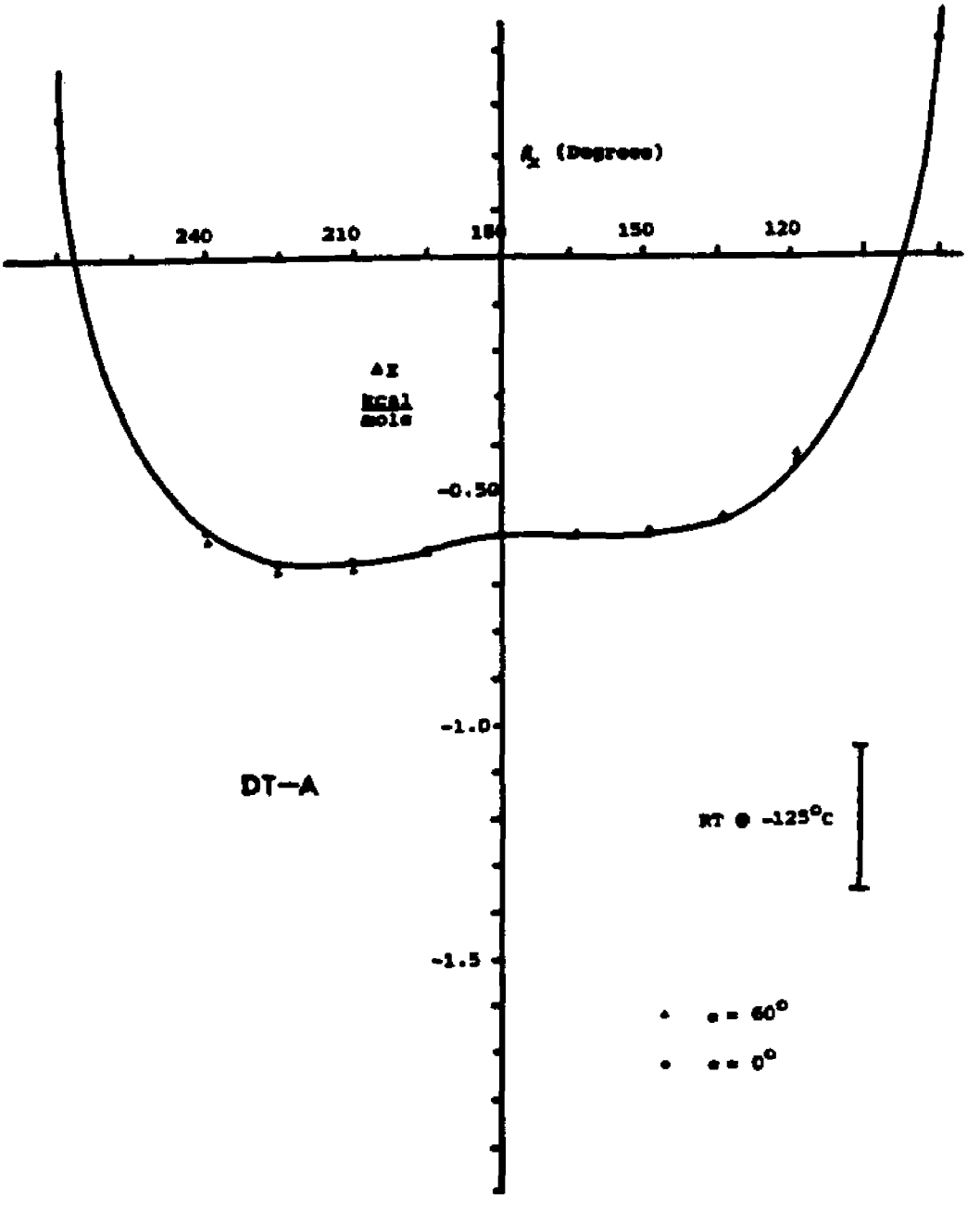

Figure A8. Stabilization Energy vs β_x for Dimer Type A

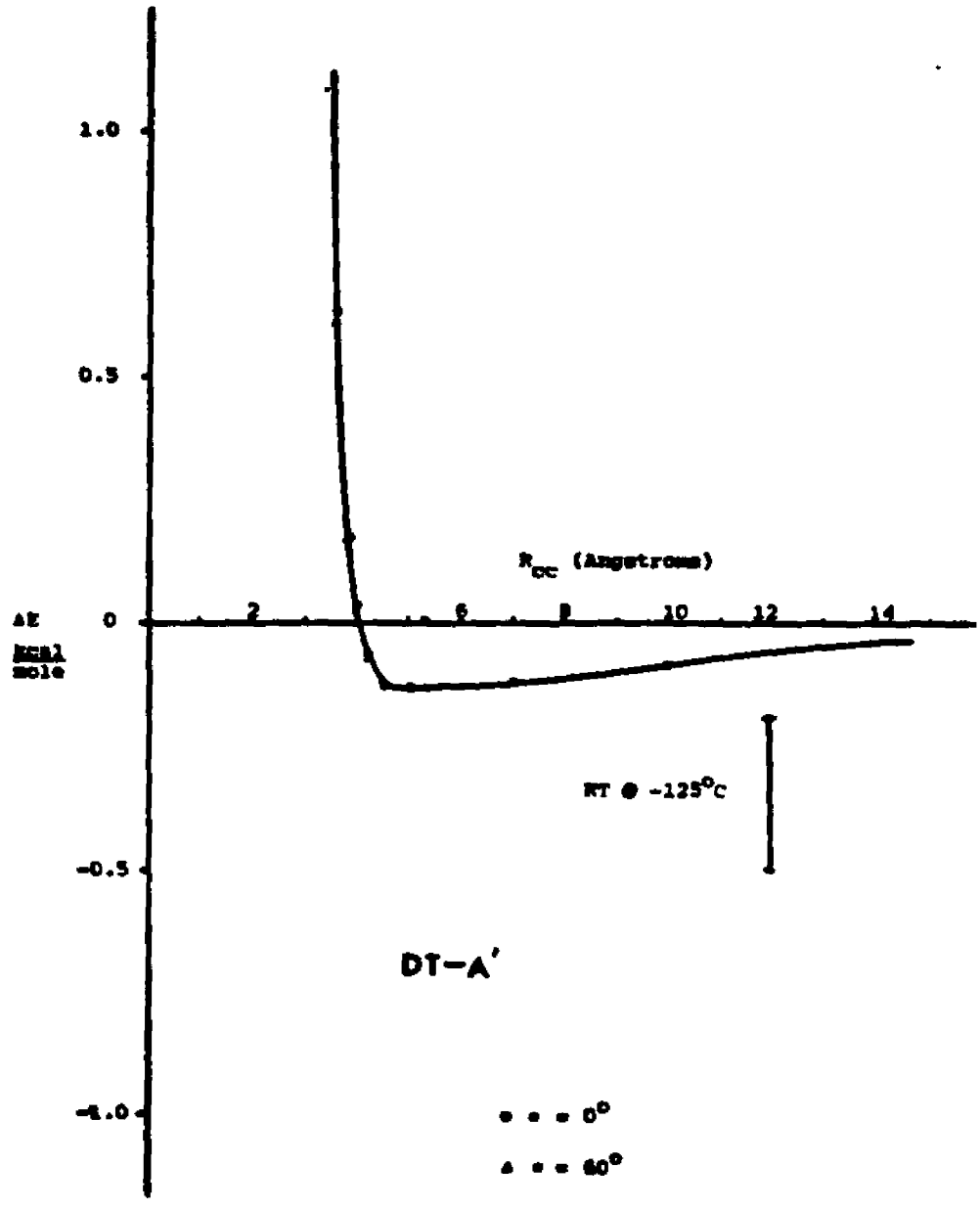

Figure A9. Stabilization Energy vs R_{CC} for Dimer Type A'

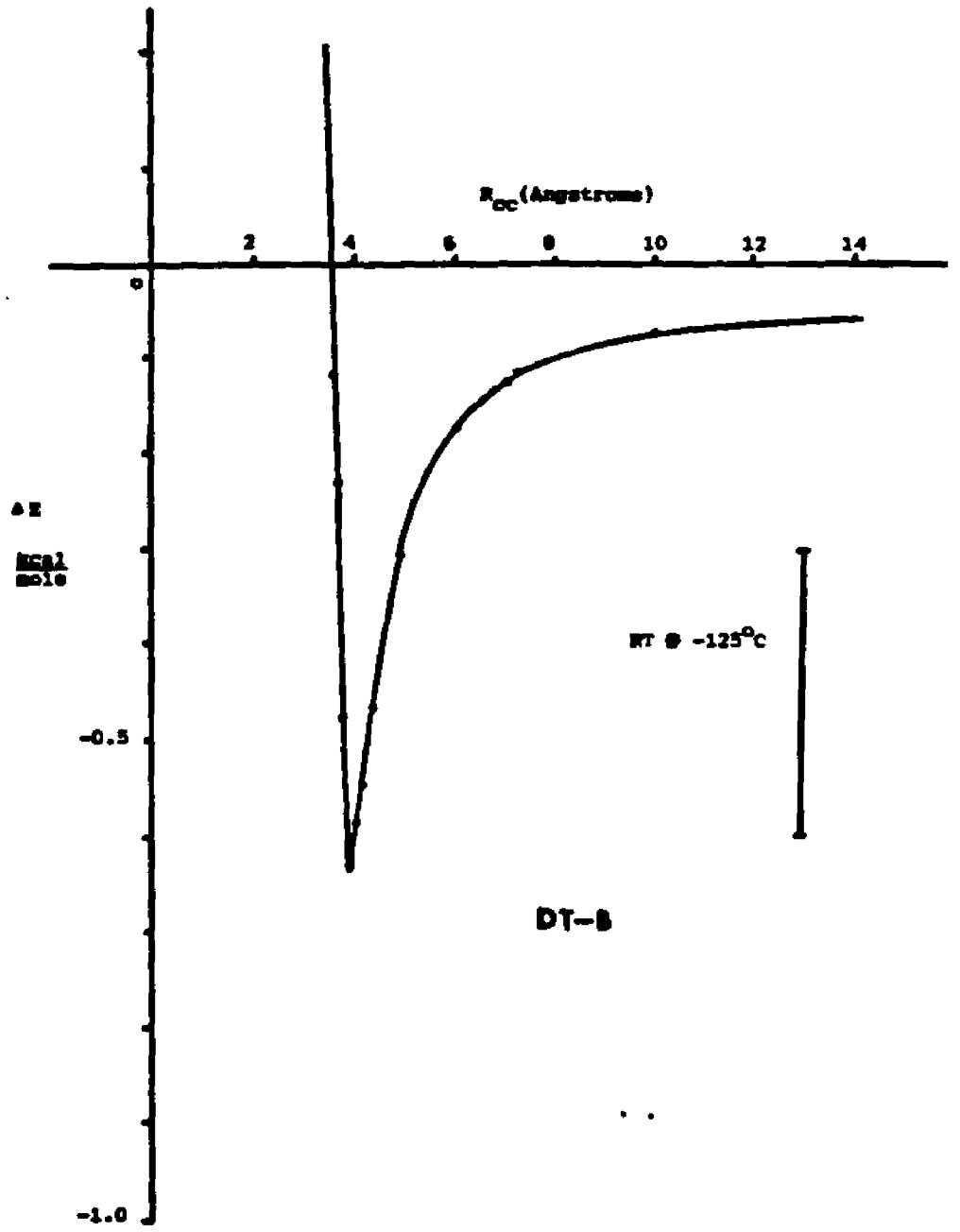

Figure A10. Stabilization Energy vs R_{cc} for Dimer Type B

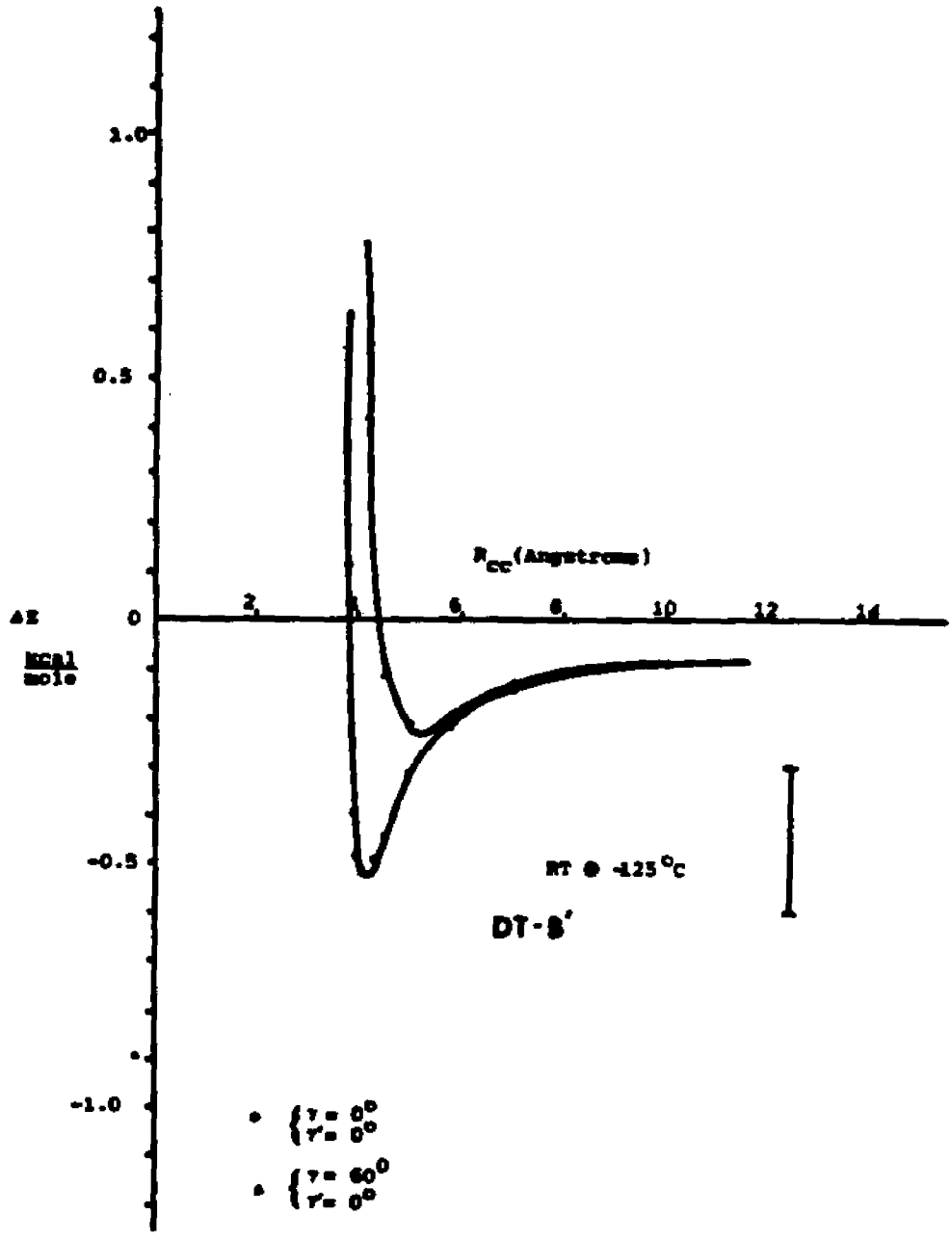

Figure All. Stabilization Energy vs R_{cc} for Dimer Type B'

density for each atom and the electronic and nuclear contributions to the total energy for the monomer and the A, B dimers can be found in Tables A4, A5, and A6, respectively. To summarize, the interaction is essentially sp in character. Deviations in linearity in the interaction would cause a decrease in the overlap between the interacting atoms. This is shown to be the case (cf. Table A4). The net ratio of H-F overlap for A/B = 1.4. The net electrostatic interaction for Dimer B is twice that for the A dimer. Usually the electrostatic contribution is the more important at the distances for these interactions, thus it would be expected that Dimer B would show more stabilization than type A. However, looking at the contributions to the total energy as well as the results in Figures A10 and A11, it can be seen that the repulsive interaction of the fluorines are also a factor.

The charge re-distribution for dimers A and B is shown in Figure A12. This distribution is the change in partial charges experienced by the atoms of each molecule as compared to the monomer. The re-distribution found in type A is typically that found in hydrogen bonded systems.[10] At first glance the charge re-distribution for type B seems to be different than that found in the A dimer. However, each molecule is now both a donor and acceptor of electron density. A net charge re-distribution on the non-interacting fluorines thus would be expected to be less than that found in the A configuration. This is actually the case. From Table A6 it can be seen that the charge re-distribution of the B dimer non-interacting fluorines is less than that found for the A dimer. So that the B dimer also typifies the hydrogen bonding situation in this case.

More detailed analysis of the nature of the interaction would

Table A4

Overlap Population Condensed to the Interacting Atoms in Dimers A,B

DT-A	H_1-F_{21}	0.0011
	F_{21}-H_1	0.0011
DT-B	H_1-F_{21}	0.0004
	F_{21}-H_1	0.0004
	H_2-F_{11}	0.0004
	F_{11}-H_2	0.0004

Table A5

Electron Density Condensed to Atoms

atom/system	Monomer	DT-A	DT-B
C_1	5.628	5.632	5.630
H_1	0.932	0.925	0.925
F_{11}	9.147	9.148	9.152
F_{12}	9.147	9.148	9.146
F_{13}	9.147	9.148	9.146
C_2	5.628	5.626	5.630
H_2	0.932	0.929	0.925
F_{21}	9.147	9.153	9.152
F_{22}	9.147	9.145	9.146
F_{23}	9.147	9.145	9.146

Table A6

CHF_3 Energy Distribution (AU)

Component	Monomer	DT-A	DT-B
$E_{electronic}$	-462.232852	-1048.629294	-1062.201307
$E_{nuclear}$	130.132801	384.428291	398.000302
.....			
E_{total}	-332.100050	-664.201003	-664.201005

require a more quantitative decomposition of the stabilization energy into electrostatic, polarization, exchange, charge transfer and coupling components.[3]

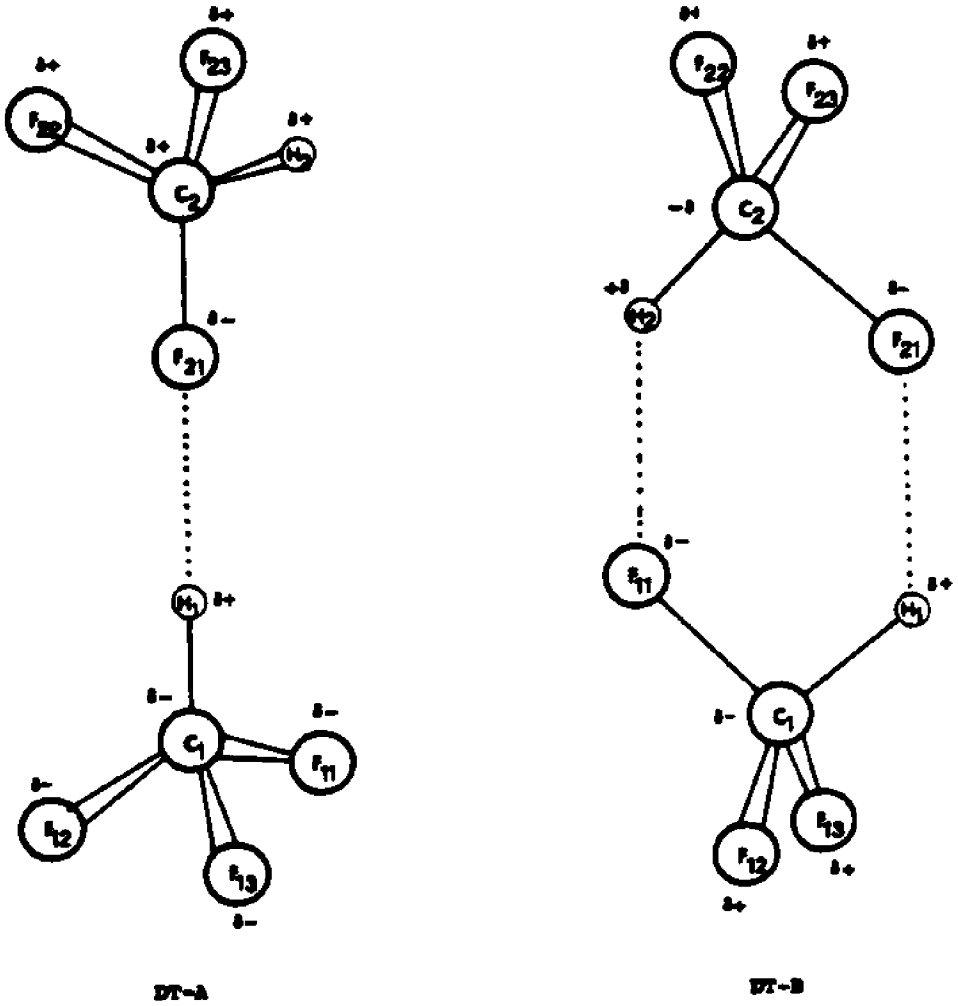

Figure A12. Charge Redistribution for Dimer Types A and B

References

1. K. Morokuma and J. Winick, J. Chem. Phys. 48, 3275 (1968).
2. K. Morokuma and L. Pedersen, J. Chem. Phys. 52, 1301 (1970).
3. K. Morokuma, Accts. of Chem. Res. 10, 294 (1977).
4. P. Kollman, Accts. of Chem. Res. 10, 365 (1977).
5. Quantum Chemistry Program Exchange, Prog #236, Chemistry Department of Indiana University.
6. J. Pople, J. Chem. Phys. 51, 2657 (1969).
7. J. Pople, J. Chem. Phys. 52, 2769 (1970).
8. J. Pople, J. Chem. Phys. 54, 724 (1971).
9. J. Pople, J. Chem. Phys. 56, 5255 (1972).
10. P. Kollman and A. Leland, Chem. Rev. 72, 283 (1972).

APPENDIX B

Infra-Red Spectroscopic Investigation of Association in Gaseous Fluoroform

Infra-Red Spectroscopic Investigation of Association in Gaseous Fluoroform

In most cases of hydrogen bonding, a red shift upon association is observed.[1] However, calculations on the frequency of the C-H stretching mode as a function of force constants for the linear and bent triatomic dimer models (C---H----F) indicate that a blue shift would occur upon association. It is believed that the large blue shift of 30 cm^{-1} in the C-H stretching frequency in going from gas to liquid is related to association of CHF_3 monomers. We propose such a temperature dependent association in the liquid phase for CHF_3, based on the available experimental data and quantum mechanical calculations on dimers of CHF_3 which have shown that the most stable dimer forms exhibit stabilization energies of $\sim$ 0.7 kcal/mole-dimer. If such an association was appreciable, it might be possible by careful observation of the spectra to see a frequency shift or a change in spectral intensities which would imitate a frequency shift by observing the spectra at various temperatures. That is to say as the temperature decreases, the concentration of the associated form would increase and that of the monomer would decrease. This would be indicated by corresponding changes in the intensities of the respective C-H stretching frequencies. If a low enough temperature could be reached, one would expect to see the monomer intensity approach zero so that the net effect appears to be a frequency shift.

To see if such a blue shift or intensity change would occur, the infra-red spectrum of gaseous CHF_3 was taken at three temperatures over the frequency range of 2990 cm^{-1} to 3100 cm^{-1}; T=500°K, T=300°K, and T=200°K. The spectra were taken on a Beckman IR 12 using cells fitted with KBr windows. For the measurement at 500 degrees-K a cell was

wrapped with heater wire and insulated. A thermocouple in contact with the cell wall was used to measure the temperature. The pressure rise in the cell was determined to have no important effect on the spectra. Pressures from 20 to 80 torr were used. To study the spectra at lower temperatures, it was necessary to design a cell for this particular purpose. A diagram of the cell used is shown in Figure B1. The cell has a cooling coil mounted in the sample chamber, where the inner diameter of the coil is greater than the diameter of the window path. The cell is provided with a vacuum jacket to minimize the condensation of atmospheric water. A dry ice/acetone bath was used for cooling the gas sample. The temperature of the inlet and outlet coolant was measured, and the average of these values was used to indicate the temperature of the gas. Due to the difficulty of measuring the temperature of the gas or the pressure of the gas in this experimental situation, it was assumed that the temperature of the gas equilibrated with that of the heated wall in the high T cell or the cooling coil in the low T cell.

Typical spectra obtained at the temperatures mentioned above are shown in Figures B2 and B3. Identification of the observed peaks are found in Table B1.

As can be seen from the spectra, no measurable frequency shift occurred (frequency resolution 0.5 cm^{-1}). The only noticeable temperature effect found was an expected sharpening in peak shape as the temperature decreased and a broadening in peak shape as the temperature was increased. However, this result does not rule out the existence of an associated form. If the concentration of the associated forms is small over the temperature range examined, it could be buried under the

monomer spectra. Also, if the temperature effect on the concentration of the associated form is small, a change might not be readily observed. Consider the following equilibrium:

$$A_2(g) \rightleftarrows 2A(g) \quad , \qquad \text{B-(1)}$$

where A is the CHF_3 monomer and A_2 the dimer. The equilibrium constant can be expressed as

$$K = \frac{(1-2X)^2}{X} \quad , \qquad \text{B-(2)}$$

where X is the fraction of dimer. K is given as[5]

$$K = \frac{9.819\times10^{-7}}{P} \cdot \frac{g_o^{\,2}(m_A kT)^{3/2}\,(1-e^{-h\omega c/kT})e^{-\Delta E_s/kT}}{2\sqrt{\pi}\, m_A r_e^{\,2} h} \qquad \text{B-(3)}$$

where T and P are the temperature in deg-K pressure in atmospheres, respectively, g_o is the electronic degeneracy, m_A is the mass of CHF_3 (AMU), ω is the H----F vibrational frequency (cm^{-1}), r_e is the carbon-carbon length (Å) and ΔE_s is the stabilization energy of the dimer (cal/mole-monomer). Evaluation of this expression for various values of the hydrogen bond strength and pressure as a function of temperature yields the % dimer expected. The results are tabulated in Table B2. The boxed off area in this table would roughly correspond to the T-P conditions at which the gas spectra was taken. Note that the following values were used for the various terms in Eqn. (3); these values are based on the QM calculations (Appendix A) and a normal coordinate analysis of

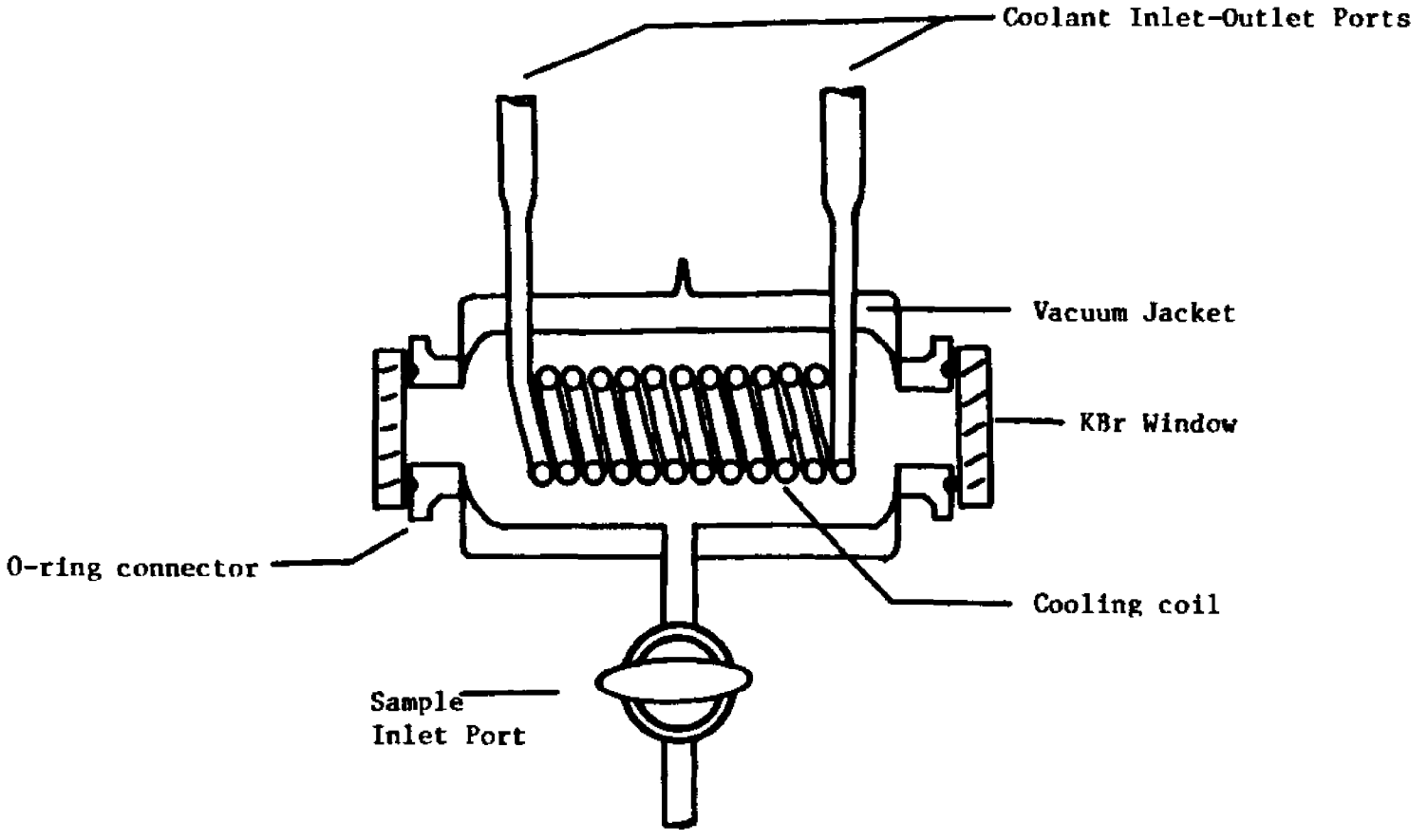

Figure B1. Low Temperature Gas IR Cell

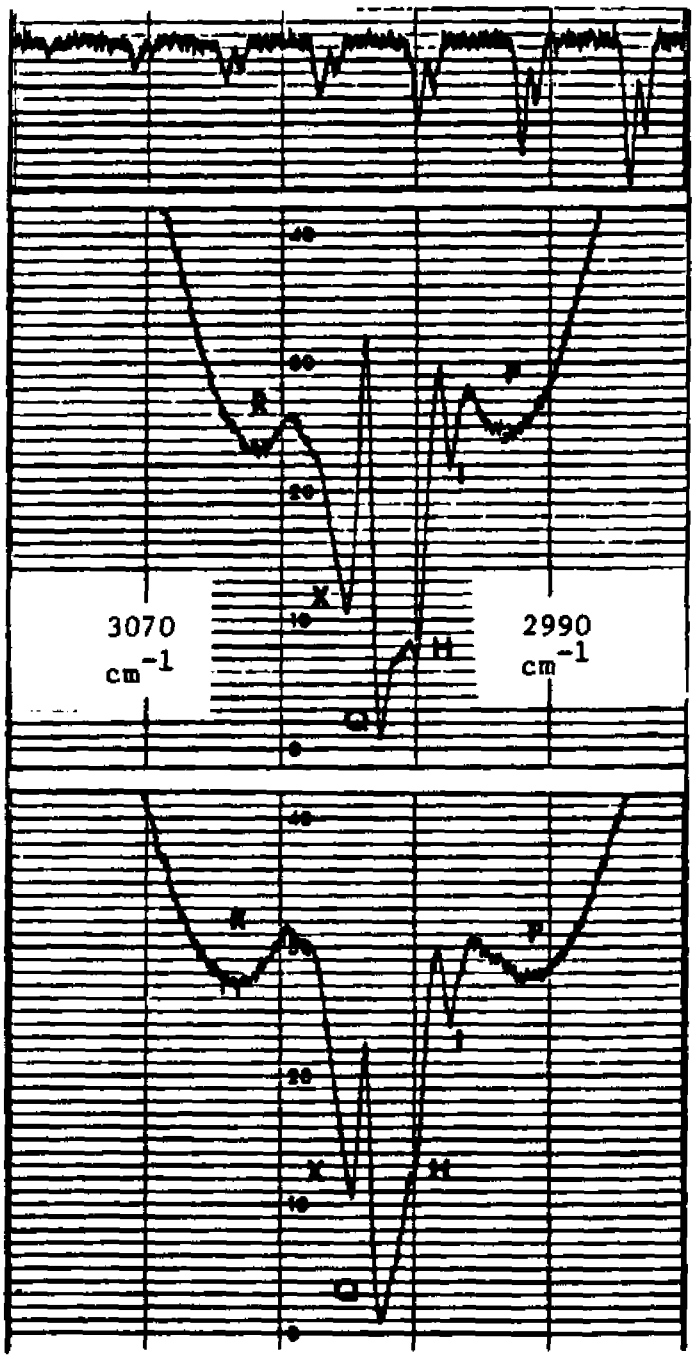

Figure B2. High Temperature Gas IR Spectrum of the C-H Vibrational Manifold in Fluoroform

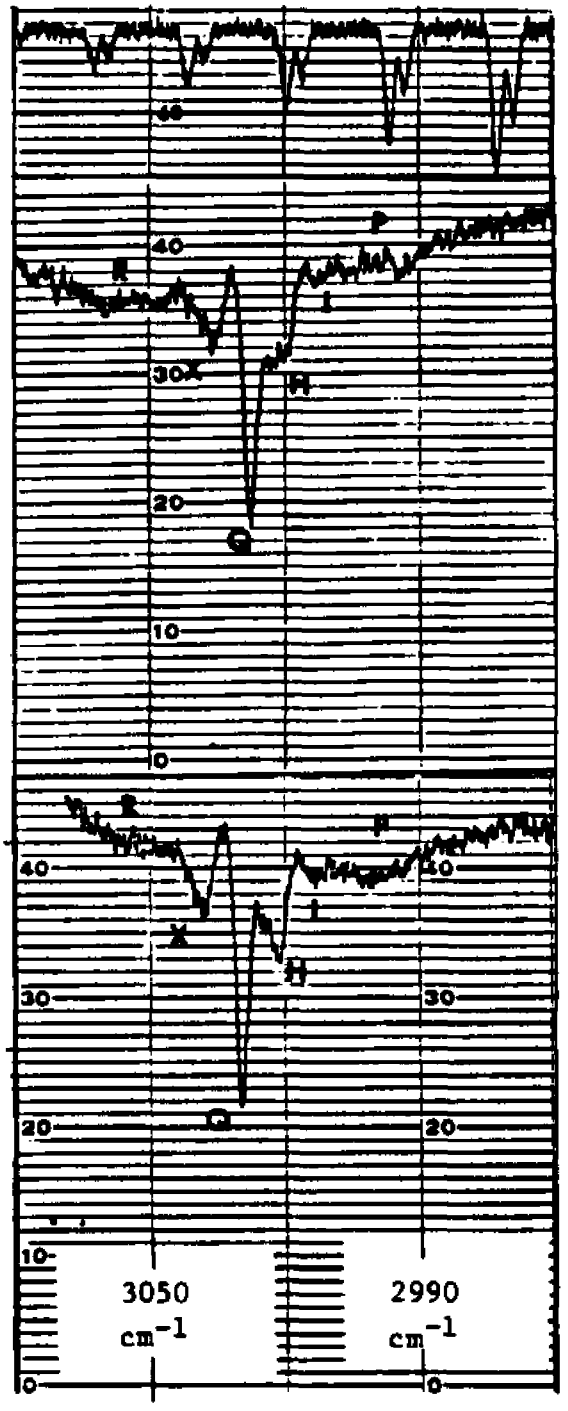

Figure B3. Low Temperature Gas IR Spectrum of the C-H Vibrational Manifold in Fluoroform

Table B1

Peak Assignment for the C-H Stretching Frequency

in CHF_3(g) Between 2990-3100 Wavenumbers^{-1}

Peak	Observed ν cm^{-1}	Literature ν cm^{-1}	Assignment
Q	3034.8	3034.2[2]	ν_1(C-H) ^{12}C
P			Rotational envelope
R			
I	3024.4	3025.0[3]	ν_1(C-H) ^{13}C
H	3029.4	3031.4[2]	Hotband
X	3040.1	3042.0[4]	Impurity? Possible Fermi Resonance?

CHF_3-dimer model systems:

$$r_e = r_{C---C} = 5.0 \text{ Å}$$

$$\omega = \omega_{A---A} = 100 \text{ cm}^{-1}$$

As can be seen, the calculated fraction of dimer is sufficiently small, at the experimental condition used, so that the monomer spectra would readily obscure that of a dimer.

Table B2

CHF_3 Dimer Fraction at Various Temperatures, Pressure and Stabilization Energies[b]

	P = 0.01 atm			P = 0.10 atm			P = 1.0 atm		
T(°K) ΔE_S[a] =	0.05	0.35	1.5	0.05	0.35	1.5	0.05	0.35	1.5
500.0	0.0	0.1	0.2	0.4	0.5	1.6	3.5	4.6	12.5
300.0	0.1	0.1	0.6	0.5	0.9	5.6	5.0	7.8	30.4
200.0	0.1	0.2	2.8	0.8	1.6	19.5	6.8	12.7	56.7
191.0	0.1	0.2	3.5	0.8	1.7	22.5	7.1	13.5	60.0
175.0	0.1	0.2	5.2	0.9	2.0	29.1	7.6	15.2	66.2
150.0	0.1	0.3	10.8	1.0	2.7	43.5	8.7	18.9	76.3
125.0	0.1	0.4	24.9	1.3	4.0	62.4	10.3	24.5	86.0
118.0	0.1	0.5	31.4	1.3	4.5	68.1	10.9	26.6	88.5

[a] ΔE_S in units of kcal/mole-monomer

[b] Units of percent

References

1. Vinogradov & Linell, Hydrogen Bonding, (New York: Van Nostrand Rheinhold Co.), 1971.

2. A. Ruoff, Spectrochimica Acta 27A, 1359 (1971).

3. P. J. Wilt, J. Mol. Spec. 58, 76 (1975).

4. H. D. Rex, J. Chem. Phys. 21, 1077 (1953).

5. F. T. Wall, Chemical Thermodynamics, (San Francisco: W. H. Freeman & Co.), 1974.

APPENDIX C

Computer Programs:

1. CRYPTIC - CRYostat Pressure Temperature Interactive Control Program
2. P9042DQ - Program to Calculate Vibrational Frequencies and Vapor Pressure Isotope Effect as a Function of Temperature

Listing of CRYPTIC

```
C     CRYOSTAT PRESSURE/TEMPERATURE INTERACTIVE CONTROL PROGRAM:KBQ/MAIN
C
C     THIS ROUTINE ALLOWS THE USER TO ENTER WHATEVER SUBROUTINE REQUIRED
C     TO PERFORM THE DESIRED TASK, THAT IS;T,P MEAS OR HEATER ADJ,ETC
C
C                              CRYPTIC/MAIN
C                          KBQ:VERSION 01 8/21/79
C                           ANTHONY M. POPOWICZ
C
C
C
      DOUBLE PRECISION TSN(100),ABSP(100),BP31(100),BP21(100),BP11(100),
     .TLNP1(100),TLNP2(100),TLNP3(100)
      DIMENSION TEMP(2,7),DAMPF(7),POWRF(7),WINDO(7),P(7),RATE(7),
     .DELTA(7)
      COMMON /BLK1/TEMP,IERR
      COMMON /BLK2/P
      COMMON /BLK3/TCNT,ICYCLE
      COMMON /BLK4/RTNT,IPRT
      COMMON /BLK5/TSN,ABSP,BP31,BP21,BP11,TLNP1,TLNP2,TLNP3,IPOINT
      COMMON /BLK6/OUT,FREQ,RLIN,DAMPF,POWRF,WINDO
      COMMON /BLK7/TSET,TINC
      COMMON /BLK8/RATE DELTA
      DO 3 I=1,7
    3 P(I)=0.0
      IPOINT=0
      CALL INSTR
    5 IERR=0
      DO 33 I=1,3
   10 IF(ITTOUR("007).NE.0) GO TO 10
   33 CONTINUE
      TYPE 101
  101 FORMAT(//'  *KBQ* (I2)? '$)
      ACCEPT 102,IROOT
  102 FORMAT(I2)
      GO TO (14,24,34,44,54,64,74,84,94,104,114,124),IROOT
      GO TO 5
   14 TYPE 111
  111 FORMAT(//'  ROUTE=TCAR (I1)? '$)
      ACCEPT 112,IOK
      IF (IOK.EQ.0) GO TO 5
      CALL TCAR
      GO TO 5
   24 TYPE 121
  121 FORMAT(//'  ROUTE=RTAR (I1)? '$)
      ACCEPT 112,IOK
      IF (IOK.EQ.0) GO TO 5
      CALL RTAR
```

```
      GO TO 5
   34 TYPE 131
  131 FORMAT(///'  ROUTE=MANAN (I1)? '$)
      ACCEPT 112,IOK
      IF (IOK.EQ.0) GO TO 5
      CALL MANAN
      GO TO 5
   44 TYPE 141
  141 FORMAT(///'  ROUTE=MAUTO (I1)? '$)
      ACCEPT 112,IOK
      IF (IOK.EQ.0) GO TO 5
      CALL MAUTO
      GO TO 5
   54 TYPE 151
  151 FORMAT(///'  ROUTE=PTIM (I1)? '$)
      ACCEPT 112,IOK
      IF (IOK.EQ.0) GO TO 5
      CALL PTIM
      GO TO 5
   64 TYPE 161
  161 FORMAT(///'  ROUTE=MUTEM (I1)? '$)
      ACCEPT 112,IOK
      IF (IOK.EQ.0) GO TO 5
      CALL MUTEM
      GO TO 5
   74 TYPE 171
  171 FORMAT(///'  ROUTE=INPUT (I1)? '$)
      ACCEPT 112,IOK
      IF (IOK.EQ.0) GO TO 5
      CALL INPUT
      GO TO 5
   84 TYPE 181
  181 FORMAT(///'  ROUTE=DBUMP (I1)? '$)
      ACCEPT 112,IOK
      IF (IOK.EQ.0) GO TO 5
      CALL DBUMP
      GO TO 5
   94 TYPE 191
  191 FORMAT(///'  ROUTE=PRESS (I1)? '$)
      ACCEPT 112,IOK
      IF (IOK.EQ.0) GO TO 5
      CALL PRESS
      GO TO 5
  104 TYPE 1101
 1101 FORMAT(///'  ROUTE=INSTR (I1)? '$)
      ACCEPT 112,IOK
      IF (IOK.EQ.0) GO TO 5
      CALL INSTR
      GO TO 5
  114 TYPE 1111
 1111 FORMAT(///'  ROUTE=CONV (I1)? '$)
```

```
      ACCEPT FT2,IOK
      IF (IOK.EQ.0) GO TO 5
      CALL CONN
      GO TO 5
  124 TYPE 1121
 1121 FORMAT(//'  ROUTE=EXIT (I1)? '$)
      ACCEPT 112,IOK
      IF (IOK.EQ.0) GO TO 5
      TYPE 1131
 1131 FORMAT(//T10,'     CRYPTIC EXIT---RUN TERMINATED
      CALL EXIT
      END
```

```
C                CRYPTIC/TCAR: SUBROUTINE 01
C
C     THIS ROUTINE MEASURES THE TEMPERATURES OF THE CRYOSTAT
C     COMPONENTS TWICE OVER A SPECIFIED PERIOD OF TIME.
C     THE ROUTINE CALCULATES TEMPERATURE CHANGES AND THE
C     RATE OF CHANGE PER COMPONENT AND PROVIDES A
C     PRINTOUT OF THIS INFORMATION.
C
C                    TCAR:VERSION 01 8/23/79
C                      ANTHONY N. POPOVICI
C
C
C
C
      SUBROUTINE TCAR
      COMMON /BLK1/TEMP,IERR
      COMMON /BLK3/TCUT,ICYCLE
      COMMON /BLK7/TSET,TINC
      COMMON /BLK8/RATE,DELTA
      DIMENSION IDATA(2,7),DATA(2,7),ICHAN(7),IDONE(7)
      IABSR="177000
      IABBUF="177002
      ICHAN(1)="15
      ICHAN(2)="415
      ICHAN(3)="1015
      ICHAN(4)="1415
      ICHAN(5)="2015
      ICHAN(6)="2415
      ICHAN(7)="3015
      IDONE(1)="214
      IDONE(2)="614
      IDONE(3)="1214
      IDONE(4)="1614
      IDONE(5)="2214
      IDONE(6)="2614
      IDONE(7)="3214
      ITRY=1
      ICYCLE=0
    5 DO 3 I=1,7
      CALL IPOKE(IABSR,ICHAN(I))
   15 ITEST=IPEEK(IABSR)
      IF (ITEST.EQ.IDONE(I)) GO TO 35
      IF (ITEST.GT.IDONE(I)) GO TO 25
      GO TO 15
```

```
 25 TYPE 11,I
 11 FORMAT(//T10,'  READ PROBLEM ON CHANNEL # ',I1)
    GO TO 9999
 35 IDATA(ITRY,I)=IPEEK(IABUF)
    IDATA(ITRY,I)=IDATA(ITRY,I)-"170000
  3 CONTINUE
    ITRY=ITRY+1
    TIME1=SECNDS(0.)
 45 TIME2=SECNDS(TIME1)
    IF (TIME2.LT.TCUT) GO TO 45
    IF (ITRY.GT.2) GO TO 55
    GO TO 5
 55 DO 13 I=1,2
    DO 13 J=1,7
    DATA(I,J)=AJFLT(IDATA(I,J))
 13 CONTINUE
    DO 23 I=1,2
    DO 23 J=1,7
    DATA(I,J)=DATA(I,J)*20.000/4096.0
 23 CONTINUE
    DO 33 I=1,2
    TEMP(I,1)=287.16-40.510*DATA(I,1)+4.2251*(DATA(I,1)**2)-0.67485*(D
   .ATA(I,1)**3)-273.15
    TEMP(I,2)=286.25-39.781*DATA(I,2)+4.0049*(DATA(I,2)**2)-0.65301*(D
   .ATA(I,2)**3)-273.15
    TEMP(I,3)=289.50-44.148*DATA(I,3)+4.9115*(DATA(I,3)**2)-0.68631*(D
   .ATA(I,3)**3)-273.15
    TEMP(I,4)=288.93-42.701*DATA(I,4)+4.8974*(DATA(I,4)**2)-0.73749*(D
   .ATA(I,4)**3)-273.15
    TEMP(I,5)=287.76-42.583*DATA(I,5)+4.6939*(DATA(I,5)**2)-0.69291*(D
   .ATA(I,5)**3)-273.15
    TEMP(I,6)=295.37-47.817*DATA(I,6)+5.9273*(DATA(I,6)**2)-0.78990*(D
   .ATA(I,6)**3)-273.15
    TEMP(I,7)=294.36-47.624*DATA(I,7)+5.8376*(DATA(I,7)**2)-0.77014*(D
   .ATA(I,7)**3)-273.15
 33 CONTINUE
    DO 43 I=1,7
    DELTA(I)=TEMP(2,I)-TEMP(1,I)
 43 RATE(I)=DELTA(I)/TCUT
    ICYCLE=ICYCLE+1
    TYPE 21,ICYCLE
 21 FORMAT(//T45,' READ # ',I6//T35,' BH ',T45,' LH ',T55,' RH ',T65,'
   . HH ',T75,' AH ',T85,' LC ',T95,' UC '//T20,' ----------------
   .----------------------------------------------------------------
   .----- ')
    DO 53 I=1,2
    TYPE 31,TEMP(I,1),TEMP(I,2),TEMP(I,3),TEMP(I,4),TEMP(I,5),TEMP(I,6
   .),TEMP(I,7)
 31 FORMAT(///'     TEMP (DEG C):   ',7(F10.3))
 53 CONTINUE
    TYPE 41,DELTA(1),DELTA(2),DELTA(3),DELTA(4),DELTA(5),DELTA(6),DELT
```

```
     .A(7)
  41 FORMAT(///'     DELTA (DEG C):  ',7(F10.3))
     TYPE 51,RATE(1),RATE(2),RATE(3),RATE(4),RATE(5),RATE(6),RATE(7)
  51 FORMAT(///'     RATE (DEG/SEC): ',7(F10.3))
     ITRY=1
     GO TO 8888
9999 IERR=1
8888 CONTINUE
     RETURN
     END
```

```
C                CRYPTIC/RTAR: SUBROUTINE #2
C
C     THIS ROUTINE MEASURES THE TEMPERATURES OF THE CRYOSTAT
C     COMPONENTS USING PLATINUM RESISTANCE THERMOMETERS.
C     DUE TO THE FACT THAT THE CAPILLARIES ARE NOT EQUIPPED WITH
C     WITH PRT'S THE THERMOCOUPLES ARE USED IN THIS CASE.
C     TEMPERATURES,TEMPERATURE CHANGES AND THE RATE OF CHANGE
C     ARE DETERMINED FOR EACH COMPONENT,AND PRINTOUT IS
C     PROVIDED. TWO MEASUREMENTS ARE MADE OVER A
C     SPECIFIED TIME PERIOD. ALSO TWO PRECISIONS IN THE A/D CONVERSION
C     ARE AVAILABLE:12BIT/15BIT PRECISION. THE LEVEL OF PRECISION
C     IS DETERMINED BY THE LEVEL OF THE REFERENCE VOLTAGE FROM THE
C     DATEL VOLTAGE CALIBRATION SOURCE,THAT IS A REF VOLT.  REATER THAN
C     0.5 VOLTS CAUSES THE ROUTINE TO PERFORM THE 15 BIT MEASUREMENT.
C     NOTE THAT THE TIME BETWEEN READINGS USING PRT'S IS THE
C     SPECIFIED WAIT TIME PLUS 40 SECONDS(EXTERNAL ELECTRONICS
C     SETTLING TIME).
C
C                    RTAR:VERSION #1 8/28/79
C                      ANTHONY M. POPOWICZ
C
C
C
C
      SUBROUTINE RTAR
      COMMON /BLK1/TEMP,IERR
      COMMON /BLK4/RTWT,IPRT
      COMMON /BLK8/RATE,DELTA
      DIMENSION IDATA(2,7),DATA(2,7),IBADB(6),IBADF(6)
      DIMENSION ICHAN(2),IDONE(2),JADDR(2),JDONE(2),SCALE(2)
      IPRT=0
      ITRY=1
      IBADB(1)="170444
      IBADB(2)="170444
      IBADB(3)="170444
      IBADB(4)="170454
      IBADB(5)="170454
      IBADB(6)="170454
      IBADF(1)="4001
      IBADF(2)="4002
      IBADF(3)="4004
      IBADF(4)="4001
      IBADF(5)="4002
      IBADF(6)="4004
```

```
      ICHAN(1)="2415
      ICHAN(2)="3015
      IDONE(1)="2614
      IDONE(2)="3214
      JADDR(1)="4401
      JADDR(2)="4405
      JDONE(1)="4600
      JDONE(2)="4604
      IPREC(1)=12
      IPREC(2)=15
      SCALE(1)=10.00
      SCALE(2)=1.000
      IADDR="177000
      IADBF="177002
    5 CALL IPOKE("170446,"4000)
      CALL IPOKE("170454,"4000)
      CALL IPOKE(IADDR,"5001)
   15 ITEST=IPEEK(IADDR)
      IF (ITEST.EQ."5200) GO TO 35
      IF (ITEST.GT."5200) GO TO 25
      GO TO 15
   25 TYPE 11
   11 FORMAT(//T10,'  READ PROBLEM ON CHAN 011(VREF) ')
      GO TO 9999
   35 IREF=IPEEK(IADBF)
      IREF=IREF-"170000
   45 VREF=AJFLT(IREF)
      VREF=VREF*10.000/4096.0
      IF (VREF.GE.0.50) GO TO 55
      J=1
      GO TO 60
   55 J=2
   60 CALL IPOKE("170446,"4000)
      CALL IPOKE("170454,"4000)
      CALL IPOKE(IDADD(6),IDADF(6))
      TIME1=SECNDS(0.0)
   65 TIME2=SECNDS(TIME1)
      IF (TIME2.GE.5.0) GO TO 75
      GO TO 65
   75 CALL IPOKE(IADDR,"4401)
   85 ITEST=IPEEK(IADDR)
      IF (ITEST.EQ."4400) GO TO 105
      IF (ITEST.GT."4400) GO TO 95
      GO TO 85
   95 TYPE 21
   21 FORMAT(//T10,'  READ PROBLEM ON CHAN 010(VSIG-REF/PRT) ')
      GO TO 9999
  105 IREFR=IPEEK(IADBF)
      IREFR=IREFR-"170000
      REFR=AJFLT(IREFR)
      REFR=REFR*10.000/4096.0
```

```
115 DO 5 I=1,2
    CALL IPOKE("170446,"4000)
    CALL IPOKE("170456,"4000)
    CALL IPOKE(IBADB(I),IBADF(I))
    TIME1=SECNDS(0.0)
125 TIME2=SECNDS(TIME1)
    IF (TIME2.GE.5.0) GO TO 135
    GO TO 125
135 CALL IPOKE(IADBR,JADBR(J))
145 ITEST=IPEEK(IADBR)
    IF (ITEST.EQ.JDONE(J)) GO TO 165
    IF (ITEST.ST.JDONE(J)) GO TO 155
    GO TO 145
155 TYPE 31,I
 31 FORMAT(//T10,'  READ PROBLEM ON CHAN #10(VBIB) PRT # ',I1)
    GO TO 9999
165 IDATA(ITRY,I)=IPEEK(IADBF)
    IDATA(ITRY,I)=IDATA(ITRY,I)-"170000
    DATA(ITRY,I)=AJFLT(IDATA(ITRY,I))
    DATA(ITRY,I)=(DATA(ITRY,I)/4096.0)*SCALE(J)+VREF-REFR
  3 CONTINUE
    DO 13 I=1,2
    N=I+3
    CALL IPOKE(IADBR,ICHAN(I))
175 ITEST=IPEEK(IADBR)
    IF (ITEST.EQ.IDONE(I)) GO TO 195
    IF (ITEST.ST.IDONE(I)) GO TO 185
    GO TO 175
185 TYPE 41,N
 41 FORMAT(//T10,'  READ PROBLEM ON CHAN # ',I1)
    GO TO 9999
195 IDATA(ITRY,N)=IPEEK(IADBF)
    IDATA(ITRY,N)=IDATA(ITRY,N)-"170000
    DATA(ITRY,N)=AJFLT(IDATA(ITRY,N))
    DATA(ITRY,N)=DATA(ITRY,N)*20.000/4096.0
 13 CONTINUE
    ITRY=ITRY+1
    IF (ITRY.LE.2) GO TO 115
    DO 23 I=1,2
    TEMP(I,1)=3.3358/DATA(I,1)+34.870+2.2008*DATA(I,1)+2.2642E-03*DATA
   .(I,1)**2-5.8296E-06*DATA(I,1)**3-273.15
    TEMP(I,2)=2.8528/DATA(I,2)+30.963+2.2742*DATA(I,2)+1.6939E-03*DATA
   .(I,2)**2-2.2344E-06*DATA(I,2)**3-273.15
    TEMP(I,3)=3.9408/DATA(I,3)+36.883+2.2471*DATA(I,3)+2.1929E-03*DATA
   .(I,3)**2-4.1826E-06*DATA(I,3)**3-273.15
    TEMP(I,4)=3.6789/DATA(I,4)+31.354+2.2489*DATA(I,4)+2.0573E-03*DATA
   .(I,4)**2-3.7857E-06*DATA(I,4)**3-273.15
    TEMP(I,5)=3.8118/DATA(I,5)+31.434+2.2452*DATA(I,5)+2.1355E-03*DATA
   .(I,5)**2-4.1016E-06*DATA(I,5)**3-273.15
    TEMP(I,6)=295.37-47.817*DATA(I,6)+5.9273*DATA(I,6)**2-0.78990*DATA
   .(I,6)**3-273.15
```

```
      TEMP(I,7)=294.36-47.624*DATA(I,7)+5.8376*DATA(I,7)**2-0.77014*DATA
     .(I,7)**3-273.15
   23 CONTINUE
      DO 33 I=1,7
      DELTA(I)=TEMP(2,I)-TEMP(1,I)
   33 RATE(I)=DELTA(I)/(RTUT*40)
      IPRT=IPRT+1
      TYPE 51,IPRT
   51 FORMAT(//T45,' READ # ',I6//T35,' BH ',T45,' LB ',T55,' RB  ',T65,
     .' BB ',T75,' AB ',T85,' LC ',T95,' UC '//T20,' ------------------
     .-------------------------------------------------------------
     .------ ')
      DO 43 I=1,2
      TYPE 61,TEMP(I,1),TEMP(I,2),TEMP(I,3),TEMP(I,4),TEMP(I,5),TEMP(I,6
     .),TEMP(I,7)
   61 FORMAT(///'      TEMP (DEG-C):   ',7(F10.3))
   43 CONTINUE
      TYPE 71,DELTA(1),DELTA(2),DELTA(3),DELTA(4),DELTA(5),DELTA(6),DELT
     .A(7)
   71 FORMAT(///'      DELTA(DEG-C):  ',7(F10.3))
      TYPE 81,RATE(1),RATE(2),RATE(3),RATE(4),RATE(5),RATE(6),RATE(7)
   81 FORMAT(///'      RATE(DEG/SEC):,7(F10.3))
      ITRY=1
      CALL IPOKE("170446,"4000)
      CALL IPOKE("170456,"4000)
      GO TO 8888
 9999 IERR=1
 8888 CONTINUE
      RETURN
      END
```

```
C                  CRYPTIC/HAHAN: SUBROUTINE 63
C
C     THIS ROUTINE ALLOWS ADJUSTMENT OF THE VARIOUS CRYOSTAT
C     HEATERS FROM THE CONSOLE TERMINAL. THE OPERATOR SPECIFIES
C     WHICH HEATERS ARE TO BE ADJUSTED, THE ROUTINE THEN REQUESTS
C     THE PERCENT POWER TO BE SUPPLIED TO THOSE PARTICULAR
C     HEATERS. THIS INPUT IS THEN REDUCED TO A FORMAT WHICH IS
C     COMPATABLE WITH THE D/A CONVERTERS. THE ROUTINE THEN
C     QUERIES THE OPERATOR WITH THE INPUT JUST SUPPLIED, IF
C     THE OPERATOR IS SATISFIED WITH THIS AS INPUT TO THE D/A'S
C     THEN THE ROUTINE LOADS THE D/A'S AND RETURNS TO KBQ.
C
C                    HAHAN:VERSION 81 8/29/79
C                      ANTHONY M. POPOVICZ
C
C
C
C
      SUBROUTINE HAHAN
      COMMON /BLK2/P
      DIMENSION W(7),V(7),IBADB(7),IBADF(7),IN(7)
      IBADB(1)="170444
      IBADB(2)="170442
      IBADB(3)="170440
      IBADB(4)="170450
      IBADB(5)="170454
      IBADB(6)="170452
      IBADB(7)="170446
      W(1)=P(1)*.1707
      W(2)=P(2)*.2839
      W(3)=P(3)*.02547
      W(4)=P(4)*.4462
      W(5)=P(5)*.4178
      W(6)=P(6)*.1391
      W(7)=P(7)*.04827
    5 DO 3 I=1,7
    3 IN(I)=0
    1 FORMAT(///T10,'  MANUAL HEATER ADJUST: ')
      TYPE 11
   11 FORMAT(///T10,'  CURRENT POWER LEVEL LISTING DESIRED(1)? ',$)
      ACCEPT 2,ILIST
    2 FORMAT(I1)
      IF (ILIST.EQ.0) GO TO 15
      TYPE 21,P(1),P(2),P(3),P(4),P(5),P(6),P(7),W(1),W(2),W(3),W(4),W(5
```

```
   .),U(6),U(7)
    TYPE 1
 21 FORMAT(///T24,' SN=1 ',T34,' LS=2 ',T44,' RS=3 ',T54,' US=4 ',T64,
   .' AS=5 ',T74,' CL=6 ',T84,' IS=7 '//T20,' ----------------------
   .---------------------------------------- '//T10,' ZP(OLD)',7
   .(4X,F6.2)//T10,'  U(OLD)'//T10,7(4X,E9.3)//T10,' ----------------
   .---------------------------------------- ')
 13 TYPE 31
 31 FORMAT(///T10,'  HEATERS(0) TO ADJUST(LIST DIR FORMAT)? ')
    ACCEPT *,IN(1),IN(2),IN(3),IN(4),IN(5),IN(6),IN(7)
    DO 33 I=1,7
    GO TO (115,125,135,145,155,165,175),IN(I)
    GO TO 33
115 TYPE 111
111 FORMAT(//T10,'  ZPSN(LIST DIR) = ')
    ACCEPT *,P(1)
    GO TO 33
125 TYPE 121
121 FORMAT(//T10,'  ZPLS(LIST DIR) = ')
    ACCEPT *,P(2)
    GO TO 33
135 TYPE 131
131 FORMAT(//T10,'  ZPRS(LIST DIR) = ')
    ACCEPT *,P(3)
    GO TO 33
145 TYPE 141
141 FORMAT(//T10,'  ZPUS(LIST DIR) = ')
    ACCEPT *,P(4)
    GO TO 33
155 TYPE 151
151 FORMAT(//T10,'  ZPAS(LIST DIR) = ')
    ACCEPT *,P(5)
    GO TO 33
165 TYPE 161
161 FORMAT(//T10,'  ZPCL(LIST DIR) = ')
    ACCEPT *,P(6)
    GO TO 33
175 TYPE 171
171 FORMAT(//T10,'  ZPIS(LIST DIR) = ')
    ACCEPT *,P(7)
 33 CONTINUE
    U(1)=P(1)*.1707
    U(2)=P(2)*.2839
    U(3)=P(3)*.02547
    U(4)=P(4)*.4462
    U(5)=P(5)*.4370
    U(6)=P(6)*.1393
    U(7)=P(7)*.04827
    V(1)=0.2661*SQRT(U(1))+0.348
    V(2)=0.1595*SQRT(U(2))+0.342
    V(3)=2.883*SQRT(U(3))+0.349
```

```
      V(4)=0.07687*SQRT(U(4))+0.555
      V(5)=0.09400*SQRT(U(5))+0.699
      V(6)=0.3121*SQRT(U(6))+0.359
      V(7)=0.9252*SQRT(U(7))+0.514
      DO 43 I=1,7
      DADF(I)=(-V(I)*2048.0/10.00)+2048.0
      IDADF(I)=INT(DADF(I))
      IDADF(I)=ABS(IDADF(I))
      TYPE 41,I,P(I),U(I),DADF(I),IDADF(I)
41    FORMAT(///T10,'  D',I1,'     ZP= ',F10.3,2X,'U= ',E9.3,2X,' VD= ',
     .F10.4,2X,' DADF= ',F10.1,2X,' IDADF= ',O6)
43    CONTINUE
      TYPE 51
51    FORMAT(//T10,'  OK TO LOAD(I1)? ')
      ACCEPT 12,IOK
12    FORMAT(I1)
      IF (IOK.EQ.0) GO TO 15
      DO 53 I=1,7
      CALL IPOKE(IDADD(I),IDADF(I))
53    CONTINUE
      TYPE 61
61    FORMAT(//T10,'  D/AS LOADED-HAHAH EXIT ')
      RETURN
      END
```

```
C                  CRYPTIC/HAUTO: SUBROUTINE 84
C
C     THIS ROUTINE AUTOMATICALLY ADJUST THE CRYOSTAT HEATERS
C     (EXCEPT FOR THE INTER SHIELD HEATER) USING DATA OBTAINED
C     FROM CALLING TCAR OR RTAR. THE FEEDBACK LOGIC IS ESSENTIALLY
C     A PROPORTIONAL CONTROL TYPE WITH BUILT IN DAMPING AND POWER
C     FACTORS. ALSO THERE ARE POWER LOCK FEATURES FOR EACH
C     HEATER SO AS NOT TO FORCE THE POWER SETTINGS TO ZERO. THIS
C     ROUTINE ATTEMPTS TO MAINTAIN THE APPROPRIATE TEMPERATURE
C     DIFFERENTIALS BETWEEN ALL COMPONENTS UP TO TSET EXCEPT FOR THE
C     REGULATED SHIELD DUE TO ITS LARGE HEAT CAPACITY TO POWER RATIO.
C     ALSO THE SAMPLE HOLDER TEMPERATURE IS FORCED TO BE LOWER THAN
C     ANY OTHER COMPONENT TEMPERATURE THROUGHOUT THE ENTIRE CONTROL
C     PROCESS.
C     TO LOOP OUT OF THE CONTROL PROCESS TYPE A CHARACTER(CR) ON THE
C     CONSOLE TERMINAL WITHIN BUT AFTER HEARING THE CONSOLE BELL
C     SOUND. A CHARACTER IN THE KB BUFFER WILL RETURN CONTROL TO KBG.
C     AN EMPTY BUFFER WILL CAUSE HAUTO TO PERFORM ANOTHER CONTROL
C     CYCLE BEFORE A KB QUERY WILL BE ATTEMPTED AGAIN.
C
C                    HAUTO:VERSION 01 9/4/79
C                      ANTHONY M. POPOVICZ
C
C
C
C
      SUBROUTINE HAUTO
      COMMON /BLK1/TEMP,IERR
      COMMON /BLK2/P
      COMMON /BLK4/OUT,FRRS,RLIN,DAMPF,POWRF,WINDO
      COMMON /BLK7/TSET,TINC
      COMMON /BLK8/RATE,DELTA
      DIMENSION DT(7),N(7),IBADB(7),IBADF(7),U(7),V(7),TS(7)
      N=0
      TS(1)=0.0
      TS(2)=0.2
      TS(3)=-2.0
      TS(4)=0.2
      TS(5)=0.2
      TS(6)=0.2
      TS(7)=0.2
      TYPE 1
    1 FORMAT(///T10,'   AUTO HEATER ADJUST: (0=TC;1=RT) SENSOR TYPE? '$)
      ACCEPT 2,ISEN
```

```
  2 FORMAT(I1)
    CALL TCAR
    IF (IERR.NE.0) GO TO 9999
    DO 3 I=1,7
    N(I)=0
  3 DT(I)=TSET-TEMP(2,I)+TS(I)
  5 IF (ISEN.EQ.1) GO TO 15
    CALL TCAR
    GO TO 20
 15 CALL RTAR
 20 IF (IERR.NE.0) GO TO 9999
    IF (R.EQ.0) GO TO 25
    TMIN=AMIN1(TEMP(2,2),TEMP(2,4),TEMP(2,5),TEMP(2,6),TEMP(2,7)
    IF (TMIN.GT.TEMP(2,1)) GO TO 25
    P(1)=0.0
    GO TO 35
 25 DO 33 I=1,6
    IF (I.EQ.3) GO TO 33
    T=TEMP(2,I)
    Q=TSET-T+TS(I)
    IF (Q.GT.WINDO(I)) GO TO 115
    R=RATE(I)-RLIM
    IF (R.GE.0.0000) GO TO 145
    IF (RATE(I).GE.0.0) GO TO 125
    N(I)=N(I)+1
    GO TO 145
115 IF (RATE(I).GT.2.0E-03) GO TO 145
    N(I)=N(I)+1
145 P(I)=(2**N(I))*(((TSET-T+TS(I))/DT(I)*POWRF(I)*DAMPF(I))
    GO TO 33
125 P(I)=P(I)
 33 CONTINUE
    T=TEMP(2,3)
    Q=TSET-T+TS(3)
    IF (Q.LE.WINDO(3)) GO TO 155
    F=(TSET-T+TS(3))/DT(3)
    IF (F.LE.FRRS) GO TO 155
    P(3)=POWRF(3)*DAMPF(3)
    GO TO 165
155 IF (RATE(3).GE.0.0) GO TO 165
    N(3)=N(3)+1
165 P(3)=(2**N(3))*(((TSET-T+TS(3))/DT(3))*POWRF(3)*DAMPF(3))
 35 DO 43 I=1,6
    PT=POWRF(I)*DAMPF(I)
    IF (P(I).GT.PT) GO TO 175
    IF (P(I).LT.0.0) GO TO 185
    GO TO 30
175 P(I)=POWRF*DAMPF(I)
    GO TO 30
185 P(I)=0.0
 30 TYPE 11,I,P(I)
```

```
 11 FORMAT(7/T10,'ZP(8',I1,')= ',F10.2)
 43 CONTINUE
    U(1)=P(1)*.1707
    U(2)=P(2)*.2839
    U(3)=P(3)*0.02547
    U(4)=P(4)*.4462
    U(5)=P(5)*.4362
    U(6)=P(6)*.1393
    V(1)=0.2441*SQRT(U(1))+0.548
    V(2)=0.1595*SQRT(U(2))+0.542
    V(3)=2.083*SQRT(U(3))+0.549
    V(4)=0.09487*SQRT(U(4))+0.358
    V(5)=0.09400*SQRT(U(5))+0.699
    V(6)=0.3121*SQRT(U(6))+0.339
    IBADD(1)="170444
    IBADD(2)="170442
    IBADD(3)="170440
    IBADD(4)="170450
    IBADD(5)="170454
    IBADD(6)="170452
    DO 53 I=1,6
    BADF(I)=(-V(I)*2048.0/10.00)+2048.0
    IBADF(I)=INT(BADF(I))
    IBADF(I)=ABS(IBADF(I))
    CALL IPOKE(IBADD(I),IBADF(I))
 53 CONTINUE
    DO 43 L=1,3
 10 IF (ITTOUR("007).NE.0) GO TO 10
 43 CONTINUE
    TYPE 21
 21 FORMAT(//T10,'  QUERY TIME')
    TIME1=SECNDS(0.0)
 45 TIME2=SECNDS(TIME1)
    IF (TIME2.GE.QUT) GO TO 55
    GO TO 45
 55 ICHAR=ITTINR()
    IF (ICHAR.GE.0) GO TO 9999
    N=N+1
    GO TO 5
9999 CONTINUE
    RETURN
    END
```

```
C                    CRYPTIC/PTIN: SUBROUTINE 05
C
C     THIS ROUTINE ACCEPTS INPUT FROM THE CONSOLE TERMINAL.
C     THIS INPUT CONSISTS OF THE PRECISION SAMPLE HOLDER
C     PRT READING, THE SPIRAL QUARTZ GAUGE COUNTER READING AND
C     THE CAPACITANCE GAUGE SIGNALS. THE ROUTINE AVERAGES MULTIPLE
C     INPUTS OF THE SAME POINT IF SO DESIRED;THEN PERFORMS THE
C     NECESSARY CONVERSIONS ON THE RAW SIGNAL. IT ALSO CALCULATES
C     THE APPROPRIATE TLNP'/P DATA AND STORES THE RESULTS FOR A DATA
C     DUMP AT THE APPROPRIATE TIME.
C
C                    PTIN:VERSION 81 9/4/79
C                      ANTHONY N. POPOVICZ
C
C
C
C
      SUBROUTINE PTIN
      COMMON /BLK5/TSH,ABSP,DP31,DP21,DP11,TLNP1,TLNP2,TLNP3,IPOINT
      DOUBLE PRECISION TEMP,DK,P3,P2,P1,P0
      TEMP=0.0D0
      IPOINT=IPOINT+1
   15 K=0
      J=IPOINT
      TSH(J)=0.0D0
      ABSP(J)=0.0D0
      DP31(J)=0.0D0
      DP21(J)=0.0D0
      DP11(J)=0.0D0
    5 K=K+1
      TEMP=TSH(J)
      TYPE 1,J
    1 FORMAT(//T10,'  INPUT TSH(OHMS) FORMAT:F10.4   TSH(',I4,')=')
      ACCEPT 2,TSH(J)
    2 FORMAT(F10.4)
      TSH(J)=TEMP+TSH(J)
      TEMP=ABSP(J)
      TYPE 11,J
   11 FORMAT(//T10,'  INPUT ABSP(CR.0) FORMAT:F10.1  ABSP(',I4,')=')
      ACCEPT 12,ABSP(J)
   12 FORMAT(F10.1)
      ABSP(J)=TEMP+ABSP(J)
      TEMP=DP31(J)
      TYPE 21,J
```

```
21 FORMAT(//T10,'  INPUT DP31(VOLTS)XSCALE:FORMAT E14.5 DP31(',I4,')
  .= '$)
   ACCEPT 22,DP31(J)
22 FORMAT(E14.5)
   DP31(J)=TEMP+DP31(J)
   TEMP=DP21(J)
   TYPE 31,J
31 FORMAT(//T10,'  INPUT DP21(VOLTS)XSCALE:FORMAT E14.5 DP21(',I4')=
  . '$)
   ACCEPT 32,DP21(J)
32 FORMAT(E14.5
   DP21(J)=TEMP+DP21(J)
   TEMP=DP11(J)
   TYPE 41,J
41 FORMAT(//T10,'  INPUT DP11(VOLTS)XSCALE:FORMAT E14.5 DP11(',I4,')=
  . '$)
   ACCEPT 42,DP11(J)
42 FORMAT(E14.5)
   DP11(J)=TEMP+DP11(J)
   TYPE 51
51 FORMAT(//T10,'  DO YOU WANT TO AVERAGE IN ANOTHER SET OF DATA?'$)
   ACCEPT 52,IOK
52 FORMAT(I1)
   IF (IOK.EQ.1) GO TO 5
   AK=FLOAT(K)
   BK=DBLE(AK)
   TSH(J)=TSH(J)/BK
   ABSP(J)=ABSP(J)/BK
   DP31(J)=DP31(J)/BK
   DP21(J)=DP21(J)/BK
   DP11(J)=DP11(J)/BK
   TSH(J)=(3.3558D0)/TSH(J)+(3.4870D01)+(2.2008D0)*TSH(J)+(2.2642D-03
  .)*(TSH(J)**2)-(5.0296D-06)*(TSH(J)**3)-2.7315D02
   ABSP(J)=(-0.19256D-13)*ABSP(J)**3+(0.16857D-08)*ABSP(J)**2+(0.1523
  .5D-01)*ABSP(J)
   DP31(J)=DP31(J)*1.0D01
   DP21(J)=DP21(J)*1.0D01
   DP11(J)=DP11(J)*1.0D01
   TYPE 61,TSH(J),ABSP(J),DP31(J),DP21(J),DP11(J),J
61 FORMAT(//T10,'   TSH(DEG-C)= ',E13.4//T10,'   ABSP(TORR)= ',E13.4/
  ./T10,'  DP31(TORR)= ',E13.4//T10,'  DP21(TORR)= ',E13.4//T10,'  DP
  .11(TORR)= ',E13.4//T10,'  POINT #= ',I4///T10,' OK TO SAVE(I1)?'$)
   ACCEPT 62,IOK
62 FORMAT(I1)
   IF (IOK.EQ.1) GO TO 25
   GO TO 15
25 P3=ABSP(J)+DP31(J)
   P2=ABSP(J)+DP21(J)
   P1=ABSP(J)+DP11(J)
   P0=ABSP(J)
   TLNP3(J)=(TSH(J)+2.7315D02)*DLOG(P3/P0)
```

```
      TLNP2(J)=(TSN(J)+2.7315D02)*DLOG(P2/P0)
      TLNP1(J)=(TSN(J)+2.7315D02)*DLOG(P1/P0)
      TYPE 71, J,TSN(J),ABSP(J),DP31(J),DP21(J),DP11(J),TLNP3(J),TLNP2(J)
     .,TLNP1(J)
   71 FORMAT(///T20,'    **********************************'//T24,' S ',I4//
     .T20,'    TSN(C)= ',B13.6//T20,'    ABSP(T)= ',B13.6//T20,'    DP31
     .(T)= ',B13.6//T20,'    DP21(T)= ',B13.6//T20,'    DP11(T)= ',B13.6
     .//T20,'    TLNP3(C)= ',B13.6//T20,'    TLNP2(C)= ',B13.6//T20,'
     . TLNP1(C)= ',B13.6//T20,'    **********************************')
      RETURN
      END
```

```
C                  CRYPTIC/NUTEN: SUBROUTINE 86
C
C     THIS ROUTINE IS USED TO SET THE NEW DESIRED TEMPERATURE FOR
C     THE NEXT POINT IN THE RUN. THE OPERATOR MUST PERFORM THIS
C     FUNCTION. IT IS NOT DONE AUTOMATICALLY AND THIS DATA IS
C     REQUIRED BY THE VARIOUS ROUTINES.
C
C                     NUTEN:VERSION 01 8/30/79
C                       ANTHONY M. POPOVICZ
C
C
C
C
      SUBROUTINE NUTEN
      COMMON /BLK7/TSET,TINC
      CALL IPOKE(%177000,%15)
    5 ITEST=IPEEK('177000)
      IF (ITEST.EQ.%214) GO TO 25
      IF (ITEST.GT.%214) GO TO 15
      GO TO 5
   15 TYPE 1
    1 FORMAT(//T10,'  READ PROBLEM ON CHAN 01 TSH/TC ')
      GO TO 9999
   25 ITSH=IPEEK(%177002)
      ITSH=ITSH-%170000
      SHT=AJFLT(ITSH)
      SHT=SHT*20.000/4096.0
      SHT=287.16-40.510*SHT+4.2251*SHT**2-0.67485*SHT**3-273.15
      TSET=SHT+TINC
   35 TYPE 11,SHT,TINC,TSET
   11 FORMAT(//T10,'   NUTEN ACTIVE:  TSH(DEG-C)= ',F10.3,5X,'INCREMENT=
     . ',F10.4,5X,' NEW TSET(DEG-C)= ',F10.3)
      TYPE 31
   31 FORMAT (//T10,'   IS THIS TSET OKT ')
      ACCEPT 2,IOK
    2 FORMAT(I1)
      IF (IOK.EQ.1) GO TO 9999
      TYPE 41
   41 FORMAT(//T10,'   INPUT THE DESIRED NEW TSET(LIST DIR)? ')
      ACCEPT *,T
      GO TO 35
 9999 CONTINUE
      RETURN
      END
```

```
C                  CRYPTIC/INPUT: SUBROUTINE #7
C
C     THIS ROUTINE ACCEPTS AS INPUT FROM THE CONSOLE TERMINAL THE
C     PROGRAM CONSTANTS AND OPERATING PARAMETERS. THESE VALUES
C     MUST BE DEFINED PRIOR TO EXECUTION OF ALL ROUTINE EXCEPT:
C     KDB,INSTR,MAMAN,PTIN,INPUT,DBUMP,PRESS,CONV. INPUT CAN BE
C     ENTERED AT ANY TIME ,HOWEVER CRE SHOULD BE TAKEN SO AS NOT
C     TO FORCE THE CRYOSTAT TO BACK TRACK IN TEMPERATURE,THAT IS
C     SET TINC AND TSET APPROPRIATELY.
C
C                    INPUT:VERSION #1 8/30/79
C                     ANTHONY M. POPOVICI
C
C
C
C
      SUBROUTINE INPUT
      COMMON /BLK3/TCUT,ICYCLE
      COMMON /BLK4/RTUT,IPRT
      COMMON /BLK6/GWT,FRRB,RLIN,DAMPF,POWRF,WINDO
      COMMON /BLK7/TSET,TINC
      DIMENSION ICODE(10)
    5 DO 3 I=1,10
    3 ICODE(I)=0
      TYPE 1
    1 FORMAT(//T10,'   INPUT OF DATA INSTRUCTIONS: LIST DIR ACCEPT FORMA
     .T'//T15,' TSET(=1)'//T15,' TINC(=2)'//T15,' TCUT(=3)'//T15,' R
     .TUT(=4)'//T15,' GWT(=5)'//T15,' POWRF(1...7)(=6)'//T15,' DAMPF(
     .1...7)(=7)'//T15,' WINDO(1...7)(=8)'//T15,' RLIN(=9)'//T15,' FR
     .RB(=10)')//T10,' LIST CODE VALUES FOR DATA INPUT(LIST DIR): ')
      ACCEPT *,ICODE(1),ICODE(2),ICODE(3),ICODE(4),ICODE(5),ICODE(6),ICO
     .DE(7),ICODE(8),ICODE(9),ICODE(10)
      DO 33 I=1,10
      GO TO (15,25,35,45,65,75,85,95,105),ICODE(I)
      GO TO 33
   15 TYPE 11
   11 FORMAT(//T10,'  TSET= ')
      ACCEPT *,TSET
      GO TO 33
   25 TYPE 21
   21 FORMAT(//T10,'  TINC= ')
      ACCEPT *,TINC
      GO TO 33
   35 TYPE 31
```

```
 31 FORMAT(//T10,'  TCUT= '$)
    ACCEPT *,TCUT
    GO TO 33
 45 TYPE 41
 41 FORMAT(//T10,'  RTUT= '$)
    ACCEPT *,RTUT
    GO TO 33
 55 TYPE 51
 51 FORMAT(//T10,'  OUT= '$)
    ACCEPT *,OUT
    GO TO 33
 65 TYPE 61
 61 FORMAT(//T10,'  POWRF(1 TO 7)= '$)
    ACCEPT *,POWRF(1),POWRF(2),POWRF(3),POWRF(4),POWRF(5),POWRF(6),POW
   .RF(7)
    GO TO 33
 75 TYPE 71
 71 FORMAT(//T10,'  DAMPF(1 TO 7)= '$)
    ACCEPT *,DAMPF(1),DAMPF(2),DAMPF(3),DAMPF(4),DAMPF(5),DAMPF(6),DAM
   .PF(7)
    GO TO 33
 85 TYPE 81
 81 FORMAT(//T10,'  WINDO(1 TO 7)= '$)
    ACCEPT *,WINDO(1),WINDO(2),WINDO(3),WINDO(4),WINDO(5),WINDO(6),WIN
   .DO(7)
    GO TO 33
 95 TYPE 91
 91 FORMAT(//T10,'  RLIN= '$)
    ACCEPT *,RLIN
    GO TO 33
105 TYPE 101
101 FORMAT(//T10,'  FRRS= '$)
    ACCEPT *,FRRS
 33 CONTINUE
    TYPE 211,TSET,TINC,TCUT,RTUT,OUT,RLIN,FRRS
211 FORMAT(///T10,'  TSET= ',F10.3//T10,'  TINC= ',F10.3//T10,'  TCUT=
   . ',F10.3//T10,'  RTUT= ',F10.3//T10,'  OUT= ',F10.3//T10,'  RLIN =
   . ',F10.3//T10,'  FRRS= ',F10.3)
    DO 43 I=1,7
    TYPE 221,I,POWRF(I),I,DAMPF(I),I,WINDO(I)
221 FORMAT(//T10,'  POWRF(',I1,')= ',F10.3,5X,'  DAMPF(',I1,')= ',F10.
   .3,5X,'  WINDO(',I1,')= ',F10.3)
 43 CONTINUE
    TYPE 231
231 FORMAT(///T10,'  INPUT OK(1)? '$)
    ACCEPT 12,IOK
 12 FORMAT(I1)
    IF (IOK.EQ.0) GO TO 5
    RETURN
    END
```

```
C                  CRYPTIC/BDUMP: SUBROUTINE BD
C
C     THIS ROUTINE DUMPS THE PRECISION DATA ONTO DISKETTE FOR LATER
C     USAGE IF SO DESIRED AS WELL AS PROVIDES A TABULAR TYPE OF
C     PRINTOUT ON THE CONSOLE TERMINAL. THIS ROUTINE SHOULD BE
C     USED JUST BEFORE THE TERMINATION OF THE RUN,HOWEVER IT CAN BE
C     USED AT ANY TIME WITHOUT CAUSING PROBLEMS FOR CRYPTIC.
C
C                    BDUMP:VERSION 81 8/30/79
C                      ANTHONY M. POPOWICZ
C
C
C
C
      SUBROUTINE BDUMP
      COMMON /BLKS/TSH,ABSP,BP31,BP21,BP11,TLNP1,TLNP2,TLNP3,IPOINT
      N=IPOINT
      TYPE 1
    1 FORMAT(1H1,4X,'N',4X,'TSH(C)',8X,'P(TORR)',5X,'BP31(TORR)',4X,' BP
     .21(TORR)',4X,'BP11(TORR)',6X,'TLNP31',8X,'TLNP21',8X,'TLNP11'//' -
     .-----------------------------------------------------------------
     .-------------------------------------')
      DO 3 I=1,N
      TYPE 11,N,TSH(N),ABSP(N),BP31(N),BP21(N),BP11(N),TLNP3(N),TLNP2(N)
     .,TLNP1(N)
   11 FORMAT(I4,8(2X,D12.6))
    3 CONTINUE
   15 TYPE 21
   21 FORMAT(//T10,'  DO YOU WANT TO DUMP ONTO DISK (DX1:) ? ')
      ACCEPT 2,IOK
    2 FORMAT(I1)
      IF (IOK.EQ.0) GO TO 5
      TYPE 31
   31 FORMAT(//T10,'  DX1: LOADED WITH A BLANK FORMATTED DISK ?')
      ACCEPT 2,IOK
      IF (IOK.EQ.0) GO TO 15
      DO 33 I=1,N
      WRITE(2,41) N,TSH(N),ABSP(N),BP31(N),BP21(N),BP11(N),TLNP3(N),TLNP
     .2(N),TLNP1(N)
   41 FORMAT(I4,8(2X,D12.6))
   33 CONTINUE
    5 CONTINUE
      RETURN
      END
```

```
C                CRYPTIC/PRESS: SUBROUTINE 09
C
C     THIS ROUTINE MEASURES THE TEMPERATURE OF THE SAMPLE HOLDER
C     USING ITS THERMOCOUPLE AS THE SENSOR, THE ABSOLUTE PRESSURE
C     AND DIFFERENTIAL PRESSURES USING THE SPIRAL QUARTZ GAUGE AND
C     CAPACITANCE GAUGES RESPECTIVELY. CONVERSIONS AND CALCULATIONS
C     ARE PERFORMED AND A PRINTOUT IS PROVIDED.
C
C                    PRESS:VERSION 01 9/4/79
C                     ANTHONY M. POPOWICZ
C
C
C
C
      SUBROUTINE PRESS
      DIMENSION ILOAD(4),IDUN(4),IDATA(4),DATA(4)
      ILOAD(1)="15
      ILOAD(2)="3411
      ILOAD(3)="4001
      ILOAD(4)="5401
      IDUN(1)="214
      IDUN(2)="3610
      IDUN(3)="4200
      IDUN(4)="5600
    5 DO 3 I=1,4
      CALL IPOKE("177000,ILOAD(I))
   15 ITEST=IPEEK("177000)
      IF (ITEST.EQ.IDUN(I)) GO TO 35
      IF (ITEST.GT.IDUN(I)) GO TO 25
      GO TO 15
   25 TYPE 11,I,ILOAD(I)
   11 FORMAT(//T10,'  READ PROBLEM ON CYCLE= ',I1,2X,'A/D LOAD= ',O6)
      GO TO 9999
   35 J=IPEEK("177002)
      IDATA(I)=J
      IDATA(I)=IDATA(I)-"170000
      DATA(I)=FLOAT(IDATA(I))
    3 CONTINUE
      DATA(1)=DATA(1)*20.000/4096.0
      DATA(1)=287.16-40.510*DATA(1)+4.2251*(DATA(1)**2)-0.67485*(DATA(1)
     .**3)-273.15
      DATA(2)=DATA(2)*100.0/4096.0
      DATA(2)=DATA(2)*1000.0
      DATA(2)=(-0.19256E-13)*DATA(2)**3+(0.16857E-08)*DATA(2)**2+(0.1523
```

```
     .5E-01)*DATA(2)
      DATA(3)=DATA(3)*100.0/4096.0
      DATA(4)=DATA(4)*100.0/4096.0
      TYPE 21,DATA(1),DATA(2),DATA(3),DATA(4)
   21 FORMAT(//T10,'  TSH= ',F10.3,2X,'DEG-C',5X,'PSOO= ',F13.3,2X,' TOR
     .R',5X,'+PCB= ',F10.3,2X,'XSCALE TORR',5X,'-PCB=',F10.3,2X,'XSCALE
     . TORR'///T10,'  DO YOU WANT ANOTHER READ ? '$)
      ACCEPT 12,INORE
   12 FORMAT(I1)
      IF (INORE.EQ.1) GO TO 5
 9999 CONTINUE
      RETURN
      END
```

```
C                    CRYPTIC/INSTR: SUBROUTINE #10
C
C     THIS ROUTINE PRINTS OUT THE OPERATING INSTRUCTIONS FOR
C     CRYPTIC AS WELL AS ACCEPTS RUN IDENTIFICATION INFORMATION FROM
C     THE OPERATOR AT THE KEYBOARD. IT ALSO PERFORMS SOME NECESSARY
C     INITIALIZATIONS. IT THEREFORE IS CALLED ONCE AUTOMATICALLY AS
C     SOON AS CRYPTIC IS LOADED AND RUN. INSTR CAN BE CALLED BY KBD
C     AT ANY TIME THE OPERATOR DESIRES.
C
C                          INSTR:VERSION #1 8/21/79
C                            ANTHONY M. POPOVICZ
C
C
C
C
      SUBROUTINE INSTR
      TYPE 101
  101 FORMAT(//T10'  NB: 1=YES; 0=NO'//T10'  PRINT INSTR(I1)?'$)
      ACCEPT 102,IWANT
  102 FORMAT(I1)
      IF (IWANT.EQ.0) GO TO 5
      TYPE 111
  111 FORMAT('1'T10,'SYSTEM OPERATING INSTRUCTIONS:'//T15'  THE MAIN
     .(KBD) ALLOWS DETERMINATION BY THE OPERATOR THE EXECUTION OF THE
     .DESIRED SUBROUTINE'//T16'  SUBR1=TCAR(CODE=1) MEASURES COMPONENT
     .TEMPERATURES USING TC-S'//T16,'  SUBR2=RTAR(CODE=2) MEASURES COMP
     .ONENT TEMPERATURES USING RT-S'//T16,'  SUBR3=MANAN(CODE=3) ALLOWS
     .THE OPERATOR TO ADJUST THE HEATERS FROM THE KEYBOARD'//T16,'
     .SUBR4=HAUTO(CODE=4) HEATER ADJUST IS DONE UNDER PROGRAM CONTROL
     .(HAUTO USES TCAR OR RTAR)'//T16,'  SUBR5=PTIN(CODE=5) ACCEPTS
     .CONSOLE INPUT OF THE PRECISION TEMP/PRESS DATA. THIS DATA IS REDUC
     .ED AND STORED'//T16,'  SUBR6=MUTEM(CODE=6) MEANS BY WHICH THE
     .OPERATOR CAN SET THE NEW DESIRED TEMPERATURE'//T16,'  SUBR7=INPUT
     .(CODE=7) ACCEPTS INPUT DATA,THAT IS, THE OPERATING PARAMETERS AND
     .CONSTANTS'//T16,'  SUBR8=DBUMP(CODE=8) PRINTS OUT AND WRITES TO
     .DISK THE PRECISION DATA'//T16,'  SUBR9=PRESS(CODE=9) READS SDS AND
     .CS PRESSURES'//T16,'  SUBR10=INSTR(CODE=10) PRINTS OUT OPERATING
     .INSTRUCTIONS,ACCEPTS RUN ID INFORMATION AND PERFORMS SOME INITIALI
     .ZATIONS(POWER TO HEATERS SET TO ZERO POWER)'//T16,'  SUBR11=CONV(C
     .ODE=11) CONVERTS KEYBOARD INPUT OF SENSOR SIGNAL VALUES TO TEMP AN
     .D PRESSURE DATA'//T16,'  SUBR12=EXIT(CODE=12) ALLOWS USER TO TERMI
     .NATE THE RUN.')
      TYPE 121
  121 FORMAT('1'////////T30,'  ********************'//T34,'  ROUTE=CODE'
```

```
   .//T55,' TCAL=   1'//T55,' RTAN=   2'//T54,' NANAN=   3'//T54
   .,' NAUTO=   4'//T55,' PTIN=   5'//T54,'MUTEN=   6'//T54,' INPUT
   .=   7'//T54,' BBUMP=   8'//T54,' PRESS=   9'//T54,' INSTR=10'//
   .T55,' CONV=   11'//T55,' EXIT=   12'//T50' **********************
   .'//T55,' NOTE: 0=NO AND 1=YES')
  5 TYPE 131
131 FORMAT('1'//T10,' WANT TO INPUT RUN ID INFORMATION(I1)? '$)
    ACCEPT 112,IWANT
112 FORMAT(I1)
    IF (IWANT.EQ.0) GO TO 25
    TYPE 141
141 FORMAT('1'//T20,,' RUN ID #= '$)
    ACCEPT 122
122 FORMAT(20H  RUN ID# GOES HERE )
    TYPE 151
151 FORMAT(//T20,' DATE = '$)
    ACCEPT 132
132 FORMAT(20H  DATE GOES HERE     )
    TYPE 161
161 FORMAT(//T20,' OPERATOR = '$)
    ACCEPT 142
142 FORMAT(25H OPERATOR NAME GOES HERE )
    TYPE 171
171 FORMAT(//T20,' SAMPLE ID = '$)
    ACCEPT 152
152 FORMAT(35H  SAMPLE ID GOES HERE              )
    TYPE 181
181 FORMAT(//T20,' SAMPLE PORT#1 = '$)
    ACCEPT 162
162 FORMAT(33H  SAMPLE PORT ID GOES HERE       )
    TYPE 191
191 FORMAT(//T20,' SAMPLE PORT#2 = '$)
    ACCEPT 162
    TYPE 201
201 FORMAT(//T20,' SAMPLE PORT#3 = '$)
    ACCEPT 162
    TYPE 211
211 FORMAT(//T20,' SAMPLE PORT#4 = '$)
    ACCEPT 162
    TYPE 221
221 FORMAT(//T5,' COMMENT(100CHAR):'$)
    ACCEPT 202
202 FORMAT(100H                                                COMMENT GOES
   .HERE                                                )
 25 CALL IPOKE("177000,"0)
    CALL IPOKE("170440,"4000)
    CALL IPOKE("170442,"4000)
    CALL IPOKE("170444,"4000)
    CALL IPOKE("170446,"4000)
    CALL IPOKE("170450,"4000)
    CALL IPOKE("170452,"4000)
```

```
      CALL IPOKE("170454,"4000)
      CALL IPOKE("170456,"4000)
      TYPE 231
  231 FORMAT(//T10,'  HAS INPUT DATA BEEN SPECIFIED AS OF YET(1) ? ')
      ACCEPT 212, IYES
  212 FORMAT(I1)
      IF (IYES.EQ.1) GO TO 15
      CALL INPUT
   15 CONTINUE
      RETURN
      END
```

```
C                    CRYPTIC/CONV: SUBROUTINE 811
C
C     THIS ROUTINE CONVERTS INPUT FROM THE CONSOLE TERMINAL FROM
C     ANALOG TO PHYSICAL DATA. THAT IS VOLTAGE,RESISTANCE AND
C     COUNTER READINGS TO PHYSICALLY SIGNIFICANT VALUES OF PRESSURE
C     AND TEMPERATURE.
C
                       CONV:VERSION 01 9/5/79
C                        ANTHONY M. POPOWICZ
C
C
C
C
      SUBROUTINE CONV
      TYPE 1
    1 FORMAT(///T10,'   THERMOCOUPLE INPUT: CODE=1 '//T10,'   RESISTANCE
     .THERMOMETER INPUT: CODE=2 '//T10,'   PRESSURE SENSOR INPUT: CODE=3
     .'//T10,'   RETURN TO KBD: CODE=0'//T10,'   NOTE INPUT LIST DIR'///
     .T10,'   CODE= '$)
    5 ACCEPT 2,ICODE
    2 FORMAT(I1)
      GO TO (15,25,35),ICODE
      GO TO 9999
   15 TYPE 11
   11 FORMAT(//T10,'  VSH= '$)
      ACCEPT *,V
      T=287.14-40.510*V+4.2251*V**2-0.67485*V**3-273.15
      TYPE 21,T
   21 FORMAT(//T10,'  TSH= ',F10.3)
      TYPE 31
   31 FORMAT(//T10,'  VLS= '$)
      ACCEPT *,V
      T=286.25-39.781*V+4.0049*V**2-0.65301*V**3-273.15
      TYPE 41,T
   41 FORMAT(//T10,'  TLS= ',F10.3)
      TYPE 51
   51 FORMAT(//T10,'  VRS= '$)
      ACCEPT *,V
      T=289.50-44.148*V+4.9115*V**2-0.68631*V**3-273.15
      TYPE 61,T
   61 FORMAT(//T10,'  TRS= ',F10.3)
      TYPE 71
   71 FORMAT(//T10,'  VUS= '$)
      ACCEPT *,V
```

```
      T=288.93-42.701*V+4.8976*V**2-0.73749*V**3-273.15
      TYPE 81,T
   81 FORMAT(//T10,'  TUB= ',F10.3)
      TYPE 91
   91 FORMAT(//T10,'  VAB= ')
      ACCEPT *,V
      T=287.76-42.583*V+4.6939*V**2-0.69291*V**3-273.15
      TYPE 101,T
  101 FORMAT(//T10,'  TAB= ',F10.3)
      TYPE 111
  111 FORMAT(//T10,'  VLC= ')
      ACCEPT *,V
      T=295.37-47.817*V+5.9273*V**2-0.78990*V**3-273.15
      TYPE 121,T
  121 FORMAT(//T10,'  TLC= ',F10.3)
      TYPE 131
  131 FORMAT(//T10,'  VUC= ')
      ACCEPT *,V
      T=294.36-47.624*V+5.8376*V**2-0.77814*V**3-273.15
      TYPE 141,T
  141 FORMAT(//T10,'  TUC= ',F10.3)
      GO TO 5
   25 TYPE 151
  151 FORMAT(//T10,'  RSH= ')
      ACCEPT *,R
      T=3.3558/R+34.870+2.2088*R+2.2642E-03*R**2-5.0296E-06*R**3-273.15
      TYPE 161,T
  161 FORMAT(//T10,'  TSH= ',F11.4)
      TYPE 171
  171 FORMAT(//T10,'  RLS= ')
      ACCEPT *,R
      T=2.8528/R+30.963+2.2742*R+1.6939E-03*R**22-5.0296E-06*R**3-273.15
      TYPE 181,T
  181 FORMAT(//T10,'  TLS= ',F11.4)
      TYPE 191
  191 FORMAT(//T10,'  RRS= ')
      ACCEPT *,R
      T=3.9408/R+30.803+2.2471*R+2.2929E-03*R**2-4.1826E-06*R**3-273.15
      TYPE 201,T
  201 FORMAT(//T10,'  TRS= ',F11.4)
      TYPE 211
  211 FORMAT(//T10,'  RUB= ')
      ACCEPT *,R
      T=3.67891/R+31.354+2.2489*R+2.0573E-03*R**2-3.7857E-06*R**3-273.15
      TYPE 221,T
  221 FORMAT(//T10,'  TUB= ',F11.4)
      TYPE 231
  231 FORMAT(//T10,'  RAB= ')
      ACCEPT *,R
      T=3.8118/R+31.434+2.2452*R+2.1355E-03*R**2-4.1016E-06*R**3-273.15
      TYPE 241,T
```

```
241 FORMAT(//T10,'  TAB= ',F11.4)
    GO TO 5
 35 TYPE 251
251 FORMAT(//T10,'  SOS(CR)= '$)
    ACCEPT *,S
    P=-0.19254E-13*S**3+0.16857E-08*S**2+0.15235E-01*S
    TYPE 261,P
261 FORMAT(//T10,'  PSOS= ',F11.4)
    TYPE 271
271 FORMAT(//T10,'  DP31,SCALE= '$)
    ACCEPT *,S,S
    P=S*S*10.000
    TYPE 281,P
281 FORMAT(//T10,'  DP31= ',F11.5)
    TYPE 291
291 FORMAT(//T10,'  DP21,SCALE= '$)
    ACCEPT *,S,S
    P=S*S*10.000
    TYPE 301
301 FORMAT(//T10,'  DP21= ',F11.5)
    TYPE 311
311 FORMAT(//T10,'  DP11,SCALE= '$)
    ACCEPT *,S,S
    P=S*S*10.000
    TYPE 321,P
321 FORMAT(//T10,'  DP11= ',F11.5)
    GO TO 5
9999 CONTINUE
    RETURN
    END
```

Listing of P9042DQ

```
C THIS IS A VARIATION OF 9042 PROGRAM FOR OBTAINING THE DIFFERENTIAL EFFECTS IN
C FREQUENCIES, LN(S/S')F FOR GAS OR LIQ PHASE, AND LN(FC/FG), DUE TO A CHANGE IN
C F-MATRIX OF GAS OR LIQUID. UP TO 24 F-MATRIX ELEMENTS MAY BE CHANGED
C SIMULTANEOUSLY IN EACH PHASE. INPUT SETS MAY BE STACKED TO PROCESS AS MANY
C DIFFERENTIAL EFFECTS AS NEEDED. ONLY ONE REFERENCE & UP TO TWO NON-REFERENCE
C ISOTOPES ARE ALLOWED FOR EACH PHASE.
C     THE ENTIRE MAIN PROGRAM BETWEEN STATEMENT NO. 90 AND THE END OF PROGRAM
C     IS REPEATED FOR EVERY ISOTOPIC SPECIES.
C *** ORDER OF INPUT:
C      1) ISOTOPE1, GAS ,NUMB=1        (=REFERENCE): READ BG(1, , ) & FF(1, , ,)
C      2)    "    , LIQ ,NUMB=2        (    "     ): READ BG(2, , ) & FF(2, , ,)
C      3) ISOTOTE2, GAS ,NUMB=3                     : READ BG(3, , )
C      4)    "    , LIQ ,NUMB=4                     : READ BG(4, , )
C      5) ISOTOPE3, GAS ,NUMB=5, IF ANY             : READ BG(5, , )
C      6)    "    , LIQ ,NUMB=6,   "               : READ BG(6, , )
C      7) ISOTOPE1, GAS ,NUMB=7,CHANGE IN F IF ANY : READ F-CHANGE INFORMATION
C      8)    "    , LIQ ,NUMB=8,     "      "      : READ F-CHANGE INFORMATION
C      9) ISOTOPE2, GAS ,NUMB=9,
C     10)    "    , LIQ ,NUMB=10,
C     11) ISOTOPE3, GAS ,NUMB=11,
C     12)    "    , LIQ ,NUMB=12,
C     13) ISOTOPE1, GAS ,NUMB=13,CHANGE IN F IF ANY: READ F-CHANGE INFORMATION
C     14)    "    , LIQ ,NUMB=14,    "      "      : READ F-CHANGE INFORMATION
C     15)
      IMPLICIT REAL*8 (A-H,O-Z)
      DIMENSION BG(6,18,18),FF(2,18,18),G(18,18),F(18,18),W(18,18),
     1DV(18),T(10),RECORD(80),NRO(170),NCO(170),NFO(170),Z(170),
     2FI(170),FJ(170),NROWG(4),NCOLG(4),DATING(4),NRL(170),NCL(170),
     3NFL(170),ZL(170),FIL(170),NRG(170),NCG(170),NFG(170),ZG(170),
     4FIG(170),IT(24),A(18,18),DG(18),DD(18),H(18,18),C(18,18),FNEW(24)


      CALL ERRSET (207,256,-1,0)
      CALL ERRSET (208,511,-1,0)

C READ GLOBAL INFORMATION FOR PRESENT MOLECULE.  "MOLECULES" ARE DIFFERENT IF
C DIFFERENT ISOTOPIC SPECIES, DIFFERENT PHASE, AND DIFFERENT F-MATRIX.  STACK
C AS MANY MOLECULES AS NEEDED, EXCEPT THAT THE TOTAL NUMBER MUST BE AN INTEGER
C MULTIPLE OF 4 OR 6
C     IND=-09 : THE PROGRAM CALLS EXIT OTHERWISE. PUT ONE BLANK CARD AT THE END
C               OF INPUT DECK.
C     NUMB    : SERIAL MOLECULE NUMBER.  SEE EXAMPLES.
C     NO      : NUMBER OF INTERNAL COORDINATES USED FOR F- & G-MATRICES
C     NRED    : NO. OF REDUNDANT COORDINATES INCLUDED IN NO.
```

```
C     IFS      : =2 IF STANDARD F-MATRIX, AND IF G-MATRIX INPUT IS PROVIDED
C              : =1 IF    "         "    , BUT NO     "      "         "
C              : =0 IF F-MATRIX IS TO BE MODIFIED.
C     NF       : NUMBER OF ELEMENTS IN FI-MATRIX.  THIS AND NOZ ARE SIGNIFICANT &
C                NEEDED ONLY WHEN NUMB=1 OR 2.
C     NOZ      : NUMBER OF ELEMENTS IN Z-MATRIX.
C     NIT      : NUMBER OF FI-MATRIX ELEMENTS TO BE CHANGED SIMULTANEOUSLY.  THIS
C                AND MODE BELOW ARE SIGNIFICANT & NEEDED ONLY WHEN
C                NUMB IS NOT 1 OR 2 AND IF KIND=1.
C     MODE     : =0 IF A CHANGE OF +1% IS IMPOSED ON EVERY F-MATRIX ELEMENT
C                   MODIFIED
C                =1 IF A CHANGE OF +0.1 MDYN/A IS IMPOSED ON EVERY ELEMENT
C                   MODIFIED
C                =2 IF EACH CHANGE IS BY +0.01 MDYN/A.
C                =3 IF EACH CHANGE IS BY +0.001 MDYN/A.
C                =4 IF NON-STANDARD CHANGES ARE MADE. THEN, FNEW INPUT IS NEEDED.
C     KIND     : =1 IF REFERENCE-GAS OR REFERENCE-LIQ MOLECULE.
C                =2 IF NON-REFERENCE MOLECULE USING THE STANDARD F-MATRIX.
C                =3 IF NON-REFERENCE MOLECULE USING A MODIFIED F-MATRIX.
C     ********* FOR FURTHER DISTINCTION AMONG KINDS, SEE "SUMMARY" BELOW.
   90 READ(5,5001) IND,NUMB,NQ,NRED,IFS,NF,NOZ,NIT,KIND,NOTEM,MODE,NCT
 5001 FORMAT(12I3)
C
C     ***************************************************************
C
C SUMMARY OF TYPICAL GLOBAL INPUT (FOR 2 NON-REFERENCE MOLECULES) FOLLOWS:
```

C DESCRIPTION OF MOLECULE	NUMB	IFS	KIND	READ	CALCULATE	SAVE	PRINTOUT
STAND-F,REFERENCE,GAS	1	2	1	G,F,T	FREQ	FREQ	F
" " ,LIQ	2	2	1	G,F	FREQ	FREQ	F
" ISOTOPE-A,GAS	3	2	2	G	FREQ,RPFR	FREQ,RPFR	NONE
" " ,LIQ	4	2	2	G	FREQ,RPFR	FREQ,RPFR	FREQ(G',G)
					LN(FC/FG)		FREQ(L',L)
							DFREQ(ISOTOPE ,PHASE)
							RPFR(G,L,D)
" ISOTOPE-B,GAS	5	2	2	G	FREQ,RPFR	FREQ,RPFR	NONE
" " ,LIQ	6	2	2	G	FREQ,RPFR	FREQ RPFR	SAME AS FOR
					LN(FC/FG)		ISOTOPE-A
MOD'D-F,REFERENCE,GAS	7	1/0	1	IT	FREQ	FREQ	CHANGE IN F
" " LIQ	8	1/0	1	IT	FREQ	FREQ	" "
" ISOTOPE-A,GAS	9	1/0	3	NONE	ALL+DIFF.	ALL+DIFF.	NONE
" " ,LIQ	10	1/0	3	"	"	"	ALL+DIFF
" ISOTOPE-B,GAS	11	1/0	3	"	"	"	NONE
" " ,LIQ	12	1/0	3	"	"	"	ALL+DIFF

```
C ****
C NOTES:+ALL MEANS ALL ITEMS APPEARING FOR CORRESPONDING SPECIES IN STAND-F
```

```
C       *DIFF MEANS DIFFERENCE, MODIFIED-F MINUS STANDARD-F
C       *ONE OR BOTH IFS'S FOR GAS & LIQ IN MODIFIED-F CAN BE 1.  REPEAT PATTERN
C        OF IFS USED FOR REF FOR ALL OTHER ISOTOPIC MOLECULES, E.G.,IF IFS=1 & 0
C        FOR REF GAS & LIQ, USE IF=1 & 0 FOR ISOTOPE-A & -B ALSO.
C     **************************************************************
      IF(IND.EQ.-9) GO TO 100
   95 CALL EXIT
  100 READ(5,5002)(RECORD(I),I=1,18)
 5002 FORMAT(9A8/9A8)
      WRITE(6,6001)(RECORD(I),I=1,18)
 6001 FORMAT(1H1,/5X,9A8,/)
  103 IF(IFS.EQ.2) GOTO 110
  104 NP=NCT
      DO 105 I=1,NQ
      DO 105 J=1,NQ
  105 G(I,J)=GG(NP,I,J)
      GO TO 130
  110 CONTINUE
      DO 112 I=1,NQ
      DO 112 J=1,NQ
      GG(NUMB,I,J)=0.0D0
  112 G(I,J)=0.0D0
      READ(5,5000)(RECORD(I),I=1,9)
 5000 FORMAT(9A8)
  113 READ(5,5003)(NROWG(L),NCOLG(L),DATING(L),L=1,3)
 5003 FORMAT(3(2I3,E18.9))
  115 DO 120 L=1,3
      IF(NROWG(L))122,610,117
  117 IF(NCOLG(L)-NROWG(L))610,118,118
  118 IF(NQ-NCOLG(L))610,119,119
  119 I=NROWG(L)
      J=NCOLG(L)
      G(I,J)=DATING(L)
      G(J,I)=G(I,J)
      GG(NUMB,I,J)=G(I,J)
  120 GG(NUMB,J,I)=G(I,J)
      GO TO 113
  122 IF(1+NROWG(L))610,130,610
  130 IF(NUMB-3)135,160,160
  135 READ(5,5004)(NRO(I),NCO(I),NFO(I),Z(I),I=1,NOZ)
 5004 FORMAT(4(3I3,F9.6))
      READ(5,5005)(FI(K),K=1,NF)
 5005 FORMAT(6F12.6)
      DO 138 K=1,NOZ
      IF(NQ-NCO(K))615,136,136
  136 IF(NCO(K)-NRO(K))615,137,137
  137 IF(NF-NFO(K))615,138,138
  138 CONTINUE
      IF(NUMB.EQ.1) GOTO 150
  140 DO 141 I=1,NOZ
      NRL(I)=NRO(I)
```

```
      NCL(I)=NCO(I)
      NFL(I)=NFO(I)
  141 ZL(I)=Z(I)
      DO 142 I=1,NF
  142 FIL(I)=FI(I)
      LG=2
      GO TO 300
  150 LG=1
      DO 151 I=1,NOZ
      NRG(I)=NRO(I)
      NCG(I)=NCO(I)
      NFG(I)=NFO(I)
  151 ZG(I)=Z(I)
      DO 152 I=1,NF
  152 FIG(I)=FI(I)
      IF(NOTEM.EQ.0) GO TO 300
      READ(5,5006)(T(I),I=1,NOTEM)
 5006 FORMAT(9F8.2)
      WRITE(6,5006)(T(I),I=1,NOTEM)
      GO TO 300
  160 IF(KIND.EQ.1) GOTO 166
  161 IF(NUMB.EQ.(NUMB/2)*2) GOTO 165
  162 LG=1
      GOTO 320
  165 LG=2
      GOTO 320
  166 IF(NIT.EQ.0) GO TO 161
      READ(5,5001)(IT(I),I=1,NIT)
      IF(MODE.NE.4) GOTO 171
      READ(5,5005)(FNEW(I),I=1,NIT)
      IF(NUMB.EQ.(NUMB/2)*2) GO TO 168
      DO 167 I=1,NIT
      J=IT(I)
  167 FIG(J)=FNEW(I)
      GO TO 171
  168 DO 169 I=1,NIT
      J=IT(I)
  169 FIL(J)=FNEW(I)
  171 IF(NUMB.EQ.(NUMB/2)*2) GOTO 175
  172 LG=1
      DO 173 I=1,NOZ
      NRO(I)=NRG(I)
      NCO(I)=NCG(I)
      NFO(I)=NFG(I)
  173 Z(I)=ZG(I)
      DO 174 I=1,NF
  174 FI(I)=FIG(I)
      GO TO 180
  175 LG=2
      DO 176 I=1,NOZ
      NRO(I)=NRL(I)
```

```
      NCO(I)=NCL(I)
      NFO(I)=NFL(I)
  176 Z(I)=ZL(I)
      DO 177 I=1,NF
  177 FI(I)=FIL(I)
  180 IF(IFS.NE.0) GO TO 300
      IF(MODE.GE.1) GO TO 190
  181 DO 185 I=1,NIT
      J=IT(I)
  185 FI(J)=FI(J)*1.01D0
      GO TO 300
  190 DO 195 I=1,NIT
      J=IT(I)
      M=-MODE
  195 FI(J)=FI(J)+10.D0**M
  300 CONTINUE
      DO 305 I=1,NQ
      DO 305 J=1,NQ
  305 FF(LG,I,J)=0.0D0
      DO 310 K=1,NOZ
      I=NCO(K)
      J=NRO(K)
      M=NFO(K)
      FF(LG,I,J)=FF(LG,I,J)+Z(K)*FI(M)
  310 FF(LG,J,I)=FF(LG,I,J)
      IF(NUMB.EQ.2) GO TO 6
      IF(NUMB.NE.1) GOTO 320
      WRITE(6,6004)
 6004 FORMAT(1HO,'STANDARD F-MATRIX FOR GAS:')
      WRITE(6,6005)
 6005 FORMAT(1HO,'              1           2           3           4
     1       5           6           7           8           9
     210')
      DO 312 I=1,NQ
  312 WRITE(6,6006) (FF(1,I,J),J=1,NQ)
 6006 FORMAT(9X,10F12.6)
      GO TO 320
    6 WRITE(6,6007)
 6007 FORMAT(1HO,'STANDARD F-MATRIX FOR LIQ:')
      WRITE (6,6005)
      DO 315 I=1,NQ
  315 WRITE(6,6006) (FF(2,I,J),J=1,NQ)
  320 DO 325 I=1,NQ
      DO 325 J=1,NQ
  325 F(I,J)=FF(LG,I,J)
  340 NR1=0
      IEGEN=0
  342 CALL HDIAG(G,NQ,IEGEN,A,NR1)
  343 DO 350 J=1,NQ
      IF(0.0005D0-G(J,J))347,345,345
  345 DG(J)=0.0D0
```

```
      GO TO 349
  347 BG(J)=G(J,J)
  349 DO 350 I=1,NQ
  350 U(I,J)=A(I,J)*DSQRT(BG(J))
  390 DO 400 J=1,NQ
      DO 395 L=1,NQ
      DD(L)=0.0D0
      DO 395 K=1,NQ
  395 DD(L)=DD(L)+F(L,K)*U(K,J)
      DO 400 I=1,NQ
      H(I,J)=0.0D0
      DO 400 M=1,NQ
  400 H(I,J)=H(I,J)+U(M,I)*DD(M)
  402 NR=0
      IEGEN=0
  404 CALL HDIAG(H,NQ,IEGEN,C,NR)
  406 DO 408 I=1,NQ
  408 DV(I)=DSQRT(DABS(H(I,I)/5.88852D-7))
      CALL THERM (NQ,NRED,DV,KIND,NUMB,IFS,LG,T,NOTEM,NCT,IT,MODE,NIT,
     1FNEW)
      GO TO 90
  610 WRITE(6,6002) NROWG(L),NCOLG(L),DATING(L)
 6002 FORMAT(1H0,' G-MATRIX ERROR. THE CARD READS ',2I3,F12.6)
      GO TO 95
  615 WRITE(6,6003) NRO(K),NCO(K),NFO(K),Z(K)
 6003 FORMAT(1H0,' Z-MATRIX ERROR. THE CARD READS ',2I3,F12.6)
      GO TO 95
      END
      SUBROUTINE HDIAG(H,N,IEGEN,U,NR)
      IMPLICIT REAL*8 (A-H,O-Z)
CHDIAGHIHDI3, FORTAN II DIAGONALIZATION OF A REAL SYMMETRIC MATRIX BY
C     THE JACOBI METHOD.
C     CALLING SEQUENCE FOR DIAGONALIZATION
C     CALL HDIAG( H, N, IEGEN, U, NR)
C     WHERE H IS THE ARRAY TO BE DIAGONALIZED.
C     N IS THE ORDER OF THE MATRIX, H.
C     IEGEN MUST BE SET UNEQUAL TO ZERO IF ONLY EIGENVALUES ARE TO BE
C     COMPUTED.
C     IEGEN MUST BE SET EQUAL TO ZERO IF EIGENVALUES AND EIGENVECTORS
C     ARE TO BE COMPUTED.
C     U IS THE UNITARY MATRIX USED FOR FORMATION OF THE EIGENVECTORS.
C     NR IS THE NUMBER OF ROTATIONS.
C     A DIMENSION STATEMENT MUST BE INSERTED IN THE SUBROUTINE.
C     DIMENSION H(N,N), U(N,N), X(N), IQ(N)
C     COMPUTER MUST OPERATE IN FLOATING TRAP MODE
C     THE SUBROUTINE OPERATES ONLY ON THE ELEMENTS OF H THAT ARE TO THE
C     RIGHT OF THE MAIN DIAGONAL. THUS, ONLY A TRIANGULAR
C     SECTION NEED BE STORED IN THE ARRAY H.
      DIMENSION H(18,18),U(18,18),X(18),IQ(18)
      IF (IEGEN) 15,10,15
   10 DO 14 I=1,N
```

```
      DO 14 J=1,N
      IF(I-J)12,11,12
   11 U(I,J)=1.0D0
      GO TO 14
   12 U(I,J)=0.0D0
   14 CONTINUE
   15 NR = 0
      IF (N-1) 1000,1000,17
C     SCAN FOR LARGEST OFF DIAGONAL ELEMENT IN EACH ROW
C     X(I) CONTAINS LARGEST ELEMENT IN  ITH ROW
C     IQ(I) HOLDS SECOND SUBSCRIPT DEFINING POSITION OF ELEMENT
   17 NNI1=N-1
      DO 30 I=1,NNI1
      X(I) = 0.0D0
      IPL1=I+1
      DO 30 J=IPL1,N
      IF(X(I)-DABS( H(I,J))) 20,20,30
   20 X(I)=DABS(H(I,J))
      IQ(I)=J
   30 CONTINUE
C     SET INDICATOR FOR-SHUT-OFF.RAP=2**-27,NR=NO.OF ROTATIONS
      RAP=7.4505805960-9
      HDTEST=1.0D38
C     FIND MAXIMUM OF X(I) S FOR PIVOT ELEMENT AND
C     TEST FOR END OF PROBLEM
   40 DO 70  I=1,NNI1
      IF (I-1) 60,60,45
   45 IF(XMAX-X(I)) 60,70,70
   60 XMAX=X(I)
      IPIV=I
      JPIV=IQ(I)
   70 CONTINUE
C     IS MAX. X(I) EQUAL TO ZERO, IF LESS THAN HDTEST,REVISE HDTEST
      IF (XMAX) 1000,1000,80
   80 IF( HDTEST) 90,90,85
   85 IF (XMAX - HDTEST) 90,90,148
   90 HDIMIN = DABS ( H (1,1) )
      DO 110  I=2,N
      IF (HDIMIN - DABS ( H (I,I))) 110,110,100
  100 HDIMIN=DABS (H(I,I))
  110 CONTINUE
      HDTEST=HDIMIN*RAP
C     RETURN IF MAX.H(I,J)LESS THAN(2**-27)DABS(H(K,K)-MIN)
      IF (HDTEST-XMAX) 148,1000,1000
  148 NR= NR+1
C     COMPUTE TANGENT, SINE AND COSINE,H(I,I),H(J,J)
  150 TANG=DSIGN(2.0D0,(H(IPIV,IPIV)-H(JPIV,JPIV)))*H(IPIV,JPIV)/(DABS(H
     1(IPIV,IPIV)-H(JPIV,JPIV))+DSQRT((H(IPIV,IPIV)-H(JPIV,JPIV))**2+
     24.0D0*H(IPIV,JPIV)**2))
      COSINE=1.0D0/DSQRT(1.0D0+TANG**2)
      SINE=TANG*COSINE
```

```
      HII=H(IPIV,IPIV)
      H(IPIV,IPIV)=COSINE**2*(HII+TANG*(2.0D0*H(IPIV,JPIV)+TANG*H(JPIV,
     1JPIV)))
      H(JPIV,JPIV)=COSINE**2*(H(JPIV,JPIV)-TANG*(2.0D0*H(IPIV,JPIV)-TANG
     1*HII))
      H(IPIV,JPIV)=0.0D0
C     PSEUDO RANK THE EIGENVALUES
C     ADJUST SINE AND COS FOR COMPUTATION OF H(IK) AND U(IK)
      IF ( H(IPIV,IPIV) - H(JPIV,JPIV)) 152,153,153
  152 HTEMP = H(IPIV,IPIV)
      H(IPIV,IPIV) = H(JPIV,JPIV)
      H(JPIV,JPIV) =HTEMP
C     RECOMPUTE SINE AND COS
      HTEMP = DSIGN (1.0D0, -SINE) * COSINE
      COSINE =DABS (SINE)
      SINE =HTEMP
  153 CONTINUE
C     INSPECT THE IQS BETWEEN I+1 AND N-1 TO DETERMINE
C     WHETHER A NEW MAXIUM VALUE SHOULD BE COMPUTE   SINCE
C     THE PRESENT MAXIMUM IS IN THE I OR J ROW.
      DO 350 I=1,NMI1
      IF(I-IPIV)210,350,200
  200 IF (I-JPIV) 210,350,210
  210 IF(IQ(I)-IPIV) 230,240,230
  230 IF(IQ(I)-JPIV) 350,240,350
  240 K=IQ(I)
  250 HTEMP=H(I,K)
      H(I,K)=0.0D0
      IPL1=I+1
      X(I) =0.0D0
C     SEARCH IN DEPLETED ROW FOR NEW MAXIMUM
      DO 320 J=IPL1,N
      IF ( X(I) -DABS( H(I,J)) ) 300,300,320
  300 X(I) = DABS(H(I,J))
      IQ(I)=J
  320 CONTINUE
      H(I,K)=HTEMP
  350 CONTINUE
      X(IPIV) =0.0D0
      X(JPIV) =0.0D0
C     CHANGE THE ORDER ELEMENTS OF H
      DO 530 I=1,N
      IF (I-IPIV) 370,530,420
  370 HTEMP = H(I,IPIV)
      H(I,IPIV)= COSINE*HTEMP + SINE*H(I,JPIV)
      IF ( X(I) - DABS( H(I,IPIV)) )380,390,390
  380 X(I) = DABS(H(I,IPIV))
      IQ(I) = IPIV
  390 H(I,JPIV) = - SINE*HTEMP + COSINE*H(I,JPIV)
      IF ( X(I) - DABS ( H(I,JPIV)) ) 400,530,530
  400 X(I) = DABS(H(I,JPIV))
```

```
      IQ(I) = JPIV
      GO TO 530
  420 IF(I-JPIV) 430,530,480
  430 HTEMP = H(IPIV,I)
      H(IPIV,I) = COSINE*HTEMP + SINE*H(I,JPIV)
      IF ( X(IPIV) - DABS(H(IPIV,I)) ) 440,450,450
  440 X(IPIV) = DABS(H(IPIV,I))
      IQ(IPIV) = I
  450 H(I,JPIV) = - SINE*HTEMP + COSINE*H(I,JPIV)
      IF (X(I) - DABS( H(I,JPIV)) ) 400,530,530
  480 HTEMP = H(IPIV,I)
      H(IPIV,I) = COSINE*HTEMP + SINE*H(JPIV,I)
      IF ( X(IPIV) - DABS( H(IPIV,I)) ) 490,500,500
  490 X(IPIV) = DABS(H(IPIV,I))
      IQ(IPIV) = I
  500 H(JPIV,I) = - SINE*HTEMP + COSINE*H(JPIV,I)
      IF ( X(JPIV) - DABS( H(JPIV,I)) )510,530,530
  510 X(JPIV) = DABS(H(JPIV,I))
      IQ(JPIV) = I
  530 CONTINUE
C     TEST FOR COMPUTATION OF EIGENVECTORS
      IF(IEGEN) 40,540,40
  540 DO 550 I=1,N
      HTEMP=U(I,IPIV)
      U(I,IPIV)=COSINE*HTEMP+SINE*U(I,JPIV)
  550 U(I,JPIV)= -SINE*HTEMP+COSINE*U(I,JPIV)
      GO TO 40
 1000 RETURN
      END
      SUBROUTINE TRANS(AX,BX,CINT,CX,N)
      IMPLICIT REAL*8 (A-H,O-Z)
      DIMENSION AX(18,18),BX(18,18),CINT(18,18),CX(18,18)
    1 DO 5 I=1,N
      DO 5 J=1,N
      CINT(I,J)=0.0D0
    4 DO 5 K=1,N
    5 CINT(I,J)=CINT(I,J)+AX(I,K)*BX(J,K)
    6 DO 12 I=1,N
      DO 12 J=1,N
      CX(I,J)=0.0D0
      DO 10 K=1,N
   10 CX(I,J)=CX(I,J)+BX(I,K)*CINT(K,J)
      IF(0.00005-DABS(CX(I,J)))12,12,11
   11 CX(I,J)=0.0D0
   12 CONTINUE
   13 RETURN
      END
      SUBROUTINE REAR(A,N)
C THIS SUBROUTINE REARRANGES A ONE-DIMENSIONAL ARRAY A INTO DESCENDING ORDER.
C N IS THE NUMBER OF ELEMENTS IN A.
      IMPLICIT REAL*8 (A-H,O-Z)
```

```
      DIMENSION A(18),IT(18),B(18)
      DO 10 I=1,N
   10 IT(I)=0
      NC=1
   15 DO 20 I=1,N
      IF(IT(I).EQ.0) GOTO 21
   20 CONTINUE
   21 C=A(I)
      II=I
      DO 25 I=1,N
      IF(C.GE.A(I)) GOTO 25
      IF(IT(I).EQ.1) GOTO 25
      C=A(I)
      II=I
   25 CONTINUE
      B(NC)=C
      IT(II)=1
      NC=NC+1
      IF(NC.LE.N) GOTO 15
      DO 30 I=1,N
   30 A(I)=B(I)
      RETURN
      END
      SUBROUTINE THERM (NQ,NRED,DV,KIND,NUMB,IFS,LG,T,NOTEM,NCT,IT,MODE,
     1NIT,FNEU)
C THIS IS A 9042D-VERSION OF SUBROUTINE "THERMD". RPFR, ITS PHASE-DIFFERENCE,
C AND THEIR CHANGES DUE TO CHANGES IN F-MATRICES ARE COMPUTED.  ALL PRINTOUTS
C OF PROGRAM 9042D EXCEPT FOR THE ALPHAMERICS AND STANDARD F-MATRICES ARE
C DONE IN THIS SUBROUTINE.
      IMPLICIT REAL*8 (A-H,O-Z)
      DIMENSION DV(18),T(10),DVR(2,18),DVI(2,18),DVS(48,18),Y(2,24),
     1YS(6,24),D1(18),D2(18),D3(10),D4(18),D5(18),D6(18),D7(18),D8(18),
     2D9(18),D10(10),D11(10),D12(10),D13(10),D14(10),IT(24),FNEU(24)
      NQ=NQ-NRED
      NM1=NUMB-1
      CALL REAR(DV,NQ)
      IF(KIND.NE.3) GOTO 100
    5 NP=NCT
      NP1=NP-1
      DO 10 L=1,NOTEM
      X=0.0D0
      DO 7 I=1,NQ
      UR=1.4385*DVR(LG,I)/T(L)
      UI=1.4385*DV(I)/T(L)
      X=X+DLOG(UI/UR)+(UR-UI)/2.0D0+DLOG((1.0D0-DEXP(-UR))/(1.0D0-DEXP(
     1-UI)))
    7 CONTINUE
   10 Y(LG,L)=X
   11 DO 15 I=1,NQ
   15 DVI(LG,I)=DV(I)
      IF(LG.EQ.2) GOTO 20
```

```
      MQG=MQ
      GO TO 500
   20 DO 25 I=1,MQG
      D1(I)=DVR(1,I)-DVR(2,I)
      D2(I)=DVI(1,I)-DVI(2,I)
      D4(I)=DVR(1,I)-DVS(1,I)
      D5(I)=DVI(1,I)-DVS(NP1,I)
      D6(I)=DVR(2,I)-DVS(2,I)
      D7(I)=DVI(2,I)-DVS(NP,I)
      D8(I)=D4(I)-D6(I)
   25 D9(I)=D5(I)-D7(I)
      NL=MQG+1
      DO 30 I=NL,MQ
      D6(I)=DVR(2,I)-DVS(2,I)
   30 D7(I)=DVI(2,I)-DVS(NP,I)
      DO 35 L=1,NOTEM
      D3(L)=Y(2,L)-Y(1,L)
      D10(L)=(Y(1,L)-YS(NP1,L))*1.D2
      D11(L)=(Y(2,L)-YS(NP,L))*1.D2
      D12(L)=D11(L)-D10(L)
      D13(L)=T(L)*D3(L)
      D3(L)=D3(L)*1.D2
      D14(L)=T(L)*D12(L)
   35 D12(L)=D12(L)*1.D2
   40 WRITE(6,6001)
 6001 FORMAT(1H0,'                                FREQUENCY (CM-1)
     1                          REDUCED PARTITION FUNCTION RATIO')
      WRITE(6,6002)
 6002 FORMAT(1X, '-------------------------------------------------
     1-------------------------------------------------------------
     2----')
      WRITE(6,6003)
 6003 FORMAT(1X, '           GAS                    LIQUID
     1 PHASE-SHIFT')

      WRITE(6,6004)
 6004 FORMAT(1X, '---------------------- ---------------------- -----
     1-----------------')

      WRITE(6,6005)
 6005 FORMAT(1X, '  REFERENCE    ISOTOPE    REFERENCE    ISOTOPE    REFE
     1RENCE    ISOTOPE     TEMP       GAS        LIQ     100*DIFF   T*DI
     2FF')
      WRITE(6,6006)
 6006 FORMAT(1X, '------------ ---------- ---------- ---------- -----
     1------ ---------- -------- -------- -------- -------- -----
     2----')
      WRITE(6,6007)
 6007 FORMAT(1H0)
      DO 45 I=1,MQG
   45 WRITE(6,6008) DVR(1,I),DVI(1,I),DVR(2,I),DVI(2,I),D1(I),D2(I)
```

```
6008 FORMAT(1X,6F12.3)
     DO 46 I=NL,NQ
  46 WRITE(6,6009) DVR(2,I),DVI(2,I)
6009 FORMAT(25X,2F12.3)
     WRITE(6,6007)
     DO 50 L=1,NOTEM
  50 WRITE(6,6010) T(L),Y(1,L),Y(2,L),D3(L),D13(L)
6010 FORMAT(73X,F10.2,2F11.5,2F10.4)
  60 WRITE(6,6011)
6011 FORMAT(1HO,///1X,' EFFECT OF MODIFIED F-MATRIX FOLLOWS:
    1VALUES UNDER "CHANGE IN REDUCED PARTITION FUNCTION RATIO" ARE 100*
    2ACTUAL ')
     WRITE(6,6012)
6012 FORMAT(1HO,'                              CHANGE IN FREQUENCY (CM-1)
    1                        CHANGE IN REDUCED PARTITION FUNCTION RATIO')
     WRITE(6,6002)
     WRITE(6,6003)
     WRITE(6,6004)
     WRITE(6,6005)
     WRITE(6,6006)
     WRITE(6,6007)
     DO 65 I=1,NQG
  65 WRITE(6,6008) D4(I),D5(I),D6(I),D7(I),D8(I),D9(I)
     DO 70 I=NL,NQ
  70 WRITE(6,6009) D6(I),D7(I)
     WRITE(6,6007)
     DO 75 L=1,NOTEM
  75 WRITE(6,6010) T(L),D10(L),D11(L),D12(L),D14(L)
     GO TO 500
 100 DO 105 I=1,NQ
 105 DVS(NUMB,I)=DV(I)
     IF(KIND.NE.1) GO TO 200
 110 DO 115 I=1,NQ
 115 DVR(LG,I)=DV(I)
     IF(NUMB.LE.2) GOTO 500
 120 IF(LG.EQ.2.AND.IFS.EQ.0) GOTO 125
     IF(LG.EQ.1.AND.IFS.EQ.0) GOTO 121
     GO TO 500
 121 WRITE(6,6013) NODE
6013 FORMAT(1HO,' GAS F-MATRIX BEING MODIFIED:  NODE = ',I3)
     GO TO 130
 125 WRITE(6,6014) NODE
6014 FORMAT(1HO,' LIQUID F-MATRIX BEING MODIFIED:  NODE = ',I3)
 130 WRITE(6,6015) (IT(I),I=1,NIT)
6015 FORMAT(1X,' IT(I) = ',2013)
     IF(NODE.NE.4) GOTO 500
     WRITE(6,6016) (FNEW(I),I=1,NIT)
6016 FORMAT(1X,' FNEW(I)= ',5F12.6)
     GO TO 500
 200 DO 210 L=1,NOTEM
     X=0.000
```

```
      DO 207 I=1,MQ
      UR=1.4385*DVR(LG,I)/T(L)
      UI=1.4385*DV(I)/T(L)
      X=X+DLOG(UI/UR)+(UR-UI)/2.0D0+DLOG((1.0D0-DEXP(-UR))/(1.0D0-DEXP(
     1-UI)))
  207 CONTINUE
  210 YS(NUMB,L)=X
  211 DO 215 I=1,MQ
  215 DVI(LG,I)=DV(I)
      IF(LG.EQ.2) GOTO 220
      MQG=MQ
      NL=MQG+1
      GO TO 500
  220 DO 225 I=1,MQG
      D1(I)=DVR(1,I)-DVR(2,I)
  225 D2(I)=DVI(1,I)-DVI(2,I)
      DO 235 L=1,NOTEM
      D3(L)=YS(NUMB,L)-YS(NM1,L)
      D13(L)=T(L)*D3(L)
  235 D3(L)=D3(L)*1.D2
  240 WRITE(6,6001)
      WRITE(6,6002)
      WRITE(6,6003)
      WRITE(6,6004)
      WRITE(6,6005)
      WRITE(6,6006)
      WRITE(6,6007)
      DO 245 I=1,MQG
  245 WRITE(6,6008) DVR(1,I),DVI(1,I),DVR(2,I),DVI(2,I),D1(I),D2(I)
      DO 246 I=NL,MQ
  246 WRITE(6,6009) DVR(2,I),DVI(2,I)
      WRITE(6,6007)
      DO 250 L=1,NOTEM
  250 WRITE(6,6010) T(L),YS(NM1,L),YS(NUMB,L),D3(L),D13(L)
  500 RETURN
      END
```